
COLLEGE OF AGRICULTURE, ENGINEERING AND SCIENCE

# COUPLED HEAT AND MASS TRANSFER IN SOLAR-POWERED LIQUID DESICCANT ADIABATIC DEHUMIDIFIER AND REGENERATOR FOR AIR CONDITIONING APPLICATIONS

**Oyieke Andrew Young Apuko**

**213571041**

Thesis submitted in fulfilment of the requirements of the award of the degree of Doctor of Philosophy in Mechanical Engineering

Supervisor

**Prof. Freddie L. Inambao**

**July 2020**

"As the candidate's academic supervisor, I agree to the Submission of this Thesis"

PROF. FREDDIE L. INAMBAO .....

**Name of Supervisor** **Signature**

# DECLARATION 1 - PLAGIARISM

I, **Oyieke Andrew Apuko Young**, declare that;

1. The research reported in this thesis, except where otherwise indicated, is my original research.
2. This thesis has not been submitted for any degree or examination at any other university.
3. This thesis does not contain other persons' data, pictures, graphs or other information, unless specifically acknowledged as being sourced from other persons.
4. This thesis does not contain other persons' writing, unless specifically acknowledged as being sourced from other researchers. Where other written sources have been quoted, then:
   (a) Their words have been re-written but the general information attributed to them has been referenced.
   (b) Where their exact words have been used, then their writing has been placed in italics and inside quotation marks and referenced.
5. This thesis does not contain text, graphics of tables copied and pasted from the internet, unless specifically acknowledged, and the source being detailed in the thesis and in the references sections.

Signed:

.....

# DECLARATION 2 - PUBLICATIONS

The following papers have been published:

1. **Oyieke Andrew.Y.A** and Freddie L Inambao (2020); A review of coupled heat and mass transfer in adiabatic liquid desiccant dehumidification and regeneration systems; Advances and opportunities. *International Journal of Low-Carbon Technologies*; ctaa031: https://doi.org/10.1093/ijlct/ctaa031 (published online: 25th May 2020)

2. **Andrew Y A Oyieke**, Freddie L Inambao (2020); Experimental assessment of heat and mass transfer characteristics of solar powered adiabatic liquid desiccant dehumidifier and regenerator *International Journal of Low-Carbon Technologies*; ctaa013. https://doi.org/10.1093/ijlct/ctaa013 (Published online: 17 April 2020)

3. **Oyieke Andrew.Y.A** and Freddie L. Inambao (2019). Stochastic Generation of Artificial Weather Data for Subtropical Climates Using Higher-Order Multivariate Markov Chain Model, *International Journal of Mechanical Engineering and Technology*, 10(6), 2019, pp. 120-134. 9http://www.iaeme.com/IJMET/issues.asp?JType=IJMET&VType=10&IType=60

4. **Andrew Y A Oyieke**, Freddie L Inambao (2018). Interfacial heat and mass transfer analysis in solar-powered, packed-bed adiabatic liquid desiccant regeneration for air conditioning, *International Journal of Low-Carbon Technologies*, Vol 13, Issue 3, , pp. 277-285,(https://doi.org/10.1093/ijlct/cty029)

5. **Andrew Y A Oyieke**, Freddie L Inambao (2019). Multi-layered Artificial Neural Network for performance prediction of an adiabatic solar liquid desiccant dehumidifier, *International Journal of Low-Carbon Technologies*, Vol 14, Issue 3, Pg. 351-363, (https://doi.org/10.1093/ijlct/ctz022)

6. **Andrew Y A Oyieke** and Freddie L. Inambao (2019). Performance Prediction of an Adiabatic Solar Liquid Desiccant Regenerator using Artificial Neural Network, *International Journal of Mechanical Engineering and Technology*, 10(3), pp. 496-511. http://www.iaeme.com/IJMET/issues.asp?JType=IJMET &V Type=10&IType=3

In all the above listed papers, I **Oyieke Andrew Young Apuko** was the main and corresponding author, whilst Prof. Freddie L. Inambao was the co-author and my research supervisor.

Signed: .....

# ACKNOWLEDGEMENT

Praise, honour and glory be to the Lord God Almighty, our creator and sustainer for the privilege of life, good health and unending blessings in the course of my work and studies

This work has been designed, executed and compiled under the invaluable guidance and positive support from my supervisor; Professor Freddie L. Inambao of the Discipline of Mechanical Engineering at the University of KwaZulu-Natal. His research vision, technical expertise, sincerity, attitude, dynamism and motivation has always inspired me to conduct research and professionally present the findings to peers in the engineering spectrum. Therefore, I would like to express my deep and sincere gratitude to him and his family for the overwhelming support. It has been a prodigious honour and privilege to be accorded the opportunity to work and study under his direction

Most importantly, I would like to express my sincere appreciation to my parents; Washington and Cathleen Oyieke, my wife; Hellen, my son; Ricky, and all my siblings for their unconditional and relentless love, patience, kindness, understanding and support. They always encouraged and supported me from the start to the accomplishment of this work; they have been my source of strength and courage. May God bless you all.

I also wish to thank my employer, the Mangosuthu University of Technology (MUT) for granting me time and financial support through University Capacity Development Grant (UCDG), which facilitated the success of this work.

I wish to thank all my colleagues at the workplace (MUT), and to a large extent, GES Research Group (UKZN) for every support accorded to me throughout my study. I wish you the best in your work, studies and future projects.

The contributions of the entire staff and fellow students in the Discipline of Mechanical Engineering and the entire University of KwaZulu-Natal from whom I have benefited throughout my stay and the duration of my study cannot go unnoticed.

Last but not least, I'm very thankful to Brian and Migan Cockwell for their accommodation hospitality, care and support. The level of comfort I experienced in your facility is second to none. May God bless you.

# ABSTRACT

With energy aggressively becoming an important environmental as well as economic issue in the past decade, there is an increased need to develop energy efficient systems especially in built environments. Air conditioning process is one of the top energy consumers in buildings which requires urgent intervention particularly in the dehumidification stage. The dehumidification process in the conventional vapour compression system (VCS) involves cooling and warming the air and ends up using a large amount of energy. The main aim of this study is to develop a reliable energy efficient and alternative system to conventional VCS to reduce humidity in conditioned air. The liquid desiccant system (LDS) has been considered for this purpose by considering enhanced the heat and mass transfer occurrence between air and liquid desiccant in a packed counterflow adiabatic dehumidifier and regenerator both experimentally and by theoretical modelling to significantly reduce the energy uptake. The LDS was preferred due to its flexibility in operation, elimination of organic and inorganic contaminants and low operating temperatures that favours the use of renewable energy from solar.

A small scale experimental rig of a packed bed adiabatic dehumidifier and regenerator driven by solar energy via a hybrid photovoltaic/thermal (PV/T) module was built to study the coupled heat and mass transfer phenomenon due to the optimization, over-estimation, low effectiveness and significant carry-over challenges recorded in existing literature. The experiment was set up under a controlled environment with temperature, humidity ratio and flow-rates of air and desiccant as variables both at inlets and outlets of the packed-bed dehumidification and regeneration columns. The leading performance analysis indices were the effectiveness and moisture removal/condensation rates (MRR). For the given inlet conditions, the increase in inlet air humidity ratio significantly reduced the regenerator effectiveness and MRR, while causing increased dehumidifier effectiveness and MRR. Varying the airmass flow rate progressively upwards, improved the regenerator effectiveness by 15% while, that of the dehumidifier reduced by 43%. The MRR generally showed low sensitivity to the air and LiBr flow rates while the dehumidifier effectiveness reduced by 32% as the generator effectiveness increased by 15%. As the solution concentration increased, the MRR decreased significantly by up to 4 kg/s while the effectiveness improved with increased LiBr concentration. Similarly, the regenerator, MRR decreased with increase in concentration while the effectiveness increased by up to 5% within the same range of concentration. The optimal solution flow rate for best performance of both regenerator and dehumidifier was 0.5 kg/h which resulted in highest temperature of 68.14$^o$ C. The results provided reliable data upon

which the theoretical models can be formulated and validated.

A 3D predictive numerical thermal model based on falling liquid stream with constant thickness in counter-flow configuration was developed and solved by a combination of separative appraisal and stepwise iterative technique. Despite the success recorded with some existing well-formulated single and multidimensional numerical and analytical performance prediction and analysis models of heat and mass transfer, they still don't offer the degree of flexibility required for performance in the external domains. The 3D model mitigated the above bottlenecks and provided results which showed that during the dehumidification and regeneration processes, an increase in airflow rate per unit length and desiccant solution flow rate per unit area resulted in increased thermal and mass exchange coefficients but with varying proportions. As the Lewis number increased, both the heat and mass transfer constants decreased significantly for the dehumidifier and regenerator vessels. A 74% increase in Lewis number caused a decrease in heat and mass transfer coefficients by 10% and 77%, respectively. Comparisons conducted at various levels of input and output of the experimental and predicted dehumidifier and regenerator MRR, effectiveness, heat and mass transfer coefficients revealed sublime conformity. The variation of dehumidifier effectiveness was within $\pm 6.2\%$ while that of the regenerator was $\pm 2.9\%$. The MRR was within $\pm 2\%$ and $\pm 1.2\%$ conformity for dehumidifier and regenerator, respectively. The heat transfer coefficients were within $\pm 9.7\%$ and $\pm 2.8\%$ for the dehumidifier and regenerator respectively. The average deviations of $\pm 3.5\%$ and $\pm 8.2\%$ were achieved during dehumidification and regeneration procedures.

In the simulation of weather parameters, typical meteorological year (TMY) and test reference year (TRY) weather tools have often been used. However, in both cases, the extreme low and high points are successively disregarded which means that the actual prevailing hourly mean settings are not precisely represented. To offer a reliable and effective alternative, a simplified higher order multivariate Markov chain model was developed founded on a combination of a mixture-transition and stochastic technique to project the solar radiation, air humidity, ambient temperatures as well as wind speeds and their interrelationships in sub-tropical climates. Multivariate Markov chain provides flexibility for use in circumstances where dynamic sequential and categorical weather data for a given region is required. The generic simulation of weather parameters was produced from 20 years of actual weather conditions using a stochastic technique. The series of weather parameters developed were then implemented in the simulation of solar powered air dehumidification and regeneration processes. The outcomes indicated that the model was devoid of constraints and more accurate in the estimation of variable parameters implying that a properly designed solar-powered liquid desiccant air conditioning

system is capable of supplying the majority of the latent cooling load. The generated and validated meteorological parameters were to be used theoretical modelling of adiabatic regenerator performance.

A simplified analytical model was also developed from which interfacial air-desiccant interaction was analysed for structured mellapak-packed vertical columns using lithium bromide (LiBr) solution. The empirical and artificial stochastic weather data was fed into the model, and the resulting differential equations solved simultaneously using separative evaluation and step by step iterative procedure. The regeneration rate and effectiveness improved with the upsurge in mass flow rate but reduced with a rise in humidity ratio. The liquid desiccant solution concentration increased by 30% during when solar radiation peak hours. The obtained theoretical outcomes of the model matched with experimental results within an acceptable deviation range of ± 5%.

An Artificial Neural Network (ANN) algorithm was also developed and used to provide an exhilarating alternative that solved complex computational glitches in prediction, optimization and control of coupled heat and mass transfer phenomenon. A reinforced-technique of supervised learning based on error correction principle combined with perceptron convergence theorem was applied. The learning ensued basically as soon as an error was encountered enabling the perceptron learning process to converge after a definite number of iterative steps. Each neuron was allocated a net and activation function indicating the possible combination of network outputs inside the neuron. Every link between neurons was assigned a variable weight factor which allowed each neuron to produce a summation of all its input weights resulting in an internal activity. The activation process of the network solely depended on the applied threshold which was mathematically formulated. The learning loop containing input formats, error calculation and adjustment was varied using sets of various input-output examples until an acceptable response level of network sum of square error was achieved. Knowing the technique of input data format, expected output and type of modelling task, the number of nodes for input and output was easily determined. The ANN algorithm offered dispersed exemplification, learning and oversimplification capability, adaptability, error forbearance and intrinsic statistical dispensation with comparatively little energy intake. The MRR was best predicted by configurations 6-12-12-1 and 6-4-4-1 for dehumidifier regenerator respectively while effectiveness was superlatively predicted by structures 6-6-1 and 6-14-1 respectively, all within a mean variation of less than ±1%.

# Contents

# List of Figures

# List of Tables

# Chapter1

# INTRODUCTION

Moisture removal in industrial as well as domestic processes and applications is often a drainer in so far as air conditioning energy is concerned. Air conditioning is an essential building service that cools and dehumidifies the process air, at the same time; define the level of comfort for a given population of occupants in a built environment. The level of comfort of occupants greatly depends on the air temperature and humidity in their environment. Cooling is relatively straight forward involving temperature gradient while moisture removal (dehumidification) is a costly process in terms of energy consumption and maintenance costs.

Conventional Vapour Compression Systems (VCS) condenses the moisture by overcooling the air to dew point and the heating it again to the comfort temperature level allowing the precipitation of vapour and decrease in the total moistness. This reduction is achieved by utilising cooling spirals which further reduces the humidity and consequently, dry-bulb temperature as illustrated in Figure 1.1a. The dehumidification process is superseded by warming the air stream to a suitable temperature H. The aggregate practice often takes up a substantial amount of energy in air cooling and then a rewarm stage C-H employing sizzling hot water, electricity or condensed refrigerant loops.

The most reliable alternative to the VCS is the desiccant technology which dates back to 1930s and has recently revolutionised moisture regulation the built environment air circulation and comfort levels. Whereas solid-state desiccants pioneered this technology, liquid desiccant systems (LDS) also emerged in the late 1960s as a consequence of ever-escalating energy and environmental challenges.

In contrast to the VCS, desiccant systems operate differently as cold liquid/solid desiccant freely absorb moisture from the exposed immediate atmosphere, up to saturation vapour pressure. It has been established that, for liquid desiccants, the saturation vapour pressure unevenly rise exponentially as the temperature rises. LDS employ the hygroscopic characteristics of a saline solution to absorb moisture from the air when the low vapour-pressure desiccant solution directly contacts the comparative moisture-rich air-stream at elevated vapour pressure. The occurrence of this process can be demonstrated psychrometrically in figure 1.1b as the air experiences a constant enthalpy state A-D while flowing through the dehumidifier. The air dry-bulb temperature reduces from D-C by a sensible cooling coil before distribution to conditioned spaces. There is less power required for this process as matched to the comparable solid desiccant wheel (SDW).

The regenerator requires a higher desiccant temperature to expel the absorbed water particles and re-concentrate the dilute desiccant solution to a near initial state. Liquid desiccants require lower temperatures to regenerate than their solid counterparts. Once the desiccant is regenerated, it is cooled, and can then be used again in the conditioner. The regeneration heat required for liquid desiccant regeneration is by far lower than that of solid equivalents. However, a more innovative approach to extra effective desiccant regeneration process is to cause ultrasonic disruption to the liquid being regenerated as suggested by (Yao and Liu, 2014).

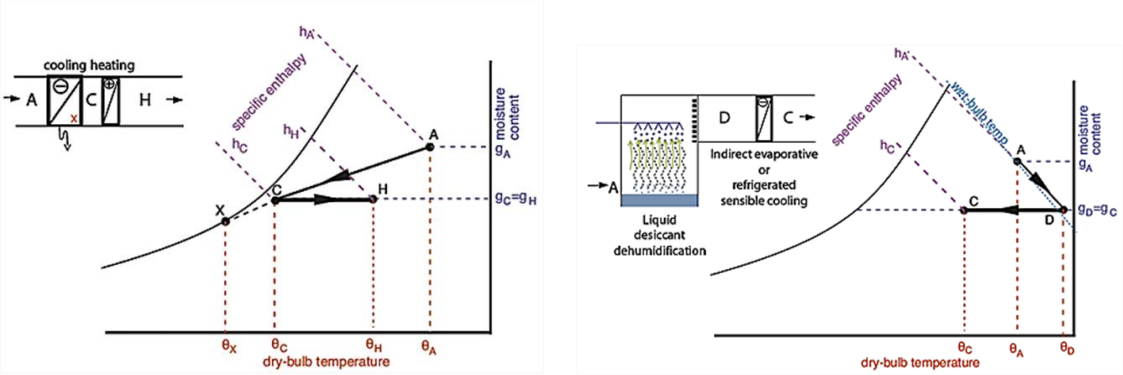


(a) (b)

Figure 1.1: Psychrometric representation of the dehumidification process by (a) cooling and reheating (b) desiccant and sensible cooling (Dwyer, 2014)

Desiccants, when used in solid-state, frequently take the form of a revolving wheel stuffed with sodium silicate (silica gel) shown in figure 1.2. When the wheel revolves, the desiccant permeates interchangeably over a distinct air-stream allowing moisture adsorption to alternative air-stream that rids of the desiccant of moisture (regeneration). Typically, only 60% surface area of the wheel is involved in the course of dehumidification, and there is absolutely no desiccant carried over to the process air. However, during the regeneration process residual 40% of the wheel surface area is bombarded by a stream of hot water, steam or hot gases ordinarily circulated through the heating coil. Solid desiccant wheel (SDW) requires a constant cycle of extensive heating and cooling in the dehumidification process. In both cases, an enormous amount of energy is wasted. Typically, successful regeneration of silica gel occurs between temperatures of 60$^o$C and 70$^o$C, even though in practice, temperatures go higher for guaranteed operational efficiency. This high-temperature operation is energy-intensive and further adds to the exorbitant cost of the system

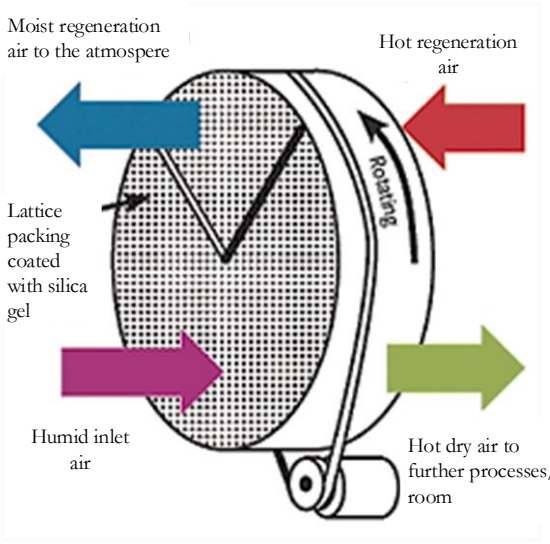


Figure 1.2: Typical of a solid desiccant wheel

On the other hand, the advent of application of liquid desiccant technology in air conditioning systems (LDACS) dates back to as early as 1969 but has only gained renewed impetus in the past decade as an effective technique of extracting moisture from process air. In addition to their potential of utilizing low-grade energy provided by the solar collector, environmental friendliness is a core benefit compared to the energy-intensive conventional VCS and SDW (Koronakia et al., 2014).

## 1.1 Basic features and operation liquid-desiccant dehumidification and regeneration (LDDR)systems

The conceivable arrangements of the constituents of LDDR systems extensively vary, with the type of desiccant and the use. A basic schematic diagram of liquid desiccant dehumidification and regeneration system for air-conditioning applications is presented in figure 1.3. The system basically consists of dehumidifier, regenerator, desiccant reservoirs (both weak and concentrated) and heat exchanger. In instances where the scheme is largely used to restrain the replacement air humidity, the size of the dehumidifier should be designed to condition only the incoming circulation air portion. The regeneration heat may be supplied by waste heat, solar radiation and other low-grade sources even though the unit is not incorporated in the diagram.

As the moist air comes into contact with sprinkled crystals of desiccant flowing over a controlled surface area, mass transfer takes place thus enabling water vapour to be absorbed by the desiccant. Similarly regeneration occurs in a packed vessel where weak solution is passed over a stream of air of elevated temperature which causes

water particles in the desiccant to separate and escape with the air. the resulting solution is re-concentrated to near initial concentration levels. The cycle is repeated under controlled and monitored environment. The reservoir serves the purpose of collecting the dilute or concentrated solution so as to ensure continuity in supply. The reservoirs are fitted with an auxiliary sub-heater to prevent crystallization of the desiccant solution which may lead to clogging of distribution pipes. The heat exchanger is configured to remove the sensible heat from the conditioned air as dictated by the defined comfort levels of a a particular location (Dwyer, 2014). For this study a solar energy unit is incorporated to facilitate regeneration process and potential energy saving as presented in a simplified typical layout in figure 1.4.

The possible dehumidification proves the effectiveness and reliability of the desiccant/regenerator vessel as a result of the probable change in vapour pressure relative to the incoming air and desiccant. The use of LDS is preferably most appropriate for highly humid and temperate (tropical) locations enriched with low-grade heat and expensive energy costs. A small sensible-to-latent heat ratio mainly makes an LDS appropriate. Operations characterised by extrication of dehumidification and sensible cooling, e.g. refrigerated food cupboards, can also benefit from LDS.

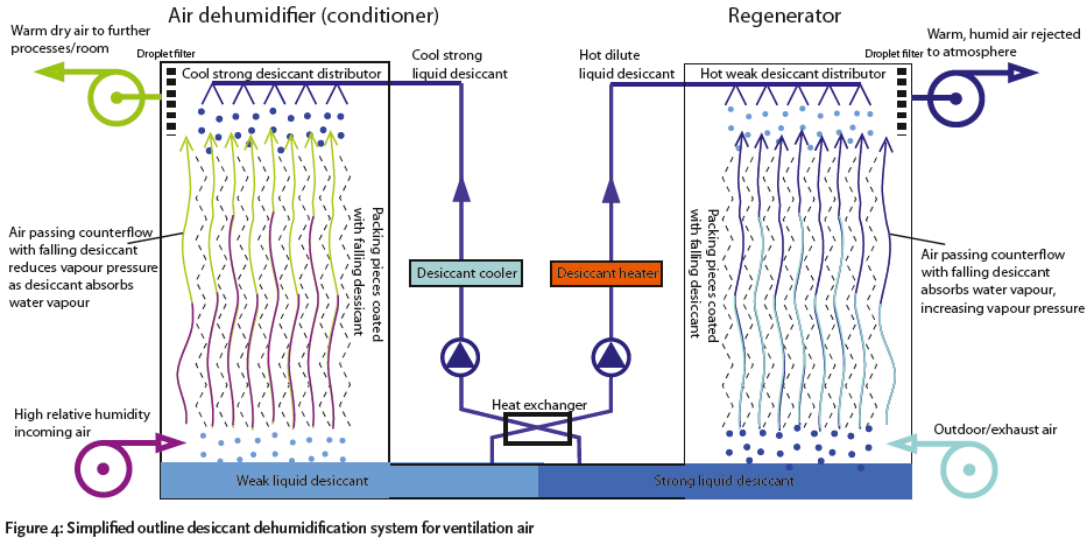


Figure 4: Simplified outline desiccant dehumidification system for ventilation air

Figure 1.3: Simple desiccant dehumidification and regeneration system for air conditioning applications (Dwyer, 2014)

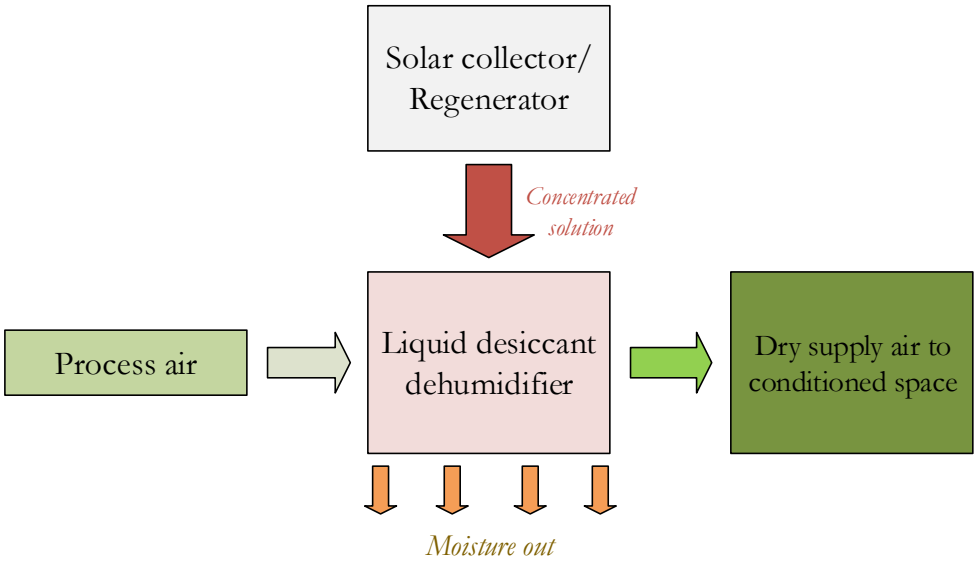


Figure 1.4: A typical solar powered liquid desiccant dehumidification and regeneration layout

The structural configurations of the regenerator and dehumidifier are similar except for extra insulation layer and air filtration mechanism to guard against ambient heat proliferation on dehumidification process. For effectiveness of heat and mass transfer, both vessels are equipped with similar packing materials. However, each process is a reverse of another for instance, during regeneration, the vapour pressure for heated dilute desiccant solution is greater than that of the ambient air hence the mass transfer of water vapour happens from the liquid solution to the air. This action causes the weak solution to regain its original concentration in readiness for circulation through he dehumidifier.

Mass transfer is driven by the vapour pressure difference between the process air and the desiccant solution, thus, for effective regeneration, the weak solution's temperature has to be increased. A conventional heat exchanger is included for this purpose, but it adds to the cost of the whole process in terms of maintenance and power consumption. A more convenient and cost effective option is to use solar energy for heating. Therefore, the role of the heat exchanger becomes auxiliary and only supplementary during the non-sunshine hours (Mei and Dai, 2008)

For effective dehumidification process, the liquid desiccant's temperature has to be lowered in order to reduce its vapour pressure as low as possible. This operation is achieved in the intermediary heat exchanger through which the weak and concentrated desiccant streams flow. The weak solution is effectively preheated while the strong solution is cooled and channelled to their respective areas of application.

An additional insulation layer on the dehumidifier helps to maintain the low vapour pressure ideal for mass transfer by preventing fluctuation of solution temperature.

The major energy intake ensues in the course of regeneration, which can be supplied by low-grade waste energy or renewable sources. The former is highly attractive but scarce while the latter is abundant and free in the form of solar energy. Moreover, their applicability is boosted by provision of energy storage option.

Placed side by side, a comparison can be drawn between LDACS and conventional VCACS to draw clear insurmountable distinctions which can be used to guide selection and inform choices. See table 1.1.

Table 1.1: Measuring instruments and specifications

| **Property** | **Conventional ACS** | **Liquid desiccant ACS** |
|---|---|---|
| Initial cost | Same | Same |
| Running costs | High | 40% savings |
| Moisture regulation | moderate | Precise |
| Interior air quality | moderate | Decent |
| Initial system set-up | Fair | Fairly complex |
| Power source | Electric, thermal, natural gas | Low-grade energy |
| Energy storing ability | Bad | Good |

## 1.2 Liquid desiccants

Liquid desiccants are aqueous solutions structured in their chemical compositions, to have a high affinity to water and are used as drying agents. They possess high abilities to absorb water vapour from any moist environment in contact with them. The selection of the type of desiccant suitable for a particular application is a sensitive process which requires advanced knowledge and consideration of a range of operational properties. The most important factors are cost, availability, thermo-physical properties, energy storage density, boiling point, regeneration temperature, corrosivity, toxicity, and vapour pressure, among others. However, the vapour pressure has shown prominence in the available literature as having the greatest influence on mass transfer in moist air-desiccant mixture (Mei and Dai, 2008).

Some of the well-known desiccant solutions are Triethyle glycol (TEG), Lithium Chloride (LiCl), Calcium Chloride ($CaCl_2$), and Lithium Bromide (LiBr) among others. As unadulterated salts, these liquid desiccants have essentially zero vapour pressure. For instance, 40% LiCl solution at $30^oC$ has a saturation vapour pressure good enough to give $3.7^oC$ dew-point temperature when contacted with humid air. $CaCl_2$ is less expensive than LiCl by approximately 10%; however, a 50/50 mixture of the duo provides saturation vapour pressure identical to that a solitary solution

of LiCl Eduardo et al. (2013). Due to their corrosiveness to metallic surfaces, their application is limited, especially with metallic ducts.

Combinations of one or two solutions in proportionate ratios have also been tried for enhanced performance. As established by Conde (2004), a carefully weighted combination of LiCl and $CaCl_2$ can give rise to a more cost-effective mixture with desirable vapour pressure for air conditioning applications. A good liquid desiccant at low temperature and high concentration should have a lower vapour pressure, than that of the humid air for effective mass transfer and absorption of water vapour.

LiCl is mostly preferred because of its stability, low vapour pressure and relatively inexpensive in comparison to other alternatives. On the other hand, $CaCl_2$ leads in terms of availability and less costliness but less effective in moisture absorption due to its relatively high vapour pressures and instability at certain inlet air and solution concentration conditions. LiBr presents itself as an intermediate desiccant solution in terms of costs and vapour pressures. TEG was the first to be discovered for air dehumidification in industrial applications; however, due to its high viscosity and very low vapour pressure, it is often characterized by high rates of carry-over to the process air in conditioned spaces (Mei and Dai, 2008).

At very high concentrations and low temperatures, the desiccants exhibit lower saturation temperatures. But, when the Concentration is raised to about 50%, they portend grave danger of crystallisation which may jam the system. The LDs under certain conditions can also act to screen out microbial adulteration of the inbound air-stream. In a fairly recent development, potassium formate desiccant was tested and found to be a suitable substitute, inexpensive, less corrosive, more effective and ecologically subtle, mainly applicable in hot and highly-humid conditions. Though some quality queries are still being raised like the unpleasant smell, and biological decomposition warrants further exploration (Dwyer, 2014).

Liquid desiccants (LD) are either used as solitary or blends of multiple solutions. In an attempt to improve LD water sorption and applicability in air dehumidification, some investigative efforts have been dedicated to thermodynamic characterisation (McNelly, 1979; Ertas and Kiris, 1992; Park et al., 1997; Morillon et al., 1999; Kaita, 2001; Younus et al., 1198; de Lucas et al., 2003).

The process of absorbing water and subsequent elimination from the air is referred to as dehumidification (absorption) and the vessel in which it happens is known as the dehumidifier. The regenerator reverses the initial concentration of the diluted desiccant exiting the dehumidifier. Regeneration as an important process requires high temperature and this impact on both the cooling capacity and energy utilization efficiency of the air conditioning system. The regeneration of the desiccant

happens when subjected to some degree of thermal energy from the solar collector that allows the water to evaporate (desorption) and desiccant re-concentrated again to near initial concentration in readiness for another absorption cycle. Therefore, the dehumidifier and regenerator units play very critical roles in air conditioning process (Koronakia et al., 2014).

## 1.3 Packing materials

Packing materials provide a larger surface area for heat and mass transfer between desiccant solution and air. In a packed column, the liquid desiccant is sprayed on the top of the packing material while air is passed across, parallel or counter current depending on the configuration. The dehumidification and regeneration process performance greatly depends on the packing; therefore, proper consideration must be given to the choice of material and subsequent arrangement.

The two existing modes of packing arrangements are random, in which irregularly shaped pieces are positioned in no definite order in the column and structured, comprised of regular shapes with fixed geometries of solution-air passages. In random packing, there is often an unpredictable distribution of liquid flow over packing material surface which complicates the process, especially when higher desiccant loads are desired. There is also a possibility of desiccant flow along the column walls and channels which may adversely affect the heat and mass transfer process. Examples are Pall rings, rosette rings and ladder rings.

The structured packing on the hand offers a uniform path and regular contact area for the air-desiccant mixture, ensuring less resistance to desiccant flow due to their geometric pattern. In this category are a wavy plate, grid packing materials and silk net materials are the most commonly used. These packing materials offer a low-pressure drop on the air-side, flexibility in manipulation and a higher rate of mass transfer. However, vulnerability to corrosion and logging is a major drawback which needs close attention.

The dehumidification process is initiated by applying desiccant liquid spray particles from above the packing medium through which conditioned air flows depending on the configuration. The packing material surface area acts as a catalyst for air-desiccant interfacial heat and mass transmission. Therefore, the selected packing material must be able to provide a surface area large enough to enable complete air-desiccant interaction which defines the dehumidifier/regenerator effective application.

The choice of packing medium greatly depends on the wetted surface pressure drop,

which is closely linked to the operational energy for the feed air blowers. In this regard, the wetted pressure drop for both regular and irregular packing materials was predicted Gandhidasan (2002) with the aid of a steady-state model. It was shown that the regular packing offered superior pressure drop than the irregular counterparts, a feature that enabled categorization and characterization according to their pressure drop limitations as well as capabilities. However, the random packing materials could also be ordered accordingly to realize better pressure drops according to Lazzarin et al. (1999).

Experimental performance comparison between the regular and irregular packing material fronted by Chung et al. (1996); Bravo et al. (1986) also showed that the structured achieved higher effectiveness and heat-mass exchange as well as lower pressure drop. The air-desiccant interfacial range is typically appraised using volumetric zoning, empty space ratio and packing material strata positioning during design and choice. The empty space ratio and air resistance are inversely proportional and must be accorded utmost consideration in addition to the packing intermission range. Typically 6 - 8 mm spacing is taken as optimum to maximize heat and mass exchange.

Likewise, the equivalent diameter as defined by Al-Farayedhi et al. (2002) equally plays a pivotal role in the forecasting of heat-mass transmission. An arithmetic mean of the varying channel hydraulic radius and cross-sectional area precisely estimates the equivalent diameter. The nominal interfacial area defined by the wetting ratio or soaked proportion of packed layers also a vital determinant of the effectiveness of packing medium in so far as mass-heat exchange is concerned. The soaked proportion varies for several filling materials due to their distinct flow path geometry and surface textures. Gandhidasan (2004) proposed a modest method of estimation of the nominal interfacial areas for various desiccant contractors.

The elevation and span of the contactor material also present crucial guiding constraints in the design of the dehumidification system. Besides the determination of packing materials as a function of mass exchange quotient, the superiority principles should be observed so as not to compromise the integrity of the packing material. In other words, the material must not collapse when drenched in the desiccant solution over an extended duration. Subsequently, the material stuffing sheets should remain in shape under the sufficient incoming air-velocity.

The heat and mass transfer process is therefore affected by the aforementioned factors such as, the configuration of the dehumidifier/regenerator, the type of desiccant and packing materials used. It is however, complex to demarcate the distinct boundary between interfacial heat and mass exchange between the desiccant solu-

tion and air and hence for simplicity the transfer phenomena are thus considered to be coupled and happen simultaneously. Moreover, the accuracy of the mathematical models depends on the method and correlations used to predict these heat and mass transfer processes.

This study explores the heat and mass transfer performance of solar-powered liquid desiccant dehumidifier and regenerator using LiBr through experimental and theoretical modelling. The experimental evaluation was performed to establish the influence of various input parameters on heat and mass transfer coefficients, moisture removal rate and effectiveness. For theoretical simulation, sets of artificial weather variables were generated using multivariate Markov chain model. Additionally, a numerical three dimensional (3D) model was developed for coupled heat and mass transfer process during dehumidification and regeneration in adiabatic liquid desiccant systems based on the energy and mass conservation laws. The model was validated with experimental results then used to optimize the dehumidification and regeneration processes and provide fundamental design data in LDAC system. The ANN technique is also employed via a multi-layered algorithm to corroborate the performance characteristics of the adiabatic dehumidifier/regenerator.

## 1.4 Research motivation

The escalated climate change, as well as environmental pollution world over, has necessitated the need for improved inhaled air quality supplied in sufficient quantity and at meticulous temperature and humidity. Coupled with increased air pollution, the increased clean air requirement piles pressure on the energy intake, particularly in the subtropical climates especially experienced in the coastal areas of South Africa.

The average yearly per capita energy use in South African built environment is approximately 358 kWh/m$^2$ of which 30% goes to the HVAC because of the prolonged cooling seasons of enormous magnitudes. Faced by the reality of fast depletion of fossil fuels, a serious intervention and exploration of substitute energy sources to accommodate the current upsurge in demand is required. However, with the prolonged cooling load challenges experienced in hot and humid subtropical regions, there is a profusion of solar radiation. For instance, a majority of locations in South Africa experience above 2500 hours of sunlight annually. The mean daily solar radiation range from 4.5 - 6.5 kWh/m$^2$ which translate to approximately 220 W/m$^2$. This fact drives the need to explore solar energy for air conditioning applications especially a novel solar-power liquid desiccant dehumidification and regeneration systems

Numerous predictive heat and mass transfer mathematical models are in existence

for regenerator and dehumidifier performance which assumes the constant mass flow rate and liquid desiccant concentration. This concept often yields very high desiccant to air volume flow ratios making it difficult to estimate the optimum air-desiccant flow ratios since the low quantity of water removed by the desiccant is neglected. The negligible water vapour removal results in low effectiveness and large liquid desiccant carry-over to the process air, which reflects in not only economic losses, but also serious health hazards if the desiccant vapours are inhaled.

In order to curtail the aforementioned challenges, an investigative as well as predictive study of coupled heat and mass transfer performance of an adiabatic solar-powered liquid desiccant dehumidification and regeneration system is required, particularly in the subtropical climate. Hence, the need for this study.

## 1.5 Aim and objectives of study

Solar radiation is plentiful, readily available, reasonably inexpensive and non-polluting to the environment and qualifies as a driver to the LDACS, which offers an alternative to VCS. However, due to its unpredictability as a component of the weather and climatic variations, the solar energy may periodically be unavailable to meet the air conditioning demand. The effective operation of LDACS is also influenced by a variety of other climatic variables which complicates the in-depth computations due to many input factors. As the desiccant and air mingle, a trade-off of heat and mass occur at the same time. Therefore, to assess the performance of liquid desiccant dehumidifier/regenerator system, complete mastery of the combined heat-mass exchange manifestation is necessary. For investigative and predictive performance assessment of solar-powered adiabatic dehumidifier/regenerator, the following objectives are set forth;

i. To perform an experimental procedure to determine the optimal heat and mass transfer performance characteristics of solar-powered dehumidifier and regenerator.

ii. To formulate a predictive three dimensional numerical models of heat and mass transfer coefficients for solar powered adiabatic dehumidifier and regenerator.

iii. To stochastically generate artificial weather data for subtropical climate characterized by multiple variables

iv. To develop an analytical model for theoretical analysis of the interfacial heat and mass transfer occurrence in a solar-powered adiabatic regenerator.

v. To develop an Artificial Neural Network (ANN) algorithm to control and pre-

dict the performance of solar-powered dehumidifier and regenerator.

## 1.6 Contributions to engineering science

The results of this research are expected to yield original contributions in coupled heat and mass transfer processes in liquid desiccant adiabatic dehumidifier and regenerator concerning experimentation as well as formulation and validation of a three dimensional (3D) numerical model in counter-flow mode. The tangible outcomes have been compiled in forms of published articles in peer-reviewed journals. Among the underlying contributions are outlined thus:

- Provision of heat and mass transfer coefficients applicable in design, sizing and optimizing of the LDAC systems.
- Provision of artificial weather data for tropical climates based on several variables applicable in the simulation of virtual all weather driven processes inputs.
- Development of a multi-layered artificial neural network algorithm capable of accepting several inputs to be used for performance prediction of dehumidifier and regenerator.
- Publication of various articles in peer-reviewed and Q-rated international journals availed as open access to widen the knowledge covered in the area of study.

## 1.7 Scope of the research

The study has been structured to accomplish the specified objectives regarding Liquid desiccant technology, with more emphasis on the coupled heat and mass transfer characteristics in adiabatic dehumidifier and regenerator powered by solar energy. Both experimental and theoretical methodologies have been used in the present case. A small scale experimental rig was constructed and used to obtain the data analysed and projected for full scale application. The theoretical evaluation was based on both numerical, analytical and artificial intelligence techniques whose results were compared and validated with the respective experimental data.

Since the regeneration process requires slightly higher desiccant temperatures to reduce the moisture-holding capacity, research has shown that heat energy can be provided by industrial low-grade waste heat or solar energy. This study only focuses mainly on the solar radiation generated thermal and electrical energy via a flat plate hybrid photovoltaic/thermal module for effective liquid desiccant dehumidification and regeneration.

The geographical location influences the solar energy potential based on seasonal meteorological conditions. The measured, as well as artificially generated solar radiation values used throughout this study, was specific to the coastal city of Durban, South Africa. However, the findings can be extrapolated to regions with similar subtropical weather characteristics.

Even though there are different types of solar operated regenerator and dehumidifiers, the presented study was centred primarily on the adiabatic, and packed-bed vessel with structured counter-flow configuration. The other types may have been mentioned in the report merely for informational purposes and not analysis.

## 1.8 Organization of the Thesis

This thesis is comprised of eight parts ordered as successive chapters whose details are provided as follows:

1. **Chapter 1** presents an introduction to the desiccant dehumidification technologies with particular emphasis on the liquid desiccant dehumidification and regeneration. A brief background and need for the LDAC technology is also provided. A systematic layout of the preliminary content of the report is given in terms of defining the research objectives, motivation and the general organization.

2. **Chapter 2** offers a comprehensive systematic review of the relevant literature related to solar energy application in liquid desiccant dehumidification and regeneration processes. It covers the critical review of the various existing experimental assessment procedures and the resulting heat and mass correlations, mathematical models of heat and mass transfer for various configurations. Various critical conclusions are drawn that justifies the need for more work in this subject area. This review article was submitted to the Q1-rated International Journal of Low carbon Technologies, and is currently under review, to be published in volume 15, Jan 2020.

3. **Chapter 3** presents an experimental assessment of heat and mass transfer characteristics of a solar-powered adiabatic liquid desiccant dehumidifier and regenerator. The effects of solar radiation, humidity ratio, air and desiccant flow-rates, and solution concentration on MRR and effectiveness were effectively analysed. A 3-D numerical model was developed to determine heat and mass transfer coefficients based on the falling fluid stream principle. The effects of air and desiccant flow rates on heat and mass transfer coefficients were also determined, and finally, the results from the model were validated using

experimental data. This chapter has been submitted to the Q1-rated International Journal of Low carbon Technologies, and is currently under review, to be published in volume 15, Jan 2020.

4. **Chapter 4** presents a higher-order multivariate Markov chain model developed and used to stochastically generate artificial weather data based on subtropical climates applicable to the simulation of any system requiring a solar application. The model was able to precisely predict and generate data for solar radiation, ambient temperature, relative humidity and wind speed. This chapter is presented in the form of a published article in the Q3-rated international journal of mechanical engineering technology volume 10, June 2019.

5. **Chapter 5** provides a detailed presentation of the theoretical interfacial heat and mass transfer occurrence in a solar-powered adiabatic liquid desiccant regenerator filled with Mellapack packing. A solar energy model fed with artificial weather characteristic inputs generated in chapter 4 as well as an analytical thermal model was developed to analyse the interfacial interaction between air and LiBr desiccant solution. The performance was analysed in terms of moisture removal rate and effectiveness attaining interesting outcomes. The content of this chapter was published in the Q1-rated International Journal of Low carbon Technologies, volume 13, June 2018.

6. **Chapter 6** gives the performance prediction of a solar-powered adiabatic LiBr desiccant dehumidifier using a modest multiple layered artificial neural network algorithm. The best algorithm patterns with the best performance levels for moisture removal rate and effectiveness, respectively, were established. The ANN algorithm predicted results were compared to the experimental values, showing precise alignments for MRR and effectiveness. The effects of desiccant and air temperatures and humidity ratio were also determined. The content of this chapter was published in the Q1-rated International Journal of Low carbon Technologies, volume 14, June 2019.

7. **Chapter 7** presents the performance prediction of an adiabatic solar-powered liquid desiccant regenerator using artificial neural network. In a similar format as chapter 6, the best algorithm patterns with the best performance levels for moisture removal rate and effectiveness respectively were established. The ANN algorithm predicted results were compared to the experimental values, showing precise alignments for MRR and effectiveness. The effects of desiccant and air temperatures and humidity ratio were also determined. The content of this chapter was published in the Q3-rated International Journal of Mechanical Engineering Technologies, volume 10 in March 2019.

8. **Chapter 8** highlights a concise collection of the key conclusions made on the entire study and pertinent additional proposals made founded on the achieved outcomes.

# Chapter2

## A review of coupled heat and mass transfer in adiabatic liquid desiccant dehumidification and regeneration systems; Advances and opportunities

This chapter offers a comprehensive systematic review of the relevant literature related to solar energy application in liquid desiccant dehumidification and regeneration processes. It covers the critical review of the various existing experimental assessment procedures and the resulting heat and mass correlations, mathematical models of heat and mass transfer for various configurations. Various critical conclusions are drawn that justifies the need for more work in this subject area. This chapter has been published in the Q1-rated International Journal of Low carbon Technologies.

**Andrew Y A Oyieke**, Freddie L Inambao; A review of coupled heat and mass transfer in adiabatic liquid desiccant dehumidification and regeneration systems; Advances and opportunities *International Journal of Low-Carbon Technologies*,

https://doi.org/10.1093/ijlct/ctaa031 Published online: 25 May 2020

# A review of coupled heat and mass transfer in adiabatic liquid desiccant dehumidification and regeneration systems; advances and opportunities

Andrew A. Y. Oyieke* and Freddie L. Inambao
*Discipline of Mechanical Engineering, University of Kwazulu-Natal, Mazisi Kunene Road, Glenwood, Durban 4041, South Africa.*

## Abstract

In this paper, a comprehensive technical review of liquid desiccant (LD) dehumidification and regeneration techniques is presented. The operational features, processes and performance indices of various flow configurations of adiabatic dehumidifier and regenerator are extensively covered. The heat and mass transfer assessment is presented in terms of past experimental and modelling evaluations and procedures. The existing adiabatic dehumidifier/regenerator heat and mass transfer models are categorized into finite difference, effectiveness-number of transfer units and simple empirical correlation models. The respective performance prediction models are critically analysed in details and compared in terms of assumptions, iterative procedures, solution methods, accuracy, computation time, output variables and applications. The solar regenerator models are also highlighted with a focus on the collector module. The ideal settings, formulation procedures, current state-of-the-art and opportunities for improvements are outlined. The review provides meaningful insight into the research status and available opportunities in the LD adiabatic dehumidifier and regenerator modelling and optimization as well as conceptualization of the applicable models. Finally, some very impactful suggestions for improvement and further research are outlined.

*Keywords:* coupled heat and mass transfer; adiabatic; regenerator/Dehumidifier; solar-powered liquid desiccant;

*Corresponding author:
youngoyieke@yahoo.com

Received 20 January 2020; revised 24 April 2020; editorial decision 28 April 2020; accepted 28 April 2020

## 1. INTRODUCTION

The rising requirements for air-conditioning, predominantly in the hot-humid subtropical climates such as in African and Mediterranean countries, have triggered a substantial intensification in demand for energy sources. Power plants experience highest loads in summer season and frequently hardly accomplish sufficient supply of the total demand. Through appropriate know-how, solar-cooling can relieve and eradicate the problem if utilized because the energy consumption is highest during the periods of high solar radiation. Liquid desiccant air conditioning (LDAC) is one such technology that has the potential of using low-grade solar thermal energy in the process of dehumidification and regeneration under adiabatic conditions.

The configuration of the adiabatic dehumidifier and regenerator is such that air–desiccant interactions are by direct contact and net energy, as well as mass transfer rates, are zero.

The most common types of dehumidifiers and regenerators are vertical columns filled with packing materials through which air–desiccant contact is enabled or spray towers [1]. In the latter, the misty desiccant liquid is spewed freely on the processed air path. However, the major drawback is the possibility of desiccant carry-over with the process air in addition to the complexity of spray head optimization.

The packed-column dehumidifier/regenerator is compact in design and provides prolonged interaction time and minimal carry-over as was proved in a verification study covering modelling and practical investigation [2]. The adiabatic type of

International Journal of Low-Carbon Technologies 2020, 00, 1–20

doi:10.1093/ijlct/ctaa031

dehumidifier is prone to low effectiveness due to escalation of desiccant temperature by the ensuing latent heat. However, a carefully balanced air–desiccant flow rates minimizes the temperature rise and risks of carry-over but care must be taken not to weigh down the coefficient of performance (COP).

The theory of liquid desiccant (LD) dehumidification and regeneration is firmly hinged on the intricately coupled heat and mass transfer manifestation. Whereas a temperature gradient spearheads the heat transmission, the mass exchange is caused by the air–desiccant interfacial vapour pressure gradient. In practice, during LD dehumidification and regeneration processes, a substantial amount of heat is produced during the phase alteration and dilution. However, the former is negligibly smaller than the latter and is always ignored in the formulation of heat and mass transfer models [3].

The assessment of heat and mass transfer process is based on interfacial film, penetration and surface renewal theories as pioneered by [4]. The film was defined as the slim still interfacial region where mass exchange resistance is highest. Based on this definition, a simple two-film theory was introduced [5]. However, the two-film approach ignores the convective component of mass exchange besides difficulty in allocating the depth of the sub-layers. Therefore, its application is only limited to steady-state conditions. Considering these and many more limitations in other studies, there is a critical need for thorough scrutiny of the existing theories and principles derived from various studies of LD dehumidification and regeneration.

This paper aims to provide meaningful insights into the research status and available opportunities in the adiabatic LD dehumidification and regeneration techniques. To unravel the gaps and provide some very impactful suggestions for improvement and further research, an extensive review of experimental and modelling procedures of heat and mass transfer assessments under varying conditions and configurations has been conducted.

# 2. DEHUMIDIFIERS

The packed bed adiabatic dehumidifiers are often characterized by high heat-mass exchange effectiveness due to its big air–desiccant interfacial area with comparatively modest geometric structure. However, there is a likelihood of high air pressure drop through the packing medium as well as high desiccant temperature in the course of moisture exchange. The high desiccant temperature is undesirable and needs to be regulated for effective moisture control. Internally cooled dehumidifiers (outside the scope of the present study) offer a temporary remedy to the heating problem; however, efficient design with optimized air–desiccant flow rates efficiently eliminates the setback [6].

## 2.1. Performance indices

The key performance appraisal indices for the packed bed adiabatic dehumidifier and regenerator that are predominantly used are effectiveness and moisture removal rate. The dehumidifier effectiveness is a unitless ratio of humidity ratio differences between inlet, exit and saturation conditions as follows [7]:

$$\varepsilon_{deh} = \left(\frac{\omega_i - \omega_o}{\omega_i - \omega_e}\right), \tag{1}$$

where w is the humidity ratio in $kg/kg_{dryair}$, while subscripts *i*, *o* and *e* are an inlet, outlet and equilibrium conditions, respectively, and $\omega_e$ is stated in relation to the inlet desiccant temperature Td and the atmospheric pressure Pa as follows:

$$\omega_e = 0.622\left\{\frac{0.6107\exp\left(\frac{17.27T_d}{T_d-237.3}\right)}{P_a - 0.6107\exp\left(\frac{17.27T_d}{T_d-237.3}\right)}\right\}. \tag{2}$$

Moisture removal rate $\epsilon$ is, by definition, directly proportional to the humidity ratio difference at outlet and inlet conditions so long as the mass flow rate $\dot{m}$ a and $\dot{m}$ d are constants. This ratio takes care of the latent heat capacity of the conditioned air and can also be mathematically formulated in terms of desiccant c concentration as well.

$$\xi_{deh} = \dot{m}_a(\omega_i - \omega_o) = \dot{m}_d\left(\frac{\chi_i}{\chi_o} - 1\right) \rightarrow \chi_i > \chi_o, \tag{3}$$

where the subscripts *a* and *d* represent states of air and desiccant, respectively. The desiccant's concentration defines the proportion and quantity of vapour expended to or engrossed from the air.

## 2.2. Permanence optimization

Numerous parameters such as air and desiccant inlet temperature, air and desiccant flow rates, concentration, inlet air humidity and the geometrical structure of the packing material influence the dehumidification process. Therefore, to achieve the optimum operational point, there have to be well-balanced proportions of these parameters. The L/G ratio is one such parameter that potentially considers the air and desiccant flow rates. However, the air vapour pressure determines the humidity ratio while that of the desiccant solution depends on the temperature and concentration.

An optimization strategy based on flow rate ratio and energy preservation was proposed and implemented comparatively on both the adiabatic and internally cooled dehumidifier in [1]. Li *et al.* [8] examined various air–desiccant flow rate ratios and determined the optimized theoretical dehumidification performance under flexible scenarios. The lower the desiccant flow rate, the patchy the fluid on the packing surface. On the other hand, too high fluid flow results in very little change in concentration that impacts on the regeneration effectiveness. Therefore, the mass flow rate ratio presents a very significant performance optimization quantity.

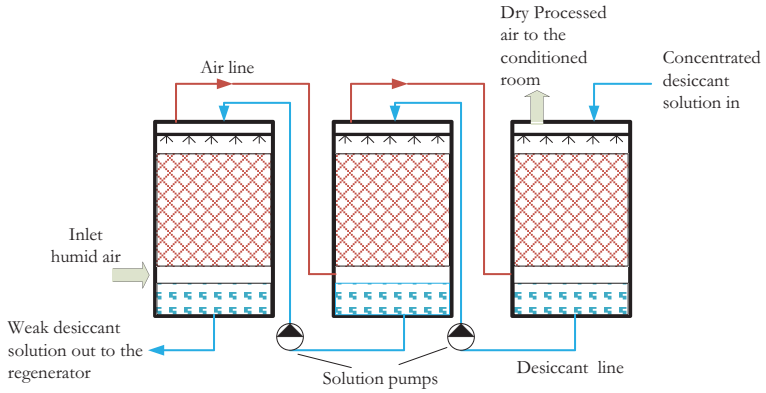


**Figure 1.** *Multi-stage LD dehumidifier recovery systems.*

The correlation depicting the interactions of unitless factors such as Nusselt, Reynolds and Sherwood numbers can be found in [9]. Additionally, using the effectiveness number of transfer units (NTU) model, the relationships for Nusselt and Sherwood numbers can be formulated as functions of mass transfer as well as Reynolds number as a significant determinant of heat transfer [10].

### 2.3. Multi-stage LD dehumidifiers

The dehumidification process can be staggered in multiple stages to limit the effects of increased desiccant temperature on mass transfer capabilities of the dehumidifier. According to Jiang *et al.* [11], dehumidification vessels can be connected in series where the air from one stage is passed through subsequent stages. This arrangement increases the effectiveness beyond that of a single stage.

The concentration of desiccant varies from stage to stage, starting with the weakest. Since both the less concentrated solution and inlet humid air possess high vapour pressures, the interaction thereof results in decreased dry air with relatively lower vapour pressure. As the process continues to the next stage, more concentrated solution interacts with the air and further reduces the vapour pressure until the last step where the vapour difference is almost at equilibrium. The multiple stages eliminate the irredeemable losses associated with the single-stage processes.

A simplified diagram is shown in Figure 1. The inter-stage desiccant solution flow rate is relatively low, but the aggregated cumulative flow becomes large depending on the number of stages prompting increased inlet-to-exit desiccant concentration variation. The variation provides a conducive platform for the implementation of the regeneration process.

## 3. REGENERATORS

The regenerator is a very vital part of LDAC system in which the dilute solution is re-concentrated to near initial conditions with the aid of low-grade thermal energy from solar and industrial waste heat. The regenerators can be classified as packed or unpacked. The packed type is similar in construction to the dehumidifier except that the process is reversed. The desiccant liquid is heated externally and then pumped to the packed bed regeneration vessel.

The temperature of the less concentrated solution is raised to desirable points where its moisture-holding capacity is weakened. Due to the sporadic and fickle nature of solar radiation and demand-constrained low-grade thermal energy, it is always necessary to include a supplementary heater. In the unpacked regenerator configuration, usually, the solution is heated in the heat exchanger or solar collector plate.

### 3.1. Performance evaluation

The goal of the desiccant regeneration process is to improve its concentration undoubtedly. The degree to which the concentration improves is critical to the effectiveness of the vessel.

The effectiveness is defined in terms of the ratio of the difference in air humidity ratios between inlet and exit as follows [7]:

$$\varepsilon_{reg} = \left(\frac{\omega_o - \omega_i}{\omega_e - \omega_i}\right). \tag{4}$$

On the other hand, the MRR expression is formulated in terms of the desiccant concentration as follows:

$$\xi_{reg} = \dot{m}_a\,(\omega_o - \omega_i) = \dot{m}_d\left(\frac{\chi_o}{\chi_i} - 1\right) \rightarrow \chi_o > \chi_i. \tag{5}$$

The outlet desiccant concentration would be higher than the inlet conditions if the regenerators work well. It should, however, be remembered that the desiccant temperature is the underlying cause of concentration change.

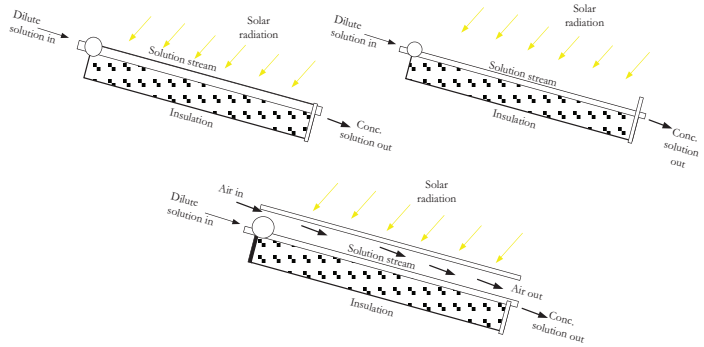


**Figure 2.** *The various configurations of solar regenerators.*

## 3.2. Types of solar collector regenerators

The conversion of solar radiation into usable thermal energy for application in desiccant regeneration primarily occurs in a solar thermal collector. This energy becomes available as a substitute of complement to the conventional heat sources. The thermal collector idea where the solution was heated in an open collector was originally introduced by Kakabaev *et al.* [12].

The solar regenerators can be classified as direct, where the dilute desiccant from the dehumidifier gets heated in the collector or indirect and where an intermediary liquid absorbs heat in the collector and then heats the desiccant via a heat exchanger. The direct type offers a more effective mode of solar energy exploitation as the fluid absorbs the maximum radiation available to the collector leading to higher temperatures. A cautious approach should be to include a complementary heater on the regenerator to cater for any unforeseen variations in solar radiation.

The solar regenerators can further be used in open, closed, natural or forced convection modes, as shown in Figure 2. Among these categories, the forced convection mode dominates in application due to its verified high effectiveness.

The construction and features of these modes are detailed as follows.

### 3.2.1. *Open-mode*

In the open mode of the solar regenerator, the dilute desiccant glides on the tilted collector surface exposed to the ambient atmosphere. Due to the higher vapour pressure of the desiccant liquid compared to the atmospheric air, the mass exchange process is triggered. Subsequently, the convective, conductive radiative and evaporative heat exchange occurs, causing the desiccant solution to free water vapour to the atmosphere.

The working principle, as well as physical components, have improved over the years, after the rigorous experimental tests [12, 13]. The feasibility of open-cycle solar regeneration and cooling in high humidity environments was explored using computational simulation [14]. Various accurate procedures for determining heat and mass exchange have also been laid out ranging from analytical model [15] and numerical methods [16–18]. Despite the enormous positive gains reported in the literature, there are still challenges associated with energy loss to the atmosphere and high dependability on meteorological conditions, especially with the occurrence of gales and storms.

### 3.2.2. *Closed-mode*

The closed-mode solar regenerator, as the name suggests, is fully covered so that the liquid being regenerated circulates without contact with the bare atmosphere. The top of the collector is glazed to trap the radiated heat from the sun, which is then absorbed by the desiccant stream flowing uniformly on the absorber surface. The evaporated water vapour condenses on the glazing and then directed towards the exit. The desiccant stream leaves the regenerator with a significant increase in concentration [19].

The temperature rise of the desiccant is indicative of the convective, conductive, radiative and evaporative/condensation thermal energy exchange. Due to lack of deficiency of ventilation, the closed-mode regenerators are often characterized by low effectiveness since the vapour pressure change is minimal. The condensed water on the glazing is likely to increase the desiccant vapour pressure and lower the regeneration capacity.

### 3.2.3. *The natural and forced convection solar collector regenerator*

The convective solar regenerator more or less the same as the closed-mode with a slight difference at the ends where there is provision for ventilation. There is an open channel for air flow either naturally or under the influence of a fan (forced).

For effective operation, the natural convection-mode solar regenerator must be able to provide the flexibility of varying the air channel height and inlet desiccant properties. However, because of the unpredictable and disorderly moving air direction, some stationary air may be trapped in the solution stream and affect the overall regenerative performance of the unit. In addition to the aforementioned natural convection-mode, the forced convection type offers access to the regulation of the inflowing air flow rate with ease. When the air flow is kept uniform and smooth, the pressure drop becomes regulated and ensures effectual regeneration output.

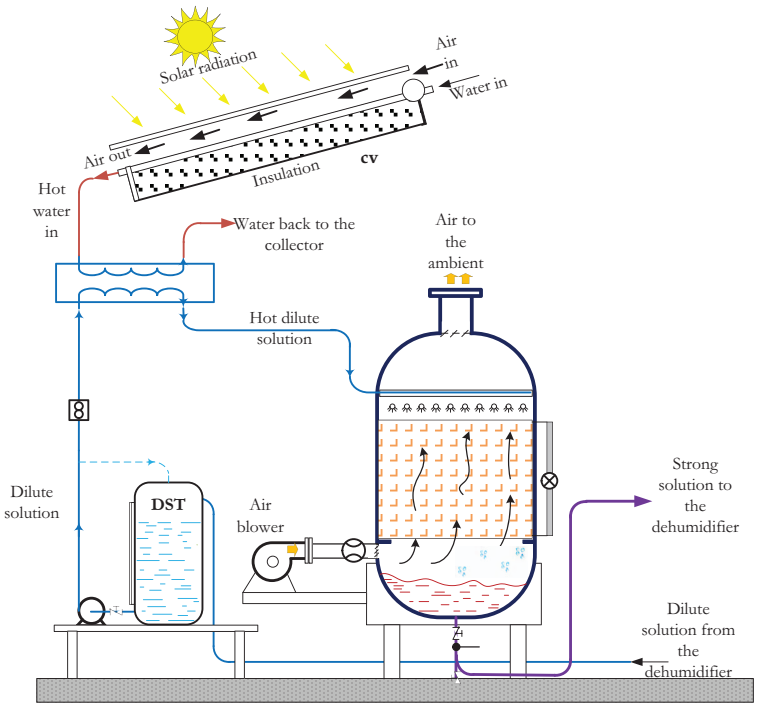


**Figure 3.** *Solar-powered indirect LD regeneration.*

In both cases, the solar radiation intensity has a significant influence on the mass exchange and outgoing solution temperature [20]. Another determining factor for heat and mass exchange performance is the regenerator length [21]. The theoretical comparison of the natural and forced convection modes in terms of their vaporization rates with and without glazing was presented in [22]. The forced flow convective mode may be configured to unidirectional or bi-directional where air and desiccant flow in same and opposing directions respectively. The former tends to provide the best mass transfer performance [23, 24].

Several factors contribute to the enhancement and optimization of the regenerator effectiveness. The spacing dimension of the glass cover, inlet solution and air temperatures are critical. The glass cover fixed at 70 mm optimized the mass exchange performance. On the other hand, the air–desiccant temperatures are inversely proportional to the desiccant flow rate [25, 26].

#### 3.2.4. *The indirect solar regenerators*

The indirect solar regenerator scheme involves a secondary fluid heated by the solar panel, which then comes in to contact with the weak desiccant solution and exchanges heat in a heat exchanger. The weak solution is then transferred to the packed regenerator for ultimate regeneration. Even though the heating effectiveness is low due to losses in the heat exchanger, the overall generation effectiveness is better than the direct counterpart. A simplified graphic illustration of the indirect solar-powered regenerator is shown in Figure 3.

#### 3.2.5. *The multi-stage regenerator*

Taking into account the previously stated benefits of solar collector regenerators, the associated mass exchange optimization challenges still needs urgent attention. As the weak solution flow over the collector, its concentration increases and vapour pressure reduces, further shrinking the air–desiccant vapour pressure difference. Because of the small difference, the regeneration becomes problematic, hence the need for regeneration in multiple phases.

The multi-stage regeneration utilizes the low thermal intensity to heat the dilute solution while the somewhat concentrated solution's temperature is raised by a stronger heating element, thereby achieving a higher energy use ratio. An illustrative diagram of a multi-stage regeneration process is shown in Figure 4. The multi-stage regeneration process combines effortlessly with the solar collector system in an indirect configuration to make use of heated water or air to provide sufficient desiccant regeneration temperature.

## 4. HYBRID AIR CONDITIONING SYSTEMS

The performance and energy savings of vapour compression system (VCS) and vapour absorption system (VAS) can immensely be improved by incorporating and LDAC for better air humidity management. A combined heat pump and LD dehumidifier attain enhanced energy-saving capability up to 35% [27, 28]. A combined LDAC-VAS system could improve the overall COP by 50%, while significant electric power savings was achieved by

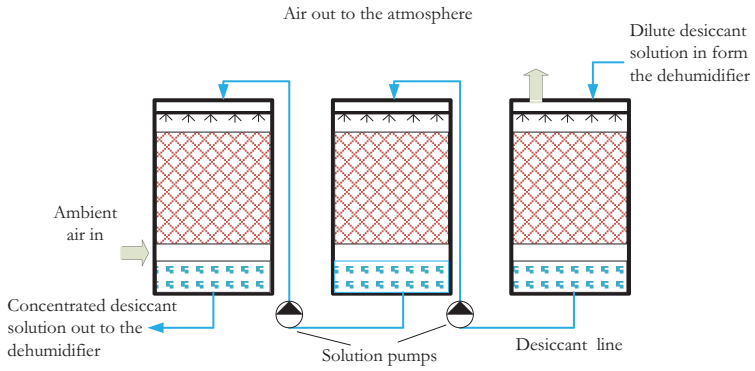


**Figure 4.** *Multi-stage LD regeneration.*

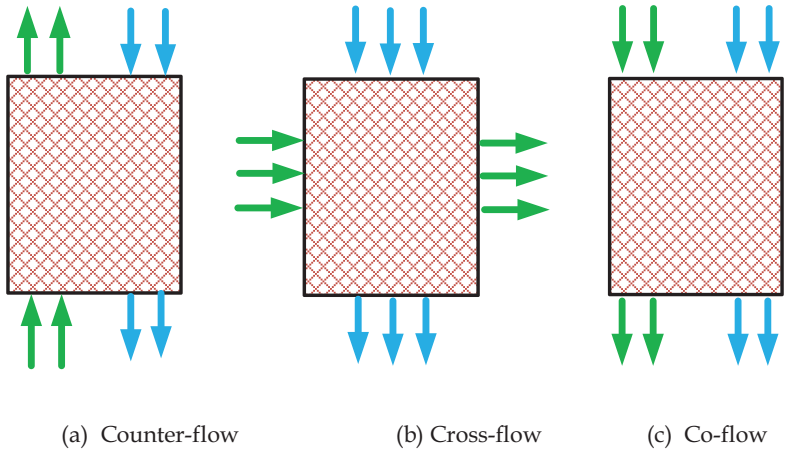


**Figure 5.** *The most common packed dehumidifier and regenerator configuration.*

incorporating LDAC and VCS in a single system with reduced size and mass flow rates [29, 30].

For the optimal aggregate performance of the hybrid air conditioning system, the geometrical properties of the dehumidifier/regenerator were investigated in addition to the solar collector configuration and dimensions in [31]. Sick *et al.* [32] conducted performance analysis of both hybrid VAS and VCS systems based on meteorological seasons and obtained exciting outcomes. Among the two systems when compared, the hybrid VAS required a large quantity of desiccant solution; hence, the solar collector heating load is increased, while the hybrid VCS needs preheating of conditioned air that weighs down on the energy demand.

The hybrid conventional and LDAC systems are capable of sufficiently supplying the cooling loads under the independent influence of solar energy or low-grade thermal source. In addition to the VCS and VAS, LD dehumidification and regeneration also combines well with heat pumps and co-generation systems in cooling and heating to form a hybrid system having more exceptional general performance than individual stand-alone systems.

## 5. FLOW CONFIGURATIONS ADIABATIC DEHUMIDIFIER AND REGENERATOR

The packed LD dehumidifiers and regenerators are classified according to the air and desiccant flow directions relative to one another in the vessel. Three distinct categories exist, namely parallel-flow (co-flow), counter-flow and cross-flow as shown in Figure 5.

The collection of literature on the development of adiabatic packed bed dehumidifier and regenerator vessels are analysed in terms of experimental, modelling as well as combined strategies. The methods, variables and selected results are systematically provided.

### 5.1. Co-flow

Chen *et al.* [33] experimented to determine the heat and mass transfer coefficient for a vertical film dehumidifier using $CaCl_2$ desiccant solution. The overall heat and mass transfer coefficient were established as a function of inlet and outlet status in terms

of logarithmic temperature difference. However, in comparison to the existing data from the literature, an overestimation and underestimation of mass and heat transfer respectively were realized. Further sensitivity analysis revealed that the mass transfer rate increased with an increase in liquid solution flow rate.

Liu *et al.* [34], with suitable and realistic assumptions, formulated a coupled heat and mass transfer phenomenon model and developed its solution analytically concerning humidity ratio and temperature of air and humidity ratio, temperature and effectiveness of the desiccant in co-flow, cross-flow and counter-flow configurations. As an extension of coupled heat and mass transfer theory, Liu *et al.* [35] configured LD packed bed dehumidifier/regenerator both in co-flow and counter-flow regimes to study the respective desiccant–air interactions. Further comparison between the two configurations, revealed that the co-flow exhibited lower and higher mass transfer during dehumidification and regeneration, respectively.

Rahama *et al.* [36] developed a numerical model of LD dehumidification/regeneration process using CaCl2 based on the borderline and interfacial states of air and desiccant liquid. The control volume method and iterative algorithm techniques were used to formulate, the finite difference (FD) equations defining the preservation of energy, mass and momentum for both air and desiccant solution were created and solved numerically. Correlations for heat and mass transfer coefficients at dehumidifier and regenerator stages were generated using mean Sherwood and Nusselt numbers and compared with a deviation of 15% with those in the existing literature. However, it was noted that, due to underestimation of some parameters, the processes were time intensive, difficulty and carry-over were not guaranteed.

A 2D dynamic model was developed by Diaz *et al.* [37] to examine the influence of changes in temperature and concentration of LD in a co-flow design dehumidifier.

The boundary conditions were prepared for adiabatic and constant temperature scenarios taking into account the wall effects, which were then, implemented in the model. The resulting sets of equations were solved by the implicit FD technique and compared with the experimental results from the literature. The interfacial correlations for Nusselt and Sherwood numbers were also developed.

Desiccant concentration, regeneration effectiveness and air-side pressure drops were the subjects of additional experimental study by Longo *et al.* [38] on 1" pall ring element structured and Mellapack 205Y randomly packed column desiccant regenerators using hygroscopic solution H2O/LiBr in a counter-flow configuration. The measured parameters, fluid properties, formulated correlations and known constants were implemented in a computer code solved by step-by-step iterative technique.

In the recent study of Peng *et al.* [39], the dimensionless heat loss coefficient and total temperature differences were considered as variables in solving mass transfer equations in a solar regenerator for both counter-flow and co-flow configurations. The numerical solution of the model revealed both liner and parabolic relationships between a limited NTU and dimensionless air temperature. Backed by a parametric study on the inlet parameters, a conclusion that counter-flow regeneration configuration exhibited superior performance compared to the co-flow counterpart under similar operating conditions was drawn.

Tanda *et al.* [40], in the study of the dehumidifier, used polyethylene glycol desiccant solution, to experimentally determine the correlation of mass transfer, taking into account the desiccant properties and nozzle dimensions. A couple of correlations was developed for the gas phase mass transfer in which one incorporated physical properties of desiccant nozzle diameter and the other, surface tension. The comparison of predicted and experimental results from literature yielded 18% and 10% variations for the former and latter, respectively. However, much as their conclusion recommended application of these correlations for a wide range of operational parameters, a limitation caveat to units with specific nozzle diameters arose.

## 5.2. Counter-flow

The inception of counter-flow LD dehumidification technology was first conceived in [41] where independent models for heat and mass transfer coefficients under adiabatic conditions were formulated for liquid and gaseous states. In the advancement of this idea, the performance of a packed column cross-flow tower was predicted using an analytical model in [2]. The derived expressions were solved using a combination of iterative and successive substitution procedures, allowing for an initial guess of liquid outlet temperature and obtain the remaining lengthwise nodal temperatures of the column. Better regeneration at higher liquid flow rate but poor at low liquid temperature was achieved.

In an attempt to validate their analytical model, Factor *et al.* [2] experimented with evaluating and comparing the effectiveness of lithium bromide (LiBr) and monoethylene-glycol (MEG) LDs in air dehumidification. Interestingly, MEG tests failed to produce satisfactory results for heat and mass transfer coefficient correlations due to its lower vapour pressure while LiBr provided a promising trend that fits well on the analytical data. Further, optimum mass transfer and drop were proposed to lie between 0.5 and 0.8, respectively.

In terms of LD temperatures, 68°C or higher was suggested for the regeneration process while for effective dehumidification, a range 25°C–30°C was considered adequate.

Lof *et al.* [42] expressed and evaluated the rates of heat and mass transfer in terms of ordinary differential equations (ODEs) with various assumptions. An experimental study was also conducted employing LiCl LD to validate the model with regards to the respective heat and mass transfer coefficients at different air flow rates, humidities and temperatures. The results showed an agreement within 10% with those of the theoretical model.

Gandhidasan *et al.* [43] investigated the performance of a counter-flow packed column dehumidifier with ceramic Rasching rings and carbon Berl saddles using $CaCl_2$ LD. Guided by the Treybal model [41], they formulated the interfacial heat and mass transfer coefficients both for the liquid and gas phases. Subsequently, heat and mass transfer coefficients showed higher sensitivity to inlet flow rate and concentration of desiccant

solution but an insignificant response to variations in air inlet temperature and flow rate as well as desiccant solution's inlet temperature. Hence, a highly concentrated solution at low temperature combined with a low flow rate of air was recommended for a highly effective dehumidification process. In a related study, Gandhidasan *et al.* [44] analysed the regeneration process of CaCl2 LD by an analytical model whose solution predicted mass water evaporation rate. An essential correlation for vapour pressure was developed in addition to ratios of dimensionless vapour pressure and temperature variance. Besides their previous study recommendations, the concept of solution pre-heating was introduced as an enhancing technique for an effective regeneration process regardless of the solution's flow rate.

Ullah *et al.* [45] evaluated on the effect of air and LD inlet parameters on the dehumidifier performance, applied moisture removal effectiveness to quantify and set the lowest theoretical limit of air outlet humidity ratio with fluid inlet conditions. Similar recommendations were made in concurrence with the earlier findings of Gandhidasan *et al.* [43] that, for effective dehumidification process, desiccant liquid at high concentration and low temperature together with little air flow rate was recommended.

A simplified dehumidifier/regenerator effectiveness model for predicting heat and mass transfer processes for LiBr was developed by Stevens *et al.* [10] based on the cooling tower model they initially formulated. Weighing their findings against the FD model of [2], an excellent fit was realized, but against experimental data, only enthalpies and temperatures of air and solution matched precisely while remarkable differences were shown especially in humidity ratio and outlet air temperature due to the overestimation of the Lewis number that was assumed to be unit. In comparison to other experimental data from the literature, the effectiveness model varied by between 1% to 23% concerning energy balances.

Inter-facial heat and mass transfer in the dehumidification process was studied by Ertas *et al.* [46] for both $CaCl_2$ and LiCl LDs. The possibility of blending the two solutions at a ratio of 50% LiCl to 50% CaCl2 and studying its performance as a cost-effective liquid desiccant (CELD) was explored. The LiCl exhibited better performance in terms of liquid phase mass transfer coefficient at higher flow rates. CELD showed more promising and realistic prosperities but had negligible alteration of liquid phase heat transfer in comparison to both $CaCl_2$ and LiCl but better mass transfer than $CaCl_2$.

Elseyad *et al.* [47] developed another FD model for predicting progressive lengthwise heat and mass transfer effectiveness of LD dehumidifier/regenerator using $CaCl_2$ solution. The focus was on inlet parameters such as air and solution temperatures, flow rates and concentration to generate the primary expressions that were solved numerically by applying the Runge–Kutta integration scheme combined with Nachtsheim–Swigert iteration technique. The solution demonstrated that the heat and mass transfer effectiveness was improved as the liquid mass flow rate increased at reduced air mass flow rate.

An adiabatic dehumidifier with air–desiccant in counter-flow configuration and random packing was studied by Chung *et al.* [48] applying aqueous LiCl desiccant solution. These parameters affected the overall mass transfer coefficient with a similar trend though less sensitivity was shown towards the desiccant flow rate. In a related study, Chung *et al.* [49] presented different correlations for various packing materials and mixtures of a couple of desiccants for predicting moisture removal efficiencies.

The 40% LiCl and 95% triethylene glycol (TEG) solutions were used for the dehumidification process. Using vapour pressure of pure water as the dehumidification driving force, the Ullah [45] model was modified by neglecting liquid concentration that resulted in a more precise prediction of desiccant solution and column efficiency relationship. This study provided a breakthrough since only a mean discrepancy of 7% was obtained when experimentally validated using different packing materials, liquid properties and column lengths.

In addition to their earlier work, Chung *et al.* [50] performed experiments under adiabatic and thin-film air–liquid interface conditions to determine the dimensionless heat and mass transfer correlations using Buckingham pi theorem. Both structured and random packings were evaluated with LiCl desiccant solution in which total liquid phase and gas phase, heat and mass transfer coefficients were obtained respectively. Impressive overall dimensionless coefficients were obtained and compared to existing experimental data from literature at less than 10% discrepancy.

An elaborate experimental work was conducted by on an air–desiccant counter-flow system of both random and structured packing bed column of varying depths [51]. The mass transfer correlations for LiBr desiccant solution were developed. A higher mass transfer coefficient was realized for random packing as opposed to structured counterpart with a lower degeneration rate recorded in the dehumidifier. However, owing to the broader mass transfer area of structured packing, they extrapolated a higher deterministic mass transfer rate of in random packing by a factor of 0.05 above structured packing.

Guided by the previous works of [2, 41], Oberg *et al.* [52] developed an FD model for heat and mass transfer prediction in an air 95% TEG, counter-flow adiabatic dehumidifier. The performance evaluation was based on dehumidification effectiveness and rate, subsequently, empirical correlations were derived from existing literature and implemented in a computer simulation code that revealed a convergence level of 0.05°C and 0.0001 kg TEG/kg solution for inlet desiccant temperature and concentration, respectively. A discrepancy of over 15% was recorded, which amounted to an over prediction of the dehumidifier performance.

Lazzarini [53] offered a theoretical assessment of the dehumidification process using $CaCl_2$ and LiBr LDs in a packed column counter-flow configuration that was later validated by experimentation. Basing their formulations on the models by [2, 41, 43, 52], a computer procedure was coded and used to evaluate the performance of the adiabatic counter-flow dehumidifier. An over prediction of reduction in the humidity of above 20% was achieved weighed against experimental data. However, the adiabatic conditions, as assumed, was confirmed to be true since the tower heightwise changes in air-side and solution-side enthalpies were 20%. As expected, better dehumidification was achieved at

low temperatures and high concentrations of the solution, specifically for LiBr, a concentration of about 45% and between 20°C and 30°C was recommended.

Radhwan *et al.* [54] presented a solar-powered LD system by mathematical modelling in which fourth-order Runge–Kutta integration scheme and Nachtsheim–Swigert iteration techniques were applied to the concentrated $CaCl_2$ solution to generate unidimensional expressions for the dehumidifier. The crucial system evaluation parameters such as solar utilization factor, system thermal ratio and desiccant replacement factor for both dehumidification and regeneration processes were assessed. A solution air flow rate ratio of 1:2.5 was recommended making the system to be most suitable for highly humid climatic conditions.

Martin *et al.* [55] explored the energy consumed in the adiabatic regeneration process of air using 95% TEG configured in a counter-flow scheme under high flow rate conditions by the experimental procedure. Using similar assumptions as [52], they generated an FD model whose findings agreed well with the investigational figures within 15% discrepancy. Consequently, air flow rate, humidity ratio, desiccant concentration and the temperature had a significant effect on the regenerator performance in addition to the packing elevation. Later on, in related developments, Fumo *et al.* [56] applied the same principles to evaluate the effectiveness of LiCl dehumidification and regeneration processes with slight modifications in the model to include wetted surface area due to superior surface tension properties over TEG. The uneven spreading of desiccant at the above tower was also taken into consideration in which similar trends of results were recorded.

Gandhidasan *et al.* [7] used the experimental results of [56] to corroborate a modest model of dimensionless temperature and vapour-pressure difference ratios. Apart from showing a decrease in condensation rate as inlet water temperature increases, the results of the model and experiments compared within 10.5% discrepancy. Longo *et al.* [57] presented an experimental and theoretical study on chemical dehumidification and regeneration of air in a counter-flow random packed column using H2O/KCOOH solution in comparison to conventional hygroscopic solutions $H_2O$/LiCl and $H_2O$/LiBr for typical air conditioning ranges. Basing their theoretical analysis on [41], a consistent reduction in humidity reduction was observed in both cases using the respective hygroscopic salt solutions.

$CaCl_2$ was used under low flow conditions to study adiabatic dehumidification and regeneration processes by [58] theoretically. A single dimension numerical model was formulated by establishing boundary expressions for quasi-equilibrium condition using similar assumptions as [2, 43]. Additionally, a numerical solution for the 1D model for heat and mass transfer for real conditions was provided and presented on a standard psychrometric chart. A combination of higher desiccant flow rate at low temperature produced better dehumidification while the high desiccant temperature at high flow rate resulted in active regeneration. As a continuation, Ren *et al.* [59] went further to formulate a pair of coupled differential equations under similar conditions and provided their analytical solutions. The analytical model proved inaccurate and inconsistent, particularly when a big solution temperature difference is involved in the process due to the assumption of constant change in flow rate and concentration of the solution.

In an attempt to establish realistic design parameters for a structured packing LD system using TEG, Elsarrag *et al.* [60] performed experimental procedures whose results were used to validate an FD model they had earlier created. No significant influence on performance was noted for liquid–air flow rate ratio above 2, while regeneration process showed more sensitivity to desiccant temperature and concentration. Still using the same TEG solution, Elsarrag *et al.* [61] scrutinized the solution seepage and carry-over into the process air concerning pressure drop. The heat and mass transfer empirical correlations and experimental exponentiations from the study, as mentioned above, were adopted to corroborate the FD model, which showed decent agreement. Similar results were obtained in terms of the dependence of heat transfer effectiveness on high air flow rates and packing elevation.

Chen *et al.* [62] analytically solved the heat and mass transfer model for an adiabatic dehumidifier/regenerator both in parallel and counter-flow configurations. The air–desiccant flow rate ratio went up as the solution temperature increased while keeping concentration low, thus allowing for the natural deduction of optimum values and validation of selected parameters against experimental data from literature presented a deviation of ±10%. The influence of inlet and operational factors was the main objective of the empirical study by [63] about the regeneration and dehumidification using LiCl LD. An extreme value of 7.5 g/m$^2$s, in 20% concentration at a temperature of 77.5°C was obtained. An optimum specific humidity ratio at the inlet was established for maximum tower efficiency that provided maximum dehumidification rate.

Jian *et al.* [64] generated different heat and mass transfer correlations for TEG, LiCl and CaCl2 desiccant solutions and performed parametric analysis on dehumidification effectiveness. They found out that increasing desiccant–air flow ratio with all the desiccants resulted in better dehumidification effectiveness. However, solution concentration and inlet temperature coupled with inlet air temperature and packing height had adverse effects on the dehumidification effectiveness in varying proportions for each desiccant solution used. Liu *et al.* [65] did extensive work in comparing two different direct contact scenarios, namely air–water and air–desiccant schemes using handling zone dividing method. Due to higher surface tension harboured by LD compared to water, the latter was found to have more spread on the packing compared to water as represented on a psychrometric chart. The counter-flow configuration showed a better mass transfer performance during dehumidification while the co-flow pattern was proper for regeneration.

Tu *et al.* [66] implemented the FD model by [59] on modular computer simulator to study an innovative and less energy demanding LD system utilizing LiCl solution.

A high inlet temperature of desiccant range of 80°C–85°C was recommended for the regenerator to gag crystallization. Tretiak *et al.* [67] constructed and investigated a counter-flow sorption and desorption system utilizing clay and $CaCl_2$ LD. Different

models from the literature were compared to the formulated desiccant pressure drop correlation with satisfactory convergence. Keeping equilibrium humidity ratio unaltered, Babakhani [68] made a remarkable contribution by providing a novel analytical solution for heat and mass transfer process. Differential equations for typical constraints were formulated whose results compared correctly with the comprehensive and consistent experimental data from literature on desiccant humidity ratio, temperature and concentration peaking at 5% deviation while the air temperature was at 7%, respectively.

Peng *et al.* [69] developed an analytical model recommended for the design of LD systems capable of evaluating heat and mass transfer occurrence under transient and low flow conditions. The average volumetric approach was used to obtain a non-equilibrium heat and mass transfer coefficients. However, the model showed a weak sensitivity to high flow conditions and could not be used to predict the dehumidifier/regenerator performance under varying or fluctuating loads. In addition to their previous study, Babakhani *et al.* [70] used similar assumptions and evaluation parameters to develop an analytical mathematical model and presented its solution with regards to the desiccant regeneration process in both random and structured packing.

Gandhidasan *et al.* [71] used an artificial neural network (ANN) analysis technique to study the performance of LiCl dehumidifier with random packing. The dimensionless temperature ratio contributed to better dehumidification rate. The ANN predicted the condensation rate and desiccant concentration with high accuracy against experimental data. Spray towers are known to cost less but have very large carry-over, low dehumidification effectiveness and small air-side pressure drop. In respect of these weaknesses, Kumar [72] performed experimental studies on air dehumidification using $CaCl_2$ in a modified spray tower to achieve a near-zero carry-over. The reduction in droplet velocity and increasing wetting surface significantly contributed to the improved performance and reduced carry-over of desiccant droplets to near zero.

### 5.3. Cross-flow

Al-Farayedhi *et al.* [73] tested three different desiccant solutions: $CaCl_2$, LiCl and CELD in a cross-flow structured packing column. The heat and mass transfer coefficient correlations for air–liquid phases were also developed and compared the outcomes for each fluid. A tight fit was obtained between theoretical and experimental literature volumetric heat and mass transfer coefficients, suggesting that the correlations reliably predicted the performance of the packed column with extraordinary accuracy. With regards to mass transfer performance, LiCl was preferred while higher heat transfer was exhibited by $CaCl_2$. A numerical model to evaluate the heat and mass transfer phenomenon in a cross-flow dehumidifier packed with honey-comb paper material was developed by [74]. A more significant Nusselt number was observed at the inlet conditions of the liquid, which gave a strong indication of better heat and mass transfer performance process. The results of the dimensionless parameters were further compared to experimental data from literature and obtained good agreement.

Liu *et al.* [75] developed an empirical correlation for predicting the heat and mass transfer process in a cross-flow LiBr LD dehumidifier, which was validated with experimental data with high accuracy and outlining the benefits thereof. In a similar assessment, using LiBr aqueous desiccant solution Liu *et al.* [76] constructed a testbed for performance analysis of a cross-flow, celdek structured packing regenerator. Correlation for regenerator effectiveness and moisture removal rate predicted performance of 95% of total runs to within $\pm$10% discrepancy and an average of 3.9% with the experimental data. Using the same setup, Liu *et al.* [77] further formulated a theoretical model for heat and mass transfer characteristics of a cross-flow dehumidifier and regenerator based on the NTU, moisture and enthalpy effectiveness. In comparison to the experimental data, impressive theoretical projection outcomes of enthalpy and moisture effectiveness were observed at deviations of 7.9% and 8.8%, respectively, for dehumidification process while 5.8% and 6.9% were obtained for the regeneration process. Liu *et al.* [78] using their previous model, formulated an analytical solution for heat and mass transfer occurrence in a cross-flow dehumidifier guided by the analogy of heat exchangers. A comparison of the results of analytical solution with experimental outcomes coupled with numerical solutions from literature employing similar LiBr desiccant solution was done, giving a significant deviation of $\pm$20% for enthalpy and moisture effectiveness, due to their earlier finding of varying Lewis number which in the contrary was taken to be constant in this case.

The combined NTU and Lewis number methods were used by [79] to predict the heat and mass transfer in the dehumidification process using LiCl LD. The concept of separative evaluation was used to evaluate combined heat and mass transfer coefficients that were then validated with experimental data in terms of humidity and air–desiccant temperatures showing deviations of 10%, 6% and 12%, respectively. Moon *et al.* [80] through experimental study, provided mass transfer data of a $CaCl_2$ cross-flow dehumidifier with structured packing. An attempt to compare the results with those of counter-flow in [49] and cross-flow in [75] failed to show good agreement. Given this development, a novel empirical correlation was formulated with regards to dehumidifier effectiveness whose outcomes fitted well within the range of 0.4–0.8 at $\pm$10% discrepancy with the experimental values.

Zhang *et al.* [81] performed experiments on a cross-flow structured packing dehumidifier and regenerator using LiCl aqueous desiccant solution under different operating conditions in summer and winter. However, lower overall mass transfer coefficients were observed at higher liquid temperatures. Correlations for dimensionless mass transfer coefficient for the regenerator and dehumidifier were further developed, which compared within $\pm$20% against predicted values. In another evaluation of the structured packing, using $CaCl_2$, Bansal *et al.* [82] considered both adiabatic conditions and when subjected to internal cooling and compared the performance indices for the two scenarios. The optimum air–liquid flow rate ratio that gave peak dehumidifier effectiveness was established. The internally cooled set up was

shown to provide superior performance in terms of efficacy and moisture removal rate compared to the adiabatic system.

In addition to their earlier study, Liu *et al.* [83] compared the performance LiBr and LiCl desiccant solutions in air dehumidification and individual regenerative evaluation through experimental procedures. Correlations were derived for volumetric mass transfer coefficient and moisture removal rate under identical temperature and vapour pressure ranges. The LiCl was found to perform better than LiBr subjected to same mass flow rates in the dehumidification process while LiBr outperforms LiCl in the regeneration process, especially under same volumetric flow rates.

Pineda *et al.* [84] considered the possibility of incorporating a heat exchanger within a dehumidifier to enhance performance in freezing environments. Using $CaCl_2$ desiccant solution, subjected to almost freezing state, they derived 3D numerical model for a cross-flow dehumidifier. The expression for heat exchanger effectiveness was derived upon which sensitivity analysis on humidity ratio, the outlet temperature of air and desiccant concentration were based.

Structured packing dehumidifier/regenerator employing $CaCl_2$ desiccant solution in a cross-flow orientation was also experimentally investigated in [85]. Higher inlet solution temperatures enhanced moisture removal rate and mass transfer coefficient but grossly inhibited the regenerator efficiency. On dehumidification vessel, this high desiccant temperature significantly lowered the mass transfer coefficient as well as moisture removal rate but improved productivity. On the life cycle cost evaluation, it was established that the system had a probable payback period of 11 months and contributed to 31% annual cost savings.

In the work of Gao *et al.* [86], lithium chloride (LiCl) desiccant solution was used to experimentally study the performance of a cross-flow, celdek structured packing air dehumidifier based on stepwise regression analysis technique. Enthalpy and moisture efficiencies were their main parameters characterization on which the influence of desiccant/air inlet parameters and structure/size of packing were assessed, leading to fascinating outcomes. In comparison to the predicted values of moisture and enthalpy efficiencies, 91.2% of the total experimental runs showed a discrepancy of within $\pm 10\%$ with an average of 4.2%.

In a more recent development, Bakhtiar *et al.* [87] introduced the COP as the cooling capacity per energy input for computation of the real system's performance efficiency. The experimental set up for analysing the total energy consumption in a room versus energy change indicated that dehumidification effectiveness and COP were better at low airspeeds. Yonggao *et al.* [63] in their experimental study on dehumidification and regeneration of LD in a cooling air conditioning system outlined the effects of temperatures (of heating source, desiccant and air), humidity and desiccant concentration on the dehumidification and regeneration rates. They generated mass transfer coefficients based on experimental results obtained and formulated empirical correlations between regeneration mass transfer coefficients, heating temperature and desiccant.

From the above literature, it is evident that counter-flow configuration has received more attention than the others because of its high effectiveness and moisture absorption and desorption rates.

## 6. THEORETICAL MODELS FOR ADIABATIC DEHUMIDIFIER AND REGENERATOR

The performance of adiabatic dehumidifier and regenerator is influenced by the rate of coupled heat and mass exchange. Thus, the effectiveness of the dehumidifier/regenerator is a function of the quantity of water vapour absorbed or expelled at the air–desiccant interface. Significant progress in the theoretical analysis has been detailed leading to predictive modelling of adiabatic dehumidifier/regenerators. From the information gathered in existing literature, the available modelling strategies are reliably summed up as the FD, effectiveness-NTU (e-NTU) and simplified algebraic correlation models [88].

The first two models are a bit complex, involving the solution of collective steady-state and momentum expressions to determine the velocity spectrum within the packed column followed by temperature and concentration dispersal by heat and mass equilibrium equalities. Such burdensome solution procedures are time consuming and take up large computer memory; hence, their popularity is waning compared to the simplified correlation-based counterparts. The simplified models have everyday use in prediction of long-term aggregate characteristic outputs of dehumidifier/regenerator systems [21].

### 6.1. FD model

The FD model is more popular due to its precision and unambiguous computational connotation. The formulation of the FD model is based on the segregation of the dehumidifier/regenerator into regions and considering an elemental air–desiccant interfacial area, as shown in Figure 6a. Treybal [41] founded the FD technique of predictive analysis of adiabatic dehumidification process and later modified by [2] to characterize the counter-flow adiabatic dehumidifier.

For simplicity, some assumptions were made, which informed the formulation of fundamental control equations. Taking the mass balance in the elemental volume:

$$dm_d = m_a d\omega, \tag{6}$$

where subscripts $d$, $a$ and $w$ represent desiccant, air and water vapour states, respectively, m is the specific mass flowrate in kg/m$^2$s and $\omega$ is the air humidity ratio. The change in air humidity is obtained in terms of the interfacial heat and mass exchange rates and the respective partial pressure $P$ as follows:

$$\frac{d\omega}{dz} = -\frac{\beta' M_w A}{m_a} \ln\left\{\frac{1 - P_d/P_i}{1 - P_a/P_i}\right\}, \tag{7}$$

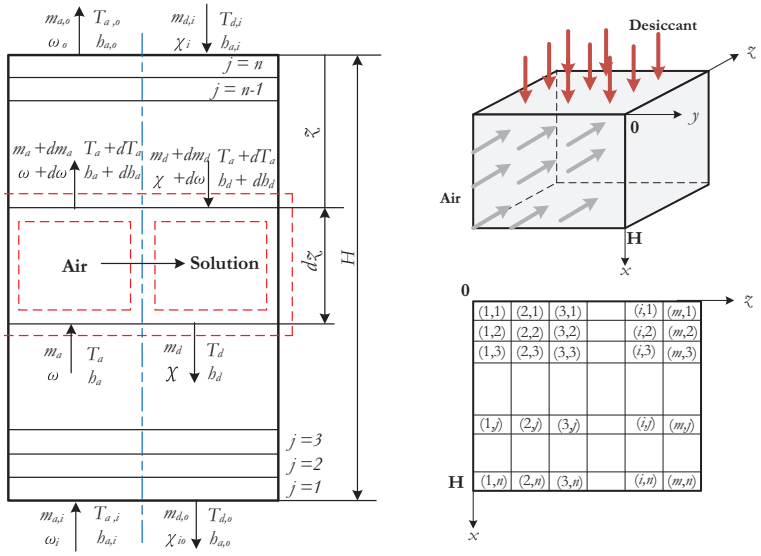


**Figure 6.** *The air–desiccant interfacial differential elements [88].*

where M is the molar mass in g/mole, A is the specific surface area per unit volume in m2/m3 and b is the mass transfer coefficient in kg/m$^2$s.

The change in temperature T is obtained in terms of interfacial air–desiccant useful heat transmission and the air-side energy balance expressed as:

$$\frac{dT_a}{dz} = -\frac{\gamma_a' A\,(T_a - T_s)}{G_a Cp_a} \tag{8}$$

$$\gamma_a' A = -\frac{m_a Cp_w \left(\frac{d\omega}{dz}\right)}{1 - \exp\left[m_a Cp_w\,(d\omega/dz)\,/\gamma_a A\right]}, \tag{9}$$

where $\gamma_a A$and $\gamma_a' A$ represent the actual (sensible) and corrected air-side heat transmission coefficient. The correction considers the influence of mass exchange on temperature achieved by Ackermann method. Therefore, the solution bounds can be defined as $z = 0$; $T_d = T_{d,\,i}$; $m_d = m_{d,i}$; $\chi = \chi_i$; $z = H$; $T_a = T_{a;i}$; $m_a = m_{a;i}$; $\omega = \omega_i$.

The derived complex differential expressions can only be solved by numerical integration using a combination of iterative and successive substitution procedures, allowing for an initial guess of liquid outlet temperature and obtain the remaining column heightwise nodal temperatures.

Gandhidasan *et al.* [89] used the FD model to establish how specific properties such as pressure drop, heat and mass transfer coefficients vary along the packed tower. Similarly, the experimental data of [52, 56] were verified using FD model and later on some modifications were made to the packing exterior to take care of the insufficient wetting of packed bed by incorporating a correction factor.

However, Khan *et al.* [90] assumed that the combined heat and mass exchange was steered by air phase, and hence the interfacial temperature was equivalent to that of the solution.

The rate of heat transmitted across the interface was also equivalent to the inlet air, thus:

$$m_a Cp_a dT_a = \gamma_a A\,(T_d - T_a)\,dz. \tag{10}$$

Likewise, the interfacial mass exchange was equivalent to the humidity change:

$$m_a d\omega = \beta_a A\,(\omega_e - \omega)\,dz. \tag{11}$$

The change in specific air enthalpy becomes:

$$dh_a = Cp_a dT_a + d\omega\left[Cp_w\,(T_a - T_r) + \lambda\right]. \tag{12}$$

Combining the Equations 10, 11 and 12, a simplified expression of change in air enthalpy h is obtained:

$$\frac{dh_a}{dz} = \frac{NTU.Le}{H}\left\{(h_e - h_a) + \lambda\left(\frac{1}{Le} - 1\right)(\omega_e - \omega)\right\}, \tag{13}$$

where *Le* and *NTU* are the Lewis number and number of thermal units, respectively, defined as:

$$Le = \frac{\gamma}{\beta Cp_a} \tag{14}$$

$$NTU = \frac{\beta AV}{m_a}. \tag{15}$$

These relationships in Equations 13, 14 and 15 showed that heat and mass exchange were combined and should be considered together. The FD model has also found extensive use in cross-flow configurations of dehumidifier and regenerator in [91, 92]. Of interest is the FD model developed in [76] for heat and mass exchange based on Figure 6b from which the main energy balance, humidity and concentrations equations are expressed as follows:

$$\frac{m\prime_a}{H}.\frac{dh_a}{dz}+\frac{1}{L}.\frac{\partial\left(m\prime_d h_d\right)}{\partial x}=0 \tag{16}$$

$$\frac{m\prime_a}{H}.\frac{d\omega}{dz}+\frac{1}{L}.\frac{\partial\left(m\prime_d\right)}{\partial x}=0 \tag{17}$$

$$d\left(m'_d\chi\right)=0, \tag{18}$$

where $m'$ is the mass flow rate in kg/s. The air–desiccant interfacial thermal and mass exchange was the same as Equation 13 and the change in humidity in the z-plane was:

$$\frac{d\omega}{dz}=\frac{NTU}{L}\left(\omega_e-\omega\right). \tag{19}$$

The values of *NTU* varied according to the corresponding experimental data. Based on the same principle, a 2D heat and mass exchange numerical FD model that was precisely validated with experimental data was proposed [93, 94].

Due to the complex nature of heat and mass transmission process in the packed bed dehumidifier/regenerator, the solution of FD models often rely heavily on experimental correlations. For instance, the fractional vapour pressure, interfacial mass exchange constants and area are such parameters. However, since the assumption of equivalent heat-mass exchange and packing specific areas ignores the desiccant solution surface tension, an insufficient surface wetting is often experienced. Therefore, to avoid minimizing the heat-mass exchange area, a correlation ratio that incorporated the surface tension of the fluid was formulated as follows [56]:

$$\frac{a_w}{a_t}=1-\exp\left\{-1.45\left(\frac{\sigma_c}{\sigma_d}\right)^{0.75}\left(\frac{L}{a_i\mu_d}\right)^{0.1}\times\left(\frac{L^2a_t}{\rho_d{}^2g}\right)^{-0.05}\left(\frac{L^2}{\rho_d\sigma_d a_t}\right)^{0.2}\right\}, \tag{20}$$

where $a_w$ and $a_t$ are the wetted and actual total packing surface areas, respectively, $\sigma$ is the fluid surface tension and $L$ is the length of the packing. Additionally, Longo *et al.* [57] developed an extended FD model that also estimated the pressure drop along the column height.

In summary, the majority of the models in the literature only show the reliance of dehumidification/regeneration process on operating conditions but largely ambiguous when it comes to the solution of film flow mass exchange. The FD model is best suited for investigative assessment of performance parameters of LD dehumidifier/regenerator with in-depth and precise outcomes.

## 6.2. Effectiveness $\varepsilon$-NTU model

The $\varepsilon$-*NTU* model assumes that the temperature and equilibrium enthalpy is directly proportional and that for effective heat-mass exchange, solution balance is devoid of vapour infiltration. Coupled with the presumptions of FD, a simple computational $\varepsilon$-*NTU* was developed by Stevens *et al.* [10] for LD heat-mass exchange.

Similar basic governing equations as FD are used:

$$m_a dh_a=m_d dh_d+h_a dh_{ad}. \tag{21}$$

The differential mass balance is:

$$dm_d=m_a d\omega_a. \tag{22}$$

The air-side enthalpy-mass balance is obtained as:

$$m_a dh_a=Cp_a m_a d\omega_e+A_w dV\left\{\gamma\left(T_d-T_a\right)+\beta\left(\omega_e-\omega_a\right)\right. . \tag{23}$$

The Le and NTU are computed by Equations 15 and 14. However, assuming negligible change in solution flow rate, the *Le* becomes unity and therefore the fundamental equations modifies to:

$$\frac{d\omega}{dV}=\frac{NTU}{V}\left(\omega_e-\omega_a\right) \tag{24}$$

$$\frac{dT_d}{dV}=\frac{NTU\left(h_e-h_a\right)}{VCp_d m_d}. \tag{25}$$

The dehumidifier/regenerator effectiveness in a counter-flow configuration is then computed in combination with the NTU and the conventional heat-exchanger capacitance ratio m∗ as follows:

$$\varepsilon=\frac{1-e^{-NTU(1-m^*)}}{1-m^*e^{-NTU(1-m^*)}} \tag{26}$$

The capacitance ratio is simplified as follows:

$$m^*=\frac{m\prime_a Cp_{sat}}{m\prime_{d,i}Cp_d}, \tag{27}$$

where $Cp_{sat}$ is the equilibrium specific heat capacity = ($dh_e = dT_d$).

The exit air and saturation enthalpies are obtained by:

$$h_{a,o}=h_{a,i}+\varepsilon\left(h_e-h_{a,i}\right) \tag{28}$$

$$h_e=h_{a,i}+\frac{\left(h_{a,o}-h_{a,i}\right)}{1-e^{-NTU}}. \tag{29}$$

And the air outlet humidity ratio is computed by:

$$\omega_o=\omega_e+\left(\omega_i-\omega_e\right)e^{-NTU}. \tag{30}$$

However, in circumstances where the fluid flow rate is lower than the air flow rate, the Stevens' NTU model becomes inappropriate, hence, the $m_a$ in Equation 15 is replaced with the least flow

rate. Alternatively, a disconcertion method in [95] can be used to correct the $\varepsilon$-$NTU$ model accordingly to account for non-linear relationships between $\omega_a$ and $h_{e,d}$, $Cp_d$ and vaporization heat.

Tao *et al.* [96] proposed a 2D numerical $\varepsilon$-$NTU$ model to predict the performance of the system resulting in a realization of low regeneration temperature of 55°C, which is easily obtainable from solar energy or waste exhaust heat. The ensuing formulations are illustrated in Equations 31 to 34 whose results were well in agreement with the experimental data.

$$\frac{dt_w}{dz} = \frac{NTU_h}{L}\,(t_w - t_s) \tag{31}$$

$$\frac{dh_a}{dz} = \frac{NTU_h.Le}{H}\left\{(h_e - h_a) + r\left(\frac{1}{Le} - 1\right)(\omega_e - \omega_a)\right\} \tag{32}$$

$$\frac{d\omega_a}{dz} = \frac{NTU_m}{L}\,(\omega_e - \omega_a) \tag{33}$$

$$NTU_h = \frac{\beta A}{Cp_w m_w}; NTU_m = \frac{\alpha_m A}{m_a}; Le = \frac{\gamma}{\beta Cp_m}. \tag{34}$$

In the latest experiments, the $Le$ has been proved to be ~1.2 for practicality, instead of unity as previously assumed. Subsequently, the non-unity $Le$ can be infused in the modified $NTU^*$ distinctly accounted for in by the $NTU$-$Le$ product. By revisiting the model in [90], a simplified analytical solution was provided under adiabatic conditions for a packed bed dehumidification and regeneration chamber by [62]. However, the assumption of constant solution concentration throughout the vessel negated the applicability of the model in low flow states. Lui *et al.* [77] used the $\varepsilon$-$NTU$ model to evaluate the operational effectiveness of a cross-flow dehumidifier by considering the air humidity ratio and temperature variations coaxial to the desiccant flow and desiccant temperature variations being in line with the airflow direction.

## 6.3. The simplified empirical correlation models

Based on the information gathered from literature, the FD and $\varepsilon$-$NTU$ are both numerically complex and requires iterative computations making them unsuitable for hourly performance assessment. This drawback has resulted in the formulation of more hourly friendly correlations based on empirical and fitted-parametrized numerical data. Khan *et al.* [90] analysed thousands of data categories using FD model and formulated a simple empirical model connecting the outlet humidity ratio to air and desiccant temperatures deduced as follows:

$$\omega_o = \omega_i + n_1\omega_i + n_2 T_{d,i} + n_3 T^2{}_{d,i} \tag{35}$$

$$\omega_o = m_o + m_1\omega_i + m_2 T_{a,o} + m_3 T^2{}_{a,o}, \tag{36}$$

where $n$ and $m$ are constants established by least square technique. These equations were particularly derived and fitted for explicit concentration conditions and flow rate ratios that may not be universally applicable. Therefore, more reliable empirical correlations for adiabatic dehumidifier/regenerator configured in counter-flow and cross-flow were formulated for enthalpy-moisture effectiveness and moisture removal rate in [7, 44, 75], respectively. Thus, temperature gradient and water vapour were formulated as dimensionless ratio as follows:

$$Cp_a\overline{T}\left(T_{a,i} - T_{d,i}\right) + \frac{M_w}{M_a}.\frac{\lambda}{P_i}P\left(P_{a,i} - P_{d,i}\right) = \frac{m_s}{m_a}Cp_d\left(T_{a,i} - T_{d,i}\right), \tag{37}$$

where the partial vapour pressure is related to the moisture removal rate e as:

$$P_{d,i} = P_{a,i} - \frac{\varepsilon P_i M_a}{m_a - M_v} \tag{38}$$

And the exiting solution temperature being:

$$T_{d,o} = \frac{T_{d,i} - \varepsilon T_{c,i}}{(1-\varepsilon)}. \tag{39}$$

Therefore, the moisture removal rate becomes

$$\xi = \frac{1}{\lambda}\left[\frac{m'_d Cp_e \varepsilon}{(1-\varepsilon)}\left(T_{d,i} - T_{c,i}\right) - m'_a Cp_e\overline{T}\left(T_{a,i} - T_{d,i}\right)\right], \tag{40}$$

where $\overline{T}$ and $\overline{P}$ are the dimensionless temperature and pressure difference ratios, $\lambda$ is the latent heat of vaporization, $\varepsilon$ is the heat exchanger effectiveness and $c$ represents the critical conditions. This method assumed different inlet air–desiccant temperatures and no heat losses between the dehumidifier and the adjacent heat exchanger.

Clen *et al.* [62] formulated an analytical model for both co- and counter-flow dehumidifier configurations founded on the FD technique of [90]. The following correlation constants were presented and conveniently used to simplify the correlation.

$$K_a = Le.Cp_a T_a + \lambda\omega \tag{41}$$

$$K_d = Le.Cp_d T_d + \lambda\omega_e \tag{42}$$

A combination of thermal mass conservation and transmission equations resulted in the flow-wise variation of $K_e$ formulated and solved to obtain the values of air moisture content and temperature as follows:

$$\frac{dK_e}{dz} = m^*\frac{NTU}{H}\left\{h_{a,i} + \frac{1}{m^*}\left(K_e - K_{e,o}\right) + (L_e - 1)\,Cp_a T_a - K_e\right\}. \tag{43}$$

Another analytical exposition of a unidimensional model of [59] resulted in two linked ODEs whose solutions were deduced in the form of

$$\Delta\omega_M = C_1 e^{\lambda_2 NTU_z} + C_2 e^{\lambda_1 NTU_z} \tag{44}$$

$$\Delta\vartheta = K_1 C_1 e^{\lambda_2 NTU_z} + K_2 C_2 e^{\lambda_2 NTU_z}. \tag{45}$$

However, the correlations were based on the assumption that the solution saturation humidity ratio was singularly hinged on

the solution temperature. Hence, the method only applicable to very low variations in desiccant concentration and flow rate.

A simplified analytical model for adiabatic dehumidifier and regenerator was developed by [68, 70] based on moisture temperature gradients and mass balance differential Equations 6, 7 and 8. The integral solutions of these equations gave rise to the following correlations whose solutions enabled the determination of air–desiccant outlet conditions:

$$\omega = \omega_{int} - (\omega_i - \omega_{int}) \exp\left(-\gamma\overline{M}NTU_z\right) \tag{46}$$

$$T_a = C_1 + C_2 \exp\left(-\theta NTU_z\right) - \frac{\beta}{\left(\gamma\overline{M}\right)^2 - \gamma\overline{M}\theta} \exp\left(-\gamma\overline{M}NTU_z\right) \tag{47}$$

$$T_a = \frac{1}{R_c Le}\left[ - C_2 \exp\left(-\theta NTU_z\right) + \frac{\gamma\overline{M}\beta}{\left(\gamma\overline{M}\right)^2 - \gamma\overline{M}\theta} \exp\left(-\gamma\overline{M}NTU_z\right) \right] + T_a \tag{48}$$

$$\ln \chi = -R_m (\omega_i - \omega_{int}) \exp\left(-\gamma\overline{M}NTU_z\right) + C_3 \tag{49}$$

$$\mathrm{m}_s = m_a (\omega_i - \omega_{int}) \exp\left(-\gamma\overline{M}NTU_z\right) + C_4. \tag{50}$$

Based on the earlier numerical model of [77], a simplified analytical model was conceptualized by [35] assuming constant solution concentration and flow rate. Sets of predictive correlations for moisture and enthalpy effectiveness of cross-flow dehumidifier were formulated as follows:

$$\eta_h = C_o(\Delta h_i)^{C_1 - 1}.(\omega_i)^{C_2}.(m_a)^{C_3}.(\dot{m}_{zi})^{C_4} \tag{51}$$

$$\eta_w = b_o(\Delta h_i)^{b_1}.(\omega_i)^{b_2 - 1}.(\dot{m}_a)^{b_3}.(\dot{m}_{zi})^{b_4}. \tag{52}$$

An improved analytical model applicable to precise prediction of real-time optimized performance with the aid of Levenberg–Marquardt method parameter identification and correlations for effectiveness of various packings using LiCl and TEG solutions were proposed considering air–desiccant flow rates and temperature, packing geometry and interfacial saturation states [50, 97]. The humidity ratios were correlated thus

$$\frac{\omega_o}{\omega_i} = \frac{C_1 \exp\left(C_2\left(T_{a,i}/T_{d,i}\right)\right)}{\xi_i C_3} \tag{53}$$

$$\omega_e = \frac{C_4 \exp\left(C_5/T_{d,i}\right)}{\xi_i C_6}. \tag{54}$$

Yonggao *et al.* [63] generated mass transfer coefficients based on experimental results and formulated empirical correlations between regeneration mass transfer coefficients, heating temperature and desiccant concentrations as shown in Equation 56. While correlations between dehumidification rates with respect to inlet air humidity dry bulb temperature as shown in Equations 57 and 58, respectively.

$$\varepsilon = \frac{1 - (\omega_o/\omega_i)}{1 - (\omega_e/\omega_i)}. \tag{55}$$

Yonggao *et al.* [63] generated mass transfer coefficients based on experimental results and formulated empirical correlations between regeneration mass transfer coefficients, heating temperature and desiccant concentrations as shown in Equation 56. While correlations between dehumidification rate with respect to inlet air humidity dry bulb temperature as shown in Equations 57 and 58, respectively:

$$\alpha_{reg} = -341.5314 + 16.1876T_h - 0.2552{T_h}^2 \ (\chi = 20\%) \tag{56}$$

$$m_d = 111.5157 - 22.9969\omega_{a,i} + 1.5379{\omega_{a,i}}^2 - 0.0329{\omega_{a,i}}^3 \tag{57}$$

$$\dot{m}_d = 11.0939 + 1.0912T_{a,i} - 0.0352{T_{a,i}}^2 + 3.7641x10^3{T_{a,i}}^3. \tag{58}$$

In summary, the three major categories of predictive models applicable to packed bed adiabatic dehumidifiers and regenerators have been covered in terms of assumptions, formulations and applications. The FD takes the lead in accuracy and suitability for design optimization but takes much memory due to the iterative nature of its solution procedure. Because of the unidimensional nature of FD models, they are best suited for counter-flow configurations.

The *ε-NTU* can be formulated in 2D and mostly applicable to cross-flow dehumidifier/regenerators. Less memory space and time during the solution process is one strong point of this kind of model. However, it is less accurate compared to the FD model, which justifies why less research is reported in the literature on *ε-NTU* models.

Both the FD and *ε-NTU* models are conditioned for specific circumstances, hence lacking the universality of use. For improved accuracy, simplicity and universal applications, some additional assumptions and modifications have been introduced guided by the experimental data to mimic the exact conditions. The ensuing models are simple and highly efficient in long-term predictions since no iterative procedures are required in their solutions. The details of the model comparison are presented in Table 1.

## 6.4. The solar regenerator models

Due to the simplicity in construction, the solar collector/regenerator presents more avenues for analysis than packed bed types. The solar collector/regenerator models are majorly built on the elemental control volume fundamental equations. These equations are formulated in terms of momentum, energy and concentration balances and variations that enable the velocity contour, temperature and concentrations to be profiled [21].

An analytical process of computing the quantity of water vapour evaporated from the dilute desiccant solution under the influence of climatic variables as well as inlet conditions of the solution was introduced in [98]. Both fixed and adjustable fluid

**Table 1.** *Comparison of models for packed bed adiabatic dehumidifier and regenerator.*

| **Model category** | **Assumptions** | **Iterations** | **Solution** | **Accuracy** |
|---|---|---|---|---|
| FD | - Minimal | - Expansive | - Numerical | - Most |
| $\varepsilon$ –*NTU* | - More | - Minimal none | - Numerical/analytical | - Good |
| | - Vast | | - Analytical | - Poor |
| **Model category** | **Computation** | **Outputs** | **Application** | |
| Finite different | Long | - All variables | - Parts design | |
| | | - Output variations | - Sensitivity analysis | |
| | | | - Performance prediction | |
| | | | - System optimization | |
| $\varepsilon - NTU$ | Short | - Selected variables | - System design | |
| | | - Outlet conditions | - Sensitivity analysis | |
| | | | - Annual performance prediction | |
| Simple correlation | Short | - Performance indices | Annual performance assessment | |
| | | - Outlet conditions | | |

stream breadth to assess the performance of solar regenerator with various simplification assumptions were used.

The control volume fundamental equations were formulated as follows.

Considering the fluid stream:

$$\gamma_d \frac{\partial^2 u_d}{\partial y^2} + \rho_d g = 0 \tag{59}$$

$$u_d \frac{\partial^2 T_d}{\partial x} = \delta_d \frac{\partial^2 T_d}{\partial y^2} \tag{60}$$

$$u_d \frac{\partial^2 C_d}{\partial x} + D_d \frac{\partial^2 C_d}{\partial y^2}. \tag{61}$$

Considering the air stream:

$$\frac{\partial P}{\partial x} = \mu_d \frac{\partial^2 v_d}{\partial y^2} \tag{62}$$

$$u_a \frac{\partial^2 T_a}{\partial x} = \delta_a \frac{\partial^2 T_a}{\partial y^2} \tag{63}$$

$$u_a \frac{\partial^2 C_a}{\partial x} + D_a \frac{\partial^2 C_a}{\partial y^2}. \tag{64}$$

And the interfacial mass balance equation is:

$$k_d \frac{\partial^2 T_a}{\partial y} = k_a \frac{\partial^2 C t_a}{\partial y} + \rho_a D_a h_{fg} \frac{\partial^2 C_a}{\partial y} \tag{65}$$

$$\rho_d D_d \frac{\partial^2 C_d}{\partial y} = \rho_a D_a \frac{\partial^2 C_a}{\partial y}. \tag{66}$$

For varying fluid stream breadth:

$$\rho_d = \sqrt[3]{\frac{3 m_d \gamma_d}{\rho_d g}}, \tag{67}$$

where $\rho_d$ is the stream thickness. For improved accuracy of solar regeneration collector, a wide-ranging data from experimental assessment of LD solar regeneration upon which the correlations of moisture removal rates were based were generated [14, 21]. In other experimental analysis, the heat and mass exchange occurrence is correlated in form of Nusselt number, and the Chilton–Colbarn correlation is widely used.

$$\frac{\gamma_a}{\beta_a} = \rho_a C p_a \sqrt[3]{\left(\frac{\alpha_a}{D_a}\right)^2} \tag{68}$$

### 6.5. Common assumptions in coupled heat and mass exchange model formulations

In summary, for convenience, unambiguity and simplification of the models, numerous fundamental postulations have to be made from which an interesting trend has emerged. Table 2 shows the most commonly used assumptions in coupled heat and mass transfer prediction model formulations, classified according to accuracy, practicability and variability.

## 7. CONCLUSIONS

Given the above-reviewed literature, LDACS have been advanced as energy efficient in comparison to the conventional VCS with recommendations for the possible use of low-grade waste heat and renewable energy such as solar for dehumidification and regeneration processes. Various scholarly works have been brought forth dating back to 1969. However, with technological advancement and knowledge evolution, new technologies and improvements have emerged with regards to system design and configurations. Of more importance is the fact that various theoretical (numerical and analytical) models for heat and mass transfer process analysis in dehumidification and regeneration processes raises the LDACS technology to a different level. Flow configurations and

**Table 2.** *Summary of heat and mass transfer modelling assumptions in LDDR systems.*

| Accuracy | Assumptions |
|---|---|
| Up to ±10% | (1) Adiabatic conditions |
| | (2) Unidirectional heat and mass transfer |
| | (3) Insignificant thermal resistance in liquid phase |
| | (4) Uniform heat and mass transfer areas |
| | (5) Air-solution interfacial thermal saturation |
| | (6) Uniform desiccant interfacial temperature |
| | (7) Insignificant desiccant evaporation desiccant vaporization |
| | (8) Unequal and varying air and desiccant inlet temperatures |
| Up to ±20% (over-estimation) | (9) Unidimensional heat and mass exchange in the air–desiccant flow direction |
| | (10) Confined thermal and mass exchange constants in the module |
| | (11) Even dispensation of desiccant within the packing material |
| Not true (in practice) | (12) Completely established inlet velocity contour |
| | (13) Laminar flow |
| | (14) Uniform thermophysical air and desiccant characteristics |
| | (15) Insignificant water absorption/desorption rates with respect to fluid flow |
| | (16) Uniform film breadth |
| | (17) Uniform wall temperature |
| | (18) Uniform desiccant latent heat of condensation |
| | (19) Constant and steady air velocity |
| Constant | (20) Air and desiccant characteristics |
| | (21) Temperature borderline states |
| | (22) Desiccant concentration and flow rate inside the column |
| Negligible | (23) Solution energy-balance water losses |
| | (24) Liquid phase heat resistance |
| | (25) Absorption compared to latent heat |
| | (26) Vapour condensation rate in comparison to the solution flow rate |
| | (27) Heat energy during air–desiccant mixing |
| | (28) Pumps and air blowers power consumption |
| | (29) Water vapour diffusion |
| | (30) Heat loss within the column |

patterns have also been extensively investigated. In this regard, the counter-flow arrangement is viewed to be more effective in terms of heat and mass transfer compared to the co-flow and cross-flow counterparts.

For validation of the theoretical models, various experimentations have also been carried out using different single and combinations of desiccant solutions to investigate the effects of inlet air/desiccant conditions on the performance output. However, uncertainties still exist to date concerning optimum air desiccant flow ratios, heat and mass transfer area relationships and wetting ratios due to inconsistencies in assumptions used during modelling and analysis. These uncertainties arise from the use of unidimensional and 2D models that do not present realistic scenarios; therefore:

- More accurate 3D models need to be considered with a view of improving the performance.
- More experimental and analytical studies are still needed to broaden the conceptualization and improve the existing systems' overall performance, predictability, use and cost.
- Most of the critical variables and thermophysical properties of the desiccant solution are assumed to be constant in theory while in practical essence, they are varying.
- These assumptions oversimplify the models to the extent of underestimating the dehumidifier and regenerator performance characteristics and should be treated as variables.
- Most of the existing thermal and mass exchange mathematical models consider steady states of dehumidifier/regenerator performances, and hence, there is a need for more advanced transient theories for dynamic operations.
- Majority of the work has been focused on the outlet conditions of various parameters. However, the heat and mass exchange modelling within the dehumidifier and regenerator is still limited and needs some renewed interest.
- Although the solar-powered LDAC systems have the capability of independent temperature and humidity regulation, their reliance on meteorological status presents operational instabilities that hamper their extensive usage. Therefore, the hybrid LDAC and conventional VCS or VAS can reliably improve the stability

## ACKNOWLEDGEMENTS

The authors grateful for the financial and material support provided by the College of Agriculture, Engineering and Science

(CAES) and the Green Energy Solutions (GES) research group of the University of Kwazulu-Natal (UKZN) as well as Mangosuthu University of Technology (MUT).

## REFERENCES


[1] Zhao Y, Shi MH. Comparison of dehumidifier in solar desiccant air conditioner system. *Acta Energiae Sol Sin* 2002;**23**:32–5.

[2] Factor HM, Grossman G. A packed bed dehumidifier/regenerator for solar air conditioning with liquid desiccants. *Sol Energy* 1980;**24**:541–50.

[3] Lowenstein AI, Gabruk RS. The effect of absorber design on the performance of a liquid-desiccant air-conditioner. *ASHRAE Trans* 1992;**98**, 712–20.

[4] Nernst W. Theory of reaction velocity in heterogeneous systems. *Z Phys Chem* 1904;**47**:52–5.

[5] Whitman W. The two-film theory of gas absorption. *Chem Metall Eng* 1923;**29**:146–8.

[6] Mei L, Dai YJ. A technical review on use of liquid-desiccant dehumidification for air conditioning application. *Renew Sustain Energy Reviews* 2008;**12**:662–89.

[7] Gandhidasan P. A simplified model for air dehumidification with liquid desiccant. *Sol Energy* 2004;**76**:409–16.

[8] Li Z, Chen Y, Liu XH. Matching conditions for flow rate and heat in the heat and mass transfer process between humid air and liquid desiccant. *Heat Ventilation and Air Conditioning* 2005;**35**:103–10.

[9] Ali A, Vafai K, Khaled ARA. Analysis of heat and mass transfer between air and falling film in a cross-flow configuration. *Int J Heat Mass Transf* 2004;**47**:743–55.

[10] Stevens DI, Braun JE, Klein AS. An effectiveness model of liquid-desiccant system heat/mass exchangers. *Sol Energy* 1989;**42**:449–55.

[11] Jaing Y, Li Z, Chen XL *et al.* Liquid desiccant air conditioning system and its applications. *Heating Ventilation and Air Conditioning* 2004;**34**:88–98.

[12] Kakabaev A. Absorption solar regeneration unit with open regeneration of solution. *Appl Sol Energy* 1976;**5**:62–72.

[13] Kakabaev A, Klyshchaeva A, Khandurdyev A *et al.* Experience in operating a solar absorption cooling plant with open solution regenerator. *Geliotekhnika* 1977;**4**:73–6.

[14] Yang Yan WJ. Simulation study for an open-cycle absorption solar cooling system operated in humid area. *Energy* 1992;**17**:649–55.

[15] Collier RK. The analysis and simulation of an open cycle absorption refrigeration system. *Sol Energy* 1979;**23**: 357–366.

[16] Peng CSP, Howell JR. Analysis of open regenerators for absorption cooling applications—comparison between numerical and analytical models. *Sol Energy* 1982;**28**:265–8.

[17] Kumar SD. Modelling of the thermal behaviour of a solar regenerator for open cycle cooling systems. *Sol Energy* 1989;**33**:287–95.

[18] Gandhidasan P. A simple analysis of an open regeneration system. *Sol Energy* 1983;**31**:343–6.

[19] Gandhidasan P. Theoretical study of tilted solar still as a regenerator for liquid desiccants. *Energ Conver Manage* 1983;**23**:97–101.

[20] Kakabaev A, Klyshchaeva A, Tuiliev S *et al.* Experimental study of thermos-technical characteristics of glazed solution regenerator. *Geliotekhnika* 1978;**14**:42–5.

[21] Yutong L, Hongxing Y. Experimental study on an open-cycle solar collector regenerator using liquid desiccant for air conditioning. *Int J Green Energy* 2010;**7**:273–88.

[22] Nelson DJ, Wood BD. Evaporation rate model for a natural convection glazed collector/regenerator. *J Sol Energy Eng* 1990;**112**:51–7.

[23] Ji LJ, Wood B. Performance enhancement study of solar collector/regenerator for open-cycle liquid desiccant regeneration. *Proceedings of the 1993 American Solar Energy Society Annual Conference*, 1993, **Number 93** American Solar Energy Society (ASES).

[24] Saman WY, Said SA, Hanna MG. Design and evaluation of a solar regenerator for liquid desiccant system. *Proceedings ISES Solar World Congress*, Hamburg, 1987.

[25] Yang R, Wang PL. The optimum glazing height of a glazed solar collector/regenerator for open cycle absorption. *Energy* 1994;**19**:925–31.

[26] Alizadeh S, Saman WY. An experimental study of forced flow solar collector/regenerator using liquid desiccant. *Sol Energy* 2002;**73**:345–62.

[27] Parsons BK, Pesaran AA, Bharathan D *et al.* Improving gas fired heat pump capacity and performance by adding a desiccant dehumidification system. *ASHRAE Trans* 1989;**95**:835–44.

[28] Yadav YK, Kaushik SC. Psychometric techno-economics assessment and parametric study of vapor compression and solid/liquid hybrid air-conditioning system. *Heat Recov CHP* 1991;**11**:563–72.

[29] Khalid Ahmed CS, Gandhidasan P, Farayedhi AAAL. Simulation of a hybrid liquid desiccant based air-conditioning system. *Appl Therm Eng* 1997;**17**:125–34.

[30] Dai YJ, Wang RZ, Zhang HF *et al.* Use of desiccant cooling to improve the performance of vapour compression air conditioning. *Appl Therm Eng* 2001;**21**:1185–202.

[31] Ania FN, Kannan KS, Badawi EM. The effect of absorber packing height on the performance of a hybrid liquid desiccant system. *Renew Energy* 2005;**30**:2247–56.

[32] Sick F, Bushulte TK, Klein SA *et al.* Analysis of the seasonal performance of hybrid liquid desiccant cooling systems. *Sol Energy* 1988;**40**:211–7.

[33] Chen YM, Sun CY. Experimental study on the heat and mass transfer of a combined absorber-evaporator exchanger. *Int J Heat Mass Transf* 1997;**41**:961–71.

[34] Liu XH, Jiang Y, Chang XM *et al.* Analytical solution of coupled heat and mass transfer process in liquid desiccant air dehumidification/regenerator. *Energ Conver Manage* 2007;**48**:2221–32.

[35] Liu XH, Jiang Y. Coupled heat and mass transfer characteristic in a packed bed dehumidifier-regenerator using liquid desiccant. *Energ Conver Manage* 2008;**49**:1357–66.

[36] Rahamah A, Elsayed MM, Al-Najem NM. A numerical solution for cooling and dehumidification of air by falling film desiccant film in parallel-flow. *Renew Energy* 1998;**13**:305–22.

[37] Diaz G. Numerical investigation of a transient heat and mass transfer in a parallel flow liquid desiccant absorber. *Heat Mass Transf* 2010;**46**:1335–44.

[38] Longo GA, Gasparella A. Experimental analysis on desiccant regeneration in a packed column with structured and random packing. *Sol Energy* 2009;**83**:511–21.

[39] Peng D, Zhang X. An analytical model for coupled heat and mass transfer processes in solar collector/regenerator using liquid desiccant. *Appl Energy* 2011;**88**:2436–44.

[40] Tanda T, Shirai K, Matsumura Y *et al.* New correlation for mass transfer characteristics of spray column. *Ind Eng Chem Res* 2011;**50**:13554–60.

[41] Treybal RE. 1969. *Mass Transfer Operations*3rd edn. New York: McGraw-Hill.

[42] Lof GOG, Lenz TG, Rao S. Coefficients of heat and mass transfer in a packed bed suitable for solar regeneration of aqueous lithium chloride solutions. *J Sol Energy Eng* 1984;**106**:387–92.

[43] Gandhidasan P, Kettleborough CF, Rifat Ullah M. Calculation of heat and mass transfer coefficients in a packed tower operating with a desiccant-air contact system. *J Sol Energy Eng* 1986;**108**:123–8.

[44] Gandhidasan P. Reconcentration of aqueous solutions in packed bed: a simple approach. *J Sol Energy Eng* 1990;**112**:268–72.

[45] Ullah MR, Kettleborough CF, Gandhidasan P. Effectiveness of moisture removal for an adiabatic counter-flow packed tower absorber operating with cacl2-air contact system. *J Sol Energy Eng* 1988;**110**:98–101.

[46] Ertas A, Anderson EE, Kavasogullari S. Comparison of mass and heat transfer coefficients of liquid desiccant mixtures in a packed bed column. *J Energy Resour Technol* 1991;**113**:1–6.

[47] Elsayed MM, Gari HN, Radhwan AM. Effectiveness of heat and mass transfer in packed beds of liquid desiccant system. *Renew Energy* 1993;**3**:661–8.

[48] Chung TW, Ghosh TK, Hines AL. Dehumidification of air by aqueous lithium chloride in a packed column. *Sep Sci Technol* 1993;**28**:533–50.

[49] Chung TW. Predictions of moisture removal efficiencies for packed-bed dehumidification systems. *Gas Separ Purif* 1994;**8**:265–8.

[50] Chung TW, Ghosh TK, Hines AL. Comparison between random and structured packings for dehumidification of air by lithium chloride solutions in a packed column and their heat and mass transfer correlations. *Ind Eng Chem Res* 1996;**35**:192–8.

[51] Potnis SV, Lenz TG. Dimensionless mass-transfer correlations for packed-bed liquid-desiccant contactors. *Ind Eng Chem Res* 1996;**35**:4185–93.

[52] Oberg V, Goswami DY. Experimental study of the heat and mass transfer in a packed bed liquid desiccant air dehumidifier. *J Sol Energy Eng* 1998;**120**:289–97.

[53] Lazzarin RM, Gasparella A, Longo GA. Chemical dehumidification by liquid desiccants: theory and experiment. *Int J Refrig* 1999;**22**: 334–47.

[54] Radhwan AM, Elsayed MM, Gari HN. Mathematical modelling of solar operated liquid desiccant, evaporative air conditioning system. *J King Abdulaziz Univ Eng Sci* 1999;**11**:119–41.

[55] Martin V, Goswami DY. Heat and mass transfer in packed bed liquid desiccant regenerators; an experimental investigation. *J Sol Energy Eng* 1999;**121**:162–70.

[56] Fumo N, Goswami DY. Study of an aqueous lithium chloride desiccant system: air dehumidification and desiccant regeneration. *Sol Energy* 2002;**72**:351–61.

[57] Longo GA, Gasparella A. Experimental and theoretical analysis of heat and mass transfer in a packed column dehumidifier/regenerator with liquid desiccant. *Int J Heat Mass Transf* 2005;**48**:5240–54.

[58] Ren C, Jiang Y, Tang G *et al.* A characteristic study of liquid desiccant dehumidification/regeneration processes. *Sol Energy* 2005;**79**:483–94.

[59] Ren C, Jiang Y, Zhang Y. Simplified analysis of coupled heat and mass transfer processes in packed bed liquid desiccant-air contact system. *Sol Energy* 2006;**80**:121–31.

[60] Elsarrag E, Elmagzoub M, Ali E *et al.* Design guidelines and performance study on a structured packed liquid desiccant air conditioning system. *HVAC/R Res* 2005;**11**:319–37.

[61] Elsarrag E. Dehumidification of air by chemical liquid desiccant in a packed column and its heat and mass transfer effectiveness. *HVAC/R Res* 2006;**12**:3–16.

[62] Chen XY, Li Z, Jiang Y *et al.* Analytical solution of adiabatic heat and mass transfer process in packed-type liquid desiccant equipment and its application. *Sol Energy* 2006;**80**:1509–16.

[63] Yin Y, Zhang X, Chen Z. Experimental study on dehumidifier and regenerator of liquid desiccant cooling air conditioning system. *Build Environ* 2007;**42**:2505–11.

[64] Jain S, Bansal PK. Performance analysis of liquid desiccant dehumidification systems. *Int J Refrig* 2007;**30**:861–72.

[65] Liu XH, Jiang Y. Handling zone dividing method in packed bed liquid desiccant dehumidification/regeneration process. *Energ Conver Manage* 2009;**50**:3024–34.

[66] Tu M, Ren CQ, Zhang LA *et al.* Simulation and analysis of a novel liquid desiccant air conditioning system. *Appl Therm Eng* 2009;**29**:2417–25.

[67] Tretiak CS, Abdallah NB. Sorption and desorption characteristics of a packed bed of clay-cacl2 desiccant particles. *Sol Energy* 2009;**83**: 1861–70.

[68] Babakhani D, Soleymani M. An analytical solution for air dehumidification by liquid desiccant in a packed column. *Int Commun Heat Mass Transf* 2009;**36**:969–77.

[69] Peng SW, Pan ZM. Heat and mass transfer in liquid desiccant air-conditioning process at low-flow conditions. *Commun Nonlinear Sci Numer Simul* 2009;**14**:3599–607.

[70] Babakhani D, Soleymani M. Simplified analysis of heat and mass transfer model in liquid desiccant regeneration process. *J Taiwan Inst Chem Eng* 2010;**41**:259–67.

[71] Gandhidasan P, Mohandes MA. Artificial neural network analysis of liquid desiccant dehumidification system. *Energy* 2011;**36**:1180–6.

[72] Kumar R, Dhar PL, Jain S. Development of new wire mesh packings for improving the performance of zero carryover spray tower. *Energy* 2011;**36**:1362–74.

[73] Al-Farayedhi AA, Gandhidasan P, Al-Mutairi MA. Evaluation of heat and mass transfer coefficients in a gauze-type structured packing air dehumidifier operating with liquid desiccant. *Int J Refrig* 2002;**25**:330–9.

[74] Dai YJ, Zhang HF. Numerical simulation and theoretical analysis of heat and mass transfer in a cross flow liquid desiccant air dehumidifier packed with honeycomb paper. *Energ Conver Manage* 2004;**45**:1343–56.

[75] Liu XH, Qu KY, Jiang Y. Empirical correlations to predict the performance of the dehumidifier using liquid desiccant in heat and mass transfer. *Renew Energy* 2006;**31**: 1627–1639.

[76] Liu XH, Jiang Y, Chang XM *et al.* Experimental investigation of the heat and mass transfer between air and liquid desiccant in a cross-flow regenerator. *Renew Energy* 2007;**32**:1623–36.

[77] Liu XH, Jiang Y, Qu KY. Heat and mass transfer model of cross flow liquid desiccant air dehumidifier/regenerator. *Energ Conver Manage* 2007;**48**:546–54.

[78] Liu XH, Jiang Y, Qu KY. Analytical solution of combined heat and mass transfer performance in a cross-flow packed bed liquid desiccant air dehumidifier. *Int J Heat Mass Transf* 2008;**51**:4563–72.

[79] Yin Y, Zhang X. A new method for determining coupled heat and mass transfer coefficients between air and liquid desiccant. *Int J Heat Mass Transf* 2008;**51**:3287–97.

[80] Moon CG, Bansal PK, Jain S. New mass transfer performance data of a cross-flow liquid desiccant dehumidification system. *Int J Refrig* 2009;**32**:524–33.

[81] Zhang L, Hihara E, Matsuoka F *et al.* Experimental analysis of mass transfer in adiabatic structured packing dehumidifier/regenerator with liquid desiccant. *Int J Heat Mass Transf* 2010;**53**:2856–63.

[82] Bansal P, Jain S, Moon C. Performance comparison of an adiabatic and an internally cooled structured packed-bed dehumidifier. *Appl Therm Eng* 2011;**31**:14–9.

[83] Liu XH, Yi XQ, Jiang Y. Mass transfer performance comparison of two commonly used liquid desiccants: LiBr and LiCl aqueous solutions. *Energ Conver Manage* 2011;**52**:180–90.

[84] Pineda SM, Diaz G. Contribution of an internal heat exchanger to the performance of a liquid desiccant dehumidifier operating near freezing conditions. *Int J Therm Sci* 2011;**50**:2304–10.

[85] Bassuoni MM. An experimental study of structured packing dehumidifier/regenerator operating with liquid desiccant. *Energy* 2011:**36**(5), pages 2628–2638 .

[86] Gao WZ, Lui JH, Cheng YP *et al.* Experimental investigation on the heat and mass transfer between air and liquid desiccant in a crossflow dehumidifier. *Renew Energy* 2012;**37**:117–23.

[87] Bakhtiar A, Rokhman F, Hwan CK. A novel method to evaluate the performance of liquid desiccant air dehumidifier system. *Energ Buildings* 2012;**44**:39–44.

[88] Luo Y, Yang H, Lu L *et al.* A review of the mathematical models for predicting the heat and mass transfer process in the liquid desiccant dehumidifier. *Renew Sustain Energy Rev* 2014;**31**:585–99.

[89] Gandhidasan P, Rifat Ullah M, Kettleborough CF. Analysis of heat and mass transfer between a desiccant-air system in a packed tower. *J Sol Energy Eng* 1987;**109**:89–93.

[90] Khan AY, Ball HD. Development of a generalized model for performance evaluation of packed-type liquid sorbent dehumidifiers and regenerators. *ASHRAE Trans* 1992;**98**:525–33.

[91] Luo YM, Shao SQ, Xu HB *et al.* Dehumidification performance of [emim] bf4. *Appl Therm Eng* 2011;**31**:2772–7.

[92] Luo YM, Shao SQ, Qin F *et al.* Investigation of feasibility of ionic liquids used in solar liquid desiccant air-conditioning. *Sol Energy* 2012;**86**: 2718–24.

[93] Niu RP. Modeling and Numerical Simulation of Dehumidifier Using LiCl Solution as the Liquid Desiccant. *Advanced Materials Research*,(2011) vol.**383-390** pages 6568–73
[94] Woods J, Kozubal E. A desiccant-enhanced evaporative air conditioner: numerical model and experiments. *Energ Conver Manage* 2012;**65**: 208–20.
[95] Ren CQ. Corrections to the simple effectiveness-ntu method for counterflow cooling towers and packed-bed liquid desiccant–air contact systems. *Int J Heat Transf* 2008;**51**:237–45.
[96] Tao Z, Xiaohau L, Jingjing J *et al.* Experimental analysis of an internally cooled liquid desiccant dehumidifier. *Build Environ* 2013;**63**: 1–10.
[97] Wang XL, Cai WJ, Lu JG *et al.* A hybrid dehumidifier model for real-time performance monitoring, control and optimization in liquid desiccant dehumidification system. *Appl Energy* 2013;**111**:449–55.
[98] Mesquita LCS, Harrison SJ, Thomey D. Modelling of heat and mass transfer in parallel plate liquid desiccant dehumidifier. *Sol Energy* 2012; **80**:1475–82.

# Chapter3

## Experimental assessment of heat and mass transfer characteristics of solar-powered adiabatic liquid desiccant dehumidifier and regenerator

In this chapter, an experimental evaluation of heat and mass transfer characteristics of a solar-powered adiabatic liquid desiccant dehumidifier and regenerator is presented. The effects of solar radiation, humidity ratio, air and desiccant flow-rates, and solution concentration on MRR and effectiveness were effectively analysed. A 3-D numerical model was developed to determine heat and mass transfer coefficients based on the falling fluid stream principle. The consequence of air and desiccant flow-rates on heat and mass transfer coefficients were also identified, and finally, the results from the model were validated using experimental data. This chapter has been published in the Q1-rated International Journal of Low carbon Technologies.

**Andrew Y A Oyieke**, Freddie L Inambao; Experimental assessment of heat and mass transfer characteristics of solar-powered adiabatic liquid desiccant dehumidifier and regenerator *International Journal of Low-Carbon Technologies*,

https://doi.org/10.1093/ijlct/ctaa013 Published online: 17 April 2020

# Experimental assessment of heat and mass transfer characteristics of solar-powered adiabatic liquid desiccant dehumidifier and regenerator

Andrew Y. A Oyieke*, Freddie L. Inambao
*Discipline of Mechanical Engineering, University of KwaZulu-Natal, Mazisi Kunene Road, Glenwood, Durban 4041, South Africa*

## Abstract

Coupled heat and mass transfer performance of an adiabatic solar-powered liquid desiccant dehumidification and regeneration scheme using lithium bromide(LiBr) solution has been conducted experimentally as well as numerically under subtropical climatic conditions. The application of a vacuum insulated photovoltaic and thermal module to provide desiccant regeneration heat as well as electrical power to drive the air fans and liquid pumps have been explored. A square channelled ceramic cordierite packing with a varying channel density of 20–80 $m^2/m^3$ has been used to establish the optimum direct air-LiBr contact ratio for maximum effectiveness. The aggregate crammed vertical dehumidifier and regenerator operational indices featured were effectiveness, moisture removal rate (MRR), heat and mass transfer constants and Lewis number. The influence of solar radiation, humidity and L/G ratios, air–desiccant flow rates and concentration on the indices have been scrutinized in details. A 3D predictive numerical thermal model based on falling liquid stream with constant thickness in counter-flow configuration has been developed and solved by a combination of separative appraisal and stepwise iterative technique. The heat and mass exchange coefficients significantly increased with the increase in Lewis number, air and desiccant flow rates for both the dehumidifier and regenerator vessels. The predicted results of heat and mass transfer coefficients, effectiveness and MRRs have been validated with experimental measurements within a general acceptable conformity of less than ±10%.

*Keywords:* coupled heat and mass transfer; solar; adiabatic regenerator/dehumidifier; liquid desiccant

*Corresponding author: youngoyieke@yahoo.com

Received 16 December 2019; revised 10 February 2020; editorial decision 1 March 2020; accepted 1 March 2020

## 1 INTRODUCTION

Liquid desiccant technology has emerged as the most effective and preferred state-of-the-art vapour extraction technique from the processed air within the various dehumidifier and regenerator configurations. The preference is due to the flexibility in operation, elimination of organic and inorganic contaminants and low operating temperatures that favours the use of renewable energy from the sun [1]. The solar radiation supplies the low-grade regeneration heat to the desiccant solution, which loses water particles to the atmospheric air during the direct-contact interaction within the regenerator vessel. The air–desiccant interaction results in water vapour extraction and dispersion from the process air and diluted liquid desiccant, respectively. The water particles exchange process creates a combined thermal and mass transmission phenomenon at the fluid–air interaction phase.

The experimental tests on solar-driven combined thermal and mass transmission in liquid desiccant regeneration and absorption technology date back to the late sixties [2]. Since then, various modifications of solar regeneration systems have emerged in the forms of experimental evaluations and validations on glazed and unglazed flat plate modules [3], enclosed and open zones, forced flow arrangements [4], psychometrics, feasibility and actualization [5–7]. The heat and mass exchange correlation constants found from investigational assessments of an open-cycle forced convection solar regenerator are obtainable in [8–13]. Combinations of theoretical examination and experimental justification of

International Journal of Low-Carbon Technologies 2020, 00, 1–19

doi:10.1093/ijolct/ctaa013 Advance Access publication

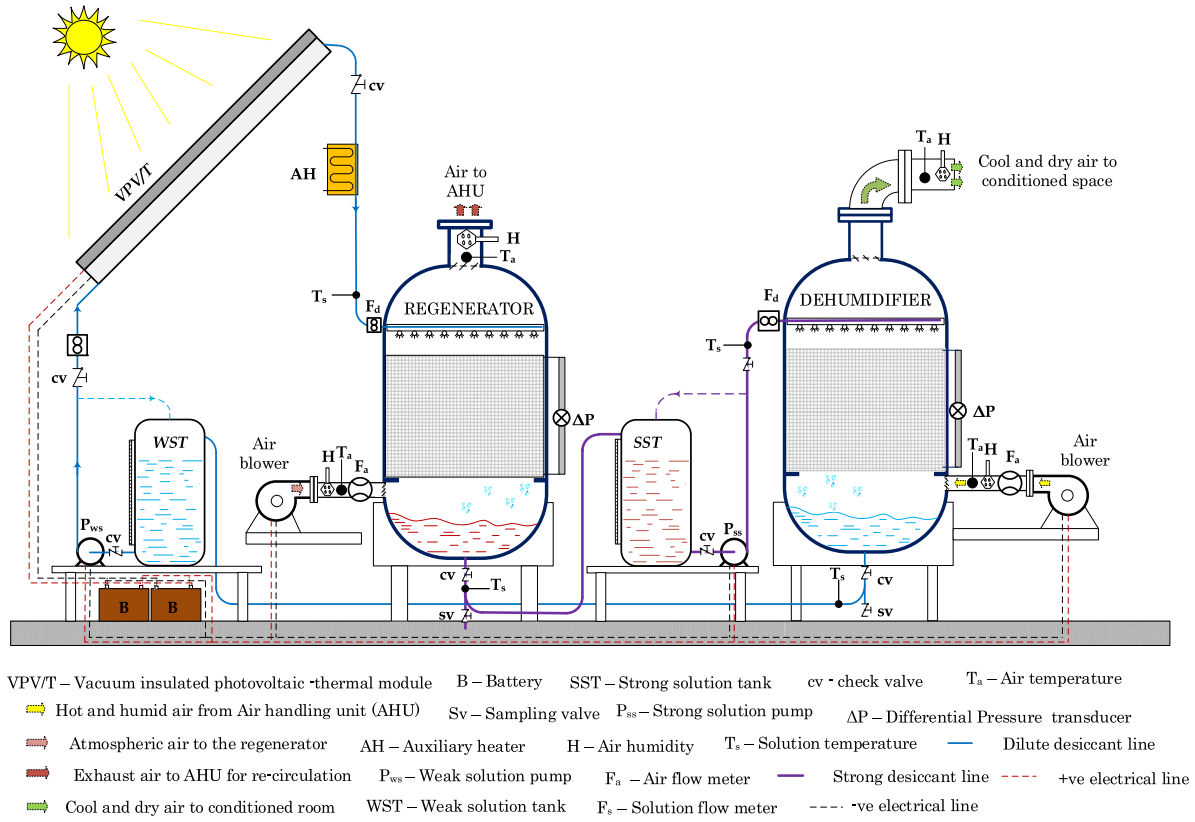


**Figure 1.** *The diagrammatic representation of the experimental setup.*

heat and mass exchange factors during chemical dehumidification and regeneration in different configurations using various desiccant solutions such as lithium chloride (LiCl) [14–17], triethylene glycol (TEG) solution [18], H2O/KCOOH [19], lithium bromide (LiBr) [20, 21] have been explored in details in packed columns. The performance comparison of structured and randomly packed dehumidifier/regenerator [22, 23] under transient conditions [24, 25] have also yielded satisfactory outcomes.

Most of the theoretical studies in the literature are based on the adiabatic conditions, unidirectional and uniform thermal and mass exchange areas [26]. Conversely, the presumption that constant thermal and mass transfer zone is equivalent to the explicit expanse of packing, ignores the effects of liquid surface tension; hence, mass transfer is reduced due to insufficient wetting of the packing material surface. Consequently, the impact of the mean solution heat on unitless parameters is unaccounted for as well. The solution to these problems is often obtained by logarithmic and arithmetic temperature difference methods. However, these techniques do not adequately consider the contribution of individual parameters like flow rate, moisture content, temperature and humidity ratio (HR) on the heat and mass exchange constants. Therefore, this work seeks to examine the heat and mass transfer constants and correlations hinged upon the experimental data obtained under local settings and establish the impact of the aforementioned individual factors on the overall operation of the liquid desiccant system in terms of effectiveness and moisture removal rate (MRR) of the dehumidifier/regenerator packed with square channel ceramic cordierite (CC).

## 2 EXPERIMENTAL SETUP AND PROCEDURE

The configuration and arrangement of the experiment shown in Figure 1 comprises of four major segments: the airline, desiccant loop, vacuum insulated photovoltaic and thermal (VPV/T) module, dehumidification chamber and regenerator vessel. In the dehumidification chamber, the incoming air temperature and humidity were initially raised to a predetermined level for the packed bed dehumidifier vessel. Air enters the vessel's lower end and exit from the top while LiBr desiccant solution comes in at the top and exits at the bottom. Within the vertical column, the air–desiccant mixture experiences a counter-flow interaction over a crammed section during which, heat and mass exchange occurs.

During the dehumidification process, air losses water vapour to the desiccant solution because of the vapour pressure difference. The chemical reaction between highly concentrated LiBr and water particles is given in Equation 1. The reaction is in two stages; firstly, the endothermic breakage of the ionic bond between $Li^+$ and $Br^-$. Secondly, the exothermic bonding ($Li^+..H_2O$) and

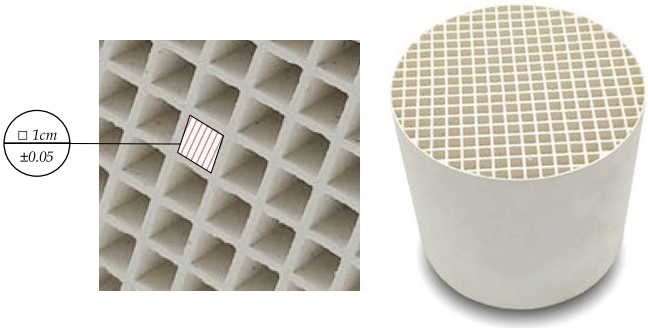


**Figure 2.** *The CC honey comb packing.*

($Br^{-}..H_2O$) during dissolution; thus, sensible heat is released due to temperature difference. At the same time, at the phase change of water vapour to liquid requires latent heat of condensation, and as a consequence, the air solution mixture temperature is increased.

$$\underbrace{Li^{+}Br^{-}}_{ionic\ \ bond}\ (s) + H_2O(l) \Longleftrightarrow \underbrace{Li^{+}(aq) + Br^{-}(aq)}_{dilute\ \ solution}. \qquad (1)$$

The reverse happens in the regeneration process as atmospheric air engrosses water particles out of the heated LiBr liquid as a result of vapour pressure gradient. Latent heat of vaporization ensues when water changes phase to vapour and escapes with air while sensible heat results from air–desiccant temperature gradient as $Li^{+}$ and $Br^{-}$ fuse in an exothermic reaction to become LiBr solution. Due to the reactions, the solution's concentration increases while temperature reduces and the opposite is exact for exhaust air. Therefore, the heat and mass transfer processes transpire together as a couple and cannot stay de-linked.

The dehumidifier and regeneration columns are made of cylindrical vessels of diameter and height of 450 mm and 650 mm, respectively, with dome-shaped ends for solution spray and collection. The air duct was a 100 mm diameter circular cross-section PVC pipe while the desiccant distribution channel was a 19 mm diameter pipe. These geometrical dimensions were determined using the strategies provided in [25]. However, the adverse effects of the dimensional characteristics on the permanence of the whole set up were out of the scope for the present study. CC honey-comb packing shaped into the perforated square channel of sides $1 \pm 0.5$ cm and specific surface area of 180 $m^2/m^3$ was used to provide heat and mass exchange surface. The CC exhibits pronounced absorbency, excellent liquescent and even dispersal, extraordinary heat and biochemical oxidization resistance, low pressure-drop, outstanding separation efficiency and highly adoptive to regeneration conditions as well as a small thermal coefficient. The properties mentioned above informed the choice and consideration of CC a packing material for this study. The geometry of the channels, as shown in Figure 2, was designed to allow pressure to drop to create partial vapour pressure conducive for heat and mass transmission occurrence in the course of dehumidification and regeneration procedures.

**Table 1.** *The thermophysical properties of packing material.*

| Property | Value |
|---|---|
| Parking | Honeycomb ceramic substrate |
| Material | Ceramic cordierite |
| Nominal surface to unit volume ratio | 180 $m^2/m^3$ |
| Cross-sectional area | 0.164 $m^2$ |
| Void fraction | 0.86 |
| Equivalent diameter | 200 mm |
| Column height | 650 mm |
| Wall thickness | 1.5 mm |
| Cell density (cell per square inch) | 100 |
| Porosity | 85% |
| Max working temperature | $1400^{o}$C |
| Average aparture | 7-15 |
| Cell dimensions | 10 mm x 10 mm |
| Chemical components | $Al_2O_3$ (35.4%), $SiO_2$ (50.4%) and $MgO$ (13.5%) |

The gas-phase mixture flows in a straight channel while the liquid-phase film flows on the packing material surface under gravitational influence. The specific thermophysical properties of the CC packing is provided in Table 1. Two solution storage tanks were connected to the setup; the strong solution tank (SST) contained the concentrated solution supplied to the dehumidifier for water vapour removal, and the weak solution tank (WST) contained the weak/diluted solution emanating from the dehumidifier to be propelled towards the regenerator unit for improved concentration to near initial levels. The solution temperature from the SST to the dehumidifier was controlled at sub-minimum (below ambient). The regenerated fluid was then passed to the concentrated solution tank and the cycle continues.

The photovoltaic/thermal solar collector consists of the photovoltaic cells mounted on a heat-absorbing copper plate. Beneath the copper plate, there is a serpentine-shaped copper tubing for fluid circulation, thereby, absorbing the excess heat from the plate. The primary purpose of the VPV/T collector was to provide regeneration heat as well as electrical energy to drive the circulation pumps and fans. The vacuum insulation provided more heat retention and absorption by the desiccant solution flowing in the pipes beneath the absorber plate. The fluid circulation pump and air fans are operated by direct current power from the VPV/T. The electrical energy produced was stored in two regulated sealed valve 12 V, 100 Ah batteries (**B**), from which the power was connected to the air blowers and fluid circulation pumps ($P_{ws}$ and $P_{ss}$), thus giving the setup a self-powering characteristic. The heat transfer and power generation characteristics of the VIP/T had previously been evaluated in [27] and therefore, will not be detailed in the present study. The dimensions and specifications of the PVT are given in Table 2

There was no need for external evaporator in the whole setup as presented since the desorption system was incorporated. The pressure was atmospheric throughout the setup; thus, the expensive pressure vessel components were eliminated. Apart from the

**Table 2.** *VPV/T collector specifications.*

| Collector property | Thermal | Collector property | Electrical |
|---|---|---|---|
| Collector dimensions | 1.640 m× 0.87 m× 0.105 m | PV module power | 180 W |
| Collector area | 1.42 $m^2$ | PV cell type | Mono-crystalline |
| Collector slope | $35^o$ | PV cell dimension | 0.125 m× 0.125 m |
| Absorber type | Sheet and tube | No. of cells | 72 |
| Absorber plate thickness | 0.001 m | PV cell encapsulation | Non-encapsulated |
| Absorber plate material | Copper | Packing factor | 1.0 |
| Internal piping | Copper | Top insulation medium | **Vacuum** |
| Riser tube diameter | 0.012 m | Bottom insulation material | Fibre wool |
| Riser tube thickness | 0.007 m | Insulation thickness | 0.05 m |
| Header tube diameter | 0.022 m | Glass cover (tempered) | 0.004 m low iron |
| Header tube thickness | 0.008 m | Number of tubes and spacing | 14 and 120 mm |

**Table 3.** *Measuring instruments and specifications.*

| Instrument | Uncertainty | Range | Parameter |
|---|---|---|---|
| Thermocouple (T-type) | $0.1^oC$ | $0–80^oC$ | Temperature |
| Thermocouple (K-type) | $0.2^oC$ | $-50–+50^oC$ | Dew point temperature |
| Ultrasonic flow meter | 0.1% | 0–1600 kg/h | Mass flow rate |
| Density meter | 0.1 $kg/m^3$ | 1–9999 $kg/m^3$ | Density |
| Barometer | 0.08% fs | 0–10 mbars | Pressure |
| Digital flow meter | ± 1% fsd | 0–800 $m^3/h$ | Fluid volume flow rate |
| Pressure transducer | 0.1% fs | 0–10 mbars | Pressure drop |

use of low-grade heat energy from the sun, the system was self-powered as the electrical and thermal power from the VPV/T module was utilized. However, an auxiliary heater was incorporated to augment the regeneration heat during periods of no sunshine.

The desiccant heat and concentration in the feeder tank were kept unchanged at pre-set conditions. The strong solution pump ($P_{ss}$) transferred the solution to the spray chamber at the upper part of the dehumidification column where it was dispensed as a mist to the top of the packed bed and allowed to flow freely by gravity. The air and desiccant interaction took place in the packing chamber where thermal and mass exchange transpired as water vapour in air was transferred to the desiccant. The water absorption process enhanced the moisture content in the liquid exiting at the bottom of the packed bed as a diluted solution which then flowed to the WST.

From the WST, the weak solution was pumped to the bottom of the VPV/T module through which it steadily flowed as it was heated by solar energy depending on the solar radiation intensity. A monitored heated solution stream was then transferred to the regenerator in a similar configuration to the dehumidifier while the returning solution was collected and directed to the SST. At raised temperature, the weak solution readily lost water vapour to the air in a counter flow configuration through a packed bed in the regenerator vessel.

## 2.1 Instrumentation

Various parameters were monitored throughout the entire duration of the experiment in order to establish their various effects and dependability on other parameters and factors. The parameters of interest that were monitored and measured includes flow rates and temperatures of both air and desiccant at inlets and outlets of the vessels, the HR of air, desiccant solution density among others. The various measurements were achieved with the following instruments listed in Table 3.

In the air loop, measurements of temperature ($T_a$), humidity ratio (H) and flow rate ($F_a$) were performed both on the dehumidifier and regenerator inlet and outlets. There was two temperature, and dew point plugs restrained by T-type and K-type thermocouples respectively installed at suitable positions in the airway to sample the temperatures. The strain-gauge differential pressure transducer was used for pressure-drop ($\triangle P$) measurement along the height of the vertical column. On the other hand, the airflow rate was measured by an ultrasonic flow meter in combination with a strain gauge pressure transducer while the absolute pressure was monitored by use of a barometer.

In the desiccant loop, temperatures and flow rates were always monitored both at the inlet and outlet conditions for the dehumidifier and regenerator vessels, respectively. At least two probe ports equipped with K-type thermocouples ($T_d$) were installed on either side of inlet and outlet. Similarly, the desiccant flow rate was monitored using a digital flow-tech meter (EMFM-9) ($F_d$) with inbuilt data acquisition at inlet and outlet of each vessel. In order to determine the solution concentration, the density was sampled by use of a DS7800 density meter. Before each run, both the absorption and desorption column assemblies were cleansed using clean, freshwater and blown dry by a stream of warm air. The readings were logged at an interval of 15 seconds while the

densities were fed into a computer algorithm to determine the concentration

Before regenerator measurements, the weak solution was stored continuously in the storage tank to equalize the conditions and for uniform distribution of the temperature and concentration. The desiccant was made to flow at meagre flow rates while the airflow rate was at maximum. The flow rates were then fixed at predetermined figures, then temperature, humidity and vapour pressure values were recorded at steady states. The process was repeated until the desiccant was restored to near its initial concentration. The data collected were then applied in a computer algorithm to determine the heat and mass exchange constants along the columns, change in the moisture content of the air as well as the change in temperatures between the inlet and outlet conditions corresponding to various flow rates.

## 2.2 Experimental data uncertainties

The purpose of experimental uncertainty analysis was to scrutinize the calculated parameters, focusing on the inconsistencies in the measured parameters, applied in form of mathematical formulation. The theoretical relationships used to transform the measurements into the derived quantity are prone to bias and unavoidable indiscriminate disparities resulting from repetitive measurements. For reliability, accuracy and precision of the measured parameters such as temperature (air and desiccant), flow rate (mass and volume), density and pressure, the propagation of the errors caused by the bias and disparities into the derived quantities must be avoided. Therefore, an approximation technique that offers consistent and valuable outcome is required. The uncertainty analysis of derived determinant parameters such as moisture removal rate (MRR,$\epsilon$ ), effectiveness ($\varepsilon$) and enthalpy ($h$) was carried out for normalization using the equations adapted from [28] whose general form is given in Equation 2. The respective estimated values of uncertainties were $\pm$ 3.5%($\epsilon$), $\pm$ 2.8% ($\varepsilon$) and $\pm$ 3.8% ($h$) while those of desiccant concentration, desiccant temperature, air HR, air velocity and temperature were estimated to be $\pm$ 0.15%, $\pm$ 0.2$^o$C, $\pm$ 0.2%, $\pm$ 0.1 m/s and $\pm$ 0.2$^o$C, respectively.

$$\Delta y = \left\{\left(\frac{\partial y}{\partial x_1}\Delta x_1\right)^2+\left(\frac{\partial y}{\partial x_2}\Delta x_2\right)^2+\left(\frac{\partial y}{\partial x_3}\Delta x_3\right)^2+\ldots\ldots+\left(\frac{\partial y}{\partial x_n}\Delta x_n\right)^2\right\}^2, \quad (2)$$

where $x_1, x_2, x_3 \ldots\ldots x_n$ are various contributing parameters and y is the determined parameter. The respective individual expressions for enthalpy, effectiveness and MRR are given in Table 4.

## 2.3 Performance indicators

The overall dehumidifier and regenerator performance were assessed using effectiveness, MRR and enthalpy. The effectiveness is given as a percentage ratio of the tangible air humidity ration difference to the extreme possible as expressed in Equations 3 and 4 for the dehumidifier and regenerator.

**Table 4.** *Uncertainties of experimental data.*

| Parameter | Uncertainty equation |
|---|---|
| Enthalpy of air ($h_a$) | $\Delta h_a = \left\{2\left(\Delta\omega\frac{\partial h_a}{\partial\omega}\right)^2 + 2\left(\Delta T_a\frac{\partial h_a}{\partial T_a}\right)^2\right\}^{1/2}$ |
| Enthalpy of desiccant ($h_d$) | $\Delta h_d = \left\{2\left(\Delta\chi\frac{\partial h_a}{\partial\chi}\right)^2 + 2\left(\Delta T_d\frac{\partial h_a}{\partial T_d}\right)^2\right\}^{1/2}$ |
| Moisture removal rate ($\epsilon$) | $\Delta\epsilon = \left\{2\left(\Delta\omega\frac{\partial\epsilon}{\partial\omega}\right)^2 + \left(\Delta\nu\frac{\partial\epsilon}{\partial\nu}\right)^2 + \left(\Delta d\frac{\partial\epsilon}{\partial d}\right)^2\right\}^{1/2}$ |
| Effectiveness ($\varepsilon$) | $\Delta\varepsilon = \left\{2\left(\Delta\omega\frac{\partial\varepsilon}{\partial\omega}\right)^2\right\}^{1/2}$ |

$$\varepsilon_{deh} = \left(\frac{\omega_i - \omega_o}{\omega_i - \omega_e}\right) \times 100\% \quad (3)$$

$$\varepsilon_{reg} = \left(\frac{\omega_o - \omega_i}{\omega_e - \omega_i}\right) \times 100\%, \quad (4)$$

where, $\omega$ is the HR in $kg/kg_{dryair}$ while subscripts $R$, $D$, $i$, $o$ and $e$ are an inlet, outlet and equilibrium conditions, respectively, and $\omega_e$ is stated in relation to the inlet desiccant temperature $T_d$ and the atmospheric pressure $P_a$ as follows:

$$\omega_e = 0.622\left[\frac{0.6107\exp\left(\frac{17.27T_d}{T_d-237.3}\right)}{p_a - 0.6107\exp\left(\frac{17.27T_d}{T_d-237.3}\right)}\right]. \quad (5)$$

The extreme range of HR was accomplished when air outlet partial vapour pressure was equivalent to the inlet solution's saturation pressure to the column. The results of the experiment are captured for the solution concentration, regeneration effectiveness and pressure-drop on the air-loop moisture removal rate $\epsilon$ is by definition, is directly proportional to the HR difference at outlet and inlet conditions so long as the mass flow rate $\dot{m}_a$ and $\dot{m}_d$ are constants. Equations 6 and 7 show the mathematical formulations in terms of desiccant $\chi$ concentration as well.

$$\epsilon_{deh} = \dot{m}_a(\omega_i - \omega_o) = \dot{m}_d\left(\frac{\chi_i}{\chi_o} - 1\right) \Rightarrow \chi_i > \chi_o \quad (6)$$

and

$$\epsilon_{reg} = \dot{m}_a(\omega_o - \omega_i) = \dot{m}_d\left(\frac{\chi_o}{\chi_i} - 1\right) \Rightarrow \chi_o > \chi_i, \quad (7)$$

where the subscripts $a$ and $d$ represent states of air and desiccant, respectively. The desiccant's concentration defines the proportion and quantity of vapour expended to or engrossed from the air. The expressions in Equations 8 and 9 can be applied for the

dehumidifier and regenerator respectively to determine the outlet concentration $\chi$,

$$\chi_{o,deh} = \frac{\chi_{d,i}}{1 + \left(\frac{\varphi}{M_a}\right)} \tag{8}$$

$$\chi_{o,reg} = \frac{\chi_{d,i}}{1 - \left(\frac{\varphi}{M_a}\right)}. \tag{9}$$

It was assumed that the concentration of the desiccant at the dehumidifier outlet was the same as that of the regenerator inlet. Therefore, the heat energy balance for the VPV/T becomes

$$G_c dx = \dot{m}_a dh_a + \dot{m}_d dh_d + U_L(T_d - T_{amb}) + mh_{fg}, \tag{10}$$

where $h_a$ and $h_d$ are the air and desiccant enthalpies in J/kg, $m$ represents the amount of vapour removed in kg, $h_{fg}$ is latent energy of vaporization, $U_L$ is the total heat-loss constant, $T_d$ and $T_{amb}$ are the solutions and ambient temperatures. $G_c$ is the radiation available to the solution from the VPV/T calculated as a function of the total solar radiation $G_T$, electrical efficiency $\eta_{el}$ and collector thermal properties as adapted from [29].

$$G_c = G_T[(1 - \rho)\tau\alpha - (\tau\alpha - \tau_{pv}\eta_{el})], \tag{11}$$

where $\tau$, $\alpha$ and $\rho$ are transmittance, absorptance and reflectance of the PV cell. The interfacial equilibrium energy balance during dehumidification and regeneration is given by Equations 12 and 13.

$$Q_{e,deh} = -\dot{m}_d dh_d - \dot{m}_a dh_a \tag{12}$$

$$Q_{e,reg} = \dot{m}_a dh_a - \dot{m}_d dh_d, \tag{13}$$

where the difference in enthalpies of air and desiccant are given in Equations 14 and 15.

$$dh_a = cp_a(T - T_{ref}) + Cp_d(T_d - T_{ref}) + Q_e d\omega. \tag{14}$$

The change in solution enthalpy is given in terms of the regeneration heat and total heat gain at saturation point $T_{ref}$.

$$dh_d = cp_d(T_d - T_{ref}) + Q_{sol} d\omega_{sat}, \tag{15}$$

where $\omega_{sat}$ is the air HR at full vapour capacity point, which depends on the desiccant concentration and temperature difference.

Considering the interfacial interaction of air and desiccant solution, we can obtain the latent heat ratio of the dehumidifier and regenerator as a fraction of latent heat generated to the overall heat transferred among the air and desiccant liquid stated as follows [28].

$$\xi = \frac{\dot{m}_a \delta d\omega}{\dot{m}_a cp_a dT_a + \dot{m}_a \delta d\omega} = \frac{\dot{m}_d \delta d\omega_{sat}}{\dot{m}_d cp_d dT_d + \dot{m}_d \delta d\omega_{sat}}. \tag{16}$$

# 3 EXPERIMENTAL RESULTS AND DISCUSSION

The main determinant parameter upon which the performances of the dehumidifier and regenerator are based on the air HR. It is therefore very essential to ascertain the effect of humidity levels on the enthalpy changes of both desiccant and air. The HRs were extracted from using the psychometric principle integrated into engineers equation solver software for the points corresponding to the temperatures and humidities obtained from the experiment. The change in enthalpies was evaluated using Equations 14 and 15 and the ensuing values used to analyse the effects of air HR. From the experimental results obtained under South African subtropical climate in the coastal city Durban, the change in HR of inlet air was carefully monitored within the ranges included in Table 5 and plotted against the changes in the respective enthalpies of air and LiBr both at entrance and exit condition as shown in Figures 3 and 4.

During the dehumidification process, it was detected that the upsurge in air HR resulted in increased enthalpy of inlet air while the outlet air enthalpy significantly reduced, as shown in Figure 3a. The reduction in enthalpy was attributed to the proportionate increase in air vapour pressure due to higher HR. At higher vapour pressures, the magnitude of latent energy of condensation liberated to the air becomes larger, thus more water vapour is engrossed by the LiBr solution. However, for an increase of HR from 0.015 to 0.035 $kg_w/kg_a$, there was an increase in enthalpy gradient of 4.11% to 27.59% along the dehumidifier height and 16% overall reduction in air enthalpy between the inlet and outlet.

On the other hand, the inlet solution enthalpy showed less sensitivity to the escalation in air inlet HR while the exit solution enthalpy considerably increased, as shown in Figure 3b. The overall increase in the inlet to outlet solution enthalpy difference was 21.55%, gradually varying from 14.08% to 29.01% within the HR range. Due to the increase in HR, there is a high likelihood of moisture absorption by LiBr from the air, hence the upsurge of interfacial heat transfer potential.

During regeneration, a similar increase in air HR increased inlet air enthalpy whereas, the outlet air enthalpy reduced as shown in Figure 4a. There was an overall reduction of enthalpy of 37.26% between inlet and outlet conditions. A progressive reduction in enthalpy difference of 46.15% to 27.21% was realized. This reduction was significantly higher than the dehumidification process due to the higher air-desiccant temperature gradient during regeneration. Subsequently, the interfacial vapour pressure variation and the prospective latent heat exchange reduces along the height of the regenerator vessel.

**Table 5.** *Typical quantities and series of working and reference parameters.*

| Parameter | Symbol | Unit | Dehumidifier | | Regenerator | |
|---|---|---|---|---|---|---|
| | | | Range | Reference | Range | Reference |
| Air inlet temperature | $T_a$ | $^oC$ | 21.02–37.47 | 31 | 21.02–37.47 | 31 |
| Air flow rate | $\dot{m}_a$ | $kg/s$ | 0.51–3.2 | 2.2 | 0.51–3.2 | 2.2 |
| Air inlet humidity ratio | $\omega_i$ | $kg_w/kg_a$ | 0.0157–0.0347 | 0.0214 | 0.0157–0.0347 | 0.0214 |
| Desiccant temperature | $T_d$ | $^oC$ | 24–35 | 29 | 50–68 | 62 |
| Desiccant flow rate | $\dot{m}_d$ | $kg/s$ | 0.39–0.85 | 0.62 | 0.39–0.85 | 0.62 |
| Desiccant concentration | $\chi$ | $\%wt$ | 50–75 | 54 | 50–75 | 50 |

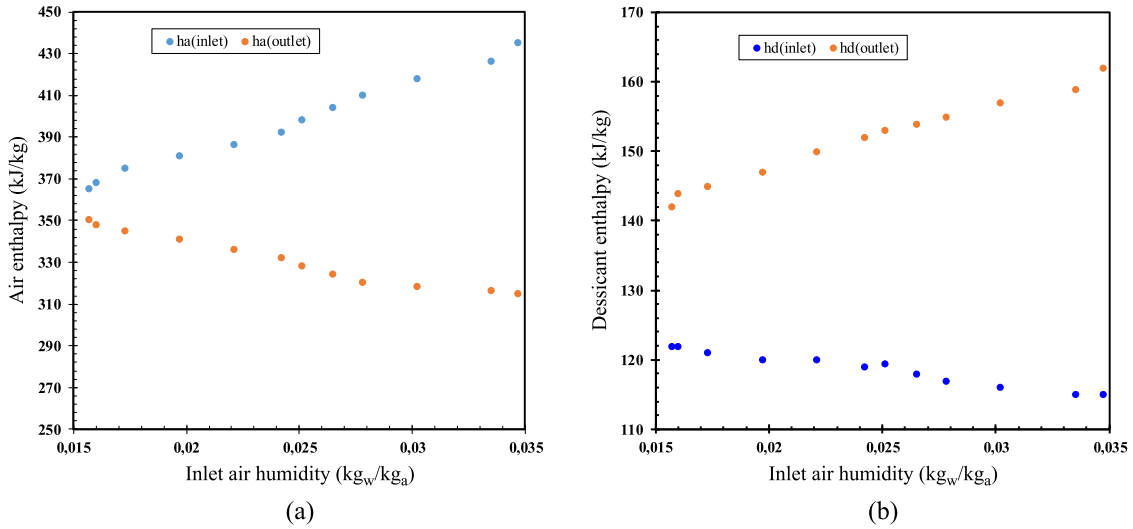


**Figure 3.** *The consequence of inlet air HR on (**a**) air and (**b**) desiccant enthalpy of the dehumidifier.*

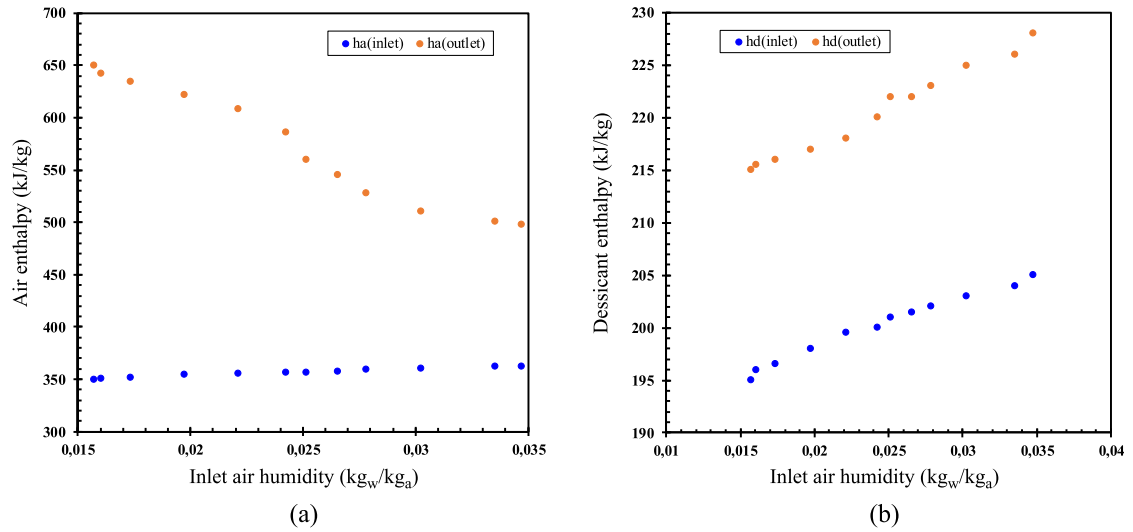


**Figure 4.** *The consequence of inlet air HR on (**a**) air and (**b**) desiccant enthalpy of the regenerator.*

Similarly, from Figure 4b, the inlet and outlet solution enthalpy changed at approximately 9.29% with a gradual increase of 8.49% to 10.09% along the height of the regenerator vessel. The increase in HR resulted in increased outlet and inlet solution enthalpies. The higher vapour pressure as a result of high HR gave rise to low moisture removal from the desiccant. Consequently, less interfacial heat transfer is experienced and hence, the slight prospect of moisture extraction from the air by the desiccant. The general

**Table 6.** *Effects of air HR on air and desiccant enthalpy.*

| Parameter | Dehumidifier | | | Regenerator | | |
|---|---|---|---|---|---|---|
| | $\omega_i$ | Inlet to outlet % (↑ / ↓) | | $\omega_i$ | Inlet to outlet% (↑ / ↓) | |
| | | $\omega_{i_{(min)}}$ (↑) | $\omega_{i_{(max)}}$ (↑) | | $\omega_{i_{(min)}}$ (↑) | $\omega_{i_{(max)}}$ (↑) |
| Air enthalpy ($kJ/kg$) | 16.1%(↓) | 4.11%(↑) | 27.6%(↑) | 37.3%(↑) | 27.21%(↑) | 46.14%(↑) |
| Desiccant enthalpy ($kJ/kg$) | 21.6%(↑) | 14.08%(↑) | 29.01%(↑) | 9.3%(↑) | 8.49%(↓) | 10.09%(↓) |
| Desiccant concentration ($kg_d/kg_s$) | 4%(↓) | 1.3% (↓) | 5.8%(↓) | 9%(↓) | 12.8%(↓) | 4.9%(↓) |
| Air humidity ratio ($kg_w/kg_a$) | 8.72%(↓) | 5.76%(↑) | 38.2%(↑) | 8%(↓) | 64.5%(↓) | 44.3%(↓) |

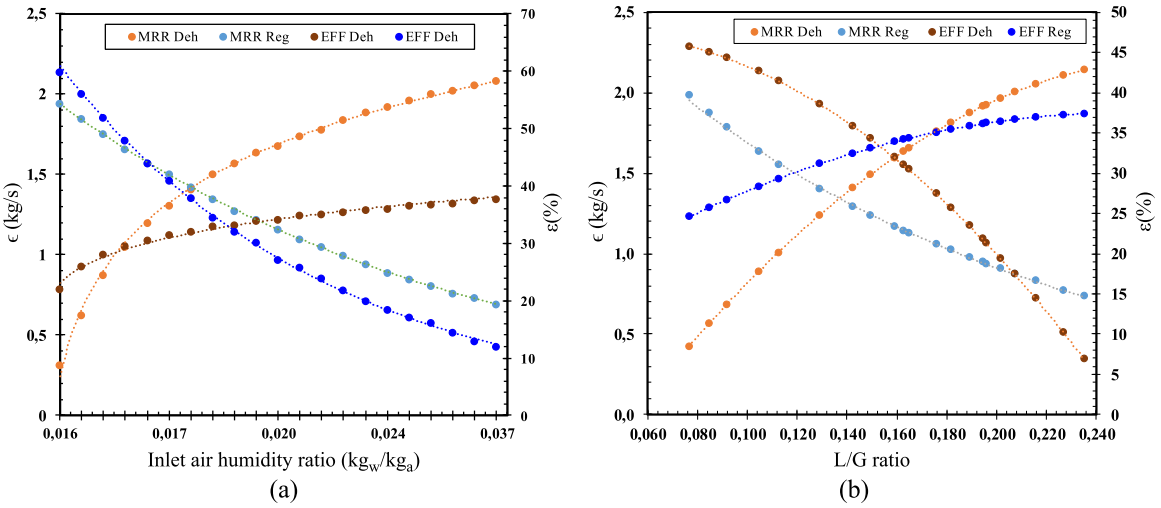


**Figure 5.** *The effect of (**a**) inlet air HR and (**b**) L/G ratio on the effectiveness ε and MRR, ϵ of the dehumidifier and regenerator.*

observation is that, as the HR increases, the solution enthalpy gradient from the packed vessel inlet increases towards the outlet through the dehumidifier height while, in the regenerator, the enthalpy gradient reduces.

Within the specified array of inlet conditions, with the increased air HR, the LiBr concentration reduces considerably in the dehumidifier as a result of more water vapour desorption from the conditioned air. On the other hand, the regeneration vessel experiences an increased outlet desiccant concentration due to vaporization of water particle into the atmosphere. It, therefore, means that, as the HR increases, the magnitude of the change in desiccant concentration from the inlet to exit of the crammed vessel reduces and increases in the dehumidifier and regenerator, respectively.

A summary of the analysed outcomes is presented in Table 6. Concerning the outlet air HR for both dehumidification and regeneration vessels, as the incoming air HR increases, the outgoing air HR reduces and increases considerably in the dehumidifier and regenerator respectively due to increased water vapour in the atmospheric air. The LiBr solution is, therefore, able to absorb as much water as possible to the saturation levels in the dehumidifier. However, in the regenerator, the air is not able to accommodate more water vapour from the LiBr solution due to the truncated vapour-pressure variance. The air–desiccant interface, therefore, becomes saturated inhibiting further heat and mass exchange.

The effects of inlet air HR and L/G ratio on the effectiveness $\varepsilon$ and MRR, $\epsilon$ of the dehumidifier and regenerator vessels are indicated in Figure 5. The influence of inlet air HR of the dehumidifier and regenerator on the effectiveness and MRR was assessed and plotted as shown in Figure 5a. A significant reduction in regenerator effectiveness from 60% to 12% was experienced as the inlet air HR increased from 0.0158 $kg_w/kg_a$ to 0.0367 $kg_w/kg_a$. The reduction was due to the fact that, as the air HR increased, the moisture-holding capacity decreased and hence less water vapour could be expelled from the desiccant, and therefore, the mass conveyance possibility is significantly reduced.

On the other hand, the increase in inlet air HR resulted in increased dehumidifier effectiveness. Within the same HR range, the dehumidifier effectiveness increased from 22% to 36%. The gradual increase was due to increased interfacial mass transfer potential of air and LiBr fed into the dehumidifier. At desiccant-air flow-rate mix of 0.5 kg/h and 0.8 kg/s respectively, the water vapour absorption was limited to the desorption capacity of the desiccant. At these conditions, the thermal-mass exchange was optimized.

Considering the same range of HR values from 0.0158 $kg_w/kg_a$–0.0367 $kg_w/kg_a$, it was noticed that the regenerator MRR decreased considerably from 1.9 kg/s to 0.7 kg/s. The reduction was due to improved vapour pressure, thus, inhibiting mass transfer at the air–desiccant interface. With higher inlet air HR,

there is less capacity to suspend more water vapour from the regenerated desiccant. There was an increased dehumidifier MRR with the increase in air HR from 0.3 kg/s to 2.2 kg/s within the same HR range. This increase was occasioned by the high affinity for the concentrated desiccant to absorb more water vapour. The lower vapour pressure in the desiccant necessitated the mass transfer process; hence, more water vapour was drawn from the process air.

The air flow-rate possess a significant consequence on the operation of the liquid desiccant dehumidification and regeneration schemes as opposed to the desiccant flow rates [28]. Therefore, the L/G ratio was altered by adjusting the airflow rate, while the desiccant flow rate remained unchanged. The effectiveness and MRR of the dehumidifier and regenerator were drawn alongside the L/G ratio, as shown in Figure 5b. The rise in L/G ratio from 0.06 to 0.24 resulted in a sharp increase in dehumidifier MRR for 0.4 kg/s to 2.15 kg/s while the regenerator MRR reduces from 2.0 kg/s to 0.8 kg/s as presented in the figure. These changes were experienced since by reducing the air mass flow rate; the L/G ratio increased; as a result, the interfacial mass transfer potential was diminished, hence, the reduction in regenerator MRR.

In contrast to the MRR, the dehumidifier effectiveness reduced from 50% to 10% while that of the regenerator increased from 29% to 41% within the same L/G ratio range of 0.06–0.24. The reduction of air mass flow meant that there was a prolonged resident time in the vessel that resulted in decelerated interfacial interaction. As a result, the dehumidifier exhibited the characteristics of a regenerator while the regenerator performance was adequately satisfactory.

Since raised LiBr solution temperatures initiate the regeneration process, it was necessary to include the VPV/T collector to aid in solar radiation conversion and conduction of heat into the circulation solution. The LiBr temperature at the exit of the VPV/T was therefore monitored and recorded for sunshine hours. The variation of outlet desiccant temperature from the collector at different flow rates is presented in Figure 6. The flow-rate was changed from 0.5–15 kg/h. It was observed that, the greater the flow-rates, the lesser the temperature increase and vice versa. At 0.5 kg/h, the temperature varied from an inlet state of 20$^o$C to a maximum of 68.14$^o$C at 12:30 hours. Alternatively, the highest flow rate considered was 15 kg/h, which resulted in a temperature rise from 20$^o$C to a maximum of 35.14$^o$C.

The implication was that at lower flow-rates, the desiccant solution gathered more heat from the collector due to more retention time. However, the risk of high stagnation temperature of the VPV/T collector was avoided by adjusting the flow rates accordingly. Therefore, the flow-rate of 0.5 kg/h through the collector was selected and maintained throughout the experiment.

The effect of solar radiation on the MRR and effectiveness of the regenerator and dehumidifier was studied under the following conditions: $\chi$ = 60 kg$_w$/kg$_a$, $\dot{m}_a$ = 0.8 kg/ms and T$_{sol,in}$ = 21 $^o$C, plotted as presented in Figure 7. The regenerator MRR and effectiveness were both observed to improve with the rise in solar radiation, implying that the mass and heat transmission potential was enriched.

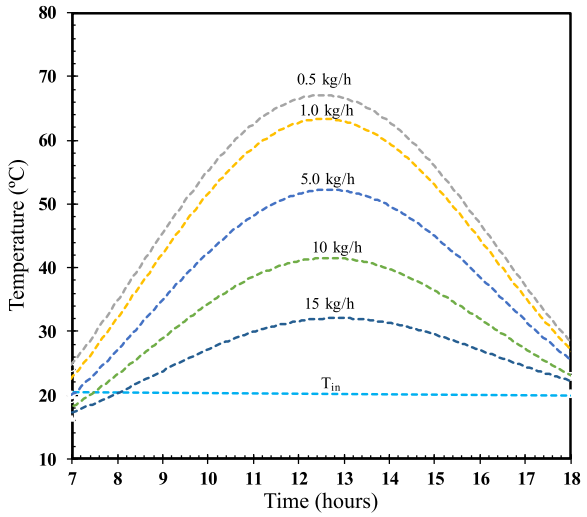


**Figure 6.** *The VPV/T collector outlet temperature variation at different flow rates with time of the day.*

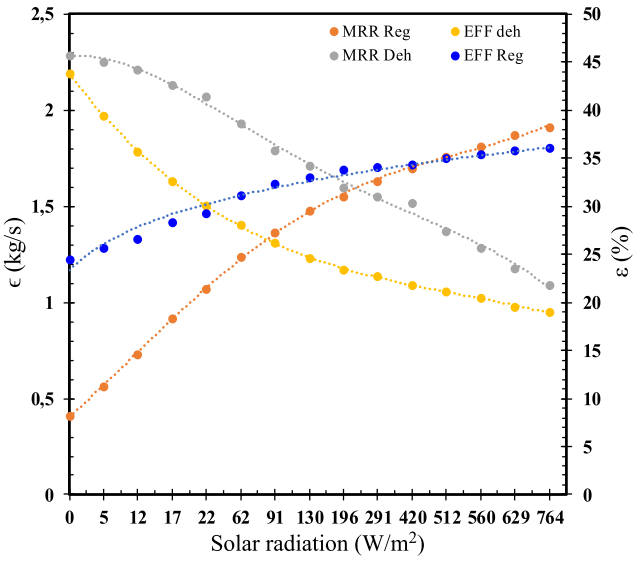


**Figure 7.** *The effect of solar radiation on MRR and effectiveness of the dehumidifier and regenerator.*

The higher the temperature of the desiccant solution, the less the capability to hold water particles hence evaporation ensued, resulting in HR difference and desiccant re-concentration to near initial condition. However, both the dehumidifier MRR and effectiveness dipped with increased desiccant temperature as a consequence of higher solar radiation. Since the dehumidifier experiences high mass transfer rates, as opposed to the high heat transfer rates in the regenerator, the temperature rise due to solar radiation worked negatively for the dehumidifier. The desiccant effectively absorbs water vapour at low temperatures, but as temperature increases, more water vapour is likely to be released from the

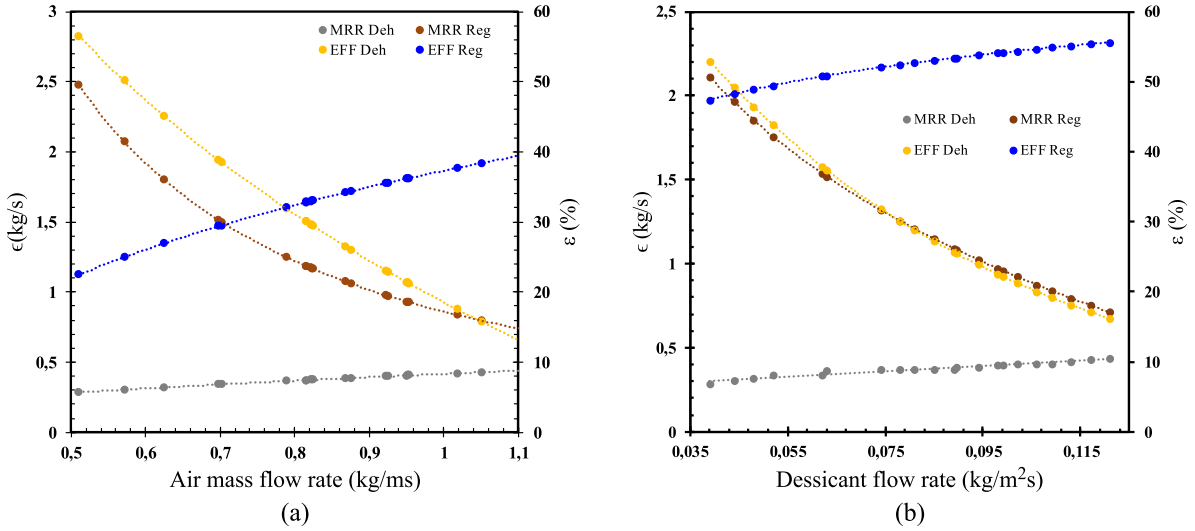


**Figure 8.** *The influence of (**a**) airflow rate and (**b**) desiccant flow rate on the MRR and effectiveness of the dehumidifier and regenerator.*

desiccant to the air, which is not the dehumidification process objective.

In order to achieve optimal performance levels of the vessels in terms of effectiveness and MRR, the air and desiccant flow rates were varied during the experiment, and the corresponding measurements were taken. Subsequently, the results were plotted, as shown in Figure 8, from which the consequence of air and desiccant mass flow rates on the effectiveness and MRR of both the dehumidifier and regenerator was studied. The air mass flow rate was changed progressively from 0.5 kg/ms to 1.1 kg/ms. Within this range, it was observed that the regenerator effectiveness increased steadily from 24% to 39% while that of the dehumidifier reduced from 56% to 13% as depicted in Figure 8a. The increase in MRR was because of the improve vapour pressure dispersion from the weak LiBr at elevated temperature, which exhibited weak moisture-holding capacity and hence increased mass transfer potential. On the other hand, the decline realized on the dehumidifier was primarily due to reduced resident time and minimized interfacial interaction of air-desiccant in the vessel hence lowering the mass transfer capability.

Similarly, the MRR showed a slight upward trend for the regenerator from 0.3 kg/s to 0.4 kg/s. There was a slight adjustment compared to that of air due to the hastened interfacial air–desiccant interaction, which hindered the mass transmission rate and resulted in low MRR. On the contrary, the dehumidifier MRR decreased significantly with the upsurge in air mass flow–rate. The MRR changed from 2.5 kg/s to 0.75 kg/s within the considered range of airflow rates. Again the mass transfer capability was lowered, which negatively affected MRR.

From Figure 8b, the influence of LiBr flow rate on MRR and effectiveness is analysed for both the dehumidifier and regenerator. The MRR curves follow the same trend as those of air; however, the only difference is the rate of change. It was observed that the regenerator MRR reduced significantly from 1.9 kg/s to 0.8 kg/s within the desiccant flow rate range of 0.04 kg/ms to 0.12 kg/ms. On the other hand, the dehumidifier MRR increased from 0.3 kg/s to 0.4 kg/s as in the previous case depicting that MRR generally shows low sensitivity to the air and desiccant flow rates. Increased desiccant flow rate of similar range reduced the dehumidifier effectiveness from 40% to 8%, a difference of 8% while the effectiveness increased by 15% from 22% to 37%.

The influence of incoming LiBr concentration on MRR and effectiveness of both the regenerator and dehumidifier is displayed in Figure 9. The LiBr concentration significantly affects the dehumidifier MRR and effectiveness, as shown in Figure 9a. As the solution concentration increases from 93% to 98%, the MRR considerably decreased from 5.8 kg/s to 1.8 kg/s. This upward change was attributed to the upright geometry of the packing profile, which enabled the solution to flow through with limited air contact, which inhibited mass transfer possibility. The effectiveness profile curve exhibited an increase from 12.5% to 23% with an increase of concentration up to 95 $kg_w/kg_a$. Further increase in concentration up to 98 $kg_w/kg_a$ resulted in a decrease of effectiveness up to 3% due to the variation in HR as correlated in [22].

Similarly, the impact of inlet solution concentration on the regenerator effectiveness and MRR is presented in Figure 9b. It was observed that the MRR decreased from 1.7 kg/s to 1.1 kg/s with an increase in concentration from 64 $kg_w/kg_a$ to 80 $kg_w/kg_a$. In contrast, the effectiveness increased from 18% to 23% within the same range of concentration. This increase was due to the low moisture-holding capacity of desiccant solution at high temperature caused by the hybrid VPV/T as well as the cooling effect of air. The surface texture and geometrical configuration of the packing in terms of smoothness and straight vertical profiles meant that less solution was in contact with the surface, resulting in low contact time due to hastened gravitational flow. For higher MRR,

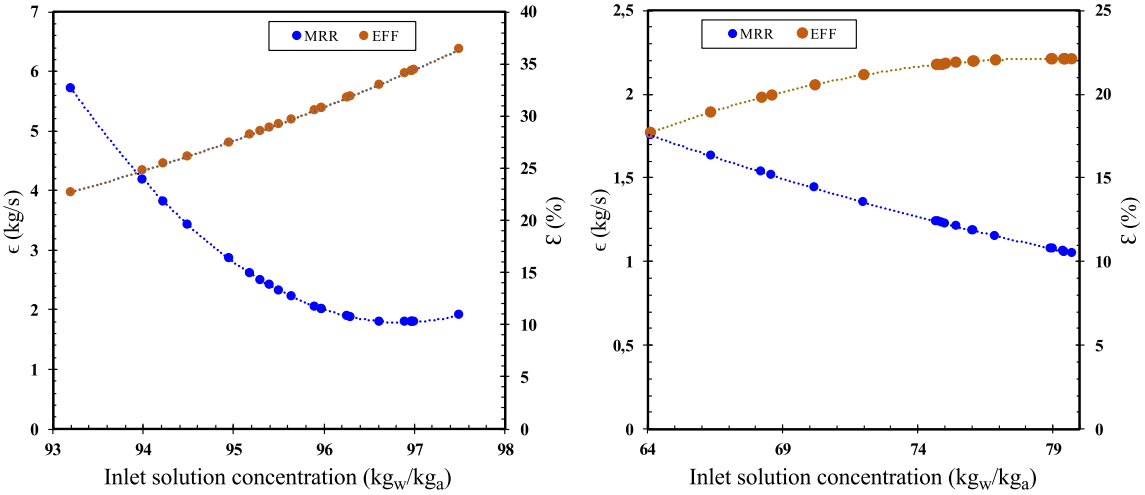


**Figure 9.** *The influence of inlet LiBr concentration on MRR $\epsilon$ and effectiveness $\varepsilon$ of (**a**) dehumidifier and (**b**) regenerator.*

it would require a corresponding increase in air mass flow in line with the findings of [30].

## 4 THE THEORETICAL MODEL

The internal structure of the dehumidifier/regenerator vessel is configured to a counter-flow mode where the desiccant flows downwards from the top countering the air stream flowing upwards from the bottom of the vessel. The vessels are packed with square channelled ceramic cordierite. Although the LiBr liquid is sprayed on the upper side of the packing, the fluid settles and flows continuously as a thin film along the square packing walls. This continuous flow is lamina and is taken to be within the range of $0 < Re_d < 4$. For descending fluid stream within this *Re* range, the prediction of fluid stream thickness and velocity characteristics is best estimated using Nusselt number analysis [31]. The ensuing expression for the stream breadth is given as:

$$\varrho = \sqrt[3]{\frac{3\dot{m}_d\mu_d}{g{\mu_d}^2}}, \tag{17}$$

where $\dot{m}_d$ is the desiccant flow rate per unit length of the packing in kg/ms, $\mu_d$ is the liquid desiccant viscosity and g is the gravitational acceleration. Taking a small elemental particle of interfacial area shown in Figure 10 in which the heat and mass transmission occurs in x, y and z planes, the following assumptions are considered in formulating the fundamental equations: (i) the dehumidification/regeneration process is adiabatic, (ii) static heat and mass transfer constants throughout the process, (iii) no heat loss caused by latent heat of condensation and evaporation and (iv) the fluid flow is continuous and laminar.

Since the water vapour absorption/desorption rate is far much lower than the LiBr solution flow rates, keeping the desiccant flow

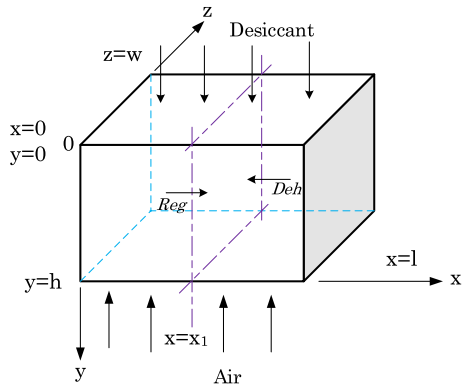


**Figure 10.** *The flow schematic of an elemental particle of interfacial area.*

rate unchanged yields a relatively stream thickness and velocity of similar invariable nature. The invariability implies that there is no interfacial velocity gradient, and therefore the velocity contour is wholly established at the beginning of the interaction span. Due to the low absorption/desorption rates, the mass flow rate towards the *y*-direction and the accompanying partial velocity *v* are significantly dominant. Therefore, the underlying expressions for the interfacial thermal and mass exchange can thus be developed [31]. Let the subscripts *a* and *d* represent air desiccant solution respectively, the fluid momentum in the *x*-plane is given as

$$\mu_d\frac{\partial^2 u}{\partial {y_d}^2} + \rho_d g = 0. \tag{18}$$

The energy balance expression is

$$v_d\frac{\partial T_d}{\partial x} = \gamma_a\frac{\partial^2 T_d}{\partial {y_d}^2}. \tag{19}$$

And mass diffusion equation becomes:

$$v_d \frac{\partial \chi_d}{\partial x} = \delta_a \frac{\partial^2 \chi_d}{\partial {y_d}^2}. \tag{20}$$

The air flows through a vertical rectangular channel of the packing whose length is considered to be extremely large compared to the width. Additionally, the depth of the channel varies form minimum at inlet to maximum at outlet, hence, the fluid flow contour is fully developed and laminar. Then the $z$ momentum equation is given as:

$$\mu_a \frac{\partial^2 v_a}{\partial {y_d}^2} - \frac{\partial p_w}{\partial z} = 0. \tag{21}$$

The energy balance expression is

$$v_a \frac{\partial T_a}{\partial z} = \gamma_a \frac{\partial^2 T_a}{\partial {y_d}^2}. \tag{22}$$

Mass diffusion equation becomes:

$$v_a \frac{\partial \chi_a}{\partial z} = \delta_a \frac{\partial^2 \chi_a}{\partial {y_d}^2}. \tag{23}$$

The equilibrium mass flow expression is formulated as

$$\varphi_a C_{p_w} \frac{\partial T_a}{\partial x} - \gamma a_d A_p \frac{\partial^2 T_a}{\partial y^2} = 0 \tag{24}$$

$$\varphi_a \frac{\partial \omega}{\partial x} - \beta a_d A_p \frac{\partial^2 \omega}{\partial y^2} = 0, \tag{25}$$

where $\varphi$ is the mass flux in kg/ms, $\gamma$ and $\beta$ are the heat and mass exchange constants, respectively, $C_{p_w}$ is the specific heat capacity of water vapour at stagnated pressure, $\delta$ is the diffusion coefficient, $A_p$ is the void space area of the packing and $P_w$ is the vapour pressure.

Considering the energy conservation on the liquid side

$$\varphi_d C_{p_d} \frac{\partial T_d}{\partial x} - \gamma a_d A_p \frac{\partial^2 T_d}{\partial y^2} = 0 \tag{26}$$

$$\varphi_d \frac{\partial \chi}{\partial x} - \beta a_d A_p \frac{\partial^2 \omega}{\partial y^2} = 0. \tag{27}$$

The interfacial characteristic equations can therefore be developed as follows:

$$\varphi_a \left( C_{p_w} \frac{\partial T_a}{\partial y} - \xi \frac{\partial \omega}{\partial y} \right) + \gamma a_d (T_a - T_d) = 0 \tag{28}$$

$$\varphi_d \left( C_{p_d} \frac{\partial T_d}{\partial y} - \xi \frac{\partial \omega}{\partial y} \right) + \gamma a_d (T_d - T_a) = 0 \tag{29}$$

$$\varphi_d \frac{\partial \chi}{\partial y} + \varphi_a \frac{\partial \omega}{\partial y} = 0 \tag{30}$$

$$\varphi_a \frac{\partial \omega}{\partial y} + \beta a_d (\omega - \omega_e) = 0, \tag{31}$$

where $\xi$ is the specific heat of dilution, the length and width-wise desiccant solution temperature variations are represented by $\frac{\partial T_d}{\partial x}$ and $\frac{\partial^2 T_d}{\partial y^2}$, respectively, while lengthwise and height-wise variation of solution concentration within the vessel are given by $\frac{\partial \chi}{\partial x}$ and $\frac{\partial^2 \chi}{\partial y^2}$. The latent heat produced during air dehumidification/regeneration processes and water vapour absorption/desorption is represented by $\xi \frac{\partial \omega}{\partial y}$ and $\xi \frac{\partial \chi}{\partial y}$, respectively. The generated interfacial heat $\gamma a_d (T_a - T_d)$ and mass transfer $\beta a_d (\omega - \omega_e)$ driven by vapour pressure difference are also considered.

Since dehumidification and regeneration processes are exothermic and endothermic respectively, the interfacial absorption/desorption heat can thus be found as a function of enthalpy of condensation/evaporation and dilution as follows:

$$\xi = h_{fg}(T_a, \omega) + \Delta h(T_a, P, \beta). \tag{32}$$

Due to the change in air and desiccant temperatures, the change in specific enthalpy is inevitable. Hence, the variation in specific enthalpy of the humid air can be found by

$$\partial h_a = Cp_a \partial T_a + \partial \omega (Cp_w (T_a - T_{amb}) + \lambda), \tag{33}$$

where $\lambda$ is the latent heat of condensation in kJ/kg. Therefore, the conditions at the boundary layer of x-y planes in the direction of z can thus be expressed as

$$x = 0; T_d = T_{d,i}; \chi = \chi_i \tag{34}$$

$$x = H; T_a = T_{da,i}; \omega = \omega_i \tag{35}$$

$$y = 0; T_d = T_a; \frac{\partial \chi}{\partial y} = 0; u = 0 \tag{36}$$

$$y = \frac{y}{2} = \frac{\omega}{2n}; T_d = T_a; \omega_a = \omega_e; \frac{\partial T_a}{\partial y} = \frac{\partial \chi}{\partial y} = \frac{\partial v_a}{\partial y} = 0 \tag{37}$$

$$y = y_p = \frac{w}{n}; \frac{\partial T_a}{\partial y} = 0; \frac{\partial \omega_a}{\partial y} = 0 \tag{38}$$

$$y = \varrho; \frac{\partial u}{\partial y} = 0 \tag{39}$$

$$y = h; v_a = 0. \tag{40}$$

Considering the above defined boundary modalities, the corresponding interfacial scenarios specified at $y = \varrho$, implies that there is no temperature gradient, hence $T_d = T_a$. However, for thermal balance of a perfect air-vapour blend, the interfacial air and solution vapour pressures are equal, thus, the interfacial concentration can be formulated in terms of molecular weight of water $M_w$ and air $M_a$ and vapour pressure $P_w$ as follows:

$$\chi_i = \frac{M_w P_w}{M_a(P_{mix} - P_w) + M_w P_w}. \tag{41}$$

The vapour pressure of water in LiBr solution can be derived in terms of temperature and concentration from the thermal properties as

$$P_w = f(T_{di}, \chi_{wi}). \tag{42}$$

The interfacial mass balance is expressed as

$$\rho_d \delta_d \frac{\partial \chi_d}{\partial y} = -\rho_a \frac{\delta_a \delta \chi_w}{\partial y}. \tag{43}$$

Similarly, the interfacial energy balance becomes

$$-k_d \frac{\partial T_d}{\partial y_d} = k_a \frac{\partial T_a}{\partial y_a} + \rho_a \delta_a \frac{\delta \chi_w}{\partial y} h_{fg}. \tag{44}$$

The component $h_{fg}$ is the latent heat of vaporization and $\delta$ is the diffusion coefficient. The value of the respective coefficients often determines the degree of heat and mass exchange. These constants can thus be established using the interfacial expression obtained from [29].

$$\gamma = \frac{\varphi_a Cp_{wv}(T_{a,o} - T_{a,i})}{\frac{1}{2}\lambda a_d \left((T_{a,o} - T_{a,i}) - (T_{d,o} - T_{d,i})\right)}, \tag{45}$$

where $\lambda$ is the volume per unit surface area of one segment of the packing material. But the packed vessel thermal and overall efficiencies are given as a function of the air and desiccant temperature difference ratios [28].

$$\eta_t = \frac{(T_{a,o} - T_{a,i})}{(T_{d,i} - T_{a,i})} = \frac{(T_{a,i} - T_{a,o})}{(T_{a,i} - T_{d,i})} \tag{46}$$

and

$$\eta_o = \frac{(T_{d,o} - T_{d,i})}{(T_i - T_{d,i})} = \frac{(T_{a,o} - T_{a,i})}{(T_i - T_{a,i})} \tag{47}$$

Equations 46 and 47 can then be substituted in Equation 45 to yield

$$\gamma = \frac{2\varphi_a Cp_{wv}(T_{d,i} - T_{a,i})\eta_t}{\lambda a_d \left((T_{d,i} - T_{a,i})\eta_t - (T_i - T_{d,i})\eta_o\right)}. \tag{48}$$

Similarly, the interfacial mass transfer coefficient is found by

$$\beta = \frac{\varphi_a}{a_d \lambda} \ln\left(\frac{1}{1-\varepsilon}\right). \tag{49}$$

In general, since the heat and mass exchange phenomenon occurs simultaneously and therefore combined, their coefficients can be correlated using Lewis number (Le), and number of thermal units (NTU) determined by

$$Le = \frac{\gamma}{\beta Cp_w} \tag{50}$$

$$NTU = \frac{\beta A_p V}{\varphi_a}. \tag{51}$$

The Equations 50 and 51 are correlated as function of the corresponding changes in enthalpy in the z direction and HR as follows:

$$\frac{\partial h_a}{\partial z} = \frac{NTU.Le}{h_a}\left[(h_e - h_a) + \lambda\left(\frac{1}{Le} - 1\right)(\omega_e - \omega_a)\right]. \tag{52}$$

From the numerical analysis, it can be established that the interfacial energy exchange between air and LiBr liquid desiccant stream is majorly subjected to the gas side temperature variation giving rise to useful heat and mass transfer rates and consequently causing potential heat gain. The coupling nature of heat and mass transfer obscures the problem and makes the solution a challenging task. Equations 44 and 52 can be conveniently solved by a combination of step by step iterative and separative evaluation methods to obtain the heat and mass transfer characteristic results that can then be compared to the experimental data. The model solution procedure involves the application of algebraic conversions of fundamental equations to group the segments at the inlet section to account for enormous variations in temperature and concentration.

## 4.1 The model solution procedure

The general outline of the solution procedure is as follows:

1. START
2. Input initial guess values for $\varphi$, $a$, $V$, $A$, $\xi$, $T_{a,i}$, $T_{d,i}$, $Cp$, T, $\eta_T$, $\delta$, $\omega_e$, $\omega_i$ and $\eta$ for the air and LiBr.
3. Initialize the values of input parameters at inlet and borderline settings and guess the interfacial temperature $T_i$.
4. Input the initial guess for the interfacial LiBr concentration and use thermodynamic equilibrium properties to obtain the concentration of vapour in air.
5. Compute the wall temperature using the heat resistance analogy.
6. Compute the liquid stream thickness $\varrho$.
7. Evaluate the ensuing energy balance matrix emanating from equation.
8. Compute the interfacial diffusive characteristics using Equations 20 and 23.
9. Using separative evaluation technique, compute $\omega$.

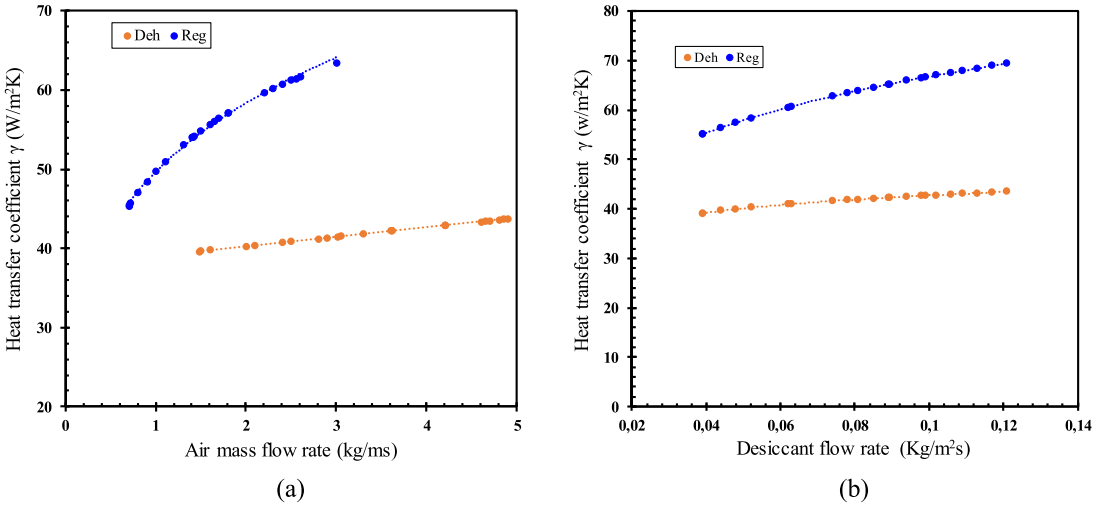


**Figure 11.** *The effect of (**a**) air and (**b**) LiBr flow rates on the heat transfer coefficient.*

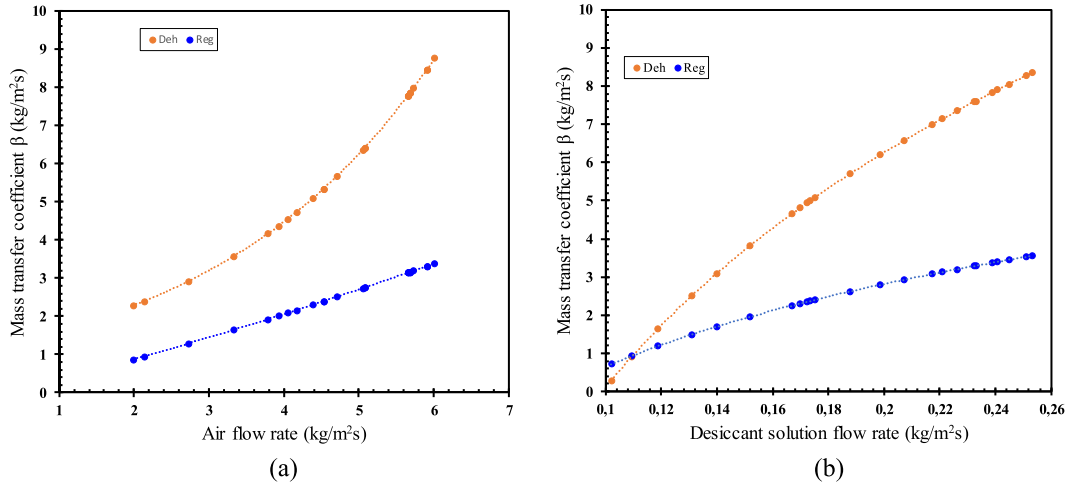


**Figure 12.** *The effect of air and LiBr flow rates on the mass transfer coefficient.*

10. Solve Equations 28, 29 and 30 to obtain $T_a$, $T_d$ and $\chi$.
11. Test if the interfacial energy balance Equation 43, is valid, if NO, recompute the interfacial temperature using Equation 44 and revert to steps 3–10. If YES, continue to the subsequent step.
12. Compute $\gamma$ and $\beta$ using Equations 48 and 49.
13. Solve Equations 50 and 51 and 52 to obtain *Le* and *NTU*.
14. STOP.

## 4.2 The numerical model results

Figure 11 shows the influence of air and LiBr flow rates on the heat transfer coefficients. During dehumidification and regeneration processes, an increase in airflow rate resulted in increased heat transfer coefficient but with varying magnitudes. For the given inlet conditions, when airflow rate per unit length of the vessel was increased from 1.48 kg/ms to 4.9 kg/ms, the heat transfer coefficient increased from 39.7 W/m$^2$K to 43.22 W/m$^2$K during dehumidification, whereas, in the regenerator, increased mass flow rate from 0.7 kg/ms to 3.0 kg/ms gave a corresponding increase in heat transfer from 54.80 W/m$^2$K to 69.44 W/m$^2$K as shown in Figure 11a.

The impact of the LiBr flow rate on the heat transfer coefficient is presented in Figure 11b. For the same range of solution flow rates from 0.039 kg/m$^2$s to 0.012 kg/m$^2$s, it was observed that the heat transfer coefficient increased steadily both in the dehumidifier and regenerator vessels. The magnitudes of the corresponding increases were from 39.16 W/m$^2$K to 43.45 W/m$^2$K and 55.05 W/m$^2$K to 69.41 W/m$^2$K, respectively. Therefore, in order to obtain optimum heat transfer coefficient, the vessels should be subjected to gradually increasing air and LiBr flow rates taking into account the risk of carry-over.

Figure 12 shows the influence of air and LiBr flow rates on the mass exchange coefficients of the dehumidifier and regener-

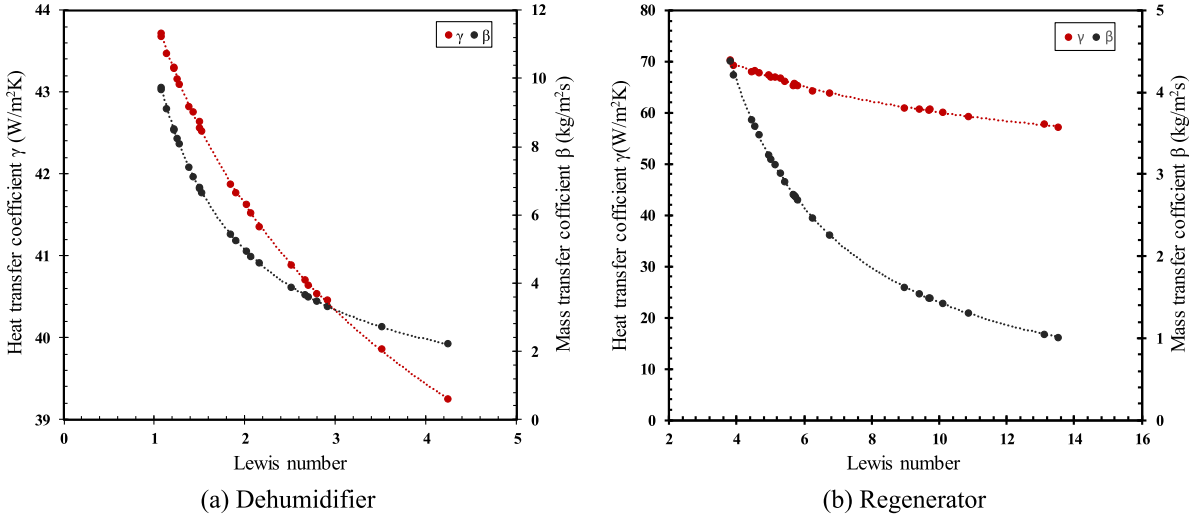


**Figure 13.** *The effect of Lewis number on the heat and mass transfer coefficients.*

ator vessels. For both vessels, it was generally observed that the respective increases in air and LiBr flow rates produced varying increases in the mass exchange coefficients. Regarding Figure 12a, when the airflow rate was varied between 1.992 kg/ms to 6.012 kg/ms while keeping desiccant solution flow rate constant, a rapid increase in mass transfer coefficient from 2.29 kg/m$^2$s to 8.78 kg/m$^2$s was realized during dehumidification process. Similarly, for the regeneration process, the same air mass flow rate range gave a gradual proliferation of the mass transferal coefficient from 0.87 kg/m$^2$s to 3.39 kg/m$^2$s.

In another scenario illustrated in Figure 12b, when the air mass flow rate per unit length was kept constant while varying the desiccant solution flow rate per unit surface area from 0.102 kg/m$^2$s to 0.2536 kg/m$^2$s, steady increases in mass transfer coefficients were realized during both dehumidification and regeneration processes. Increases of mass transfer coefficients from 0.029 kg/m$^2$s to 8.35 kg/m$^2$s and 0.71 kg/m$^2$s to 3.55 kg/m$^2$s were realized for the dehumidifier and regenerator vessels, respectively. In both cases of varying air and desiccant flow rates alternately within the specified ranges, there were significant increases of above 70% in the course of dehumidification and regeneration procedures because of the low vapour pressure and geometry of the CC packing as well as improved interfacial mass transfer potential caused by improved MRR.

The inlet parameters outlined in Table 5 were used to compute the Lewis number and plotted against the heat and mass exchange coefficients corresponding to the dehumidifier and regenerator vessels, as displayed in Figure 13. For both the dehumidifier and regenerator vessels, it was observed that as the Lewis number increased, both the heat and mass transfer constants expressively decreased as depicted in Figures 13a and 13b. These decreases were attributed to the fact that the Lewis number increases when the vapour absorption capability weakens due to reduced interfacial mass transfer. The resultant implication of the reduced mass transfer on the latent heat of vaporization and condensation is also significantly negative, and hence the heat transfer coefficient is also reduced significantly.

For the dehumidification system, the increase in Lewis number from 1.07 to 4.24 caused a decline in heat and mass transfer coefficients from 43.72 W/m$^2$K to 39.25 W/m$^2$K and 9.74 kg/m$^2$s to 2.21 kg/m$^2$s, respectively. Similarly, for the regenerator, as Lewis number increased from 3.83 to 13.54, the heat and mass transfer coefficients reduced from 70.22 W/m$^2$K to 57.23 W/m$^2$K and 4.38 kg/m$^2$s to 1.01 kg/m$^2$s, respectively. These findings were in agreement with those of [28].

## 5 VALIDATION OF THE MODEL

To ascertain the validity of numerical model outcomes, the measured data, as well as experimental outcomes, were used as a benchmark. Comparisons were conducted at various levels of inputs and outputs of different dehumidifier and regenerator thermal and mass exchange performance characteristics and indices. Since the leading performance indices of the dehumidifier and regenerator units were the MRR and effectiveness, a side-by-side comparative evaluation was done concerning projected and experimental figures for the considered range of experimental conditions at different air and desiccant solution inlet temperatures along with inlet air HR.

Figure 14 illustrates the degree of validation match between the predicted and experimental dehumidifier and regenerator vessels effectiveness. The variation of dehumidifier effectiveness was within ±6.2%, as shown in Figure 14a, while that of the regenerator was ±2.9%, as shown in Figure 14b. The lower variation experienced in the regenerator was due to the influence of solar radiation that had a powerful effect on the regeneration process. The temperature increase was significant in improving the regenerator effectiveness. On the contrary, the temperature increase worked against the definite increase in dehumidifier performance.

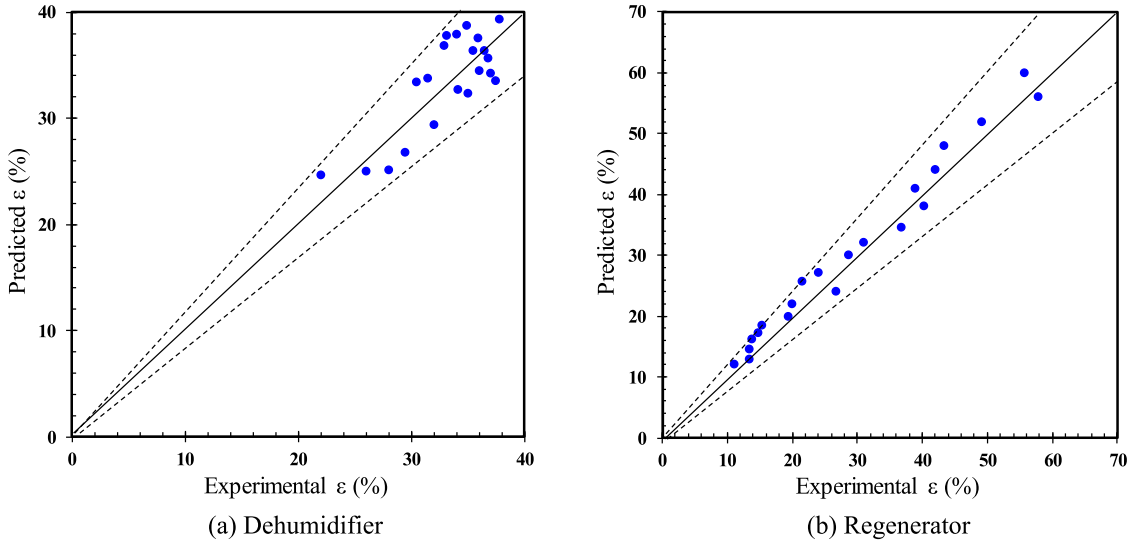


**Figure 14.** *Experimental validation of predicted effectiveness ε.*

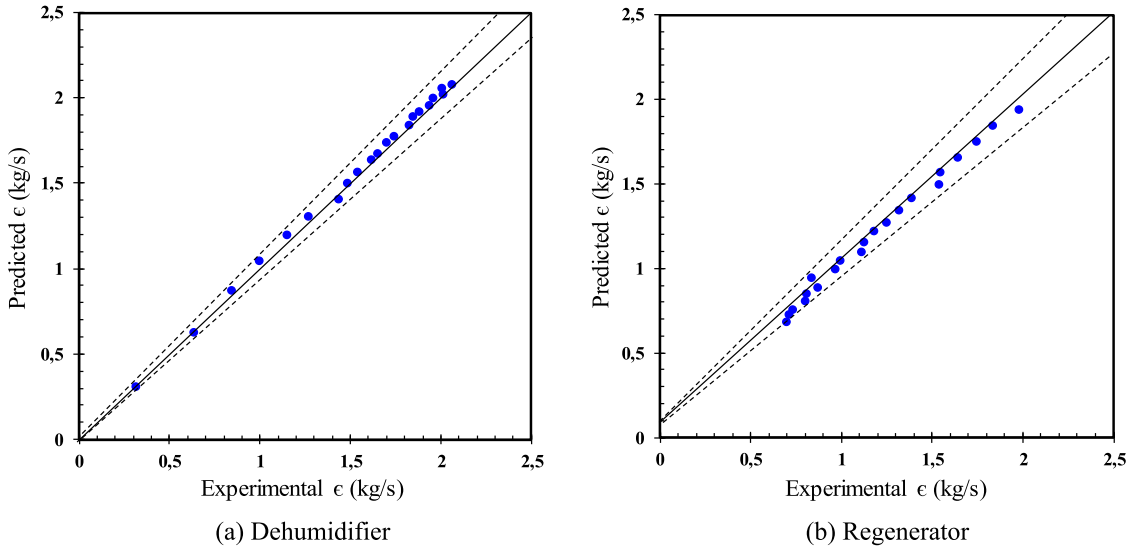


**Figure 15.** *Experimental validation of predicted MRR ϵ.*

Comparisons of the experimental and predicted MRR for the dehumidifier and regenerator is shown in Figure 15. Specifically, Figure 15a and b show the validation of predicted results with experimental data at near precise conformity within ± 2% and ±1.2% for dehumidifier and regenerator MRR, respectively. Again, the MRR of the desiccant solution was found to depend on the temperature variation provided by the solar radiation as the fluid exhibited weak moisture-holding capacity at a higher temperature than lower temperature. For the dehumidifier, the results were accurate at a lower temperature while the variation widened at a higher temperature. This occurrence of the LiBr temperature at the dehumidifier entry needed to be as low as possible for effective MRR.

A comparison between the experimental and modelled heat transfer coefficients of the dehumidifier and regenerator is presented in Figure 16. The observed average deviations between the investigational and modelled thermal transfer coefficients were ±9.7% and ±2.8% for the dehumidifier and regenerator, respectively, as shown in Figure 16a and b. Similarly, from the comparisons between the investigational and modelled mass transfer constants in Figure 17, the average deviations were ±3.5% and ±8.2% during dehumidification and regeneration processes as displayed in Figure 17a and b, respectively.

## 6 CONCLUSIONS

The heat and mass exchange performance of an adiabatic solar-powered liquid desiccant dehumidification and regeneration scheme using LiBr solution has been conducted experimentally

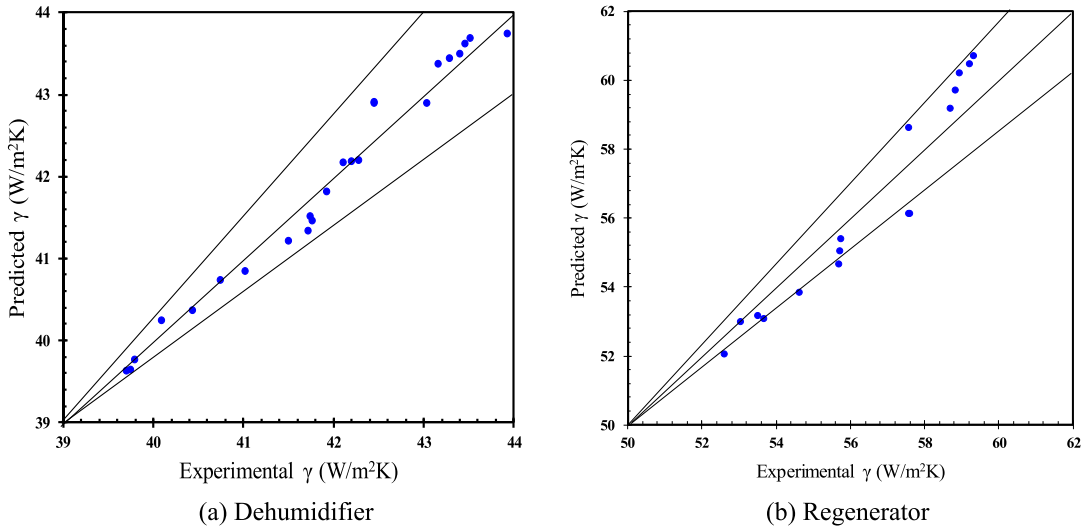


**Figure 16.** *Experimental validation of predicted heat transfer coefficient $\gamma$.*

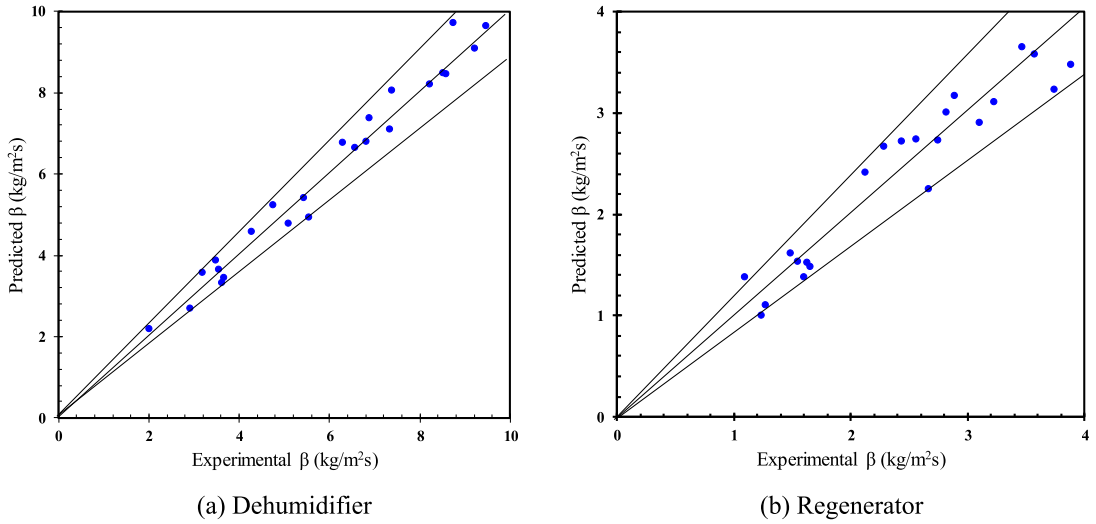


**Figure 17.** *Experimental validation of predicted mass transfer coefficient $\beta$.*

as well as numerically. Based on the analysis procedures and computational approaches, the following significant findings have featured prominently.

Based on the considered sub-tropical climatic conditions, the vacuum insulated solar photovoltaic and thermal module has shown great potential to provide desiccant regeneration heat and electrical energy to drive the system components. Additionally, the square channel structured CC has shown great potential for application as a packing material and catalyst for heat and mass transmission in the dehumidifier and regenerator vessels.

For the given inlet conditions, increased inlet air humidity caused increases in inlet air enthalpies and reduction in outlet air enthalpies during both regeneration and dehumidification process. On the contrary, the desiccant solution enthalpies reduced at inlets and increased at outlets of both dehumidifier and regenerator vessels while the incoming air humidity increased. The increase in inlet air HR also significantly reduced regenerator effectiveness and MRR, while causing increased dehumidifier effectiveness and MRR. Alternatively, the increase in L/G ratio caused an increase in dehumidifier MRR and decrease in regenerator MRR. In contrast, the dehumidifier effectiveness is reduced while that of the regenerator is improved.

Varying the air mass flow rate progressively upwards, improved the regenerator effectiveness by 15% while, that of the dehumidifier reduced by 43%. The MRR showed a slight upward trend for the regenerator of 0.1 kg/s and significantly increase of 1.85 kg/s in dehumidifier MRR. The MRR generally shows low sensitivity to the air and LiBr flow rates. For instance, increased LiBr solution flow rate within the rage of 0.04 kg/ms to 0.12 kg/ms caused a significant reduction in regenerator MRR by 0.8 kg/s while the dehu-

midifier MRR increased by 0.1 kg/s MRR. On the effectiveness, a similar margin of desiccant flow rate reduced the dehumidifier effectiveness by 32% while the generator effectiveness increased by 15%.

The desiccant concentration significantly affected the dehumidifier MRR and effectiveness. As the solution concentration increased, the MRR decreased significantly by up to 4 kg/s. The effectiveness improved with increased LiBr concentration. Similarly, the regenerator, MRR decreased with increase in concentration while the effectiveness increased by up to 5% within the same range of concentration.

The t3D predictive numerical thermal model based on falling liquid stream with constant thickness in counter-flow configuration was developed and solved by a combination of separative appraisal and stepwise iterative technique. The numerical model showed that during the dehumidification and regeneration processes, an increase in airflow rate per unit length and desiccant solution flow rate per unit area resulted in increased thermal and mass exchange coefficients but with varying proportions. As the Lewis number increased, both the heat and mass transfer constants decreased significantly for both the dehumidifier and regenerator vessels. A 74% increase in Lewis number caused a decrease in heat and mass transfer coefficients by 10% and 77%, respectively.

Comparisons conducted at various levels of input and output of the experimental and predicted dehumidifier and regenerator MRR, effectiveness, heat and mass transfer coefficients revealed sublime conformity. The variation of dehumidifier effectiveness was within ±6.2% while that of the regenerator was ±2.9%. The MRR was within ±2% and ±1.2% conformity for dehumidifier and regenerator, respectively. The heat transfer coefficients were within ±9.7% and ±2.8% for the dehumidifier and regenerator, respectively. The average deviations of ±3.5% and ±8.2% were achieved during dehumidification and regeneration procedures.
The underlying findings of this study, provides insights into the design and optimization, application of solar energy as well as CC in liquid desiccant air dehumidification and regeneration setups. Sets of reliable and consistent data upon which theoretical simulation models can be validated and empirical correlations developed have been provided. However, the biochemical reactions and biodegradability of LiBr and CC has not been considered and can be proposed for further investigations.

## REFERENCES


[1] Yonggao Y, Xiaosong Z, Chen Z. Experimental study on dehumidifier and regenerator of liquid desiccant cooling air conditioning system. *Build Environ* 2007; **42**:2505–11.

[2] Kakabayev A, Khandurdyev A. Absorption solar regeneration unit with open regeneration of solution. *Appl Sol Energy* 1969; **5**:69–72.

[3] Kakabayev A, Klyschaeva O, Khandurdyev A. Refrigeration capacity of an absorption refrigeration plant with flat plate glazed solution regenerator. *Appl Sol Energy* 1972; **8**:90–5.

[4] Kaudinya JV, Kaushik SC. Experimental validation of theoretical studies on open and forced flow solar regeneration. *Int J Sol Energy* 1986; **4**:13–33.

[5] Kaushik SC, Kumar Y, Kaundinya JV. Feasibility of an open cycle absorption solar cooling system with solution storage for continuous operation. *Int J Ambient Energy* 1991; **12**:101–6.

[6] Hawlader MNA, Stack P, Wood BD. Performance evaluation of glazed and unglazed collector/regenerator in a liquid desiccant absorbent open-cycle absorption cooling system. *Int J Sustain Energy* 1992; **11**:135–64.

[7] Davangere BS, Sheriff SA, Goswami DY. Feasibility study of a solar air conditioning system - part 1: psychometric and analysis of air conditioned zone. *Int J Energy Res*1999; **23**:103–16.

[8] Ji LJ, Wood B. Performance enhancement studies of a solar collector/regenerator for open cycle liquid desiccant regeneration. *Proceedings of the Annual ASES Conference*, American Solar Energy Society (ASES), 1993, Inc (USA), ISSN: 1062–4910.

[9] Yang R, Wang PL. Experimental study of a forced convection solar collector/regenerator for open cycle absorption cooling. *J Sol Energy Eng* 1994; **116**:194-9.

[10] Yang R, Wang PL. *Experimental study of a glazed solar collector/regenerator operated under humid climate. Int J Solar Energy* 1995; **16**:185–201.

[11] Yang R, Wang PL. Experimental study of a double glazed solar collector/regenerator for open cycle absorption cooling. *J Solar Energy Eng* 1998; **120**:253–9.

[12] Yutong Li, Hongxing Y. Experimental study on an open-cycle solar collector regenerator using liquid desiccant for air conditioning. *Int J Green Energy* 2010; **7**:273–88.

[13] Alizadeh S, Saman WY. *An experimental study of forced flow solar collector/regenerator using liquid desiccant. Solar Energy* 2002; **73**:345–62.

[14] Lazzarin RM, Gasperella A, Longo GA. Chemical dehumidification by liquid desiccants; theory and experiments. *J Refrigeration* 1999; **22**:334–47.

[15] Hennings HM. Solar assisted air conditioning of buildings—an overview. *Appl Therm Energy* 2007; **27**:1734–49.

[16] Zhang L, Hihara E, Matsuoka F, Dang C. Experimental analysis of mass transfer in adiabatic structured packing dehumidifier/regenerator with liquid desiccant. *Int J Heat Mass Tran* 2010; **53**:2856–63.

[17] Gao WZ, Lui J, Cheng YP, Zhang XL. Experimental investigation on the heat and mass transfer between air and liquid desiccant in a cross-flow dehumidifier. *Renew Energy* 2012; **37**:117–23.

[18] Chung TW, Wu H. Comparison between comparison between spray towers with and without fin coils for air dehumidification using triethylene glycol solutions and development of their heat and mass transfer correlations. *Ind Eng Chem Res* 2000; **39**:2076–86.

[19] Longo GA, Gasparella A. Experimental and theoretical analysis of heat and mass transfer in a packed column dehumidifier/regenerator with liquid desiccant. *Int J Heat Mass Tran* 2005; **48**:5240–54.

[20] Liu XH, Jiang Y, Chang XM, Yi XQ. Experimental investigation of the heat and mass transfer between air and liquid desiccant in a cross-flow regenerator. *Renew Energy* 2007; **32**:1623–36.

[21] Longo GA, Gasparella A. Experimental analysis on desiccant regeneration in a packed column with structured and random packing. *Solar Energy* 2009; **83**:511–21.

[22] Chung TW, Wu H. Comparison between random and structured packings for dehumidification of air by Licl solution in a packed bed and their heat and mass transfer correlations. *Ind Eng Chem Res* 1996; **35**:192–8.

[23] Yin YG, Zhang XS, Chen ZQ. Experimental study on dehumidifier and regenerator of liquid desiccant cooling air conditioning system. *Build Environ* 2007; **42**:2505–11.

[24] Peng SW, Pan ZM. Heat and mass transfer in liquid desiccant air conditioning process at low flow conditions. *Commun Nonlinear Sci Numer Simul* 2009; **14**:3599–607.

[25] Wang L, Xiao F, Niu X, Gao D. Experimental study of dynamic characteristics of liquid desiccant dehumidification process. *Sci Technol Built Environ* 2016; **00**:1–14.

[26] Treybal, R. E. Mass Transfer Operations, 3rd ed. McGraw-Hill, New York, 1969 edition.

[27] Oyieke AYA, Inambao FL. Performance characterisation of a hybrid flat-plate vacuum insulated photovoltaic/thermal solar power module in sub-tropical climate. *Int J Photoenergy* 2016; **1**:1–15.
[28] Naik B K, Muthukumar P. Experimental investigation and parametric studieson structured packing based liquid desiccant dehumidification and regeneration system. *Build Environ* 2019; **149**:330–49.
[29] Oyieke AY A, Inambao FL. Interfacial heat and mass transfer analysis in solar-powered packed-bed adiabatic liquid desiccant regeneration for air conditioning. *Int J Low-Carbon Tec* 2018; **13**:277–85.
[30] Zurigat YH, Abu-Arabi MK, Abdul-Wahab SA. Air dehumidification by triethylene glycol desiccant in a packed column. *Energy Conversion and Management* 2004; **45**:141–55.
[31] Park MS, Howell JR, Gray CV, Peterson J. Numerical and experimental results for coupled heat and mass transfer between a desiccant film and air in cross flow. *Int J Heat Mass Tran* 1994; **37**:395–402.

# Chapter4

## Stochastic generation of artificial weather data for subtropical climates using higher-order multivariate Markov chain model

In this chapter, a higher-order multivariate Markov chain model was developed and used to stochastically generate simulated weather data based on subtropical climates applicable to the simulation of any system requiring a solar application. The model was able to precisely predict and create data for solar radiation, ambient temperature, relative humidity and wind speed.

The contents of this chapter are presented in the form of a published article in the Q3-rated International Journal of Mechanical Engineering Technology volume 10, June 2019.

**Oyieke Andrew.Y.A** and Freddie L. Inambao, (2019) Stochastic Generation of Artificial Weather Data for Subtropical Climates Using Higher-Order Multivariate Markov Chain Model, *International Journal of Mechanical Engineering and Technology*, 10(6), 2019, pp. 120-134. Available at: http://www.iaeme.com/IJMET/issues.asp?JType=IJMET&VType=10&IType=6

**International Journal of Mechanical Engineering and Technology (IJMET)**
Volume 10, Issue 06, June 2019, pp. 120-134 . Article ID: IJMET_10_06_007
Available online at http://www.iaeme.com/ijmet/issues.asp?JType=IJMET&VType=10&IType=6
ISSN Print: 0976-6340 and ISSN Online: 0976-6359


# STOCHASTIC GENERATION OF ARTIFICIAL WEATHER DATA FOR SUBTROPICAL CLIMATES USING HIGHER-ORDER MULTIVARIATE MARKOV CHAIN MODEL

**Andrew Y. A. Oyieke* and Freddie L. Inambao**
Discipline of Mechanical Engineering, University of KwaZulu-Natal,
Mazisi Kunene Road, Glenwood, Durban 4041, South Africa
*Corresponding Author.

**ABSTRACT**

*Liquid desiccant air conditioning systems provide an efficient and less energy-intensive alternative to conventional vapour compression systems due to their ability to use low-grade energy provided by a hybrid photovoltaic and thermal solar power module. Air conditioning systems are major energy consumers in buildings especially in extreme climatic conditions and are therefore primary targets in so far as energy efficiency is concerned. Building energy performance has traditionally been simulated using typical meteorological year (TMY) and test reference year (TRY) weather tools. In both cases, the value allocation is pegged on the least nonconformity from the long-range data of the past 29 years. The extreme low and high points are successively disregarded which means that the actual prevailing hourly mean settings are not precisely represented. The multivariate Markov chain provides flexibility for use in circumstances where dynamic sequential and categorical weather data for a given region is required. This study presents a simplified higher order multivariate Markov chain analysis founded on a combination of a mixture-transition and a stochastic technique to project the solar radiation, air humidity, ambient temperatures as well as wind speeds and their interrelationships in sub-tropical climates, typically the coastal regions of South Africa. The generic simulation of weather parameters is produced from 20 years of actual weather conditions using a stochastic technique. The series of weather parameters developed are then implemented in the simulation of solar powered air dehumidification and regeneration processes. The outcomes indicate that the model is devoid of constraints and more accurate in the estimation of variable parameters implying that a properly designed solar-powered liquid desiccant air conditioning system is capable of supplying the majority of the latent cooling load.*

**Keywords**: Weather data, higher-order, multivariate Markov chain, liquid desiccant, sub-tropical climate.

**Cite this Article**: Andrew Y. A. Oyieke and Freddie L. Inambao, Stochastic Generation of Artificial Weather Data for Subtropical Climates Using Higher-Order Multivariate Markov Chain Model, *International Journal of Mechanical Engineering and Technology*, 10(6), 2019, pp. 120-134.
http://www.iaeme.com/IJMET/issues.asp?JType=IJMET&VType=10&IType=6

# 1. INTRODUCTION

Due to tremendous advances in the sector of the built environment in recent years, there has been a positive movement towards the use of renewable energy owing to the ever-increasing danger posed to the environment by conventional sources. Thus, the current trend among building specialists, architects and researchers is towards using renewable sources of energy such as solar to alleviate the high cost of conventional energy. One area of such application is the liquid desiccant air conditioning system, especially at dehumidification and regeneration stages.

The climatic characteristics in sub-tropical regions have not made it easy to include renewable energy into buildings. South Africa is one such country, with a sub-tropical climate along the coastal strip adjacent to the Indian Ocean which is where the city of Durban is located. This region experiences moderately hot and highly humid weather so ideally the air needs to be conditioned before delivery into occupied spaces. The air conditioning process is often a very costly and energy-intensive process. The use of solar energy in air conditioning has been demonstrated to curb energy costs by up to 70% [1]. This form of energy is highly dynamic and unpredictable and its application is often dependent on hourly variations.

Typical meteorological year 2 (TMY2) provides hourly solar data sets in terms of radiation and other weather-related data distributed over a period of one year. The use of TMY2 is limited to simulations of solar energy conversion systems and applications in hypothetical building performance assessments in terms of architectural configurations and geographical positioning in various parts of the world. However, they only characterize archetypical other than real circumstances which may in some occasions be deemed extreme and therefore not suitable for designing structures to withstand worst-case scenarios especially in the regions along coastal strips [4, 5].

In an attempt to solve this shortcoming, another sophisticated set of meteorological data was generated by Chan et al. [6] which involved measured data in an hourly interval for 25 years spanning from 1979 to 2003, dubbed typical meteorological months (TMM). The cumulative distribution function (CFD) for the 12 months in a year were weighed against the long term CFD. The CFD technique involves choosing the month with the least deviation as the standard month and applying this in the composition of TMY. However, since various TMYs possess different statistical inferences, the application is restricted to energy simulation in the built environment and not necessarily suitable for inclusion of other forms of energy such as wind and solar.

Various weighting parameters formed the basis of comparison of TMY and extreme weather year (EWY) weather parameters by Yang et al. [7]. The researchers concluded that weighting factors are useful in the generation of TMY data especially where renewable energy systems are concerned. For reliability and least capital costs of such energy systems, a consistent pattern of meteorological factors needs to be considered. An even more comprehensive analysis of different methods of choosing TMY available in the literature versus those from TRY has been presented by [8]. The effects of both TMY and TRY on functional capabilities of solar thermal collectors and photovoltaic (PV) cells with periodic energy retention systems in buildings was considered.

The effect of solar radiation and ambient air conditions cannot be underestimated since solar radiation provides the regeneration heat while the ambient temperature and humidity of air dictate the ability to either expel or absorb more water vapour. Wind speed determines the intensity of solar radiation reaching a surface. Existing annual solar water heating and photovoltaic weather data have less potential in the present case. The situation is compounded by the fact that it may be difficult to distinguish the effects of solar radiation and ambient air conditions on the performance of a solar-powered liquid desiccant dehumidifier and regenerator. Moreover, the weighting factor assignment to generate the corresponding TMY and TRY weather data can be tedious. It is evident that various TRY files may be needed for building simulations case by case and TMY greatly relies on weighting factors which often overestimate or understate the data points. Based on the identified gaps, a new set of reliable and more realistic and dynamic weather data needs to be developed for air conditioning applications, particularly for closed-direct liquid desiccant (LD) dehumidification and regeneration systems.

In this paper, a stochastic methodology is used to develop a higher-order multivariate Markov chain model incorporating a feedback loop with the capability of linking the observed states and the interdependence of parameters to generate yearly weather data for application in simulation of energy systems comprising multiple weather characteristics over a long period of time. Higher-order MMC models find better application in the modelling of sequential data with the capability of incorporating the long-term dependence on a sequentially measured variable such as solar LD dehumidification and regeneration systems. The main aim of this study was to formulate the governing probability matrices of the measured and predicted parameters as higher-order stochastic equations that provide a more effective method of estimation of model parameters.

## 2. MULTIVARIATE MARKOV CHAIN THEORY

The Markov chain (MC) is a stochastic process theory that can be applied in modelling multi-variable processes which occur unpredictably. Based on probability distribution theory, MC takes care of parameters that change form with a change in time, and therefore a time step variation of a past state is dictated by the assigned order. In other words, the rules of stochastic systems probability generally rely on the previous phases but only up to a given level. The multivariate Markov chain (MMC) model variables accept a modest probabilistic interpolation capable of fitting into an iterative algorithm.

A first-order MC was evidently applied in Yang et al. [9], where a generic weather data set "typical days" was generated and used in the design of an independent photovoltaic system. A bi-state MC model fed with solar radiation parameters was developed and used by Maafi and Adane [10]. A comparison between first and second MC was provided by Shamshald et al. [11] in terms of accuracy based on the wind velocity over a long period of time. Ching et al. [12] put forward a first order multivariate MC model for analysis of various sequential signals produced by a common source. Ching and Fung [13] conducted a study on demand forecast by applying an MMC model based on sequential data series and categories. Yutong and Yang [14] developed a first-order multivariate MC model and used it to generate a series of synthetic weather data for Hong-Kong based on 15-year actual weather data for simulation of solar-powered desiccant air conditioning systems. More recently, Wang et al. [15] formulated a new MMC model for the addition of first-hand data series.

A higher-order MMC model was developed and recommended by Raftery [16], however, the solution using this approach gets complicated due to the non-linear optimization problem and a global maximum and local convergence is not guaranteed. Later a mixture transition technique was used by Raftery et al. [17] to estimate and model recurring patterns. Ching et al.

[18] used the stochastic difference equation technique to generalize Raftery's models to create adequate circumstance for sequential convergence to a static distribution. Zhu et al. [19] presented a higher-order interactive hidden MMC and highlighted areas of its application. However, there are minimal meteorological applications of higher-order MMC from the available literature even though the Markov chain technique can give efficient and reliable models capable of generating changing meteorological data. The idea of higher-order MMC is introduced by extending the first-order MMC to a higher order so as to include long-term dependence on actual as well as predicted variables with the possibility of including a feedback mechanism for reliability. The majority of the applications point to the fact that higher-order MMC provides superior outcomes than the first order instances especially in the accurate estimation of unpredictable variables such as solar irradiance, ambient temperature and relative humidity. A lean and efficient non-negative matrix factorization and two-level optimization iterative algorithm that predicts unknown parameters based on scarce information is now outlined.

A multivariate MC theory can be developed in the following manner: taking n sequential categories of meteorological variables each with k possible combinations; and assuming the probability distribution sequence i at time $t = k + 1$, to rely on sequential probabilities of all states at time $t = k$, it can be deduced that:

$$\chi_{k+1}^{(1)} = \sum_{j=1}^{k} \gamma_{ij}\, \chi_k^{(j)} \quad \text{for i } = 1, 2, \ldots\ldots n \text{ and } k\ 1, 2, \ldots . n \tag{1}$$

For i = 1, 2, 3,.....n and k = 1, 2, 3,.....n; γij ≥ 0, 1 ≤ i, j ≤ n; $\sum_{j=1}^{k} \gamma_{ij}$ for $i = 1, 2, 3, \ldots . n$; $\chi_o^{(j)}$ is the probability distribution at the origin of sequence i. It, therefore, follows that the probability distribution of sequence i is greatly dictated by the weighted mean of $p^{(i,j)}\chi_k^{(j)}$. A matrix can then be generated by considering a single-step probability combination $p^{(i,j)}$ at state t and sequence j and k at time $t = k + 1$, with $\chi^{(j)}$ probability distribution of sequence j at time k. This relationship yields the matrix in equation 2:

$$\begin{bmatrix} \chi_{k+1}^{(1)} \\ \chi_{k+1}^{(2)} \\ \chi_{k+1}^{(3)} \\ \vdots \\ \chi_{k+1}^{(n)} \end{bmatrix} = \begin{bmatrix} \gamma_{11}p^{(11)} & \gamma_{12}p^{(12)} & \gamma_{13}p^{(13)} & \cdots & \gamma_{1n}p^{(1n)} \\ \gamma_{21}p^{(21)} & \gamma_{22}p^{(22)} & \gamma_{23}p^{(23)} & \cdots & \gamma_{2n}p^{(2n)} \\ \gamma_{31}p^{(21)} & \gamma_{32}p^{(32)} & \gamma_{33}p^{(33)} & \cdots & \gamma_{3n}p^{(3n)} \\ \vdots & \vdots & \vdots & \ddots & \vdots \\ \gamma_{n1}p^{(n1)} & \gamma_{n2}p^{(n2)} & \gamma_{n3}p^{(n3)} & \cdots & \gamma_{nn}p^{(nn)} \end{bmatrix} \begin{bmatrix} \chi^{(1)} \\ \chi^{(2)} \\ \chi^{(3)} \\ \vdots \\ \chi^{(n)} \end{bmatrix} \tag{2}$$

The above matrix in equation 2 can be solved by a simple linear algorithm to obtain the underlying parameters after performing a normalization procedure. In order to estimate $p^{(i,j)}$ and γij, we consider a transition probability matrix encompassing the state at *i* and j sequences respectively and generate a state matrix for data frequency. Hence, it is vital that an $m \times m$ transitional matrix for MMC model be estimated prior to solution.

Therefore, if we take the frequency $f^{(i,j)}$ in phases $l_i$ and $l_j$ within sequences $\chi^{(i)}$ and $\chi^{(j)}$ we can develop a transition frequency matrix in equation 3.

$$f^{(i,j)} = \begin{bmatrix} f_{11}^{(i,j)} & f_{21}^{(i,j)} & f_{31}^{(i,j)} & \cdots & f_{1n}^{(i,j)} \\ f_{12}^{(i,j)} & f_{22}^{(i,j)} & f_{32}^{(i,j)} & \cdots & f_{2n}^{(i,j)} \\ f_{13}^{(i,j)} & f_{23}^{(i,j)} & f_{33}^{(i,j)} & \cdots & f_{3n}^{(i,j)} \\ \vdots & \vdots & \vdots & \ddots & \vdots \\ f_{1n}^{(i,j)} & f_{2n}^{(i,j)} & f_{3n}^{(i,j)} & \cdots & f_{nn}^{(i,j)} \end{bmatrix} \tag{3}$$

The probability matrix $\hat{P}^{(i,j)}$can then be estimated from $f^{(i,j)}$ as:

$$\hat{p}^{(i,j)} = \begin{bmatrix} p_{11}^{(i,j)} & p_{21}^{(i,j)} & p_{31}^{(i,j)} & \dots & p_{1n}^{(i,j)} \\ p_{12}^{(i,j)} & p_{22}^{(i,j)} & p_{32}^{(i,j)} & \dots & p_{2n}^{(i,j)} \\ p_{13}^{(i,j)} & fp_{23}^{(i,j)} & p_{33}^{(i,j)} & \dots & p_{3n}^{(i,j)} \\ \vdots & \vdots & \vdots & \ddots & \vdots \\ p_{1n}^{(i,j)} & p_{2n}^{(i,j)} & p_{3n}^{(i,j)} & \dots & p_{nn}^{(i,j)} \end{bmatrix} \tag{4}$$

From which the exact value of $p_{l_i l_j}^{(i,j)}$ can be evaluated for as long as the following condition is met:

$$p_{l_i l_j}^{(i,j)} = \begin{cases} n\dfrac{f_{l_i l_j}^{(i,j)}}{\sum_{l_i=0}^{n} f_{l_i l_j}^{(i,j)}} & when \sum_{l_i=0}^{n} f_{l_i l_j}^{(i,j)} \neq 0 \\ 0 & other\ cases \end{cases} \tag{5}$$

We then estimate the factors γij by assuming an MMC model with a static probability vector χˆ which can be evaluated by getting the occurrence probability of a state in a sequence denoted by a stable probability vector χˆ(χˆ(1), χˆ(2), χˆ(3) . . . χˆ(n)) which relates to matrices γij and p(ij) in the following configuration matrix:

$$\hat{\chi} \approx \hat{\chi} = \begin{bmatrix} \gamma_{11}p^{(11)} & \gamma_{12}p^{(12)} & \gamma_{13}p^{(13)} & \dots & \gamma_{1n}p^{(1n)} \\ \gamma_{21}p^{(21)} & \gamma_{22}p^{(22)} & \gamma_{23}p^{(23)} & \dots & \gamma_{2n}p^{(2n)} \\ \gamma_{31}p^{(21)} & \gamma_{22}p^{(32)} & \gamma_{33}p^{(33)} & \dots & \gamma_{3n}p^{(3n)} \\ \vdots & \vdots & \vdots & \ddots & \vdots \\ \gamma_{n1}p^{(n1)} & \gamma_{n2}p^{(n2)} & \gamma_{n3}p^{(n3)} & \dots & \gamma_{nn}p^{(nn)} \end{bmatrix} \tag{6}$$

By using Ching et al.'s [13] optimization principle rule, a linear programming problem for each instance l on the parameter $\gamma = \gamma_{ij}$ which satisfies the condition set out if equation 5, can be formulated as shown in equation 7:

$$\beta = \hat{P}^{(l_1)}\hat{\chi}^{(1)}\left|\hat{P}^{(l_1)}\hat{\chi}^{(1)}\right|\hat{P}^{(l_1)}\hat{\chi}^{(1)}|\dots|\hat{P}^{(l_1)}\hat{\chi}^{(1)}\,| \tag{7}$$

A combination of equations 6 and 7 can then be implemented in the objective function in equation 8 to give the outlined parameters.

$$\begin{cases} Min_{\gamma} \qquad Min_{l}\left|\left[\sum_{l_j=1}^{m}\gamma_{ij}\hat{p}^{(j)}\hat{\chi}^{(i,j)} - \hat{\chi}^{(i)}\right]_{l}\right| \\ subject\ to \qquad \sum_{l_j=1}^{m}\gamma_{ij} = 1\ and\ \gamma_{ij} \geq 0,\ \forall_j \end{cases} \tag{8}$$

However, the solution using this approach gets complicated due to the non-linear optimization problem and a global maximum and local convergence is not guaranteed. Therefore, a higher-order MMM can be introduced by considering distinct time-dependent parameter sets given that χt is the probability matrix of MMC i.e. ($\chi^t \in \mathbb{k}m$) and βt gives the probability matrix of the observed parameter at time t i.e. ($\beta_t \in \mathbb{k}km$). It follows that in the higher-order MMC, the observed and the predicted states interactively affect each other according to linear higher order stochastic difference equations:

$$\begin{cases} \chi_t = \sum_{j=1}^{a} \gamma_j p^{(j)} \beta_{(t-j)} \\ \beta_t = \sum_{i=1}^{b} \mu_i \, M_i \chi_{(t-i+1)} \\ subject\ to \sum_{j=1}^{a} \gamma_j = \sum_{i=1}^{b} \mu_i = 1 \ and \ \gamma_j \geq 0, \ \mu_i \leq 1 \end{cases} \quad (9)$$

Where a and b are the orders of predicted and measured phases respectively and the matrices $P^{(j)}$ and $M_{(i)}$ are the jth step change-over probability matrices from the observed to predicted states and vice versa. If $a = b = 1$, then the Yutong and Ching models are generated [14, 20]. However, if $\chi^t$ is substituted into the equation for $\beta_t$, a higher-order MMC model βt is obtained as follows:

$$\beta_t = \sum_{j=1}^{a} \sum_{i=1}^{b} \mu_i \, \gamma_j M_i \, p^{(j)} \beta_{(t-i-j+1)} \quad (10)$$

Equation 10 can be solved by applying the non-negative matrix factorization method from [20]. In another scenario, second order homogeneous MMC model with value a = b = 2 can be formulated as:

$$\begin{cases} \chi_t = \gamma_j p^{(j)} \beta_{(t-1)} + (1-) Q \beta_{(t-2)} & ; \\ \beta_t = \mu_i \, M_i \chi_t + (1+\mu) N \chi_{t-1} & where \ \gamma_j \geq 0, \ \mu_i \leq 1 \end{cases} \quad (11)$$

Substituting the values of $\chi^t$ in equation 12, we get:

$$\beta t = \gamma_j \mu_i M_i p^{(j)} \beta_{(t-1)} + [(1-\gamma)\mu MQ + \gamma(1-\mu)NP]\beta_{(t-2)} + (1-\gamma)(1-\mu)NQ\beta_{(t-3)} \quad (12)$$

Therefore, a matrix $\boldsymbol{H_t}$ can be formulated as follows:

$$\boldsymbol{H}_{(t)} = \begin{bmatrix} \beta_{(t)} \\ \beta_{(t-1)} \\ \beta_{(t-2)} \\ \beta_{(t-3)} \\ \vdots \\ \beta_{(t-n)} \end{bmatrix} = \begin{bmatrix} C_1 & C_2 & C_3 & C_4 & \dots & C_n \\ 1 & 0 & 0 & 0 & \dots & 0 \\ 0 & 1 & 0 & 0 & \dots & 0 \\ 0 & 0 & 1 & 0 & \dots & 0 \\ \vdots & \vdots & \vdots & \vdots & \ddots & \vdots \\ 0 & 0 & 0 & 0 & \dots & 1 \end{bmatrix} \begin{bmatrix} \beta_{(t-1)} \\ \beta_{(t-2)} \\ \beta_{(t-3)} \\ \beta_{(t-4)} \\ \vdots \\ \beta_{(t-n)} \end{bmatrix} = C\boldsymbol{H}_{(t-1)} \quad (13)$$

Where

$$\begin{cases} C_1 = \gamma\mu MP \\ C_2 = (1-\gamma)\mu MQ + \gamma(1-\mu)NP \\ C_3 = (1-\gamma)(1-\mu)NQ \\ C_4 = (1-\gamma)(1-\mu)(\gamma-\mu)QP \end{cases} \quad 4)$$

For proper estimation of parameters γ, μ, M, N, P, Q and R, then the matrix C must be estimated first by minimizing the normalization factor as follows:

$$\underbrace{Min}_{C} \left\{ \sum_{t-4}^{T} \left\| \boldsymbol{H}_t - C\boldsymbol{H}_{(t-1)} \right\| \right\} \quad (15)$$

Based on the values of γ and μ, equation 14 represents the change-over matrix since the column sums of $C_1$, $C_2$, $C_3$ and $C_4$ are equal. The optimal estimates of the unknown parameter

can be achieved by a two-level optimization algorithm based on non-negative matrix factorization [20, 21, 22].

### 2.1. The Algorithm

**1.** Initialize W, N and h = 1.

**2.** Using the Lin sub-problem algorithm [21], solve for $P^h$, $Q^h$ and $R^h$ by minimizing $||\gamma\mu W^{(h-1)} P^{(h)} - C_1 ||_F^2, ||(1-\gamma)(1-\mu)N^{(h-1)} Q^{(h)} - C_3||_F^2$ and $||(1-\gamma)(1-\mu)(\gamma-\mu)Qh-1)R(h) - C_4||_F^3$.

**3.** By minimizing

$||C_2 - (1-\gamma)\mu W(h)Q(h) - \gamma(1-\mu)N-1)P(h)||_F^2$, solve W(h) and N (h) subject to $0 \leq W^{(h)}, N^{(h)} \leq 1$ and the total sums of $W^{(h)}$ and $N^{(h)}$ being 1.

**4.** If $||W^{(h)} - W^{(h-1)}||_F^2 + ||N^{(h)} - B^{(h-1)}||_F^{2\,(h)} <$ the tolerance, then STOP otherwise $h = h+1$ and return to step 2.

**5.** Repeat steps 1 to 4 until the function in step 4 is greater than the tolerance.

Initial guesses should be chosen randomly so as to avoid attainment of the local minimum. When the normalization of P and Q values is done, the column sums of the probability matrix will be equal to 1 and hence only the parameters minimizing the function

$$\|\gamma\mu WP - C1\|_F^2 + \|C_2 - (1-\gamma)\mu WQ - \gamma(1-\mu)NP\|_F^2 + \|(1-\gamma)(1-\mu)NQ - C3\|_F^2 + \|(1-\gamma)(1-\mu)(\gamma-\mu)QR - C4\|_F^2$$ are chosen.

## 3. APPLICATION OF THE MMC MODEL TO GENERIC WEATHER DATA GENERATION

The weather data can be decomposed into random and deterministic segments which are autocorrelated daily on an hourly basis for 20 years. A clearness index as defined in [14] and [3] is based on a time series which conveniently estimates solar radiation, temperature, humidity and wind speed which eliminates interdependencies among the weather variables. It then requires testing before any estimation procedure commences.

Before implementation of the formulated MMC model in the estimation of global solar radiation as well as humidity, wind speed and ambient temperatures, consideration must be given to the fact that past studies have shown that MMC is best applicable to studying dependent variables as reported in [14]. Therefore, we then determined through tests whether the parameters in consideration for this study fell in this category by considering an asymptotically spread parameter σ characterized by $\chi^2$ having $(n-1)^2$ degrees of freedom, $\mathbb{k}$ and $n_{ij}$ number of phases and transitions respectively, and a borderline probability for the kth column of changeover probability matrix. In the case of an independent relationship, then σ must statistically satisfy the relationship defined as:

$$\sigma = 2\sum_{j=i}^{k} n_{ij}\, ln\left(\frac{\hat{p}^{(i,j)}}{\hat{p}^{(j)}}\right) \tag{16}$$

A dependence test between variables showed that at 5 % level and 93 degrees of freedom, σ was large enough above χ2 with a corresponding value of 115. This occurrence meant that transitional phases of hourly weather parameters were dependent and thus satisfied the MMC conditions

A time phase change-over probability is independent if the MMC is stationary. To check the dependability, a complete cycle of occurrence was disintegrated into $\mathbb{k}$ mini intervals whose transitional probability matrices were then calculated and compared. If the comparison returned the same results then it could be concluded that the MMC was stationary. For this test, we used

the statistic λ which combines the $n_{(ij)}(s)$ transitions with $p\hat{}^{(ij)}(s)$ probability. The solution of equation 17 is expected to give the value of λ with χ2 exhibiting $(\mathbb{k} - 1)n(n - 1)$ degrees of freedom in order to satisfy the condition of a stationary MMC in the following manner:

$$\lambda = 2\sum_{s}^{k}\sum_{j=i}^{k} n_{ij}\, ln\left(\frac{\hat{p}^{(i,j)}}{\hat{p}^{(j)}}\right) \tag{17}$$

Generally, during this test, the solar radiation, humidity wind speed ambient temperature gave lesser values than $\chi^2$ of 17 500 at 5 % confidence level and 15 750 degrees of freedom. This evidently implies that the MMC is stationary for the mentioned weather parameters.

A pattern of weather data was then generated by considering an initial random phase *j*, then applying MMC to arbitrary values of 0 to 1 produced in a sequential generator. These values formed the basis of comparison with the components of the $j^{th}$ row in the change-over probability matrix. The ensuing states adopted were those of superior value to the total probability of the preceding phase and lower than the probability of the phases.

Taking the minimum and maximum boundary conditions of wind speeds as $V_0$ and $V_1$, and $Z_1$ random numbers falling within range 0-1, a relationship was adopted from [19] and formulated for wind speed, which was replicated hourly for all the t hours.

$$Vw = V_0 + Z_j(V_1 - V_0) \tag{18}$$

For consecutive time intervals i.e. $t_1$, $t_{2.....}$ and $t_n$ falling within the phase *i*, the former state was selected. On the other hand, the duration of phase *j* was determined by selecting a random $Z_j$ whose value was less than the cumulative probabilities $p\hat{}(t-1; j)$, $p\hat{}(t-2; j)$ $p\hat{}(t-n; j)$ provided that $(t-1)$ to $(t+L-1)$ fell within phase *j*.

The number of change-over probabilities to be predicted rises in an exponential pattern as the order of the model. This results in computational complexities which can only be overcome by incorporating more parameters. Using the data available from measurements at Mangosuthu University of Technology weather station, the hourly variation of solar radiation, wind speed, relative humidity and ambient air temperatures were used to generate a sequence of daily occurrences and subsequent changes. For the formation of data sequences for each parameter, the daily upward and downward variations were identified and marked within intervals to obtain two sets of finite discrete data sequences within the time range of $t$ = 8760 hours as follows:

$R_1 = [X_4X_2X_1X_4X_1X_4X_1 \ldots X_3X_1X_4]$, $R_2 = [X_2X_1X_3X_4X_1X_4X_1\ldots\ldots\ldots X_3X_4X_1]$

$R_3 = [X_2X_3X_2X_1X_4X_2X_3 \ldots X_1X_2X_2]$, $R_4 = [X_3X_4X_1X_2X_2X_4X_4\ldots\ldots\ldots X_1X_3X_1]$

Where the ranges $X_1 = 0 \leq R_n \leq 3\gamma$, $X_2 = R_n \leq 3\gamma$, $X_3 = R_n \leq -3\gamma$ and $X_4 = -3\gamma \leq R_n \leq 0$ represent normal upward change, maximum upward change, minimum decrease and normal decrease respectively in values of each parameter. $R_1$, $R_2$, $R_3$ and $R_4$ are the data sequences for the variations in solar radiation, ambient air temperature, wind speed and relative humidity respectively. From the above combinations, the respective changeover matrices for each parameter can be determined as follows:

$$W_{R1} = \begin{bmatrix} 1773.42 & 1060.94 & 113.07 & 1050.7 \\ 2107.84 & 1463.13 & 17.50 & 1655.57 \\ 894.85 & 535.12 & 373.07 & 990.78 \\ 670.50 & 495.20 & 925.54 & 960.96 \end{bmatrix},$$

$$W_{R2} = \begin{bmatrix} 23.75 & 28.85 & 25.95 & 27.75 \\ 30.85 & 26.15 & 27.75 & 23.25 \\ 28.75 & 18.40 & 17.54 & 26.15 \\ 27.55 & 25.45 & 26.15 & 19.75 \end{bmatrix},$$

$$W_{R3} = \begin{bmatrix} 7.95 & 4.5 & 9.9 & 4.65 \\ 7.35 & 1.6 & 6.75 & 8.5 \\ 4.0 & 3.3 & 2.65 & 7.1 \\ 3.4 & 6.95 & 7.1 & 1.6 \end{bmatrix},$$

$$W_{R4} = \begin{bmatrix} 77.5 & 71.5 & 66.5 & 89.5 \\ 91.5 & 88.5 & 86.5 & 79.5 \\ 56.0 & 58.5 & 94.5 & 82.5 \\ 58.5 & 86.0 & 58.0 & 61.0 \end{bmatrix}$$

Where $W_{R1}$, $W_{R2}$, $W_{R3}$ and $W_{R4}$ are the changeover frequency occurrences between phases of $R_1$, $R_2$, $R_3$ and $R_4$ respectively. The next procedure is to normalize the change-over occurrence matrices to determine the probability matrices as follows;

$$\hat{P}_{R1} = \begin{bmatrix} 0.0138 & 0.0138 & 0.0124 & 0.0117 \\ 0.0119 & 0.0121 & 0.0131 & 0.0115 \\ 0.0133 & 0.0098 & 0.0109 & 0.0114 \\ 0.0099 & 0.0107 & 0.0114 & 0.0098 \end{bmatrix},$$

$$\hat{P}_{R2} = \begin{bmatrix} 0.0188 & 0.0154 & 0.0177 & 0.0155 \\ 0.0144 & 0.0157 & 0.0135 & 0.0114 \\ 0.0133 & 0.0142 & 0.0149 & 0.0137 \\ 0.0111 & 0.0125 & 0.0128 & 0.0118 \end{bmatrix},$$

$$\hat{P}_{R3} = \begin{bmatrix} 0.0160 & 0.0114 & 0.0173 & 0.0151 \\ 0.0137 & 0.0129 & 0.0114 & 0.0148 \\ 0.0222 & 0.0130 & 0.0111 & 0.0104 \\ 0.0106 & 0.0133 & 0.0137 & 0.0149 \end{bmatrix},$$

$$\hat{P}_{R4} = \begin{bmatrix} 0.0126 & 0.0101 & 0.0105 & 0.0198 \\ 0.0147 & 0.0147 & 0.0163 & 0.0170 \\ 0.0185 & 0.0167 & 0.0184 & 0.0138 \\ 0.0158 & 0.0146 & 0.0164 & 0.0145 \end{bmatrix},$$

## 4. RESULTS AND DISCUSSION

After computation and solution of change-over probability matrices, the properties exhibited similar characteristics as those of the actual weather data based on a 20-year average. The actual weather data used as a basis of comparison in this study was obtained from one of the South African Universities Radiometric Networks (SAURAN) at Mangosuthu University of Technology STARLab station (STA), situated at Umlazi, Durban, South Africa on latitude, longitude and elevation of -29.97027$^o$ E, 30.91491$^o$ S and 95 m respectively. The annual hourly distribution of air ambient temperature is shown in Figure 1. The maximum and maximum values of temperature during the year are 5.7 °C and 32.2 °C. The former was experienced in the month of June while the latter occurred in February, these months corresponding to summer and winter seasons in South Africa respectively.

The relative humidity annual hourly distribution is shown in Figure 2. The predicted minimum and maximum values were 44 % and 100 % receptively for the Durban region which lies on the coastal line. The minimum RH corresponds to the winter month of July while the maximum range was recorded in the summer month of January. The annual hourly variation of wind speed was plotted as shown in Figure 3, from which the minimum and maximum values of 0.1 m/s and 13.55 m/s were recorded. The values corresponded with the winter and summer months of July and December respectively.

The total solar radiation distribution over a one-year period is shown in Figure 4. The lowest value was 0 W/m$^2$ during the non-sunshine hours while the highest value was 3391.57 W/m$^2$

experienced between the months of May and August. All the maximum and minimum values of these parameters appeared to follow the same trend as the actual measured weather data.

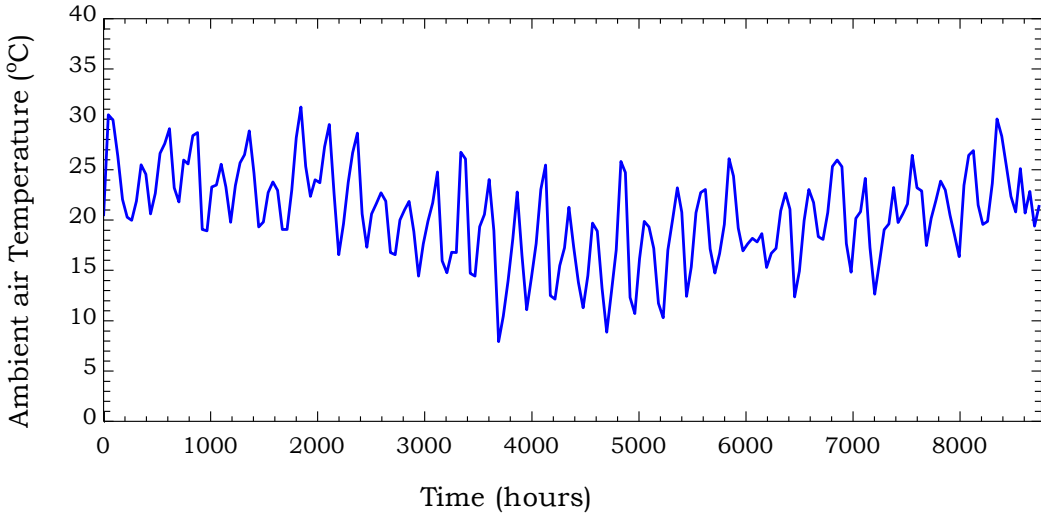


**Figure 1** Predicted annual ambient air temperature hourly distribution per year

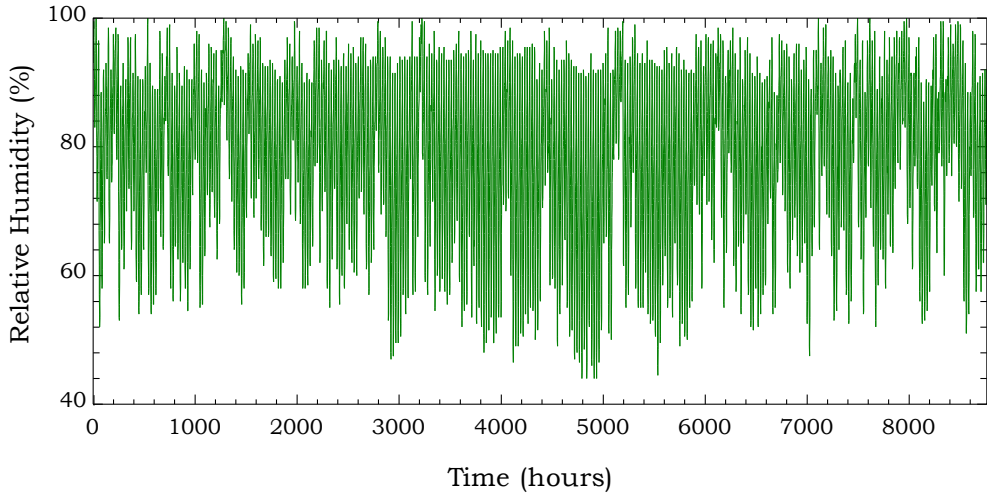


**Figure 2** Predicted annual relative humidity hourly distribution

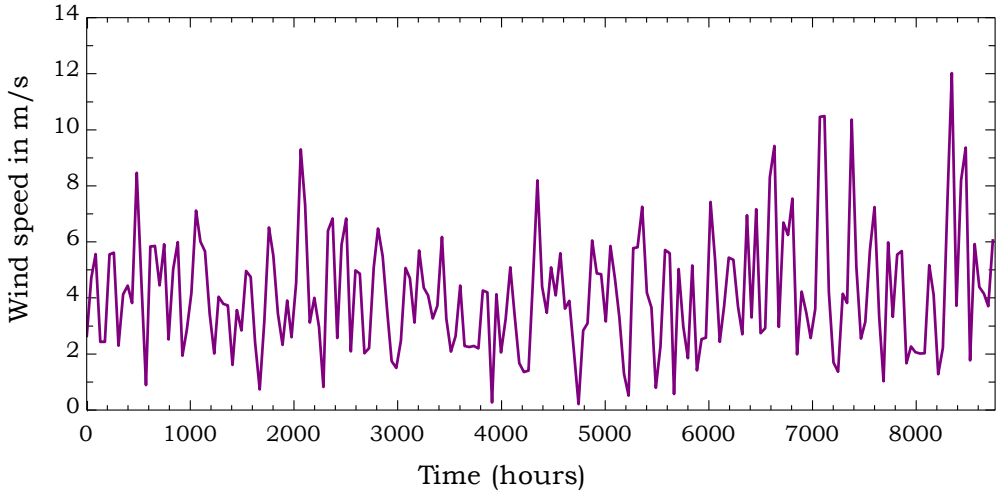


**Figure 3**. Predicted annual wind speed hourly distribution

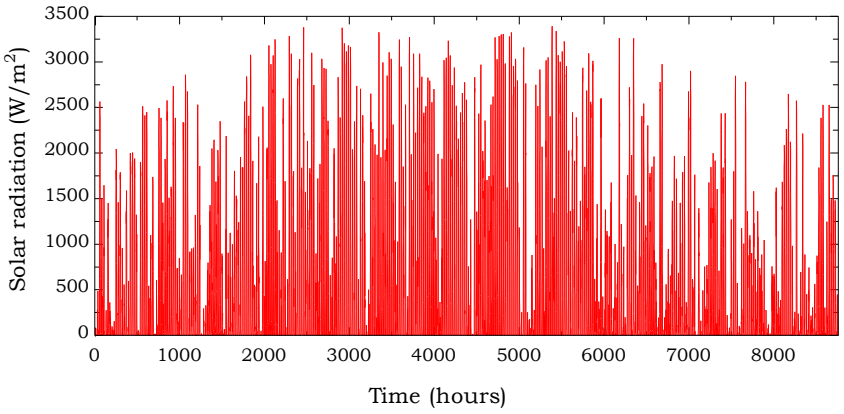


**Figure 4** Predicted annual total solar radiation hourly distribution

The data was subsequently evaluated qualitatively in terms of frequency of occurrence of different phases of the parameters as measured and predicted. The MMC model outputs were then contrasted with the probability ranges for the actual measured values. Figure 5 presents the comparisons of MMC predicted and actual weather data statistics on long term range. The individual probability comparisons are presented in Figures 5a, 5b, 5c and 5d for solar radiation, ambient temperature, wind speed and relative humidity respectively. From the analysis, the deviations of the predicted probabilities from the actual were 0.53 %, 0.5 %, 0.2 % and 0.16 % respectively, thus depicting great accuracy of the model.

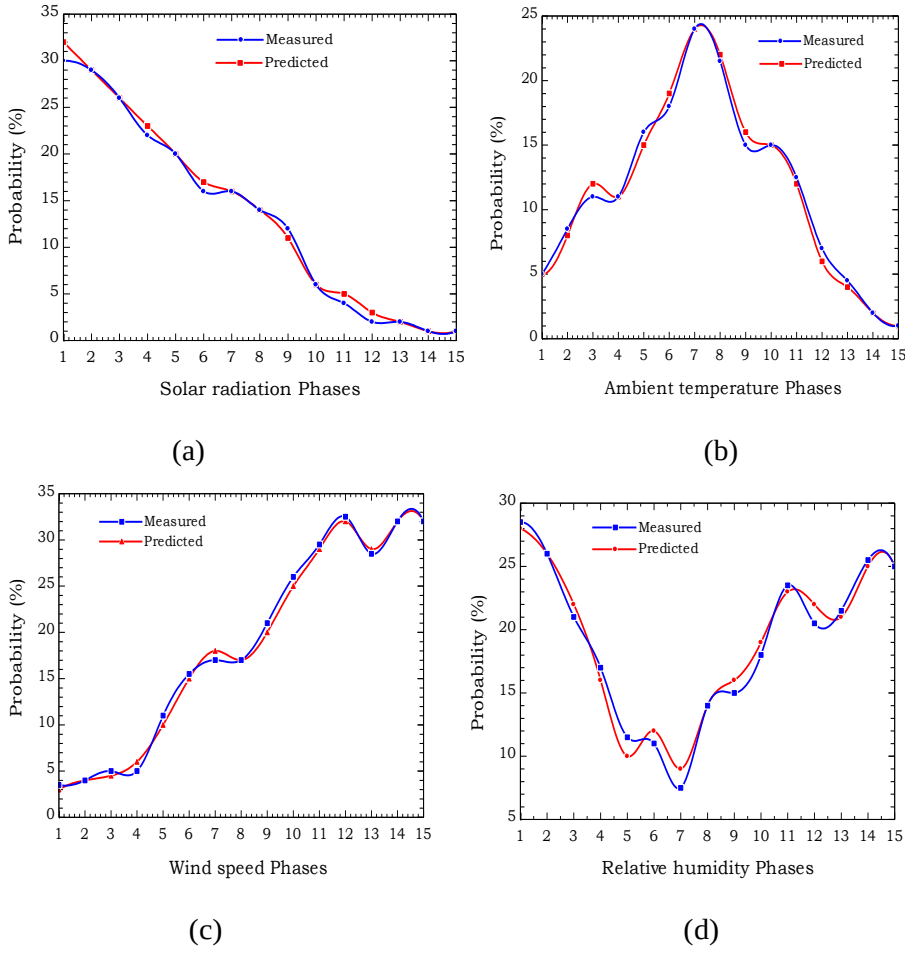


**Figure 5** Comparison of measured and MMC predicted probability distributions for (a) Solar radiation (b) Ambient temperature (c) Wind speed and (d) Relative humidity.

A more detailed comparison of annual data in terms of annual range, average deviation as well as maximum and minimum values is tabulated in Table 1. In general, the generated data displayed similar properties to the actual data in terms of range and magnitude with below 5 % marginal error.

**Table 1** Comparison of annual measured and MMC predicted weather data for Durban South Africa.

| Parameter | Predicted | | | | Measured | | | | Variation (%) | | | |
|---|---|---|---|---|---|---|---|---|---|---|---|---|
| | AV | SD | Max | Min | AV | SD | Max | Min | AV | SD | Max | Min |
| Solar rad. ($w/m^2$) | 419.5 | 248 | 1030 | 0 | 425.8 | 249.8 | 1050 | 0 | 1.48 | 0.72 | 1.90 | 0 |
| Air temp. (°C) | 20.51 | 4.57 | 32.2 | 5.7 | 21.3 | 4.61 | 32.6 | 5.72 | 3.71 | 0.78 | 1.23 | 0.35 |
| Wind speed(m/s) | 4.121 | 2.26 | 13.55 | 0.1 | 4.232 | 2.342 | 13.94 | 0 | 2.62 | 3.71 | 2.80 | 0 |
| Air humidity ($kg/kg_{dry}$) | 78.59 | 11.87 | 100 | 44 | 80.15 | 12.1 | 94 | 42.8 | 1.95 | 1.90 | -3.09 | -2.80 |

Since the extreme weather patterns under study displayed very compact curves over the annual span, it was prudent to use a shorter span to demonstrate the relationships between the measured and predicted data. For this reason, data from the summer month of February 2018 was extracted for comparison purposes. Figure 6 shows the curves predicted and the measured solar radiation distribution. There was a precise *t* between the curves laid side by side with an average variation of 0.14 %. On the air relative humidity, a side by side comparison of the predicted and measured data profiles are presented in Figure 7. The mean variation between the two sets of curves was -0.22 %.

Figure 8 shows the variation of ambient air temperature as well as wind speeds for the said month. The MMC model precisely predicted the ambient temperature to an accuracy of -0.65 % while the wind speed was estimated with a variation of -3.4 %. In all these comparisons the values fall far below the 5% limit and similar proportionate variations were cascaded through the year. These low values demonstrated that the MMC predicted values of the weather parameters generally matched the corresponding measured data with great accuracy.

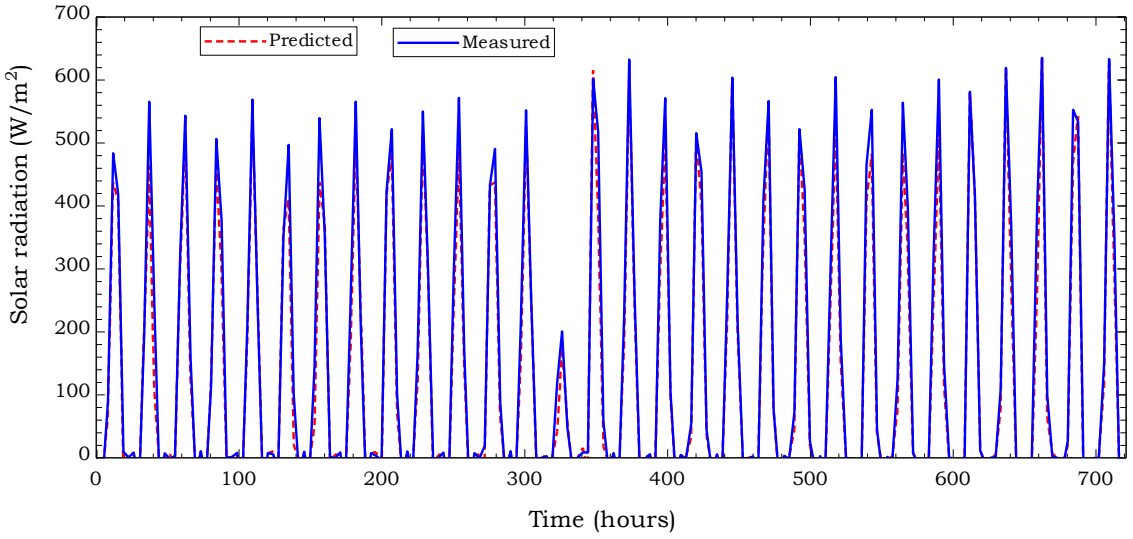


**Figure 6** Comparison between predicted and actual solar radiation hourly distribution for the month of July

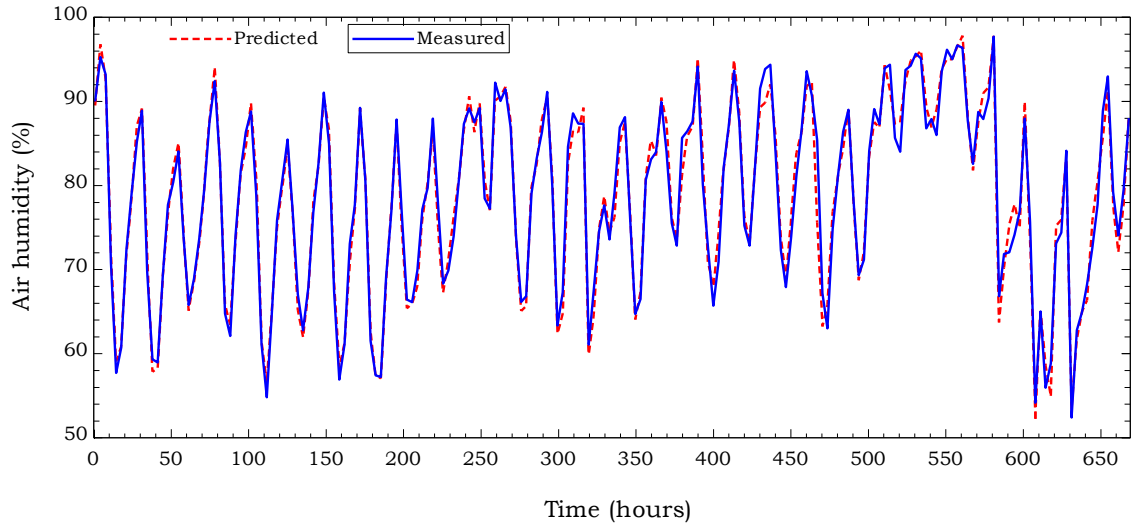


**Figure 7** Comparison between predicted and actual air humidity hourly distribution for the month of February

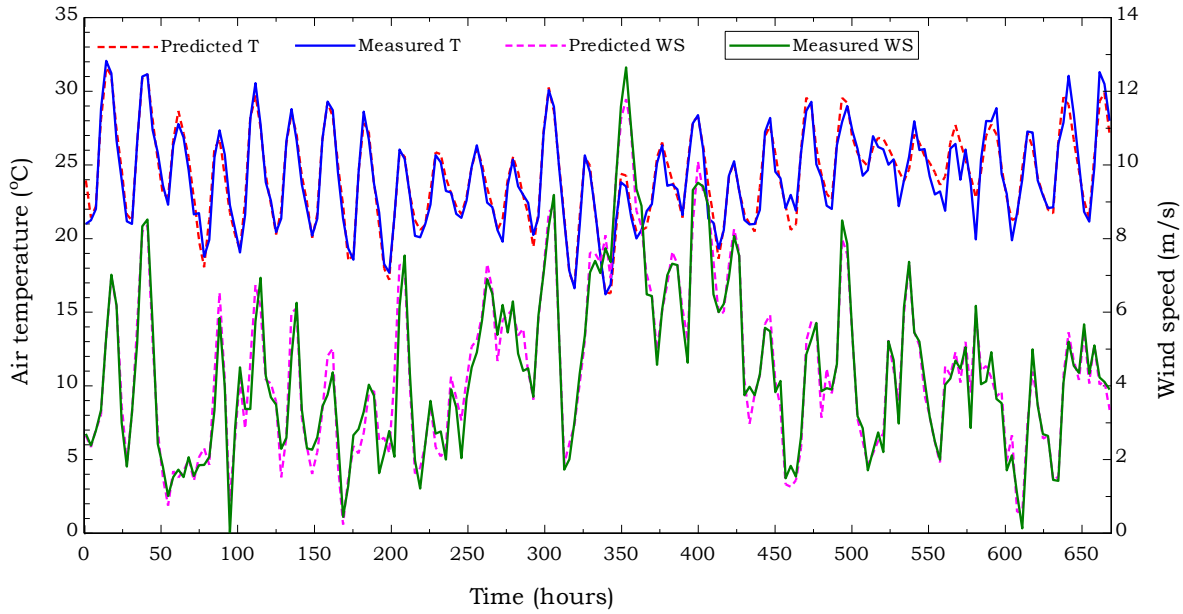


**Figure 8** Comparison between predicted and actual air humidity hourly distribution for the month of February

## 5. CONCLUSION

In this study, the theoretical modelling of MMC has been concisely presented and implemented in order to make the structure more understandable. A stochastic methodology was used to develop a higher-order multivariate Markov chain model incorporating a feedback loop with the capability of linking the observed states and the interdependence of parameters. The higher-order MMC model was then used to generate yearly weather data for application in simulation of energy systems comprising multiple weather characteristics over a long period of time.

The first order MMC was extended to a higher-order to include the long-range dependent sequences. Consequently, the number of categorical consequences were increased to obtain a distinctive and realistic estimation of weather patterns and how the parameters depend on each other. The number of phases in an occurrence was also increased to obtain as many data points as possible to the tune of the second interval to enhance accuracy.

The governing probability matrices of the measured and predicted parameters were developed as higher-order stochastic equations that provided a more effective method of estimation of model parameters. Since the MMC model is computationally simple and can reliably be implemented, the number of parameters to be estimated were equally increased with ease compared to the number earlier considered in [14]. An algorithm founded on non-negative matrix factorization and multilevel optimization was developed to estimate the unknown parameters depending on little information.

The hourly distribution of solar radiation, air temperature, air humidity and wind speeds were generated and compared to the actual measured data from a weather station. The predicted annual averages for solar radiation, air temperature, wind speed and air humidity were 419.5 W/m2, 20.51 °C, 4.121 m/s and 78.59 kg/kgdry respectively. Subsequently, the respective mean measured values were 425.8 W/m2, 21.3 °C, 4.324 m/s and 80.15 kg/kgdry. The percentage variations between the measured and predicted values were 1.48 %, 3.71 %, 2.67 % and 1.95 % respectively. All these values of percentage deviations were below 5 % implying that the higher-order MMC model estimated the corresponding parameters with great accuracy.

Higher-order MMC model in comparison to first-order MMC give a more precise prediction of categorical sequences due to computational accuracy and efficient application. The increased number of parameters and constants in this study helped to create a new MMC model of a higher order. The outcomes imply that higher-order MMC replicates the actual weather data with great accuracy. Stochastically generated artificial weather parameters can reliably be implemented in the study of the solar energized system of liquid desiccant dehumidification and regeneration. By increasing the number of sequential categories of data, it is possible to gain more explicit results and precise prediction of the sequences influencing each other. The higher-order MMC model is more truthful when the number of phases in a sequence is increased because more data is generated.

## REFERENCES

[1] Aly, A. A, Zeidan, E. B, and Hamed, A. M. Solar Powered Absorption Cycle Modelling with Two Desiccant Solutions. *Energy Conservation and Management*, **51**, 2011; pp. 2768-2776.

[2] Marion, W. and Urban, K. User's Manual for TMY2s (Typical Meteorological Years) - Derived from the 1961-1990 National Solar Radiation Data Base. *NREL Report No. TP-463-7668*. 1995. http://rredc.nrel.gov/solar/publications

[3] Marion, W. and Urban, K. New Typical Meteorological Year Data Sets. In: Campbell-Howe, R., Wilkins-Crowder, B., eds. Solar '95: Proceedings of the 1995 American Solar Energy Society Annual Conference, 15-20 July 1995, Minneapolis, Minnesota. NREL Report No. 20077.Boulder, CO: American Solar Energy Society, 1995, pp. 220-225.

[4] Marion, W. New Typical Meteorological Years and Solar Radiation Data Manual. PV Radio- metric Workshop Proceedings, 24-25 July 1995, Vail, Colorado. NREL/CP-411-20008 pp. 171-178. Acc. No. 16760. Golden, CO: National Renewable Energy Laboratory, 1995.

[5] Meteotest, Meteonorm handbook, Parts I, II and III. Bern, Switzerland: Meteotest, 2003. http://www.meteotest.ch

[6] Chan, A. L. S., Square, K. F. F., and John, Z. L. Generation of Typical Meteorological Year for Hong Kong. *Energy Conversion and Management*, **47**, 2006, pp. 87-96.

[7] Yang, H. and Lu, L. The Development and Comparisons of Typical Meteorological Years for Building Simulation and Renewable Energy Applications. *ASHRAE Trans*, 2004; **110**(2), pp. 424-431.

[8] Drury, B. C. and Linda, K. L. Rethinking the TMY: is the 'Typical' meteorological year best for building performance simulation? In: *Proceedings of BS2015: 14th Conference of International Building Performance Simulation Association*, Hyderabad, India, Dec. 7-9, 2015, pp. 2655-2662.

[9] Yang, H., Yutong, L., Lin, L. and Ronghui, Q. First-Order Multivariate Markov Chain Model for generating annual weather data for Hong Kong. *Energy and Buildings,* **43**, 2011, pp. 2371-2377.

[10] Maafi, A. Markov models in discrete time for solar radiation. In: *Proceedings of Multiconference on Computational Engineering in Systems Applications (IMACS-IEEE),* Nabeul-Hammamet (Tunisia), 1998, pp 319-322.

[11] Shamshald, A., Bawadi, M. A., Wan Hussin, W. M. W., Majid, T. A. and Sanusi, S. A. M. First and Second-Order Markov Chain Models for Synthetic Generation of Wind Speed Time Series, *Energy*, **30**, 2005, pp. 693-708.

[12] Ching, W. K., Ng, M. K., Fung, E. S. Higher-Order Multivariate Markov Chains and their Applications. *Linear Algebra and its Applications,* **428**(2), 2008, pp. 492-507.

[13] Ching, W. and Fung, E. M, A Multivariate Markov Chain Model for Categorical Data Sequences and its Application in Demand Prediction. *IMA Journal of Management Mathematics,* **13**, 2002, pp. 187-199.

[14] Yutong, L. and Yang, H. First Order Multivariate Markov Chain Model for Generating Synthetic Series of Weather Data to Evaluate the Performance of Open Cycle Desiccant Air Conditioning System. *Proceedings of the 12th International Refrigeration and Air Conditioning Conference*, Purdue University, West Lafayette, Indiana, July 4-7, 2008.

[15] Wang, C., Huang, T. Z. and Ching, W. K. A New Multivariate Markov Chain Model for Adding a New Categorical Data Sequence. *Mathematical Problems in Engineering,* 2014 https://dx.doi.org/10.1155/2014/502808

[16] Raftery, A. A Model of High-Order Markov Chains. *Journal of Royal Statistic Society,* **47**, 1985, pp. 528-539.

[17] Raftery, A. and Tavare, S. Estimation and Modelling Repeated Patterns in High Order Markov Chains with the Mixture Transition Distribution Model. *Applied Statistics*, **43**, 1994, pp. 179-199.

[18] Ching W., Fung, E. M, and Ng. M. A Higher-Order Markov Chain Model for Categorical Data Sequences. *International Journal of Naval Research Logistics,* **51**, 2004, pp. 557-574.

[19] Zhu, D., Ching, W., Elliott, R. J., Siu, T. K. and Zhang, L. A. Higher-order Interactive Hidden Markov Model and its Applications. *OR Spectrum,* **39**(4), 2017, pp. 1055-1069.

[20] Ching W., Fung, E., Ng. M., Siu, T and Li, W. A. Interactive hidden Markov models and their applications. *IMA Journal of Management Mathematics,* **18**, 2004, pp. 85-97.

[21] Lin C. Projected Gradient Method for Non-Negative Matrix Factorization. *Neural Computation*, **19**, 2007, pp. 2756-2779.

[22] Bard, J. F. Practical Bi-Level Optimization: Algorithms and Applications. Dordrecht: Kluwer Academic Publishers, 1998.

# Chapter5

## Interfacial heat and mass transfer analysis in solar-powered, packed-bed adiabatic liquid desiccant regeneration for air conditioning

This section offers a complete presentation of the theoretical interfacial heat and mass transfer occurrence in a solar-powered adiabatic liquid desiccant regenerator filled with Mellapack packing. A solar energy model fed with artificial weather characteristic inputs generated in chapter 3 as well as an analytical thermal model was developed to analyse the interfacial interaction between air and LiBr desiccant solution. The performance was analysed in terms of moisture removal rate and effectiveness attaining exciting outcomes. The content of this chapter was published in the Q1-rated International Journal of Low carbon Technologies, volume 13, June 2018.

**Andrew Y A Oyieke**, Freddie L Inambao; (2018) Interfacial heat and mass transfer analysis in solar-powered, packed-bed adiabatic liquid desiccant regeneration for air conditioning, *International Journal of Low-Carbon Technologies*, Vol 13, Issue 3, pp. 277-285, Available at: (https://doi.org/10.1093/ijlct/cty029)

# Interfacial heat and mass transfer analysis in solar-powered, packed-bed adiabatic liquid desiccant regeneration for air conditioning

Andrew Y. A. Oyieke* and Freddie L. Inambao
*Discipline of Mechanical Engineering, University of KwaZulu-Natal, Mazisi Kunene Road, Glenwood, Durban 4001, South Africa*

## Abstract

In this article, a hybrid photovoltaic–thermal (PV/T) module generating both electrical and thermal energy simultaneously has been used in a closed-cycle system to provide regeneration heat via a dynamic solar radiation model as well as electrical power relative to location, time of the day and day of the month. Electrical power generated drives the air fan, water and solution pumps, while the thermal component is used for desiccant's regeneration. This combination enhances energy efficiency of the air conditioning system. A simplified analytical model of the complex occurrence of coupled heat and mass transmission phenomenon in liquid desiccant regeneration system powered by a hybrid PV/T module is developed. The interfacial air–desiccant interaction in a structured packing vertical column using lithium bromide solution and Mellapak was analysed. The resulting differential equations are solved simultaneously using separative evaluation and step-by-step iterative procedure. The system's performance was projected with regeneration effectiveness, subject to varying temperatures of air and desiccant solution, moisture content and mass flow rate. It was established that subject to the prevailing local weather conditions, the PV/T module significantly raised desiccant temperature to a high of 67.22°C good enough for the regeneration process. The regeneration rate and effectiveness improved with upsurge in mass flow rate but reduces with a rise in humidity ratio. The optimum flow mix for effective regeneration was therefore established to be 0.847 and 0.00331 kg/min for air and desiccant solution, respectively, for maximum effectiveness of 69.3%. The liquid desiccant solution concentration increased by 30% during when solar radiation peak hours. The obtained theoretical outcomes matched with experimental results from the available literature show a permissible discrepancy of within ±20%, largely due to the fact that the simulation parameters were not the same as the prevailing experimental conditions.

*Keywords:* liquid desiccant; regeneration; solar energy; photovoltaic/thermal; air conditioning

*Corresponding author:
youngoyieke@yahoo.com

Received 26 January 2018; revised 4 June 2018; editorial decision 18 June 2018; accepted 21 June 2018

## 1 INTRODUCTION

The urgent need for energy efficiency coupled with environmental consciousness in air conditioning systems has in the recent decade, drawn attention towards liquid desiccant dehumidification and regeneration. As an innovative substitute technology to conventional vapour-compression systems, liquid desiccant air conditioning systems (LDACS) have currently gained prominence in both domestic and industrial applications due to its ability to use low-grade industrial waste heat as well as renewable sources like solar energy. The inception of solar-powered LDAC system dates back to 1980s, pioneered by Lof *et al.* [1]. Since then, the popularity of solar-powered LDACS has stepped up 3-fold with numerous advances made with emphasis in feasibility, use, energy intake and economic analysis [2].

Solar-powered desiccant schemes are categorized as closed- or open-loop configurations. A chilling unit is built in a closed-loop system utilizing water as a heat transfer medium to the desiccant. On the other hand, water is supplied from external source in an open cycle and is used as the refrigeration agent, hence replacing the need for energy-intensive condenser [3].

International Journal of Low-Carbon Technologies 2018, 1–9

doi:10.1093/ijlct/cty029

The advances of the LDAC technology was demonstrated in the experimental study by Gommed and Grossman [4] on the use of solar energy in liquid desiccant dehumidification and cooling. On the feasibility and economic analysis of solar application in LDAC systems, Li and Yang [5] and Halliday *et al.* [6] presented an open-cycle dehumidification in Hong Kong and UK environments, respectively. More recently, Aly *et al.* [3] used Matlab to simulate an open-cycle solar-powered, two-desiccant system. Closed-cycle systems of solar-powered desiccant regeneration are not so common and have very limited literature. In addition, the application of a hybrid photovoltaic and thermal (PV/T) module brings a new dimension to this technology. Direct solution regeneration through a solar collector in which the desiccant solution is the heat collecting medium has been demonstrated to be more effective compared to indirect systems [7].

This article presents a simplified theoretical breakdown of interfacial heat and mass transfer characteristics of an autonomous and self-sustainable liquid desiccant regenerator powered by PV/T collector in a closed loop through computer modelling. The theoretical models for solar radiation, solution side mass transfer, heat transfer as well as the pressure drop on the airside are developed and used to establish the influence of inlet properties of both air and desiccant solution on the regenerator effectiveness (e.g. temperatures, humidity ratio and mass flow rate) for near-zero carry-overs.

## 2 LDAC SYSTEM

A graphic illustration of a typical hybrid solar PV/T-powered LDAC system considered for this analysis is presented in Figure 1. The arrangement is made up of three major units; the dehumidifier within which strong desiccant solution is spewed from the top of a packed vertical column, while air blown from the bottom mixes with the desiccant crystals in a counterflow pattern. Strong/concentrated desiccant solution absorbs water vapour from humid air as they come into contact.

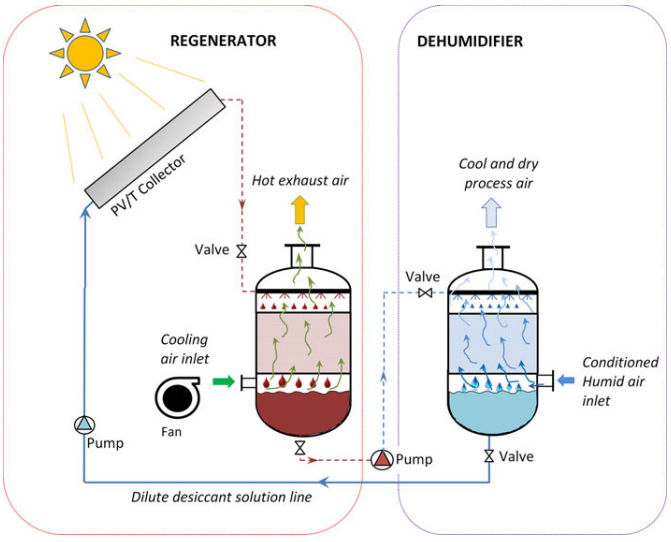


**Figure 1.** *Graphical illustration of a solar-powered direct liquid desiccant regeneration and dehumidification scheme.*

The regenerator functions in a similar manner as the dehumidifier except for heated dilute solution crystals flowing from the topside of a packed-bed vertical column where a counterflow interaction is initiated with stream of air from the bottom. The interaction results in evaporation of water molecules leaving in a strong desiccant liquid at near-initial concentration ready for recirculation in the dehumidifier.

The third unit is the hybrid PV/T collector in which both electrical power and thermal energy are generated subject to prevailing solar radiation. The PV unit converts solar radiation into electrical energy used to drive the air fans and solution pumps, while residual heat energy is absorbed and transferred to the weak/dilute desiccant solution circulating through the tubes attached to the absorber plate. The solution leaves the collector at raised temperatures. At this state, it becomes difficult to hold water vapour and is pumped to the regeneration column. Theoretical analysis was only limited to the solar radiation and interfacial interaction amongst the liquid desiccant and air in the regeneration process. The interactions in dehumidification process were not considered in this study but provided merely for easy understanding and completeness of the concept.

## 3 PERFORMANCE ANALYSIS

The performance index used for regenerator analysis was the specific effectiveness ($\varepsilon_r$) defined as:

$$\varepsilon_r = \frac{\omega_i - \omega_o}{\omega_i - \omega_e} \tag{1}$$

where $\omega_i$, $\omega_o$ and $\omega_e$ are air humidity ratios at inlet, outlet and equilibrium settings, respectively.

Equilibrium air humidity ratio was evaluated in terms of atmospheric, $p_a$ and partial vapour $p_d$ pressures of air and bulk fluid, respectively, using the following relationship.

$$\omega_e = 0.622\frac{p_d}{p_a - p_d} \tag{2}$$

According to Montieth and Unsworth [8], partial vapour pressure was further given by Teten's equation as follows:

$$p_d = 0.61078\exp\left(\frac{17.27T}{T + 237.3}\right) \tag{3}$$

where $T$ is the temperature of desiccant solution.

### 3.1 Solar energy model

The surface total incident solar radiation $G_T$ was evaluated with respect to time and day of the year and location as a function

of direct, diffuse and reflected beam radiation. The relationship adopted from the study of Aly *et al.* [3] is applied, thus,

$$G_T = R_b G_{bn} + \frac{CG_d(1 + cos\varphi)}{2} + (G_{bn} + G_d)\frac{(\Upsilon_g)(1 + cos\varphi)}{2} \quad (4)$$

where $G_b$ is the horizontal surface beam radiation, $R_b$ is the beam radiation tilt factor, $G_d$ is the diffuse sky radiation, $\varphi$ is the surface tilt angle taken to be 35°, while $\Upsilon_g$ is the ground reflectance whose value depends on the surface texture. $C$ is the diffuse radiation factor determined by Becker [9] as follows:

$$C = 1 + 0.11 \times cos(n - 15) \times 2\pi/365 \quad (5)$$

where $n$ is the number of $i$th days during the year under consideration.

The expression for beam radiation on horizontal surface $G_b$ *was* established as

$$G_b = G_{bn}\, cos\Phi \quad (6)$$

where $\Phi$ is the solar altitude angle and $G_{bn}$ is the incident beam radiation normal to the module surface on a clear day computed as a function of the solar altitude angle using the following expression:

$$G_{bn} = 1366.1\left\{1 + 0.033\, cos\left(\frac{360\iota}{365}\right)\right\} exp\left(-\frac{31}{sin\Phi}\right) \quad (7)$$

Additionally, diffuse solar radiation $G_d$ was estimated as:

$$G_d = 0.5(1 + cos\varphi)CG_{bn} \quad (8)$$

The altitude angle $\Phi$ was evaluated in terms of the latitude $L$, hour and declination angles all in a simplified expression as follows:

$$sin\Phi = sin\, L\, cos\, A + cos\, L\, cos\, A\, cos(\pm 0.25\Gamma) \quad (9)$$

where $A = (23.45\, sin\{360/365(248 + \iota)\})$

The $\pm$ implies negative and positive values of the hour angle in the morning and afternoon, respectively, while $\Gamma$ is the quantity of time in minutes, before or after confined solar noon at a particular time in consideration.

As defined in [3], the beam radiation tilt factor was formulated as the ratio of sunbeam heat on slanted and flat surfaces respectively. This relationship was further simplified and expressed as:

$$R_b = \frac{sin(L - \varphi)cos\, A + cos(L - \varphi)cos\, A\, cos(\pm 0.25\Gamma)}{sin\, L\, cos\, A + cos\, L\, cos\, A\, cos(\pm 0.25\Gamma)} \quad (10)$$

Since the main focus of this analysis was on the thermal energy component generated by the PV/T collector, the electrical energy element has not been detailed. Hence, from the total solar radiation on the collector surface, the overall heat energy available to the solution in the collector was expressed as follows:

$$G_c = G_T\{(1 - \rho)\tau\alpha - (\tau\alpha - \tau_{pv}\eta_{el})\} \quad (11)$$

where $\rho$, $\tau$, and $\alpha$ are the reflectance, transmittance and absorptance of the collector glazing and PV cells attached directly to the absorber plate, respectively. $\eta_{el}$ represents the PV/T module electrical efficiency. Therefore, taking heat energy balance for the hybrid PV/T collector, an expression was then derived as follows:

$$G_c dx = \dot{m}_a dh_a + \dot{m}_d dh_d + U_L(T_d - T_{amb}) + mh_{fg} \quad (12)$$

where $\dot{m}_a$ and $\dot{m}_d$ are air and desiccant mass flow rates, respectively, in kg/s; $h_a$ and $h_d$ are air- and desiccant-specific enthalpies, respectively, in J/kg; $m$ is the quantity of water evaporated in kg; $h_{fg}$ is the hidden heat of vaporization of water in J/kg, $U_L$ is the overall heat loss coefficient in W/m$^2$K, $T_d$ and $T_{amb}$ are the desiccant and ambient temperatures, respectively, in °C.

Likewise, the air stream energy equilibrium entering the regenerator was also derived as follows:

$$\dot{m}_a dh_a = \vartheta_a(T_d - T_a)dx - \vartheta_d(T_a - T_{amb})dx \quad (13)$$

where $\vartheta_a$ and $\vartheta_d$ are the heat transfer coefficients of air and desiccant, respectively.

## 3.2 Mass transfer

Considering a unit volume and cross section of a counterflow packed column differential segment presented in Figure 2, heat and mass exchange process occurring at the air–desiccant solution interface can theoretically be analysed based on the derivations of [2], [10], and [11].

The regeneration process was considered adiabatic and hence, negligible liquid-phase heat flow resistance was experienced. Taking both heat and mass transfer to happen in crosswise directions of air–desiccant flow on a uniform area throughout the interface, correlations and differential equations were derived

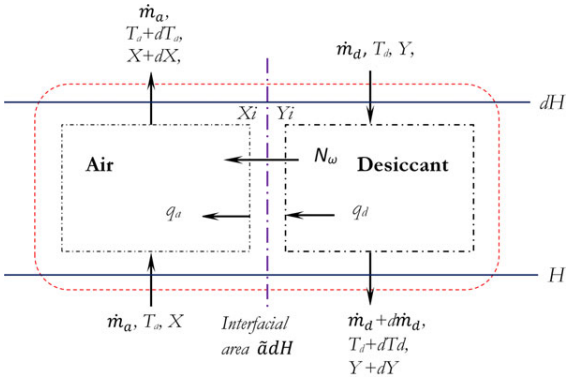


**Figure 2.** *Differential section of air–desiccant interface.*

and solved by separative evaluation and step-by-step iterative methods.

The desiccant-specific enthalpy was expressed as the sum of solution's weakening heat $\Delta Q_{sol}$ at set point $T_{ref}$ and heat gain as follows:

$$h_d = C_{p,d}(T - T_{ref}) + \Delta Q_{sol} \tag{14}$$

where $C_{p,d}$ represents desiccant-specific heat capacity at $T$ °C. On the other hand, specific enthalpy of air was formulated as:

$$h_a = C_{p,a}(T - T_{ref}) + \omega\{C_{p,w}(T_a - T_{ref}) + Q_{w,ref}\} \tag{15}$$

where $\omega$ is the humidity ratio, $C_{p,a}$ and $C_{p,w}$ are specific of dry air and water, respectively, while $Q_{w,ref}$ is the latent heat of water at reference temperature $T_{ref}$.

From the principle of conservation of mass, the correlation for water vapour content was derived as a function of air- and liquid-phase-specific mass flow rates $\dot{m}_a$ and $\dot{m}_d$, respectively, expressed as:

$$d\dot{m}_d = \dot{m}_a d\omega \tag{16}$$

### 3.2.1 Airside

The interfacial mass transfer is expressed as a function of molecular mass $M_w$ and specific molar flow rate $N_w$ of water formulated by Babakhani and Soleymani [12] as:

$$-\dot{m}_a d\omega = M_w \tilde{a} dH \vartheta_a \ln\left[\frac{1-\beta_i}{1-\beta}\right] \tag{17}$$

The airside humidity ratio was formulated by further simplifying (17) to yield a rudimentary differential equation for as follows:

$$\frac{d\omega}{dH} = -\frac{\tilde{a} M_w \vartheta_a}{\dot{m}_a} \ln\left[\frac{1-\beta_i}{1-\beta}\right] \tag{18}$$

where $\beta$ is the moisture content in air and subscript $i$ denotes initial conditions, $\tilde{a}$ is the exact active interfacial contact area in $m^2/m^3$ of packed-bed capacity which is dependent on the stuffing arrangement and operating environments given for structured packing as:

$$\tilde{a} = a_n\left(\frac{d_p \sin\theta}{4\xi}\right)\phi_t^{1.5}\left(\frac{\rho_d g}{3\mu_d \nu_d}\right)^{0.5} \tag{19}$$

where $a_n$ is the packing material's exact surface area for each single element volume, while $d_p$ is the equivalent diameter of channel, $\theta$ is the angle of inclination of packing channels, $\xi$ represents the hollow part of dry packing and $\phi_t$ is the total liquid hold up.

The air mass transfer coefficient $\vartheta_a$ is in direct proportionality to the air mean partial pressure $P_{m,a}$, but inversely proportional to the product of temperature and universal gas constant $RT$. Considering this relationship, a mathematical expression of mass transfer coefficient was developed, thus,

$$\vartheta_a = \frac{\tau_a P_{m,a}}{RT} \tag{20}$$

The constant of proportionality is the gas-phase mass transfer coefficient $\tau_a$ which depends on Reynold's $Re$ and Prandlt $Pr$ numbers for air as was formulated by Fair and Bravo [13] for structured packing and thus,

$$\tau_a = 0.0338(\partial_a/d_p) Re_a^{0.8} Pr_a^{1/3} \tag{21}$$

where $d_p$ is the equivalent packing channel diameter and $\partial_a$ is the airside molecular diffusivity. Reynoldsnumber is given by:

$$Re_a = \frac{\rho_a d_p}{\mu_a}\left\{\frac{\nu_a}{\xi(1-\phi_t)\sin\theta} + \frac{\nu_d}{\xi\phi_t \sin\theta}\right\} \tag{22}$$

where $\nu_a$ and $\nu_d$ are the superficial velocities of air and desiccant, respectively, $\phi_t$ is the total liquid residence on packing surface, while $\theta$ denotes the inclination angle of packing channel from the vertical axis.

From [14], we obtain an expression for total liquid hold up $\phi_t$ for Mellapack structured packing as follows:

$$\phi_t = 8.66 a_n^{0.83} \nu^{1.39}\left(\frac{\mu_d}{\mu_w}\right)^{0.25} \tag{23}$$

where $\mu_d$ and $\mu_w$ are viscosities for desiccant fluid and water, respectively.

### 3.2.2 Solution side

Considering the desiccant solution side, the interfacial mass transfer was found by the following correlation:

$$N_d = \vartheta_d \ln\left[\frac{1-\psi}{1-\psi_i}\right] \tag{24}$$

where $\psi$ and $\psi_i$ are the solution's bulk and interfacial preoccupation in water, while $\vartheta_d$ is the desiccant solution's mass transfer factor given as:

$$\vartheta_d = \varrho_d\left(\frac{\rho_d}{\tilde{M}_d}\right)\tilde{\psi} \tag{25}$$

where $\tilde{\psi}$ is the mean solution's molar salt preoccupation, $\tilde{M}_d$ is the desiccant's mean molar mass and $\varrho_d$ is mass transfer factor in liquid phase in structured packing derived from the study of Fair and Bravo [13] as a function of molecular diffusivity of the desiccant fluid $\partial_d$ given by:

$$\varrho_d = 2\sqrt{\{\partial_d \nu_d/\xi\phi_t \sin\theta\}\, 1/\pi d_p} \tag{26}$$

For equilibrium conditions, the exact airside interfacial mass transfers must be equal to those of desiccant side, therefore,

taking the mass balance at the interface, the airside interfacial molar mass strength in water $\beta_i$ was found by:

$$\beta_i = [1 - (1 - \beta)]\left\{\frac{1 - \psi}{1 - \psi_i}\right\}^{\vartheta_d/\vartheta_a} \tag{27}$$

This Equation (27) was then solved concurrently with air–desiccant equilibrium equation by an iterative procedure while taking the molar mass concentration $\beta$ as dependent on the humidity ratio given by the expression:

$$\beta = \frac{\omega}{\omega + M_w/M_a} \tag{28}$$

### 3.3 Heat transfer

The coupled nature of heat and mass transfer processes confirms they happen simultaneously. However, for ease of understanding, analysis of heat transfer was performed separately on the respective phases of air and liquid. The simultaneous airside interfacial sensible heat flow $q_a$ was formulated as a function of bulk air and interfacial temperatures $T_a$ and $T_i$, respectively, by taking the thermal energy balance on the airside:

$$q_a \tilde{a} dz = \sigma'_a \tilde{a}(T_a - T_i)dz \tag{29}$$

where $\acute{\sigma}_a \tilde{a}$ is the simultaneous heat transfer factor for air obtained from Ackermann correction in [15] and given as:

$$\sigma'_a \tilde{a} = \frac{-\dot{m}_a Cp_w d\omega/dH}{\left\{1 - exp\left(\frac{\dot{m}_a Cp_w d\omega / dH}{\alpha_a \tilde{a}}\right)\right\}} \tag{30}$$

where $\alpha_a$ denotes the airside heat transfer factor which was formulated for structured packing as:

$$\alpha_a = 0.0338(k_a/d_d) Re_a^{0.8} Pr_a^{1/3} \tag{31}$$

where $k_a$ is the airside thermal conductivity. Therefore, taking the thermal energy balance on the airside, we obtained

$$\begin{aligned} \dot{m}_a h_a - \dot{m}_a(h_a + dh_a) \\ + \dot{m}_a \omega \{C_{p,w}(T_a - T_{ref}) + Q_{w,ref}\} \\ = \sigma'_a \tilde{a}(T_a - T_i)dH \end{aligned} \tag{32}$$

But the enthalpy of air was taken to vary across the differential element according to the following expression.

$$\begin{aligned} dh_a = C_{p,a} dT_a + \omega C_{p,w} dT_a \\ + \dot{m}_a \omega \{\{C_{p,w}(T_a - T_{ref}) + Q_{w,ref}\} \end{aligned} \tag{33}$$

Considering (34) and (35), a differential equation for air temperature was generated, thus,

$$\frac{dT_a}{dH} = \frac{-\sigma'_a \tilde{a}(T_a - T_i)}{\dot{m}_a(C_{p,a} + \omega C_{p,w})} \tag{34}$$

And the overall heat stability of the differential control element within the packed unit was then formulated as:

$$\dot{m}_a dh_a = \dot{m}_d dh_d + \dot{m}_a d\omega h_d \tag{35}$$

Substituting (14) and (35) into (37), we get:

$$\begin{aligned} C_{p,a} dT_a + \omega C_{p,w} dT_a \\ + \dot{m}_a \omega \{C_{p,w}(T_a - T_{ref}) + Q_{w,ref}\} \dot{m}_a \\ = \dot{m}_d \{C_{p,d} dT_d + d(\Delta Q_{sol})\} \\ + \dot{m}_a d\omega \{C_{p,d}(T_d - T_{ref}) + \Delta Q_{sol}\} \end{aligned} \tag{36}$$

However, since the variation in thermal energy for dilution $d(\Delta Q_{sol})$ is negligibly small, it was ignored and a new basic differential equation for desiccant temperature emerged as follows:

$$\begin{aligned} \frac{dT_d}{dH} = \frac{\dot{m}_a}{\dot{m}_d}(C_{p,a} + \omega C_{p,w})\frac{dT_a}{dH} \\ + \{C_{p,w}(T_a - T_{ref}) + Q_{w,ref}\}\frac{d\omega}{dH} \\ - \{C_{p,d}(T_d - T_{ref}) + \Delta Q_{sol}\}\frac{d\omega}{dH} \end{aligned} \tag{37}$$

Upholding the principle of conservation of mass in the differential volume, the expression for salt content was developed as:

$$\dot{m}_d \chi = (\dot{m}_d + d\dot{m}_d)(\chi + d\chi) \tag{38}$$

where $\chi$ denotes the desiccant content in salty solution. Consequently, a basic differential equation was obtained by substituting Eqn. (16) into (38) to give;

$$\frac{d\chi}{dH} = -\chi\left(\frac{\dot{m}_d}{\dot{m}_a}\right)\frac{d\omega}{dH} \tag{39}$$

Again Eqn. (39) was solved iteratively to obtain the concentration of the desiccant solution leaving the regenerator.

## 4 RESULTS AND DISCUSSION

Apart from design parameters that were investigated by Aly *et al.* [3] and Gandhidasan [16], the PV/T module performance in desiccant regeneration was affected by the ambient properties of air such as temperature and vapour pressure.

### 4.1 The air and desiccant solution temperatures variations

The change in solution temperature during the sunshine hours of the day under consideration is shown in Figure 3. The solution conditions at the inlet and outlet followed an expected trend, i.e. the solution left the module at a higher temperature than at entry point. The variation of temperature with respect to various flow rate levels was demonstrated. It was observed that the lower desiccant flow rates corresponded to higher temperatures due to increased residence time in the module.

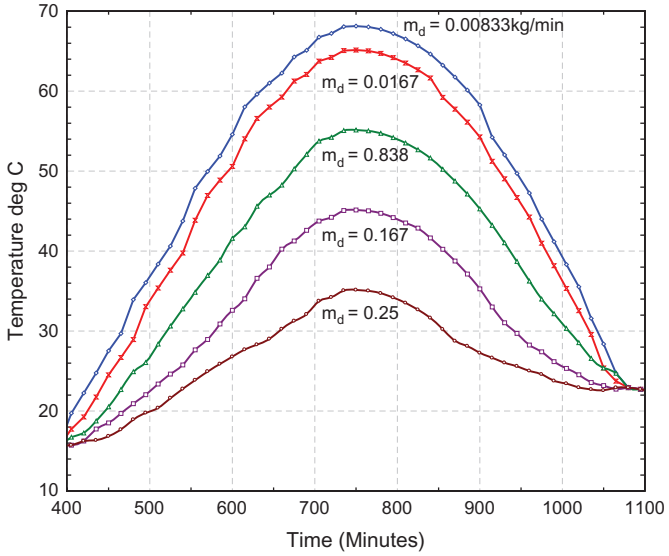


**Figure 3.** *The temperature variations of desiccant at various mass flow rates over time of day.*

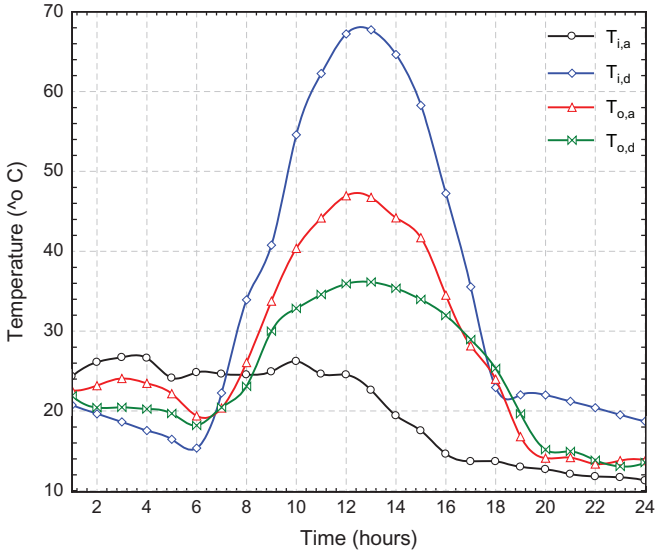


**Figure 4.** *The temperature variations of air and desiccant at entry and exit of the regenerator over time of day.*

From the previous study of Oyieke and Inambao [17], it was shown that the electrical efficiency of the PV/T module increased when a working fluid flow through and carried away residual heat. Based on this previous knowledge, apart from heating the desiccant solution, the PV/T efficiency was also kept to near maximum. Different desiccant flow rates were considered in regeneration performance evaluation. For this analysis to happen, the air flow rate $m_a$ was kept at an optimum constant value of 5.082 kg/min while varying the desiccant flow rate $m_d$. Since the mass transfer ability of desiccant solution is in direct proportionality to the water evaporation rate along the regenerator height, the mass transfer coefficient was unchanged during the iteration.

The air and desiccant temperature profiles at the regenerator entry and exit were plotted as shown in Figure 4 over a 24-h span. The desiccant solution entered the regenerator at same exit temperatures of the PV/T module. The highest inlet temperature $T_{i,d}$ exhibited was 67.22°C with a corresponding outlet temperature $T_{o,d}$ of 36.14°C at 12:30 h. However, air entered the regenerator at low temperature $T_{i,a}$ and left at elevated temperature $T_{o,a}$ signifying a gain due to the heat transfer occurrence. During 24-h day, regeneration process only occurred between 6:00 h and 18:00 h, which corresponded to the sunrise and sunset times. Outside the range of these hours, the vessel operated as a dehumidifier whose performance is not included in this work.

## 4.2 Influence of mass flow rates on regeneration effectiveness

To evaluate the influence of air mass flow rates on regenerator effectiveness, a plot is presented in Figure 5 The regeneration

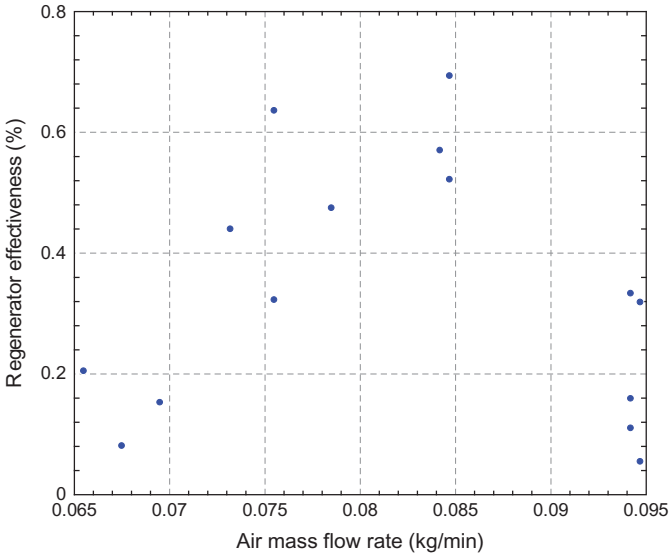


**Figure 5.** *Effect of mass flow rates of air on regeneration effectiveness.*

process occurred with the air flow rates ranging from 0.065 to 0.095 kg/min. A general observation was that effectiveness improved with the upsurge of mass flow rate. However, maximum effectiveness of 69.3% was achieved at a corresponding air flow rate of 0.0847 kg/min, beyond this value, the effectiveness begun to drop due the system's reliance on the solar energy. The maximum effectiveness was noted to occur at solar noon which on this day was seen to be at 12:30 h.

Similarly, the variation of desiccant solution's flow rate against regeneration effectiveness was plotted as shown in Figure 6. The effectiveness improved proportionally with desiccant flow rate

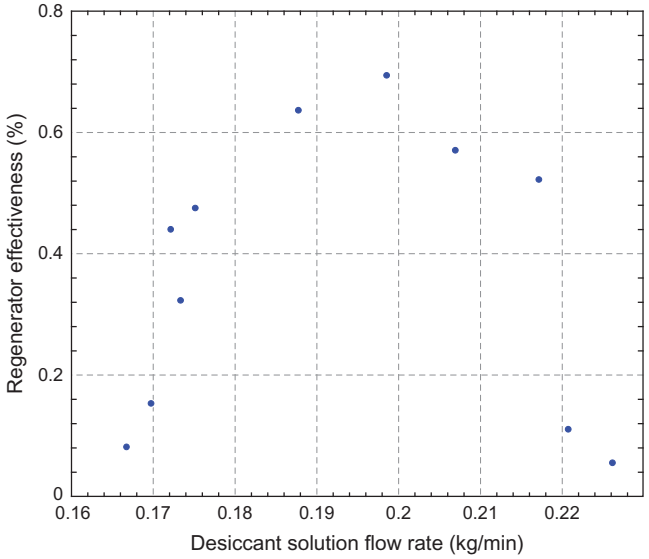


**Figure 6.** *Effect of mass flow rates of desiccant on regeneration effectiveness.*

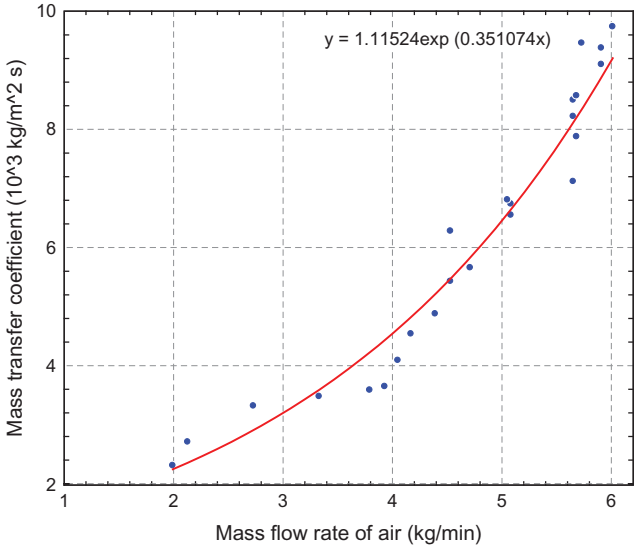


**Figure 8.** *Effect of mass flow rates of air on the overall mass transfer coefficient.*

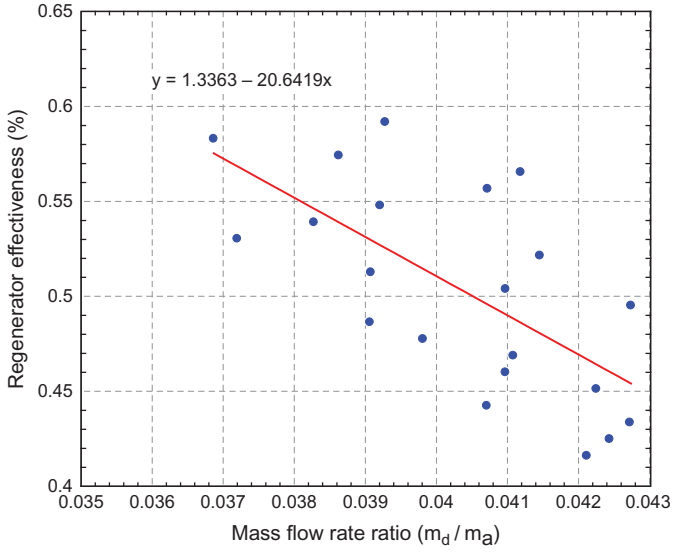


**Figure 7.** *Effect of mass flow rate ratio on regeneration effectiveness.*

like in previous case, but the maximum effectiveness was attained at a solution flow rate of 0.00331 kg/min which was below that of air. The regeneration process was observed to occur between flow rate ranges of 0.1665–0.2262 kg/min.

From these two scenarios, it was observed that maximum effectiveness was achieved at air and desiccant flow rates of 0.847 and 0.00331 kg/min, respectively. These values were taken as the optimum flow mix for effective regeneration performance of the unit. Any other values outside this combination demonstrated desiccant fluid carryover to the process air. The outlet solution concentration at this point is 82%, which is near the initial concentration, hence the confirmation of a regeneration process.

The relationship between regenerator effectiveness and mass flow rate ratio $\dot{m}_d/\dot{m}_a$ is shown in Figure 7. The effectiveness reduced with an increase in mass flow rate ratio as depicted by the negative gradient of up to 20.64. Low $\dot{m}_d$ and high $\dot{m}_a$ resulted in a low flow rate ratio, which in turn gave higher regenerator effectiveness. On the other hand, higher $\dot{m}_d$ and low $\dot{m}_a$ gave a higher flow rate ratio, which results in reduced effectiveness. Since the simulation was conducted at varying flow rates of desiccant and air at an alternating pattern, i.e. reducing one and increasing the other and vice versa, the individual instantaneous flow rate ratios appeared to be scattered but suggested a reducing trend. Therefore, it was logically concluded that for effective desiccant regeneration, the solution flow rate must be lower than the air flow rate at any instant.

## 4.3 Effect of mass flow rates on the mass transfer coefficient

The mass transfer coefficient values were calculated by an iterative procedure and the results provided in this section. As can be observed in Figure 8, the variation of overall mass transfer factor with regards to alteration of air mass flow rate was plotted. An improvement of air the mass flow rate triggered an exponential growth in overall mass transfer coefficient over the regeneration period. When air mass flow rate increased over a span of 2–6 kg/min, a corresponding increase of between 2.4 and 9.8 kg/m$^2$ in mass transfer coefficient was observed.

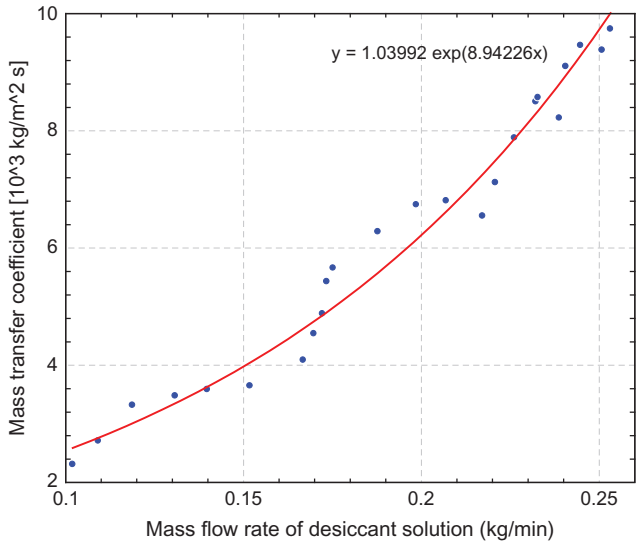


**Figure 9.** *Effect of mass flow rates of desiccant on the overall mass transfer coefficient.*

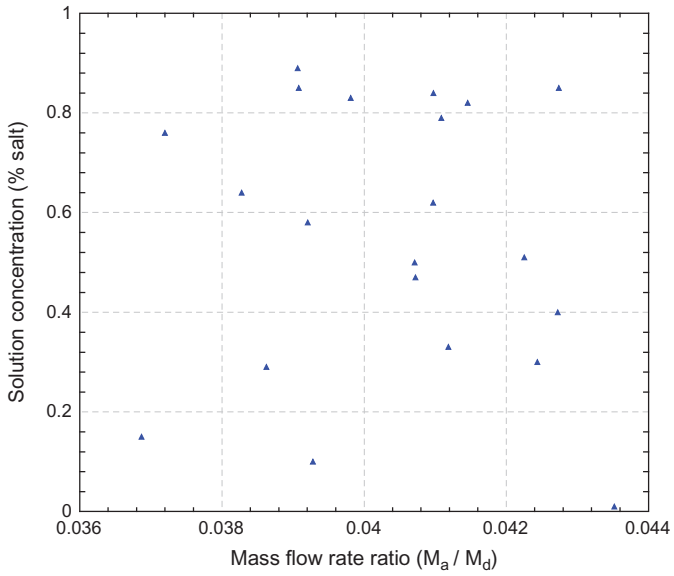


**Figure 11.** *The variation of solution concentration (**a**) during regeneration period and (**b**) with change in mass flow rate ratio.*

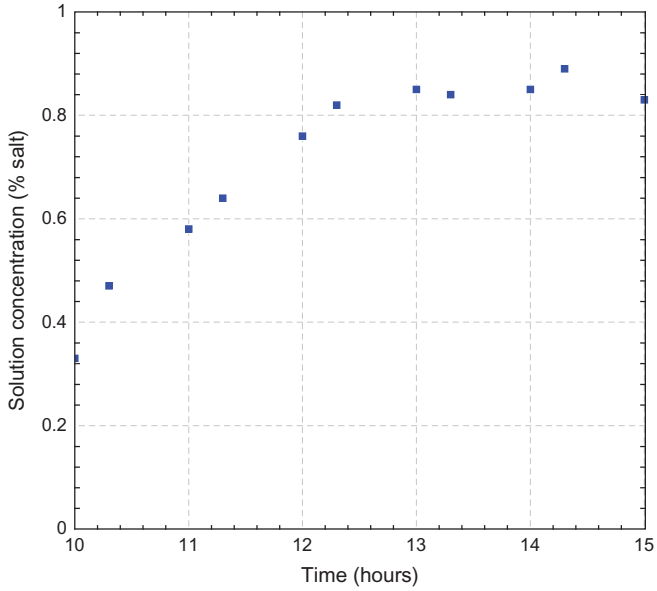


**Figure 10.** *The variation of solution concentration during regeneration period.*

Similar exponential increment of mass transfer coeffcient was realized as a result of the rise in desiccant flow rate as presented in Figure 9. When desiccant solution's flow rate varies between the range of 0.1 and 0.25 kg/min, mass transfer factor improves from 2.18 to 9.0 kg/m$^2$. This steep alteration in mass transfer factor is because of rapid rate desiccant crystallization, thus increasing the air–desiccant interfacial surface area for mass transfer.

The variation of solution concentration during the active regeneration period is shown in Figure 10. The liquid desiccant sollution at the initial concentration level of 50% was monitored during the solar peak hours from 10.00 to 15.00 h when solar radiation was at its highest. The final concentration achieved was 82%, this showed an increase of 30%. A corresponding escalation of the relative mass of water vapour per kilogram of solution of the same proportion was also realized.

However, with respect to the mass flow rate ratio, it was observed that there was an uphazard distribution with a slight reduction in concentration with an increase in the mass flow rate ratio as depicted in Figure 11. Generally, for the individual flow rates of air and desiccant, there was a negligible change in concentration with higher desiccant flow rates, while significant increase was seen with an increase in air flow rates.

## 4.4 Assessment of predicted and experimental outcomes

The average relative deviation between investigational and hypothetical outcomes are evaluated based on average deviation, Equation (40). It was realized from the existing literature that the application of PV/T in air conditioning was not a common phenomenon and had virtually not been documented prior to this study. Hence, to check the trend of some selected parameters, existing experimental results by Zhang et al. [18] were used for validation. The comparison of heat transfer coefficients predicted in this article and experimental values showed an average deviation within the range of ±20% as shown in Figure 12. This deviation is largely due to the fact that the simulation parameters were not the same as the prevailing experimental conditions. However, better results would be

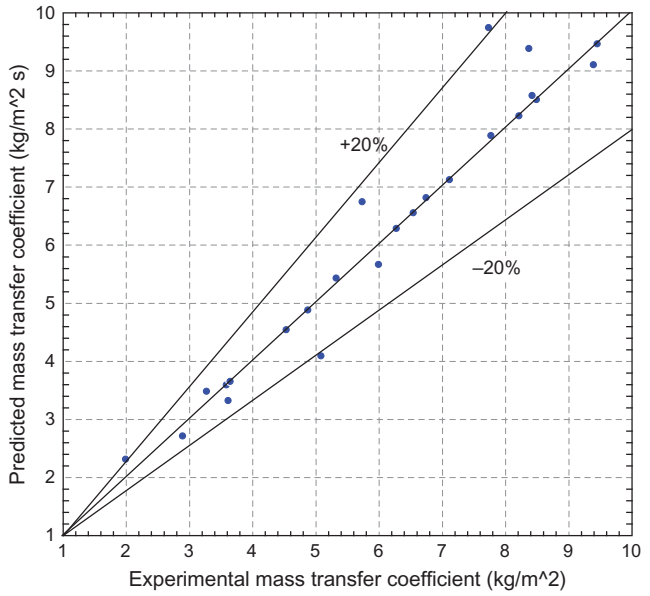


**Figure 12.** *Predicted vs experimental mass transfer factors for the regenerator.*

envisaged if experimental data for PV/T existed in the same location considered for the simulation.

$$ARD = \frac{1}{n}\sum_{i=1}^{n}\left|\frac{\varepsilon_{exp} - \varepsilon_{th}}{\varepsilon_{exp}}\right| \times 100\% \qquad (40)$$

## 5 CONCLUSION

This article has dealt with a theoretical analysis of desiccant regeneration system powered by solar energy via a hybrid PV/T. From the air and desiccant temperature profiles at entry and exit of the regenerator, the highest inlet temperature attained was 67.22°C with a corresponding outlet temperature of 36.14°C. This difference demonstrated that PV/T module could significantly raise desiccant temperature to required levels for regeneration process. The regenerator effectiveness improved proportionally with air and desiccant mass flow rates. However, the maximum effectiveness of 69.3% was achieved at a corresponding air flow rate of 0.0847 kg/min, beyond this value, the effectiveness begun to drop due the system's reliance on the solar energy. The optimum flow mix for effective regeneration was therefore established to be 0.847 and 0.00331 kg/min for air and desiccant solution, respectively. The liquid desiccant solution increased by 30% during peak hours when solar radiation was at its maximum. The final concentration achieved was 82%. Increase in air and desiccant mass flow rates caused an exponential increase in the overall mass transfer coefficient over the regeneration period.

The comparison of heat transfer coefficients predicted in this article and experimental values showed an average deviation within the range of ±20%. This deviation is largely due to the fact that the simulation parameters were not the same as the prevailing experimental conditions. However, better results would be envisaged if experimental data for PV/T existed in the same location considered for the simulation.

## REFERENCES

[1] Lof GOG, Lenz TG, Rao S. Coefficients of heat and mass transfer in a packed bed suitable for solar regeneration of aqueous lithium chloride solutions. *J Sol Energy Eng* 1984;**106**:392.
[2] Factor HM, Grossman G. A packed bed dehumidifier/regenerator for solar air conditioning with liquid desiccants. *Solar Energy* 1980;**24**:541–50.
[3] Aly AA, Zeidan EB, Hamed AM. Solar powered absorption cycle modelling with two desiccant solutions. *Energy Cons Mgt* 2011;**51**:2768–76.
[4] Gommed K, Grossman G. Experimental investigation of a liquid desiccant system for solar cooling and dehumidification. *Solar Energy* 2007;**81**:131–8.
[5] Li X, Yang H. Energy and economic performance analysis of an open cycle solar desiccant dehumidification air-conditioning system for application in Hong Kong. *Solar Energy* 2010;**84**:2085–95.
[6] Halliday SP, Beggs CB, Sleigh PA. The use of solar desiccant cooling in UK: A feasibility study. *Applied Thermal Eng* 2002;**22**:1327–38.
[7] Grossman G. Solar powered systems for cooling, dehumidification and air conditioning. *Solar Energy* 2002;**72**:53–62.
[8] Montieth JL, Unsworth MH. *Principles of Environmental Physics*, 3rd edn. Academic press, Oxford, UK, 2008.
[9] Becker S. Calculation of direct and diffuse solar radiation in Israel. *Int J Clim* 2001;**21**:1561–76.
[10] Treybal RE. *Mass Transfer Operations*, 3rd edn. McGraw-Hill, Singapore, 1969.
[11] Gandhidasan P, Ullah MR, Kettleborough CF. Analysis of heat and mass transfer between a desiccant-air system in a packed tower. *Trans ASME J Solar Energy Eng* 1987;**109**:89–93.
[12] Babakhani D, Soleymani M. Simplified analysis of heat and mass transfer model in liquid desiccant regeneration process. *J Taiwan Ins Chem Eng* 2010;**41**:259–67.
[13] Fair JR, Bravo L. Distillation columns containing structured packings. *Chem Eng Prog* 1990;**86**:19–29.
[14] Suess P, Spiegel L. Hold-up of Mellapak structured packings. *Chem Eng Prog* 1992;**31**:119–24.
[15] Longo GA, Gasparella A. Experimental analysis on desiccant regeneration in a packed column with structured and random packing. *Solar Energy* 2009;**83**:511–21.
[16] Gandhidasan P. Prediction of pressure drop in a packed bed dehumidifier operating with liquid desiccant. *Appl Therm Eng* 2002;**22**:1117–27.
[17] Oyieke AYA, Inambao FL. Performance characterisation of a hybrid flat-plate vacuum insulated photovoltaic/thermal solar power module in sub-tropical climate. *Int J Photoenergy* 2016;**1**:1–15.
[18] Zhang L, Hihara E, Matsuoka F, *et al.* Experimental analysis of mass transfer in adiabatic structured packing dehumidifier/ regenerator with liquid desiccant. *Int J Heat Mass Transf* 2010;**53**:2856–863.

# Chapter6

## Multi-layered Artificial Neural Network for performance prediction of an adiabatic solar liquid desiccant dehumidifier

This chapter covers the performance prediction of a solar-powered adiabatic LiBr desiccant dehumidifier using a modest multiple layered artificial neural network algorithm. The best algorithm patterns with the best performance levels for moisture removal rate and effectiveness, respectively, were established. The multi-layered ANN algorithm predicted results were compared to the experimental values obtained in chapter 5, showing precise alignments for MRR and effectiveness. The effects of desiccant and air temperatures and humidity ratio were also determined. The content of this chapter was published in the Q1-rated International Journal of Low carbon Technologies, volume 14, June 2019.

**Andrew Y A Oyieke**, Freddie L Inambao; (2019) Multi-layered Artificial Neural Network for performance prediction of an adiabatic solar liquid desiccant dehumidifier, *International Journal of Low-Carbon Technologies*, Vol 14, Issue 3, Pg. 351-363, Available at: (https://doi.org/10.1093/ijlct/ctz022)

# Multilayered artificial neural network for performance prediction of an adiabatic solar liquid desiccant dehumidifier

Andrew Y. A Oyieke* and Freddie L. Inambao
*Discipline of Mechanical Engineering, University of KwaZulu-Natal, Mazisi Kunene Road, Glenwood, Durban 4041, South Africa*

## Abstract

In this study, a multi-layered artificial neural network (ANN) algorithm was developed and trained to predict the performance of a solar powered liquid desiccant air conditioning (LDAC) system particularly the adiabatic packed tower dehumidifier using Lithium Bromide (LiBr) desiccant. A reinforced technique of supervised learning based on error correction principle rule coupled with perceptron convergence theorem was applied to create the algorithm. The parameters such as temperature, flow rates and humidity ratio of both air and desiccant fluid were fed as inputs to the ANN algorithm and their respective outputs used to determine dehumidifier effectiveness and moisture removal rate (MRR). The ANN model when subjected to validity tests using vapour pressure of LiBr desiccant solution at specific random temperatures and concentrations, gave astounding outcomes with precise estimation to $R^2$ values of 0.9999 for all desiccant concentration levels. Due to the variation in solar radiation, the MRR and effectiveness fluctuated with the change in desiccant and air temperatures, giving maximum differences of 0.2 g/s and 1.8% respectively between the predicted and measured values depicting a perfect match. With respect to humidity ratio, MRR was accurately predicted by ANN algorithm with maximum difference of 3.4969% while the mean variation was −0.5957%. With respect to air temperature, the dehumidifier effectiveness was perfectly predicted by the ANN algorithm to an average accuracy of 0.53% and extreme positive deviation of 4.14%. The MRR was replicated to a mean variation of 0.013% and highest point difference of 0.08%. In all the above cases, the mean and maximum differences between the ANN model and experimental values were far below the allowable limit of ± 5%, hence the algorithm was deemed to be successful and could find use in air conditioning scenarios. The ANN algorithm's capability and flexibility test of processing unforeseen inputs was accurate with negligible deviations and prospects of predicting the desiccant's vapour pressure, dehumidifier effectiveness and MRR within all ranges of temperature and concentration which then eliminates the need for use of charts.

*Keywords:* Adiabatic dehumidifier; liquid desiccant; solar; artificial neural network

*Corresponding author:
youngoyieke@yahoo.com

Received 9 January 2019; revised 15 March 2019; editorial decision 8 April 2019; accepted 9 April 2019

## 1 INTRODUCTION

The performance of liquid desiccant air conditioning system (LDACS) is key to the general energy saving in buildings, especially with the use of renewable (solar) energy and waste heat as opposed to the national grid energy. The most reliable and commonly used performance analysis indices for such systems are the dehumidification effectiveness and moisture removal/condensation rates. Based on the existing literature, the analysis of these systems has predominantly been done by theoretical modeling (both analytical and numerical), experimental (instantaneous and dynamic measurements) and Artificial Neural Networks (ANN).

Whereas theoretical analysis gives hypothetical representation of a particular condition, verification must be done using experimental data which in most cases result in a skewed variation. Even though a lot of successes have been recorded with some well defined and formulated numerical and analytical

International Journal of Low-Carbon Technologies 2019, 14, 351–363

doi:10.1093/ijlct/ctz022 Advance Access publication 24 May 2019

models, the degree of flexibility required for performance in the external domains is still not achieved. Drawing inspiration from biological neuron networks, ANN provides an exhilarating alternative with side by side scheme of numerous interlinked basic elements that solve a number of complex computational glitches usable in a wide range of applications such as prediction of a phenomenon, process optimization and control, substantive memory and recognition of patterns. Other favourable benefits of ANN over other methods include dispersed exemplification, learning and oversimplification capability, adaptability, error forbearance, intrinsic appropriate statistical dispensation with comparatively little energy intake [1].

A brief account of historical advancements in ANN research extensively appears to be triple-phased. The pioneering interest emanated in the 1940s by McCulloch [2] who developed a coherent calculus of concepts impending in nervous action. A dualistic threshold element computational model for an artificial neuron was suggested, leading to the proof that, aptly selected weights enables a carefully arranged array of neurons to execute widely accepted computations. However, the model encompassed numerous abridged assumptions that did not allow accurate replication of behaviour of biological neurons. The second phase spanned through the 1960's when Rosenblatt [3] introduced the perception convergence theorem in neurodynamics which was later to be critically analysed in [4] for shortcomings. The findings dampened the interests of researchers and scientists, resulting in about 20 years of dormant phase of ANN research.

It was until the 1980s that Hopefield [5] initiated a third phase of investigations by demonstrating an innovative ANN computational capabilities using an energy approach that a renewed impetus was triggered. The multi-layered perceptrons algorithm based on back-propagation learning was first initiated by [6]. The back-propagation technique was later re-invented by [7] through parallel distributed processing. Based on the ideas generated, modern ANN research has metamorphosed into a state of the art technology.

The application of ANN technology in HVAC systems is a fairly recent development with the current crop of investigators using assorted parameters to study the behaviour of LDACS at dehumidification stage resulting in interesting outcomes. Most notably, Gandhidasan *et al.*, [8] predicted the vapour pressures of different aqueous desiccant solutions such as; calcium chloride (CaCl), lithim chloride (LiCl) and Lithium bromide (LiBr), applied in cooling using ANN. The study led to a conclusion that, ANN offered a great platform for vapour pressure prediction potential using temperature and concentration as inputs, eliminating the requirement of obtaining the precise points. Later on, Gandhidasan *et al.*, [9] developed and applied an ANN model to analyse the connection between input and output parameters in a LiCl based randomly packed liquid desiccant dehumidification system.

Abdulrahman *et al.*, [10] implemented and validated an ANN to predict the output of Tryethylene glycol (TEG) based liquid desiccant dehumidifier subjected to several input constraints. The predicted results were compared to experimental data and showed discrepancies of 8.13% and 9.05% for water condensation rate and effectiveness respectively. Still on the same subject, Abdulrahman [11, 12] further ran performance tests on a solar-hybrid air conditioning system with LiCl desiccant solution in a packed regenerator and dehumidifier using a single and multi-layered ANN structure. Using different input data, the outputs were obtained and compared with experimental data. The moisture removal rate (MRR) and effectiveness of the regenerator were predicted within 0.71% and 1.1% deviation while for dehumidification, a maximum difference of 1.2°C and 1.9 g/kg of temperature and humidity ratio respectively. The conclusion of this work depicted ANN technique as more reliable and accurate methodology for application in LDACS. However, they lacked extensive experimental data for further training of the ANN to ensure accuracy.

The application of artificial intelligence technique in prediction of heat and mass transfer process in liquid desiccant dehumidification process however presents the most accurate conformity to the prevailing conditions under which the experiments are run. The reason being, due to its ability to train and adopt to the test conditions and produce results which are validly true representation of actual operating conditions. The details of the respective relevant ANN literature reviewed are summarized in Table 1 in terms of precess, type of liquid desiccant used, input and output parameters, applied ANN structure and symbol. The classifications forms the basis of distinguishing the relevance of the present study as the parameters are listed in the last row for comparison. The present study applies a supervised paradigm based on error-correction learning rule to develop a multi-layered perceptron and back propagation algorithm for use in prediction of performance of LDACS powered by solar energy.

## 2 DEHUMIDIFIER THEORY

The basic theoretical assessment of the functional response of the adiabatic dehumidifier in air conditioning system is arguably essential and necessary before engaging in complex evaluation techniques. The functional capability of these vessels has most often been analysed using moisture removal rate and effectiveness. Moisture removal rate is the amount of water transferred to and from the desiccant solution per given time in the dehumidifier. From this definition, MRR is the product of inlet mass flow rate of dry air and the difference in humidity ratios between inlet and outlet of the vessel. MRR can be mathematically formulated in terms of the air-side or liquid-side as follows;

$$MRR = m_a(\omega_i - \omega_o) = m_d\left(\frac{X_{out}}{X_{in}} - 1\right) \Rightarrow X_{out} > X_{in} \qquad (1)$$

Where $m_a$ and $m_d$ are the inlet air and desiccant flow rates respectively; $\omega_i$ and $\omega_o$ are the inlet and outlet humidity ratios

**Table 1.** *ANN modeling applications in air dehumidification.*

| References | Process | Liquid desiccant | Input parameters | Output parameters | Applied network structure | ANN structure symbol |
|---|---|---|---|---|---|---|
| [9] | Dehumidification | LiCL | – Air and desiccant temperature<br>– Cooling water temperature<br>– Air humidity<br>– Air and desiccant flow rates<br>– Desiccant concentration<br>– Temperature ratio | – Desiccant temperature<br>– Desiccant concentration<br>– Water condensation rate | Multiple hidden layer | 8-3-2 |
| [10] | Dehumidification | TEG | – Air and desiccant flow rates<br>– Air and desiccant temperature<br>– Air humidity<br>– Desiccant concentration | – Water condensation rate<br>Dehumidifier effectiveness | Single and Two Hidden layers | 6-1-2<br>6-2-2 |
| [11] | Dehumidification | LiCL | – Air and desiccant temperature<br>– Air and desiccant flow rates<br>– Air inlet humidity ratio | – Air and desiccant temperature<br>– Humidity ratio<br>– Dehumidifier effectiveness<br>– Moisture removal rate | Single and Two Hidden layers | 5-5-5-1<br>5-11-11-1 |
| [13] | Dehumidification and regeneration | $CaCL_2$ | – Air and desiccant temperature<br>– Air and desiccant flow rates<br>– Air humidity<br>– Desiccant concentration | – Air and desiccant temperature<br>– Air and desiccant flow rates<br>– Air humidity<br>– Desiccant concentration | Multiple hidden layer | 6-2-6 |
| [14] | Dehumidification | LiCL | – Air flow rate<br>– Desiccant temperature<br>– Air humidity ratio<br>– Air flow rate | Water condensation rate | Mamdami fuzzy models | 3-1-1 |
| Current study | Dehumidification | LiBr | – Air inlet humidity ratio<br>– Air inlet temperature<br>– Air flow rates<br>– Desiccant concentration<br>– Desiccant inlet temperature<br>– Desiccant flow rates | – Temperature<br>– Humidity ratio<br>– Moisture removal rate<br>– Effectiveness<br>– Vapour pressure | Multilayer | 6-12-12-1<br>6-4-4-1 |

in $Kg/Kg_{dryair}$ respectively while, $X_{in}$ and $X_{out}$ are the desiccant concentrations at inlet and outlet conditions respectively.

Effectiveness on the other hand is the ratio of real humidity change in air to the highest possible difference in humidity ratio; formulated as;

$$\varepsilon = \left(\frac{\omega_i - \omega_o}{\omega_i - \omega_e}\right) \times 100\% \tag{2}$$

Where $\omega_e$ humidity ratio of air at equilibrium conditions expressed as;

$$\omega_e = 0.62185\left(\frac{p_{v,o}}{P - p_{v,o}}\right) \tag{3}$$

Where P is the the aggregate pressure in mmHg and $p_{v,o}$ is the outlet vapour pressure, given by;

$$p_{v,o} = \frac{P}{62185}\left(\frac{\omega_i}{1 + \frac{\omega_i}{0.62185}} - \frac{\vartheta}{\dot{M}_a}\right) \tag{4}$$

The rate at which water vapour condenses in the dehumidifier is governed by the heat transfer occurrence between the air and desiccant solution. An expression for this manifestation is thus developed as;

$$\vartheta = \frac{1}{\kappa}\left[\frac{\dot{M}_d C_d T_d \varepsilon}{1 - \varepsilon} - \dot{M}_a C_a (T_i - T_o)_a\right] \tag{5}$$

Where; $\vartheta$ is the moisture condensation rate in $kg/ms$, $\kappa$ is the concealed heat of condensation $kj/kg$; $\dot{M}$ is the mass fluctuation in $kg/ms$; $C$ is the specific heat capacity in $kJ/kgK$ and T is the temperature in $K$. The superscripts $i$ and $o$ show the inlet and outlet conditions respectively; while $a$ and $d$ stand for air and desiccant solution respectively.

The desiccant concentration is one of the most essential parameters of consideration because it determines the rate and amount of water expended or absorbed from the air. Therefore, at outlet state, the concentration $\chi$ can be found for the dehumidifier as;

$$\chi_{d,o} = \frac{\chi_{d,i}}{1 + \left(\frac{\vartheta}{\dot{M}_a}\right)} \tag{6}$$

It should however be noted that the desiccant concentration at dehumidifier outlet was considered to be the inlet concentration for the regenerator.

## 3 ARTIFICIAL NEURAL NETWORK MODEL

Artificial neural network (ANN) is an emerging machine learning technique which uses the analogy of axon like similar interlinked processing elements known as neurons for performance prediction and estimation analysis, automatic control and pattern classification [9]. Several neurons are linked together to form an information network that can be trained by examples to achieve desired outputs from sets of input data. The interconnection provides a communication channel between successive neurons. Typically, an ANN encompasses an input, output and one or more hidden layer depending on the complexity of the system [11]. Multi-layered feed-forward neural network generally consists of L-layers with L-1 hidden layers since the front layer of input nodes is not counted. The multi-layered perceptron is in the family of feed forward networks involving unidirectional linkages between successive neuron layers. This technique allows individual computational element to apply thresholding and/or sigmoid functions by forming intricate multifaceted resolution limits that could take the form of any boolean operations.

In general, a feed-forward network configuration is said to be static because it produces a single set of outputs instead of a series of values emanating from feed inputs. Its reaction and design is not dependent on the former network condition, but a number of factors such as the number of layers needed for a particular task, nodes per layer, training sets for generalization, network reaction and generalization performance on non-training data. Even though, the back propagation multi-layered feed-forward networks are popular in sorting and function approximations purposes, some of the design factors are established by trial and error because existing theories merely offer very feeble and unreliable concepts for choosing these factors in practice. A characteristic neuron has three major elements. Firstly; sets of interconnecting links each with its own weight/strength, secondly; a summing junction for all input indicators weighted by the respective synaptic strength of neuron, and thirdly; a stimulation function for controlling the largeness of the output of the neuron, e.g a squashing function.

In the context of ANN, a learning procedure is regarded as a delicate activity of iteratively appraising the network design and linkages through weights so as to effectively accomplish a definite assignment. The capability of ANN to habitually learn from examples gives it a smart and thrilling desirability as an important benefit compared to outdated practice and methods. It follows fundamental guides such as input-output interactions from a particular assortment of characteristic examples as opposed to established procedures decided by human specialists. The learning methodology involves developing and establishing a learning paradigm or model, rules and procedures for appraising the network weights. The paradigm can be supervised, unsupervised or a combination of both. Taking into account the aforementioned factors, a reinforcement technique of supervised learning based on error-correction principle rule is best suited for application in LDACS because it enables the formulation of the system evaluation model to act as a teacher and provision of predictable outcome for each input arrangement subject to assessment procedures of the precision of outputs. This enables the ANN to predict the desired results with subtle precision.

Based on the perceptron convergence theorem, the learning ensues basically as soon as an error is encountered [3]. This enables the perceptron learning process to converge after a definite number of iterative steps. Each neuron possesses a net and activation function indicating the possible combination of network outputs in the form $\{x_j{:}1 \leq j \leq n\}$ inside the neuron. Every link between neurons was assigned a variable weight factor which allowed each neuron to produce a summation of all its input weights resulting in an internal activity level $a_i$ defined as;

$$a_i = \sum_{j=1}^{n} w_j x_{ij} \pm w_{io} \tag{7}$$

Where $\{w_{ij};1 \leq j \leq n\}$ is the synaptic weight and $w_o$ is the bias used to model minimum or maximum conditions. The activation process of the network solely depended on the applied threshold which was mathematically represented as;

$$y = \varphi(a) \tag{8}$$

For simplicity and convenience of this cluster of ANN, a logic function shown in equation 9 was used for the activation;

$$\varphi(a) = \frac{1}{1 + exp^{(-a)}} \tag{9}$$

The learning loop containing input formats, error calculation and adjustment was varied using sets of various input-output examples until an acceptable response level of network sum of square error was achieved. Knowing the technique of input data format, expected output and type of modeling task, the number of nodes for input and output was easily determined. However, there is no known theoretical limit of the number of hidden layers. For this study, the constructed general layout of the ANN configuration is presented in Figure 1 with six nodes on the input layer, 4-14 nodes on each of the two hidden layers and a one node output layer.

Prior to training of the neural network, the input and the anticipated vectors needed to be normalized as a first procedure, though not a fixed rule. Whereas, normalization also known as scaling of input data, significantly enables transposing of the inputs into statistical series housing the sigmoid stimulation function, it does not work well and tends to misrepresent dynamic data which formed the majority in this case. Therefore, an alternative was considered by linearly magnifying the data interval commensurate to the stimulation function. A linear scale was adopted by having a static linking weight to each neuron fed with linear stimulation function and a 1:1

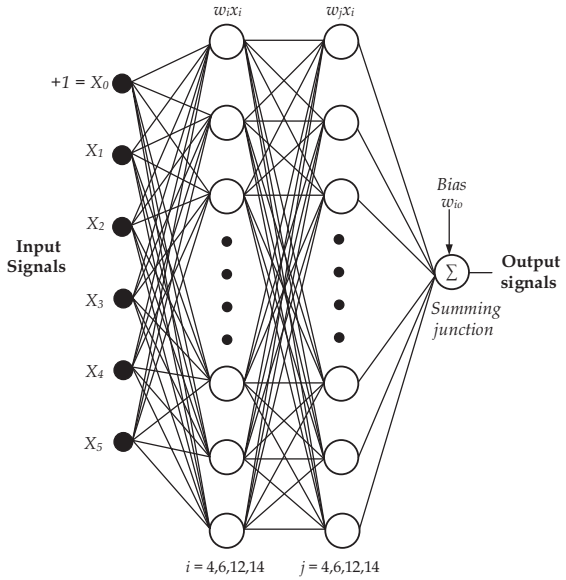


**Figure 1.** *The artificial neural network structure.*

linkage to the input stratum. This enabled the calculation of regressions with the capability of transposing any input into any output collection. Typical ranges of values used in linearisation are provided in Table 2.

## 4 ERROR BACK PROPAGATION TRAINING OF ANN

Data were first optimized to approximate the weights before training in order to obtain an acceptable outcome within the least number of epochs. An epoch is defined as the degree of repetitive application of all the training data or vectors in a single run to modify the weights of the respective nodes. It essentially implies a whole iteration procedure of a training algorithm of an ANN. MATLAB permits the setting of ultimate termination epoch for the training process. Hence, the training can be terminated in case the algorithm solution is not converging to avoid unending execution of training. A 'real-time period' of an epoch depends on the method of training; whether batch or sequential. A bunch of examples go through the learning algorithm concurrently in a single epoch prior to reorganizing the respective weights in batch training. Alternatively, successive training involves updating of weight at every instance the training vector passes over the training algorithm. Whereas, the former allows processing of large amount of non-zero input data within a short span of time, the latter provides for enhanced accuracy whether the data is defined or undefined. Therefore, sequential algorithm was preferred for the current study.

The choice of the respective weight matrices is the most important step in implementing an ANN model. In this multi-layered ANN structure, the weights terminating at each layer of

**Table 2.** *Typcal values for linearization.*

| Parameter | Symbol | Unit | Range |
|---|---|---|---|
| Air inlet temperature | $T_a$ | °C | 21.02–37.47 |
| Air flow rate | $\dot{m}_a$ | $kg/s$ | 0.051 |
| Air inlet humidity ration | $\omega_i$ | $kg_{H_2O}/kg_{da}$ | 0.0157–0.0347 |
| Desiccant temperature | $T_d$ | °C | 34.90–39.30 |
| Desiccant flow rate | $\dot{m}_d$ | $kg/s$ | 0.39–0.85 |
| Desiccant concentration | $X$ | $\%wt$ | 97 |

neurons made the weight matrix of that particular layer. However, it should be noted that the input layer was not assigned any weight matrix due to the absence of neurons in that layer. To determine the weight matrix values of each layer, an error back-propagation training (EBPT) technique was applied. Taking a set of training example in the form $\{x(j);1 \le j \le n\}$, The EBPT was achieved by initially entering all the $n$ inputs in the neural network and then calculating the expected resultant outputs $\{z(j);1 \le j \le n\}$

The training data comprised of N sets of input-output trajectories defining the task. The algorithm reduced the sum of square variation between the actual and anticipated outcomes in a back-propagation scheme. The performance of the back propagation algorithm was geared towards a predetermined slip task involving the general average of the variation of individual neurons in the output stratum and the anticipated result. The error task was formulated with an aim of varying the weight matrix $W$ in order to minimize error. Hence, the sum of square error $E$ was then calculated as follows;

$$E = \frac{1}{N}\sum_{j=1}^{n}[d_j - z_j]^2 = \frac{1}{N}\sum_{j=1}^{n}[d_j - f(w_j x_{ij})]^2 \qquad (10)$$

Where; $w_{ji}$ = weight matrix $[W_0 W_1 W_2 ... W_n]$ and $x$ = input vector $[X_0 X_1 X_2 ... X_n]$. With $j$ as the indexing constant for neurons in the output layer, $d_j$ as the constituent of the $N^{th}$ anticipated vector and $f(w_j x_{ij})$ being the component of the output of N inputs, the minimization of the objective function called for modifying instruction to change the weights of the neuron linkages. Care was taken to avoid the occurrence of a linear least square optimization problem, since lessening the error task gave rise to modification instruction to change the neuron linkage weights. Therefore, to modify the link between two adjacent neurons in layers L and L + 1 respectively without oscillation, an iterative correction factor with a momentum term was formulated as;

$$\Delta w_{ji}(n-1) = w_{ij}(n) + \mu\delta_j z_i + \beta\Delta w_{ji}(n) \qquad (11)$$

With $n$ number of iterations, the correction factor $\Delta w_{ji} = \mu\delta_j z_i$. Where index $i$ represent the units in layer L, $\mu$ is the learning rate, $z_i$ is the output of the $i^{th}$ neuron in layer L and $\delta_j$ is the error element transmitted from the preceding $j^{th}$ neuron in layer L + 1 determined for $j^{th}$ neuron in the output layer as $\delta_j = [d_j - z_j]/[1 - z_j]$ and $\delta_j = z_j[1 - z_j]\sum_m \delta_m w_{mj}$ for the $j^{th}$

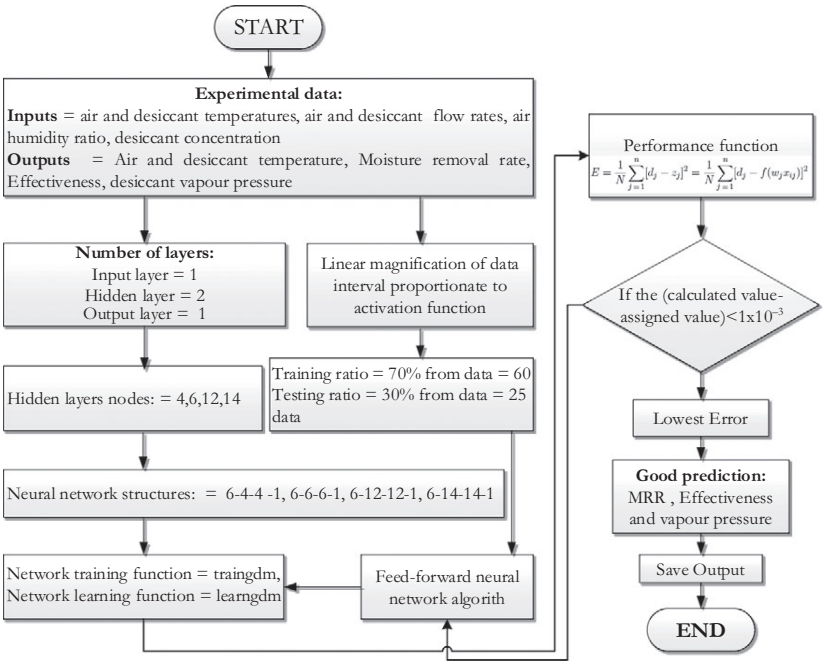


**Figure 2.** *The ANN program logical flow chart.*

neuron in hidden layer with m neurons in layer L + 2. $\beta$ is a real constant which checks the influence of previous weight modifications on the current path of traffic in the weight matrix. The feed-forward ANN algorithm is thus laid down below;

- Start
- Set the weights to trivial arbitrary values
- Arbitrarily select an input pattern $x(\mu)$
- Disseminate the signal onward over the network.
- Calculate $\delta_i{}^L$ for the output layer; $\delta_i{}^L = f'(h_i{}^L)[d^a{}_L - z_i{}^L]$, Where $h_i{}^L$ is the net input to the $i^{th}$ level while $f'$ is the derivative of the stimulation factor $f$
- Repeat procedure 4 for the subsequent levels by transmitting the error towards the back according to the expression; $\delta_i{}^l = f'(h_i{}^l)\sum_j w_{ij}{}^{i+1}\delta_j{}^{i+1}$,for $l = (L-1,...,1)$
- Modify the weights by then function; $\Delta w_{ij}{}^i = \eta\delta_i{}^l z_l{}^{l-1}$
- Go back to stage 2 and replicate the procedure until the total number of repetitions is achieved or output layer displays an error under the specified threshold (Figure 2).
- End

The feed-forward ANN algorithm was then implemented in a comprehensive logical flow chart fed with all the characteristic model parameters as shown in Figure 2.

## 5 RESULTS AND DISCUSSION

An ANN algorithm based on the reinforcement technique of supervised learning encompassing error correction principle and the perceptron convergence theorem was developed and implemented in MATLAB. For accuracy and computational intricacy of ANN algorithm, an appropriate number of training arrangements guaranteeing effective simplification was chosen. A total of eight structures was studied for both moisture removal rate and effectiveness. A regression scrutiny was performed on the experimental and predicted outcomes to establish the coefficient of determination $R^2$. This coefficient offered a degree of how distinct practical results were imitated by the algorithm, founded on the fractional aggregate deviation of respective results. For each combination of layers, the $R^2$ value were determined during training, validation and testing. Consequently, the overall values were computed to give the best performance level of each structure which informed the decision to choose the best combination.

Table 3 presents a summary of the respective patterns and their corresponding $R^2$ values during dehumidification process. Several combinations were tested and scrutinized for this purpose. Based on the respective outcomes, configurations 6-12-12-1 and 6-6-6-1 demonstrated the best performance levels for moisture removal rate and effectiveness respectively for the dehumidifier. The results informed the decision for the choice of these configurations for comparison of various parameters.

The regression of moisture removal rate for dehumidifier gave $R^2$ values spanning between 0.87 to 0.987 in training phase, 0.92 to 0.991 for validation and 0.93 to 0.995 during testing. Subsequently, the overall values varied between 0.92 and 0.988. However, the most outstanding corroboration performance for moisture removal rate was 0.988 attained by the 6-12-12-1 pattern, which exhibited a validation display of $5.899\times10^7$ at epoch-4 as demonstrated in Figure 3a. In terms of

dehumidifier effectiveness, the regression examination gave the following ranges of $R^2$ during training, validation, testing and overall. The dehumidifier effectiveness ranged from 0.81–0.989, 0.84–0.993, 0.81–0.957 and 0.82–0.983 respectively. Configuration 6-6-6-1 was the greatest performer attaining 0.983 with a validation performance display of $1.8194\times10^{6}$ corresponding to epoch-3 as shown in Figure 3b.

The prediction by ANN algorithm effectively corresponded to the measured values. The ANN configurations of 6-12-12-1 and 6-4-4-1 gave the best results for MRR of the dehumidifier and regenerator respectively during training. The best performance during training was achieved when a prediction goal was reached for the dehumidifier MRR and effectiveness output target of $0.97^{*}$(target + 0.0054) and $0.96^{*}$(Target + 0.0068) respectively against experimental values. A detailed representation of testing validation and overall are shown in Figures 4 and 5 for validation halt at epoch 4 and epoch 8, respectively. The matching $R^2$ values at these respective points were 0.987 and 0.989.

**Table 3.** *The $R^2$ values for various ANN structures during training, validation, testing and overall.*

| Performance Index | | Phase $R^2$ values | | | |
|---|---|---|---|---|---|
| | ANN Structure | Training | Validation | Testing | Overall |
| **MRR (g/s)** | 6-4-4-1 | 0.95 | 0.98 | 0.93 | 0.95 |
| | 6-6-6-1 | 0.87 | 0.92 | 0.96 | 0.94 |
| | 6-12-12-1 | 0.987 | 0.991 | 0.995 | 0.988 |
| | 6-14-14-1 | 0.89 | 0.90 | 0.94 | 0.92 |
| **Effectiveness (%)** | 6-4-4-1 | 0.95 | 0.88 | 0.94 | 0.88 |
| | 6-6-6-1 | 0.989 | 0.993 | 0.957 | 0.983 |
| | 6-12-12-1 | 0.89 | 0.88 | 1.83 | 0.77 |
| | 6-14-14-1 | 0.98 | 0.97 | 0.87 | 0.88 |

## 6 COMPARISON OF MODEL AND EXPERIMENTAL RESULTS

The main parameters of focus were the moisture removal rate and effectiveness of the regenerator and dehumidifier. However, parameters such as inlet air and desiccant temperatures and inlet air humidity ratio were also analysed in terms of their influence on the MRR and $\varepsilon$. Table 4 gives a summary of the results obtained from experiment side by side with those predicted by the algorithm. The termination of algorithm training process was initiated at the ultimate defined total epochs of 25 000 or correspondingly upon attainment of the least SSE on validation procedure, whichever come first. As a result, the prediction accuracy was determined during testing by comparing the experimental and predicted results both for MRR and effectiveness. Figure 6 shows how the predicted and experimental MRR of the dehumidifier varied and matched during the testing stage of the ANN algorithm for 6-12-12-1 configuration. The maximum difference obtained between the two profiles was 0.2 g/s. Generally, the MRR changed with the variation in temperatures as dictated by the solar radiation hence the wavy profile.

Similarly, the degree of accuracy of predicted effectiveness compared to experimental values was computed and plotted. The variation of dehumidifier effectiveness during the testing phase compared with the corresponding experimental contour in Figure 7 for ANN structure 6-6-6-1. A perfect match was achieved with a mean difference of 1.8% over a testing duration of 21 counts. The highest effectiveness value was 70% while the average for the whole period was 52%.

Since the main purpose of the system is to reduce the humidity of air to the required comfort levels by use of hygroscopic liquids hereby referred to as liquid desiccants. Therefore, the humidity ratio (HR) of inlet air is of paramount importance

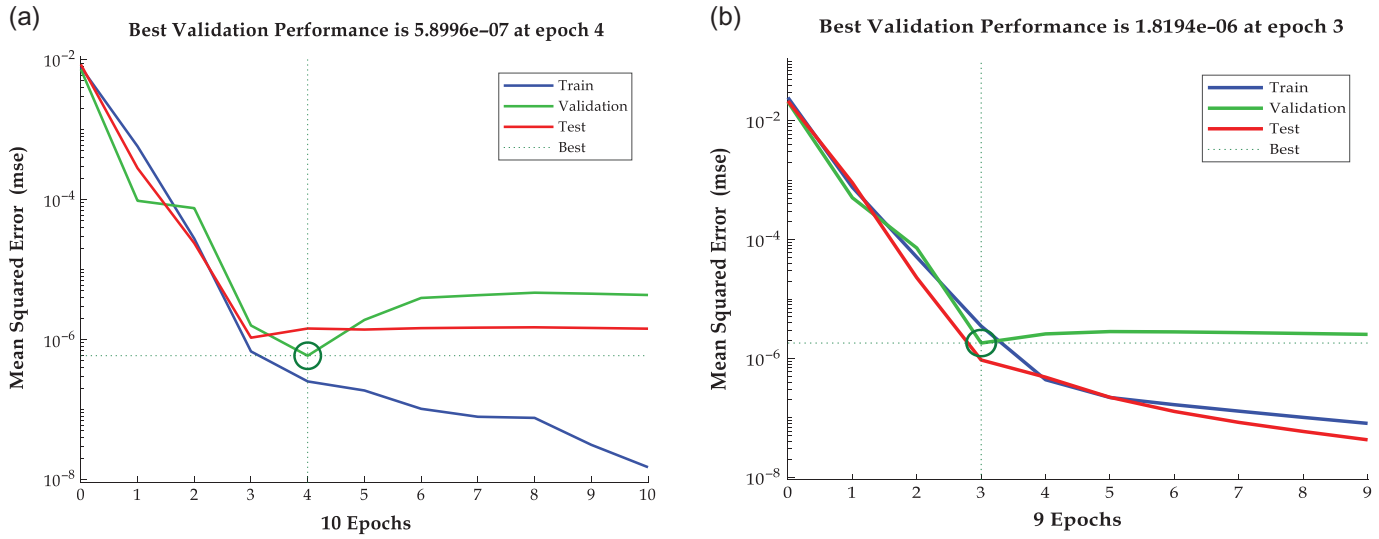


**Figure 3.** *The best fit validation outcome for the dehumidifier (a) MRR (b) effectiveness.*

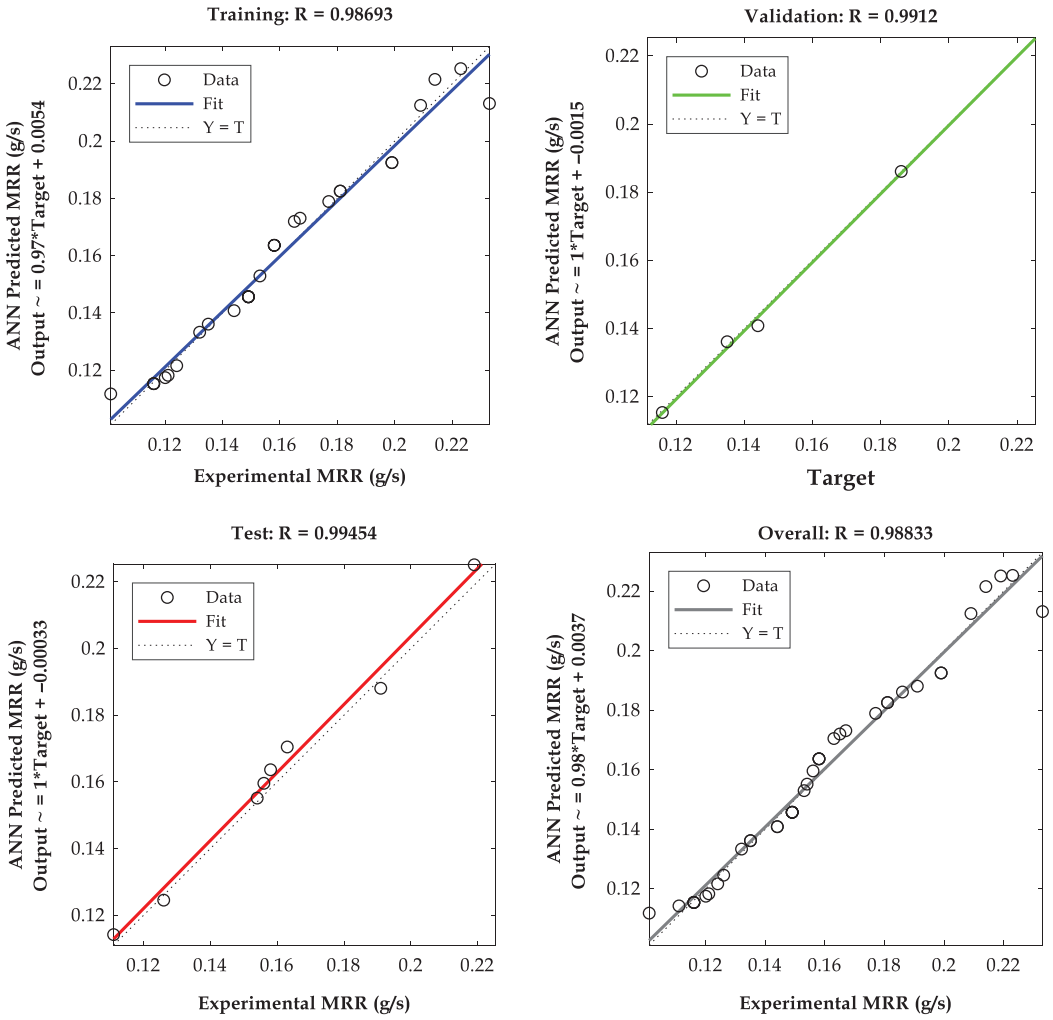


**Figure 4.** *The 6-12-12-1 ANN structure training regression validation halt at epoch 4 for dehumidifier MRR.*

in the design of LDAC systems. To this end, humidity ratio at inlet conditions was monitored and recorded. These values formed the basis for training the neural network algorithm to mimic exact experimental outcomes. The respective outcomes of the predicted parameters were compared to those obtained from experimental process.

Figure 8 shows the variations of dehumidifier MRR and effectiveness with humidity ratio of air at inlet. MRR increases steadily with increase in humidity ratio up to and optimum value of 1.6 g/kg. Further increase in humidity ratio beyond this point results in reduced MRR. The ANN algorithm accurately predicted the HR with negligible isolated variations. Of interest was the maximum observed difference of 3 4969% while the mean variation was −0,5957%. The dehumidifier effectiveness also followed the same trend as read from the secondary axis. The effectiveness steadily increased with increase in HR up to a maximum value of 54% corresponding to 0.02 kg$H_2O$/kg$^{dryair}$. Beyond this value $\varepsilon$ steadily decreases. The maximum and average variations realized were 2 6087% and −0,2053%. Overall prediction was deemed perfect since the deviations were negligible and within acceptable limits.

## 6.1 The vapour pressure

The vapour pressure is critical in the sorption process since it is the major driver of mass transfer phenomenon. Different liquid desiccant solutions posses varied vapour pressure characteristics at different operating conditions. However, the shape and contour of the curves are largely of similar inclinations. Very limited and in-exhaustive vapour pressure data is available in the existing literature for inorganic desiccants. Within the limited scope, only a few data points often gain prominence and hence calling for the interpolation and extrapolation of exact points under extended circumstances [8]. Thus, the ANN algorithm technique provides a more reliable and less tedious analysis alternative backed and trained by experimental data to generate even more intricate vapour pressure data points

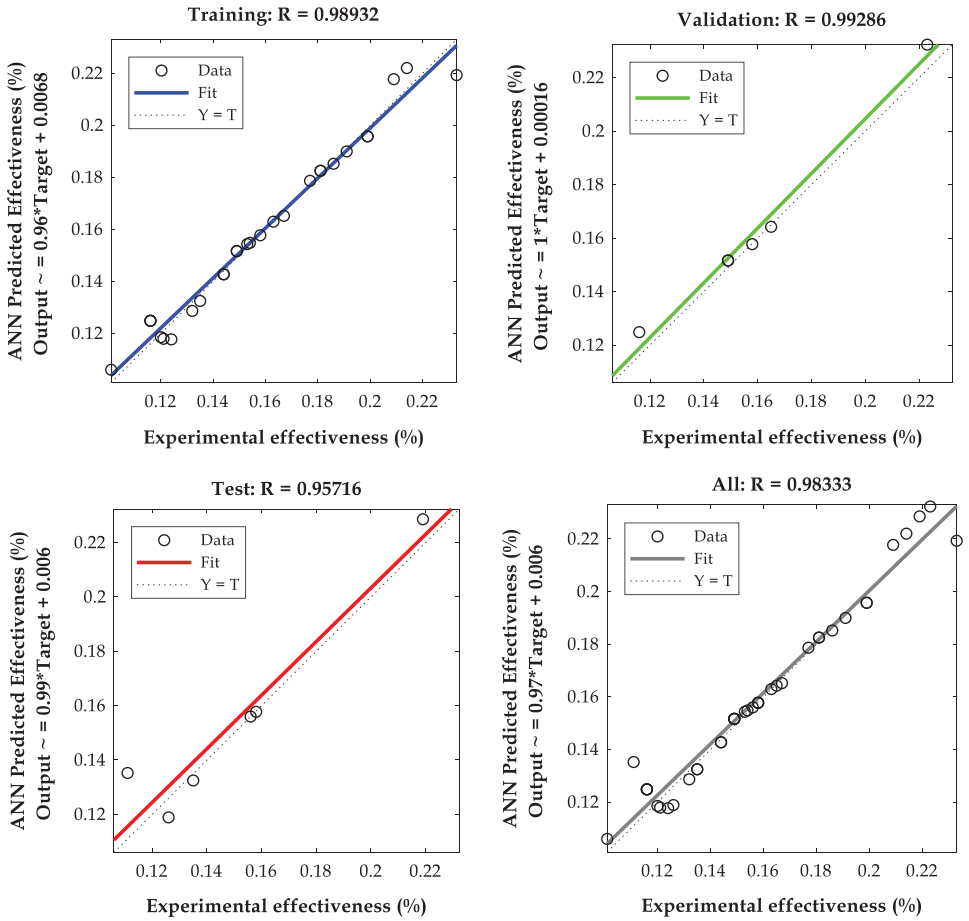


**Figure 5.** *The 6-6-6-1 ANN structure training regression validation halt at epoch 8 for dehumidifier effectiveness.*

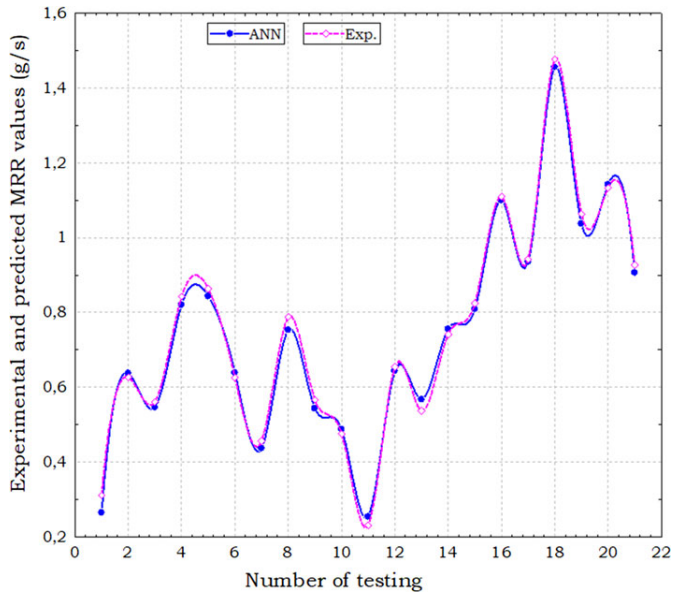


**Figure 6.** *The degree of accuracy between experimental and ANN predicted MRR values for the dehumidifier.*

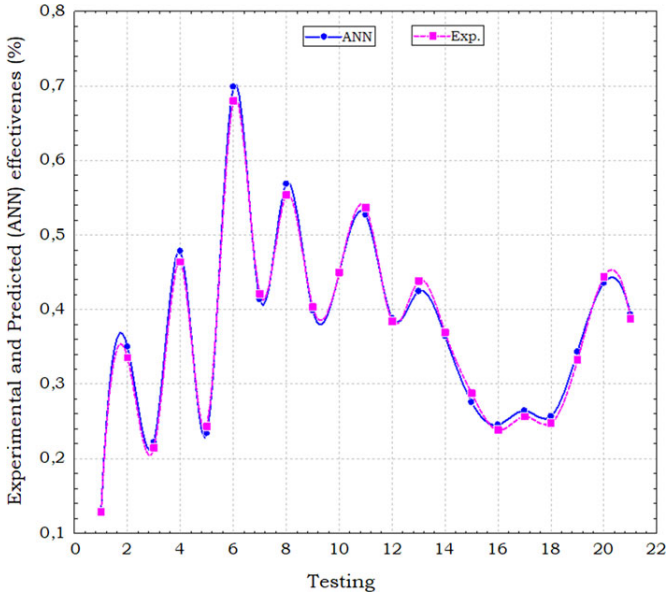


**Figure 7.** *The degree of accuracy between experimental and ANN predicted effectiveness for the dehumidifier.*

**Table 4.** *Comparison of ANN modeling results with experimental data for dehumidification process*

| $M_a$ (kg/ms) | $M_d$ (kg/ms) | $T_a$ (°C) | $T_d$ (°C) | $\omega_{in}$ ($kg_{H_2O}/kg_{dry}$) | $X_{in}$ (%$Wt$) Deh | DEHUMIDIFIER | | | | | |
|---|---|---|---|---|---|---|---|---|---|---|---|
| | | | | | | MRR (g/s): 6-12-12-1 | | | $\varepsilon$ (%): 6-6-6-1 | | |
| | | | | | | ANN | Exp | Var.(%) | ANN | Exp | Var.(%) |
| 0.51 | 0.039 | 21.02 | 37.70 | 0.0157 | 97 | 0.2649 | 0.3112 | −0.1749 | 0.1277 | 0.1285 | −0.6265 |
| 0.51 | 0.074 | 21.15 | 35.95 | 0.0158 | 97 | 0.6377 | 0.6268 | 0.0171 | 0.3502 | 0.3357 | 4.1405 |
| 0.51 | 0.082 | 21.29 | 35.12 | 0.0160 | 97 | 0.5466 | 0.5612 | −0.0268 | 0.2221 | 0.2144 | 3.4669 |
| 0.51 | 0.085 | 21.98 | 32.42 | 0.0167 | 97 | 0.8209 | 0.8425 | −0.0264 | 0.4784 | 0.4637 | 3.0727 |
| 0.51 | 0.085 | 22.45 | 35.67 | 0.0172 | 97 | 0.8435 | 0.8636 | −0.0239 | 0.2342 | 0.2434 | −3.9283 |
| 0.51 | 0.085 | 22.56 | 36.16 | 0.0173 | 97 | 0.6389 | 0.6260 | 0.0202 | 0.6988 | 0.6800 | 2.6903 |
| 0.51 | 0.085 | 22,70 | 35.30 | 0.0174 | 97 | 0.4367 | 0.4562 | −0.0447 | 0.4139 | 0.4212 | −1.7637 |
| 0.51 | 0.085 | 23.47 | 38.00 | 0.0182 | 97 | 0.7534 | 0.7879 | −0.0457 | 0.5688 | 0.5540 | 2.6020 |
| 0.51 | 0.085 | 25.51 | 39.30 | 0.0183 | 97 | 0.5436 | 0.5663 | −0.0419 | 0.3989 | 0.4034 | −1.1281 |
| 0.51 | 0.085 | 23.69 | 36.20 | 0.0185 | 97 | 0.4877 | 0.4756 | 0.0248 | 0.4500 | 0.4499 | 0.0222 |
| 0.51 | 0.085 | 25.22 | 34.70 | 0.0201 | 97 | 0.2545 | 0.2310 | 0.0925 | 0.5271 | 0.5366 | −1.8023 |
| 0.51 | 0.085 | 25.22 | 35.80 | 0.0201 | 97 | 0.6441 | 0.6544 | −0.0160 | 0.3883 | 0.3843 | 1.0301 |
| 0.51 | 0.085 | 25.96 | 35.40 | 0.0212 | 97 | 0.5676 | 0.5369 | 0.0540 | 0.4245 | 0.4384 | −3.2744 |
| 0.51 | 0.085 | 26.25 | 35.20 | 0.0217 | 97 | 0.7556 | 0.7411 | 0.0192 | 0.3646 | 0.3694 | −1.3165 |
| 0.51 | 0.085 | 27.16 | 35.80 | 0.0230 | 97 | 0.8091 | 0.8245 | −0.0190 | 0.2756 | 0.2876 | −4.3541 |
| 0.51 | 0.085 | 27.16 | 35.60 | 0.0230 | 97 | 1.0999 | 1.1094 | −0.0087 | 0.2456 | 0.2384 | 2.9316 |
| 0.51 | 0.085 | 28.03 | 35.60 | 0.0242 | 97 | 0.9355 | 0.9425 | −0.0075 | 0.2643 | 0.2563 | 3.0269 |
| 0.51 | 0.085 | 29.66 | 34.90 | 0.0266 | 97 | 1.4565 | 1.4775 | −0.0144 | 0.2567 | 0.2477 | 3.5060 |
| 0.51 | 0.085 | 33.14 | 35.60 | 0.0298 | 97 | 1.0379 | 1.0634 | −0.0246 | 0.3433 | 0.3323 | 3.2042 |
| 0.51 | 0.085 | 35.32 | 35.30 | 0.0327 | 97 | 1.1423 | 1.1335 | 0.0077 | 0.4356 | 0.4435 | −1.8136 |
| 0.51 | 0.085 | 37.47 | 35.30 | 0.0347 | 97 | 0.9065 | 0.9267 | −0.0223 | 0.3934 | 0.3878 | 1.4235 |

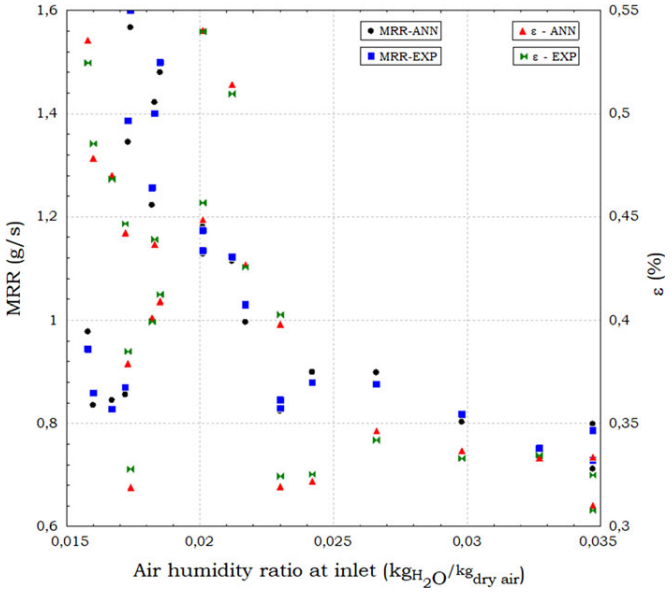


**Figure 8.** *The variation of dehumidifier MRR and ε in relation to humidity ratio of air at inlet conditions.*

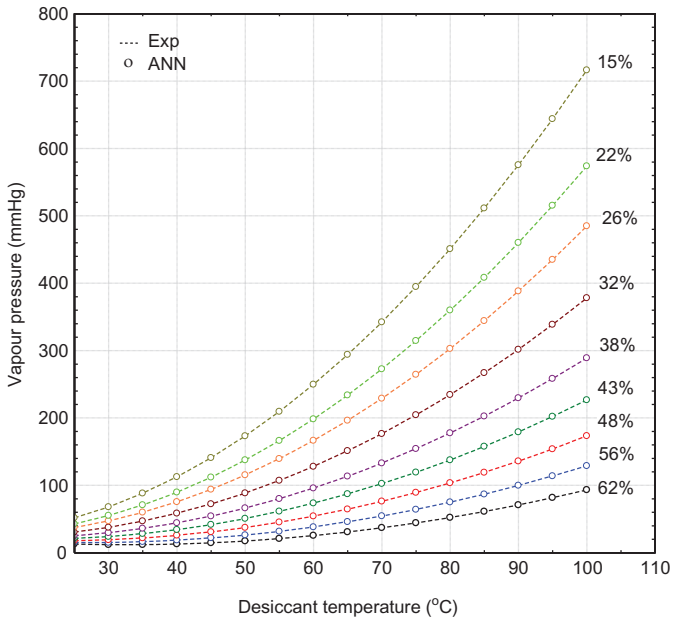


**Figure 9.** *The relationship between experimental and ANN predicted vapour pressure at varying concentration of LiBr desiccant.*

The training of ANN algorithm was enabled by a sum of 50 data points chosen randomly among the various experimental data availed. Another set of experimental data was used in the testing phase. At the end of the successful training, the test data enabled the performance of the algorithm to be predicted for different desiccant concentration levels. These predicted results were then matched with those from experiment as shown in Figure 9. The vapour pressure was low and high at high and low desiccant concentration levels respectively. Thus, giving the

desiccant the ability to attract more moisture from the air up to saturation point. The ANN algorithm was also subjected to validity tests using vapour pressure of the LiBr desiccant solution at specific random temperatures. It was evident that algorithm precisely estimated the vapour pressure to perfection with $R^2$ values of approximately 1 in all levels of desiccant concentration.

The individual temperature points and instantaneous concentrations which had not been used in training were then employed to observe the behaviour and response of the algorithm. The results convincingly agreed with negligible deviation giving and indication that the ANN algorithm had the capability and flexibility of processing predatory inputs it had not been fed with before with great accuracy. It was therefore concluded that the algorithm based ANN model exhibited promising prospects of predicting the desiccant's vapour pressure within any ranges of temperatures and concentrations which eliminates the need for use of charts for various points. Moreover, as inputs, the temperature and concentration data can be fed to the algorithm in order to give the corresponding vapour pressure. The system was trained using the actual data collected from the experiment which was earlier conducted. This was due to the fact that more actual data was needed to train the algorithm for specific applications and scenarios.

## 6.2 Effect of inlet desiccant temperature

Comparisons were drawn between predicted and measured outcomes, then analysed on the effects of desiccant and air temperatures on the performance the dehumidifier. The variation of desiccant temperature at the dehumidifier inlet in relation to MRR is shown in Figure 10. Generally, the increase in desiccant temperature gave a marginal increase in MRR of the dehumidifier. However, the stability of MRR was achieved at between 31–32°C beyond this range, the MRR was haphazardly distributed implying less sensitivity. In comparison to experimental data, ANN model predicted the desiccant temperature to a mean accuracy of −0.0124%. The highest temperature difference attained from the comparison was 0.93%.

To evaluate how dehumidifier effectiveness was affected by the varying inlet desiccant temperatures, an analysis is provided in Figure 11. Effectiveness reduced with increase in inlet desiccant temperatures beyond 32°C. This was due to the decreased ability of the desiccant liquid to hold moisture at elevated temperatures, hence the desiccant would be losing water particles instead of absorbing. In comparison to the experimental temperatures, the ANN algorithm generated values aligned perfectly to an average accuracy of 0.53% while extreme positive deviation 4.14% was realized.

## 6.3 Effect of inlet air temperature

It was observed that MRR reduced significantly with the escalation of inlet air temperature as displayed in Figure 12. Since moisture holding capacity of air increases with increase in temperature, it was increasingly becoming difficult for air to lose water vapour to the desiccant hence lower MRR. The highest MRR achieved was approximately 1.6 g/s at corresponding air temperature of 23°C. Beyond this point, there was a sharp reduction. Therefore, dehumidifier MRR exhibited very high sensitivity to air inlet temperature. The ANN algorithm replicated the experimental data to a mean variation of 0.013%, while the highest point difference was 0.08%, implying a best fit.

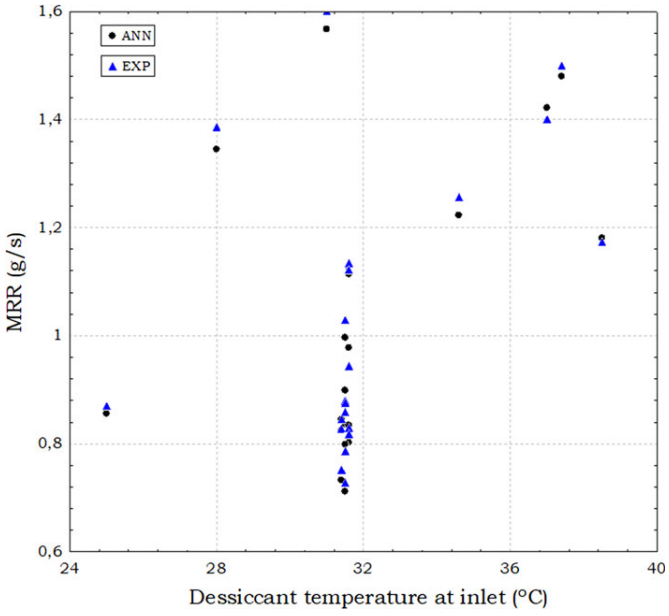


**Figure 10.** *The effect of inlet desiccant temperature on moisture removal rate of the dehumidifier MRR.*

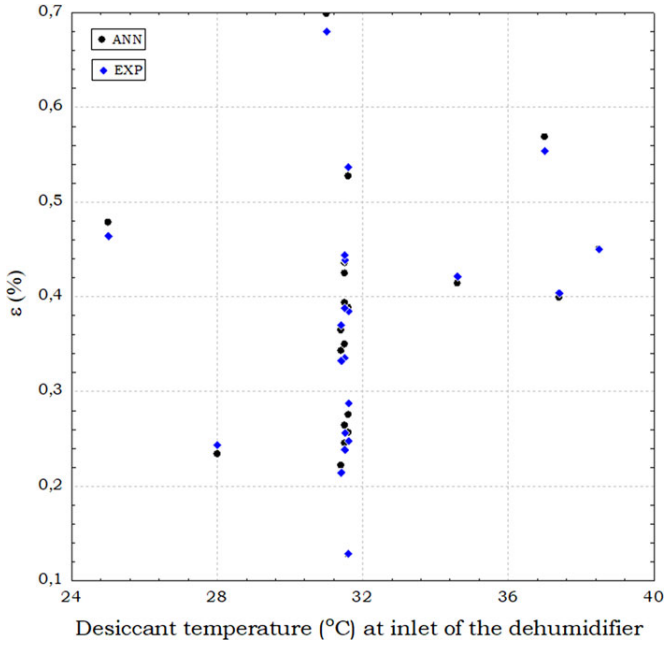


**Figure 11.** *Effect of inlet desiccant temperature on the effectiveness ε of the dehumidifier.*

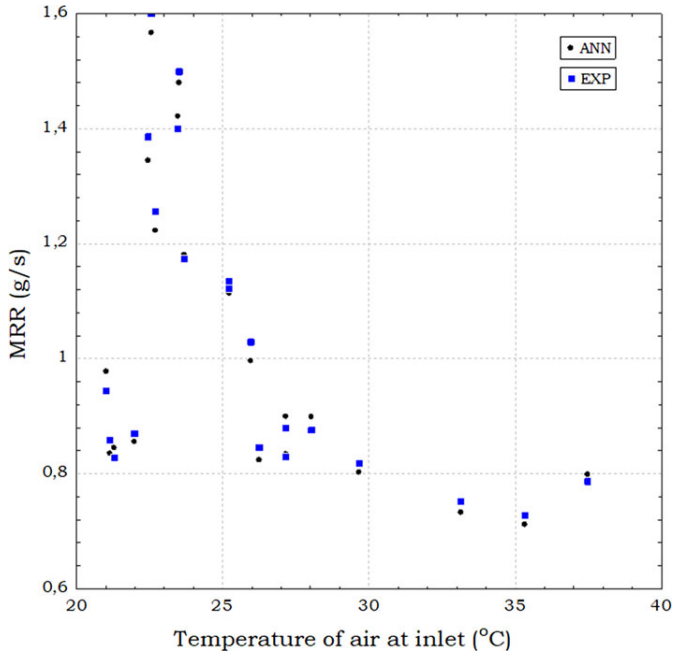


**Figure 12.** *Effect of inlet air temperature on the moisture removal rate of the dehumidifier.*

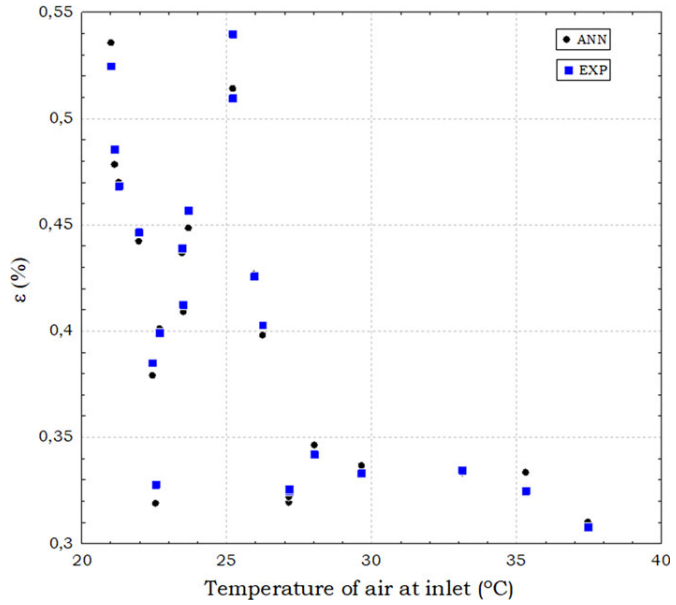


**Figure 13.** *Effect of inlet air temperature on effectiveness of the dehumidifier.*

The dehumidifier effectiveness displayed greater sensitivity to the increase in air inlet temperature. As can be seen in Figure 13, higher effectiveness values up to 54% were achieved below temperature 25°C, after which, a steady decline ensued. This scenario confirmed the assertion that air would not readily loose water at higher temperatures hence the low effectiveness. The ANN algorithm precisely predicted the experimental values to a mean and maximum variation of −0.04% and 3.21% respectively.

## 7 CONCLUSION

An ANN algorithm based on the reinforcement technique of supervised learning encompassing error correction and perceptron convergence theorem was developed and implemented in MATLAB for prediction of dehumidifier performance subjected to various inputs to get the moisture removal rate and effectiveness. Various ANN structures were considered and regression scrutiny was performed during training to establish the coefficient of determination $R^2$ upon which the best combination with the best fit was chosen. The authors had previously conducted experiments to establish the effects of temperature, humidity ratio and concentration of air and desiccant solution respectively on the main parameters of the study. The results of the experiment were used to train, test and validate the algorithm.

The accuracy of the algorithm was established to depend on the number of strata and the corresponding number of neurons. Care was taken to avoid oversimplification and/or overcomplication of the model. Based on the respective outcomes, configurations 6-12-12-1 and 6-6-6-1 demonstrated the best performance levels for moisture removal rate and effectiveness respectively for the dehumidifier. Therefore, the analysed results for various parameters and comparisons were based on the aforementioned configurations. The ANN model when subjected to validity tests using vapour pressure of LiBr desiccant solution at specific random temperatures and concentrations, gave precise estimation with $R^2$ values of 0.9999 for all desiccant concentration levels. From a detailed scrutiny of the ANN algorithm performance and upon comparing the ANN generated results to those from experiments, a series of conclusions were drawn.

The dehumidifier MRR varied with the variation in desiccant temperature as dictated by solar radiation. The maximum difference between the predicted and measured values was 0.2 g/s. A perfect match was obtained in the variation of predicted dehumidifier effectiveness during the testing phase compared to the corresponding experimental contour with a mean difference of 1.8% over a testing duration of 21 counts. The highest effectiveness value was 70% while the average for the whole period was 52%. The variation of dehumidifier MRR with respect to humidity ratio was accurately predicted by ANN algorithm with maximum difference of 3.4969%, while the mean variation was −0.5957%. For the effectiveness, the maximum and average variations were 2.6087% and −0.2053% respectively. On the variation of desiccant temperature at the dehumidifier inlet in relation to MRR, the ANN model predicted the desiccant experimental temperature to a mean accuracy of −0.0124% with the highest difference being 0.93%.

However, the dehumidifier effectiveness was affected by varying inlet desiccant temperatures as displayed by the experimental results which were in turn perfectly predicted by the

ANN algorithm to an average accuracy of 0.53%, while extreme positive deviation of 4.14% was realized. On the other hand, MRR exhibited very high sensitivity to air inlet temperature. The ANN algorithm replicated the experimental data to a mean variation of 0.013%, while the highest point difference was 0.08%. The dehumidifier effectiveness displayed greater sensitivity to the increase in air inlet temperature. The ANN algorithm precisely predicted the experimental values to a mean and maximum variation of −0.04% and 3.21% respectively.

In all the above cases, the mean and maximum differences between the ANN model and experimental values were far below the allowable limit of ±5% hence the algorithm was deemed to be suitable and could find use in air conditioning scenarios. The ANN algorithm's capability and flexibility test of processing unforeseen inputs were accurate with negligible deviations and prospects of predicting the desiccant's vapour pressure, dehumidifier effectiveness and MRR within all ranges of temperature and concentration which then eliminates the need for use of charts.

## REFERENCES


[1] Anil KJ, Mao J, Mohiuddin KM. Artificial neural networks: a tutorial. *IEEE Trans Neural Netw* 1996;**21**:31–44.

[2] McCulloch WS, Pitts W. A logical calculus of ideas immanent in nervous activity. *Bull Math Biophys* 1943;**5**:115–33.

[3] Rosenblatt R. *Principles of Neurodynamics*. Spartan Books, 1962.

[4] Minsky M, Papert S. *Perceptrons; An Introduction to Computational Geometry*. MIT Press, 1969.

[5] Hopfield JJ. Neural networks and physical systems with emergent collective computational abilities. *Natl Acad Sci* 1982;**132f**:2554–8. USA 79.

[6] Werbos P (1974). Beyond regression: New tools for prediction and analysis in the behavioural sciences. PhD thesis, Department of Applied Mathematics, Harvard University, Cambridge, Mass.

[7] Rumelhart DE, McClelland JL. *Parallel Distributed Processing; Exploration in the Microstructure of Cognition*. MIT press, 1988.

[8] Gandhidasan P, Mohandes MA. Prediction of vapour pressures of aqueous desiccants for cooling applications by using artificial neural networks. *Appl Therm Eng* 2008;**28**:126–35.

[9] Gandhidasan P, Mohandes MA. Artificial neural network analysis of liquid desiccant dehumidification system. *Energy* 2011;**36**:1180–6.

[10] Mohammed TH, Sohif BN, Sulaiman MY, *et al.* Artificial neural network analysis of liquid desiccant dehumidifier performance in a solar hybrid air-conditioning system. *Appl Therm Eng* 2013a;**59**:389–97.

[11] Mohammed TH, Sohif BN, Sulaiman MY, *et al.* Artificial neural network analysis of liquid desiccant regenerator performance in a solar hybrid air-conditioning system. *Sustainable Energy Technologies and Assessment* 2013b;**4**:11–9.

[12] Mohammed TH, Sohif BN, Sulaiman MY, *et al.* Implementation and validation of an artificial neural network for predicting the performance of a liquid desiccant dehumidifier. *Energy Convers Manag* 2013c;**67**:240–50.

[13] Zeidan EB, Aly AA, Hamed AM. Investigation on the effect of operating parameters on the performance of solar desiccant cooling system using artificial neural networks. *Int J Therm Environ Eng* 2010;**1**:91–8.

[14] Singh H, Sing J, Gill SS. Fuzzy modeling of liquid desiccant based air dehumidification system. *Int J Eng Sci Techn* 2011;**3**:2775–2785.

# Chapter7

## Performance Prediction of an Adiabatic Solar Liquid Desiccant Regenerator using Artificial Neural Network

This chapter presents the performance prediction of an adiabatic solar-powered liquid desiccant regenerator using artificial neural network. In a similar format as chapter 6, the best algorithm patterns with the best performance levels for moisture removal rate and effectiveness respectively were established. The ANN algorithm predicted results were compared to the experimental values obtained in chapter 5, showing precise alignments for MRR and effectiveness. The effects of desiccant and air temperatures and humidity ratio were also determined. The content of this chapter was published in the Q3-rated International Journal of Mechanical Engineering and Technology, volume 10 in March 2019.

**Andrew Y A Oyieke** and Freddie L. Inambao (2019). Performance Prediction of an Adiabatic Solar Liquid Desiccant Regenerator using Artificial Neural Network, *International Journal of Mechanical Engineering and Technology*, 10(3), pp. 496-511. http://www.iaeme.com/IJMET/issues.asp?JType=IJMET&V Type=10&IType=3

**International Journal of Mechanical Engineering and Technology (IJMET)**
Volume 10, Issue 03, March 2019, pp. 679-693. Article ID: IJMET_10_02_073
Available online at http://www.iaeme.com/ijmet/issues.asp?JType=IJMET&VType=10&IType=3
ISSN Print: 0976-6340 and ISSN Online: 0976-6359



# PERFORMANCE PREDICTION OF AN ADIABATIC SOLAR LIQUID DESICCANT REGENERATOR USING ARTIFICIAL NEURAL NETWORK

**Andrew Y. A. Oyieke and Freddie L. Inambao***
Green Energy Solutions Research group, Discipline of Mechanical Engineering, University of KwaZulu-Natal, Mazisi Kunene Road, Glenwood, Durban 4041, South Africa.
*Corresponding author

## ABSTRACT

*This paper presents an artificial neural network (ANN) algorithm developed and trained to predict the performance of a solar powered adiabatic packed tower re-generator using LiBr desiccant. A reinforced technique of supervised learning based on the error correction principle rule coupled with the perceptron convergence theorem was used. The input parameters to the algorithm were temperature, flow rates and humidity ratio of both air and desiccant fluid and their respective outputs used to determine regenerator effectiveness and moisture removal rate. The optimum performance of the ANN algorithm was shown by structures 6-4-4-1 and 6-14-1 for moisture removal rate (MRR) and effectiveness respectively. Upon comparison, the predicted and experimental MRR profiles aligned perfectly during training with a maximum and mean difference of 0.18 g/s and 0.11 g/s. The regenerator effectiveness profiles also agreed well with a few negligible disparities with a mean and maximum difference of 0.6 % and 1 %. With respect to humidity ratio, the algorithm predicted the experimental MRR values to maximum and mean accuracies of 0.0925 % and -0.012 %. The maximum and mean accuracies of 4.14 % and 0.53 % were realized in the prediction of experimental effectiveness by the neural network algorithm. The ANN model precisely predicted the experimental MRR with respect to inlet desiccant temperature with an average deviation of -0.5290 % while the highest difference was 3.496 % between predicted and measured temperature. With change in inlet desiccant temperature, the ANN predicted and experimental values revealed maximum and mean deviations of 2.61 % and 0.21 %. While the regenerator moisture removal rate varied proportionally with the air temperature, the predicted MRR values matched perfectly with the measured data with a mean and highest difference of -0.12 % and 3.2 %. In all the aforementioned cases, the mean and maximum differences between the ANN model and experimental values were way below the allowable limit of 5 % hence the algorithm was deemed to be successful and could find use in air conditioning scenarios.*

**Keywords**: Adiabatic regenerator, Liquid desiccant, Solar, Artificial neural network.

**Cite this Article**: Andrew Y. A. Oyieke and Freddie L. Inambao, Performance Prediction of an Adiabatic Solar Liquid Desiccant Regenerator using Artificial Neural Network, *International Journal of Mechanical Engineering and Technology*, 10(3), 2019, pp. 679-693.
http://www.iaeme.com/IJMET/issues.asp?JType=IJMET&VType=10&IType=3

# 1. INTRODUCTION

The application of desiccant materials in air conditioning systems has increasingly become popular in built environments. Liquid desiccants such as lithium bromide, lithium chloride, and calcium chloride among others have found application in most preferred systems due to flexibility in operation, ability to neutralize both organic and inorganic contaminants, and ability to work in the low regeneration temperatures provided by solar energy. The regenerator is a vessel in which a heated dilute solution comes into contact with air in a packed environment which enables heat and mass transfer phenomenon to occur. This process leads to evaporation of water particles from the desiccant to the atmospheric air and results in a strong solution to near initial concentration.

Evidence from literature shows that there has been a considerable amount of theoretical modelling and practical experimental tests performed on these units with little reference to use of artificial intelligence techniques. Even though a lot of success have been recorded with some well-defined and formulated numerical and analytical models, they still don't offer the degree of flexibility required for performance in the external domain. Drawing inspiration from biological neural networks, artificial neural networks (ANN) provide an excellent alternative with numerous interlinked neurons that are stimulated to solve a number of complex computational problems applicable in a whole range of scenarios such as prediction, process optimization and control, substantive memory, and recognition of patterns. Other favourable benefits of ANN over other methods include dispersed exemplification, learning and oversimplification capability, adaptability, error forbearance, intrinsic appropriate statistical dispensation with comparatively little energy intake [1].

ANN research was pioneered by [2] in the 1940s who suggested a dualistic threshold element computational model for an artificial neuron, with carefully selected weights in an organized array of neurons to execute widely accepted computations. Rosenblatt [3] introduced the perception convergence theorem in neurodynamics which was later critically analysed by [4] for shortcomings. Hopfield [5] further introduced the energy approach which demonstrated innovative ANN computational capabilities. The perceptron multi-layered algorithm-based back-propagation learning was first initiated by [6] and re-invented by [7] through parallel distributed processing. Based on their ideas, modern ANN research has metamorphosed into a state-of-the-art technology.

The application of ANN technology in heating, ventilation and air conditioning (HVAC) systems is a fairly recent development involving the use of assorted parameters to study the behaviour of liquid desiccant air conditioning systems (LDACS) at the regeneration stage. Gandhidasan [8] predicted the vapour pressures of different aqueous desiccant solutions (CaCl, LiCl and LiBr) applied in cooling using ANN. Later on, they developed and applied an ANN model to analyze the connection between input and output parameters in an LiCl based randomly packed liquid desiccant dehumidification system [9]. Mohammed et al. [10] implemented and validated an ANN to predict the output of a triethyle glycol (TEG) based liquid desiccant dehumidifier subjected to several input constraints. Still on the same subject, Mohammed et al. [11] and [12] ran performance tests on a solar-hybrid air conditioning system with LiCl desiccant solution in a packed regenerator using various ANN structures. Using different input data, the outputs were obtained and compared with experimental data in terms

of moisture removal rate (MRR) and effectiveness. However, due to lack of extensive experimental data for further training of the ANN the accuracy of their model was not guaranteed.

A summary of the respective relevant ANN literature reviewed is presented in Table 1 in terms of process, type of liquid desiccant used, input and output parameters, applied ANN structure and symbol. This classification forms the basis of distinguishing the relevance of the present study as the parameters are listed in the last row for comparison. The present study applies a supervised paradigm based on an error-correction learning rule to develop a multi-layered perceptron and back-propagation algorithm for use in prediction of performance of LDACS powered by solar energy.

**Table 1** ANN modelling applications in air regeneration

| References | Process | Liquid desiccant | Input parameters | Output parameters | Applied network structure | ANN structure symbol |
|---|---|---|---|---|---|---|
| [13] | Regeneration | $CaCL_{2}$- | - Air and desiccant temperature<br>- Air and desiccant flow rates<br>- Air humidity<br>- Desiccant concentration | - Air and desiccant temperature<br>- Air and desiccant flow rates<br>- Air humidity ratio<br>- Desiccant concentration | Multiple hidden layer | 6-2-6 |
| [12] | Regeneration | LiCl | - Air and desiccant inlet humidity ratio<br>- Air and desiccant inlet temperature<br>- Air and desiccant flow rates | - Temperature<br>- Humidity ratio<br>- Moisture removal rate (MMR)<br>- Effectiveness | Single and multilayer | 5-5-5-1<br>5-11-1 |
| Current study | Regeneration | LiBr | - Air inlet humidity ratio<br>- Air inlet temperature<br>- Air flow rates<br>- Desiccant concentration<br>- Desiccant inlet temperature<br>- Desiccant flow rates | - Temperature<br>- Humidity ratio<br>- Moisture removal rate<br>- Effectiveness | Multilayer | 6-4-4-1<br>6-14-1 |

## 2. REGENERATOR THEORY

The basic theoretical assessment of the functional response of the regenerator in an air conditioning system is arguably essential and necessary before engaging in complex evaluation techniques. The functional capability of these vessels have most often been analysed using MRR and effectiveness. MRR rate is the amount of water transferred to and from the desiccant solution per given time in the dehumidifier and regenerator respectively. From this definition, MRR is the product of inlet mass flow rate of dry air and the difference in humidity ratios between inlet and outlet of the vessel. This is mathematically formulated in terms of the air-side or liquid-side as follows:

$$MRR = m_a(\omega_o - \omega_i) = m_d\left(\frac{\chi_{in}}{\chi_{out}} - 1\right) \Rightarrow \chi_{in} > \chi_{out} \quad (1)$$

Where $m_a$ and $m_d$ are the inlet air and desiccant flow rates respectively; $\omega_i$ and $\omega_o$ are the inlet and outlet humidity ratios in $kg/kg_{dryair}$ respectively while, $\chi_{in}$ and $\chi_{out}$ are the desiccant concentrations at inlet and outlet conditions respectively. Effectiveness on the other hand is the ratio of real humidity change in air to the highest possible difference in humidity ratio, formulated as:

$$\varepsilon = \left(\frac{\omega_o - \omega_i}{\omega_e - \omega_i}\right) x100\% \quad (2)$$

Where $\omega_e$ is the humidity ratio of air at equilibrium conditions expressed as:

$$\omega_e = 0.62185\left(\frac{p_{v,o}}{P - p_{v,o}}\right) \quad (3)$$

Where P is the aggregate pressure in mmHg and $p_{v,o}$ is the outlet vapour pressure given by:

$$p_{v,o} = \frac{P}{62185}\left(\frac{\omega_i}{1+\frac{\omega_i}{0.62185}} - \frac{\vartheta}{\dot{M}_a}\right) \quad (4)$$

The rate at which water vapour evaporates in the regenerator is governed by the heat transfer occurrence between the air and desiccant solution. An expression for this manifestation is thus developed as:

$$\vartheta = \frac{1}{\kappa}\left[\frac{\dot{M}_d C_d T_d \varepsilon}{1-\varepsilon} - \dot{M}_a C_a (T_i - T_o)_a\right] \quad (5)$$

Where; $\vartheta$ is the moisture condensation rate in kg/m-s, $\kappa$ is the concealed heat of condensation kj/kg; $\dot{M}$ is the mass fluctuation in kg/m-s; C is the specific heat capacity in kJ/kgK and T is the temperature in K. The subscripts *i* and *o* show the inlet and outlet conditions respectively; while *a* and *d* stand for air and desiccant solution respectively. The desiccant concentration is one of the most essential parameters of consideration because it determines the rate and amount of water expended or absorbed from the air. Therefore, at outlet state, the concentration $\chi$ can be found as follows:

$$\chi_{d,o} = \frac{\chi_{d,i}}{1+\left(\frac{\vartheta}{\dot{M}_a}\right)} \quad (6)$$

It should however be noted that the desiccant concentration at dehumidifier outlet was considered to be the inlet concentration for the regenerator.

## 3. ARTIFICIAL NEURAL NETWORK MODEL

According to [9], the artificial neural network (ANN), as an upcoming machine learning technique, applies the analogy of axon-like interconnected neurons for performance prediction and estimations. These tasks are achieved by combining several neurons in a network capable of being trained using examples and input data sets to produce desired results.

The interconnection provides a communication channel between successive neurons. Depending on the complexity of the network, the main parts of a typical ANN includes an input, output and one or more hidden layers [11]. A feed-forward neural network generally consist of L-layers and L-1 hidden layers ignoring the front layer of input nodes.

A classical neuron is characterized by sets of interconnecting links with defined weights, a summing joint where all weighted inputs combine and a stimulation function for control-ling the magnitude of the outputs. The learning process intricately updates the weights of neuron connections to effectively accomplish a specific task. The capability of the ANN technique to consistently learn from examples gives it an edge over other methods. Moreover, ANN follows basic rules such as input-output interactions from an assortment of typical examples contrary to traditional procedures decided by human specialists.

A reinforcement technique of supervised learning based on the error-correction principle is best suited for application in LDACS due to its capability to formulate a system training model and provide predictable output for each input configuration. The learning process encompasses creating a learning paradigm, guides and steps for updating the network weights. Hence, the ANN can predict the desired results with high precision. Based on the [3] perceptron convergence theorem, the learning begins immediately an error occurs, thus the perceptron

learning process converges after a definite number of iterative steps. As earlier enumerated, when dealing with the dehumidifier, each neuron possesses a net and activation function indicating the possible combination of network outputs in the form of $\{x_j : 1 \leq j \leq n\}$ inside the neuron. Assigning every link between neurons a variable weight factor, each neuron to produce a sum of all inbound signal weights resulting in an internal activity level $a_i$ defined as:

$$a_i = \sum_{j=1}^{n} w_j x_{ij} \pm w_{io} \tag{7}$$

Where $\{w_{ij}: 1 \leq j \leq n\}$ is the synaptic weight and $w_o$ is the bias used to model minimum or maximum conditions. The activation process of the network solely depended on the applied threshold which was mathematically represented as:

$$y = \varphi(a) \tag{8}$$

For simplicity and convenience of this cluster of ANN, a logic function shown in equation 9 was used for the activation:

$$\varphi(a) = \frac{1}{1+e^{-a}} \tag{9}$$

The learning loop containing input formats, error calculation and adjustment was varied using sets of various input-output examples until an acceptable response level of network sum of square error was achieved. Knowing the technique of input data format, the expected output and the type of modelling task, the number of nodes for input and output was easily determined, though not fixed. For this study, the constructed general layout of the ANN configuration is presented in Figure 1 with six nodes on the input layer, 4 to14 nodes on each of the two hidden layers and a one node output layer.

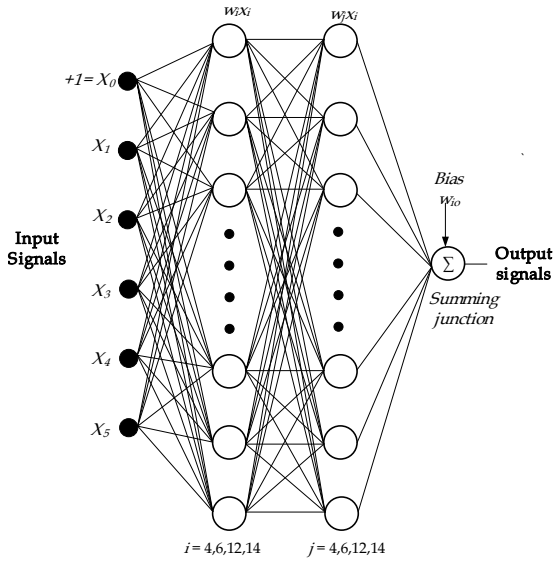


**Figure 1** The artificial neural network structure

Whereas normalization of data, also known as scaling of input data, significantly enables transposing of the inputs into statistical series housing the sigmoid stimulation function, it does not work well and tends to misrepresent dynamic data which formed the majority in this case. Therefore, an alternative was considered by linearly magnifying the data interval commensurate to the stimulation function. A linear scale was adopted by having a static linking weight to each neuron fed with linear stimulation function and a 1:1 linkage to the input stratum. This enabled the calculation of regressions with the capability of transposing any input into any output collection

## 4. ERROR BACK PROPAGATION TRAINING OF ANN

Optimized data weights were to be approximated and then trained to give desirable outcomes at the fewest number of whole iteration procedures of ANN training also known as epochs. A bunch of examples go through the learning algorithm concurrently in a single epoch prior to reorganizing the respective weights in batch training. Alternatively, successive training involves updating of weight at every instance the training vector passes over the training algorithm. Whereas, the batch training enables fast processing of numerous non-zero input data, sequential training was preferred for this study because of its precise accuracy irrespective of whether the data is defined or undefined.

The same procedure as previously laid out by the authors in analyzing the dehumidifier was followed. To establish the weight combination of each layer an error backpropagation training (EBPT) technique was used. Taking a set of training examples in the form of $\{x(j);1 \leq j \leq n\}$, all the $n$ inputs in the neural network were initially entered and then the expected outputs $\{z(j);1 \leq j \leq n\}$ were calculated. The training data comprised N sets of input-output trajectories defining the task. The algorithm minimized the mean square variation between the actual and anticipated outcomes in a back-propagation scheme. The performance of the back-propagation algorithm was geared towards a predetermined slip task involving the general average of the variation of individual neurons in the output stratum and the anticipated result. The error task was formulated with the aim of varying the weight matrix $W$ in order to minimize error. Hence, the sum of square error E was then calculated as follows:

$$E = \frac{1}{N}\sum_{j=1}^{n}\left[d_j - z_j\right]^2 = \frac{1}{N}\sum_{j=1}^{n}\left[d_j - f(w_j x_{ij})\right]^2 \quad (10)$$

Where: $w_{ji}$ = weight matrix $[W_0 W_1 W_2 :::::: W_n]$ and $x$ = input vector $[X_0 X_1 X_2 ::::: X_n]$. With $j$ as the indexing constant for neurons in the output layer and $d_j$ as the constituent of the $N^{th}$ anticipated vector and $f(w_j x_{ij})$ being the component of the output of $N$ inputs, the minimization of the objective function called for modifying instructions to change the weights of the neuron linkages. Care was taken to avoid the occurrence of a linear least square optimization problem, since lessening the error task gives rise to modification instructions to change the neuron linkage weights. Therefore, to modify the link between two adjacent neurons in layers L and L+1 respectively without oscillation, an iterative correction factor with a momentum term was formulated as:

$$\Delta w_{ij}(n-1) = w_{ij}(n) + \mu\delta_j z_1 + \beta\Delta w_{ij}(n) \quad (11)$$

With $n$ number of iterations, the correction factor was $\Delta w_{ij} = \mu\delta_j z_1$. Where index $i$ represents the units in layer $L$, $\mu$ is the learning rate, $z_i$ is the output of the $i^{th}$ neuron in layer L, and $j$ is the error element transmitted from the preceding $j^{th}$ neuron in layer L+1 determined for $j^{th}$ neuron in the output layer as $\delta j = [d_j - z_j]/[1 - z_j]$ and $\delta_j = z_j[1 - z_j]\sum_m \delta_m w_{mj}$ for the $j^{th}$ neuron in hidden layer with $m$ neurons in layer L+2. $\beta$ is a real constant which checks the influence of previous weight modifications on the current path of traffic in the weight matrix. The feed-forward ANN algorithm is thus laid down as follows:

1. **Start**
2. Set the weights to trivial arbitrary values
3. Arbitrarily select an input pattern $x(\mu)$
4. Disseminate the signal onward over the network
5. Calculate for the output layer $\delta_i^L = f'(h_i^L)[d_L^a - z_i^L]$; Where $h_i^L$ is the net input to the $i^{th}$ level while $f'$ is the derivative of the stimulation factor $f$.
6. Repeat procedure 4 for the subsequent levels by transmitting the error towards the back according to the expression; $\delta_i^L = f'(h_i^L)\sum_j w_{ij}^{i+1}\delta_j^{i+1}$, for $l = (L-1, \ldots\ldots, 1)$

7. Modify the weights by the function; $\Delta w_{ij}^{i} = \delta_{i}^{l} z_{l}^{l-1}$
8. Go back to stage 2 and replicate the procedure until the total number of repetitions is achieved or output layer displays an error under the specified threshold
9. **End**

A combination of parameters summarized in table 2 and the feedforward algorithm constituted the ANN model logic procedure and the final decision on the output.

**Table 2** ANN modelling parameters

| Item | Parameter |
|---|---|
| Liquid desiccant | Lithium bromide |
| Inputs | - Air = inlet humidity ratio, inlet temperature and flow rates,<br>- Desiccant = concentration, inlet temperature, and flow rates |
| Outputs | - Temperature, humidity ratio, moisture removal rate and effectiveness |
| Network structures | - 6-4-1, 6-6-1, 6-12-1, 6-14-1, 6-4-4-1 |
| Number of hidden layers | - 4, 6, 12, 14 |
| Training technique | - Feedforward - Error back propagation algorithm |
| Training ratio<br>Testing ration | - 70% from data = 60<br>- 30% from data = 25 |
| Training function | - traingdm |
| Learning function | - learngdm |
| Performance function | $E = \frac{1}{N}\sum_{j=1}^{n}[d_j - z_j]^2 = \frac{1}{N}\sum_{j=1}^{n}[d_j - f(w_j x_{ij})]^2$ |
| Decision Logic | - If (calculated value –assigned value) < 1 x $10^{-3}$ then lowest error. Accept output |

## 5. RESULTS AND DISCUSSION

Supervised learning based on the reinforcement technique involving the error correction rule and perceptron convergence theorem were applied to develop an ANN algorithm in MATLAB. The choice of appropriate number of training arrangements offering effective simplification was very trivial for the computational accuracy of the ANN algorithm. To determine the best ANN configuration, which would give the best training outcomes, various structures were considered for both moisture removal rate and effectiveness. The ensuing coefficient of determination $R^2$ values during training, validation and testing were used to choose the most suitable structure. However, the overall values were obtained for each combination and the best chosen.

A summary of the respective patterns and their corresponding $R^2$ values during regeneration process is presented in Table 2. Based on the respective outcomes of numerous combinations tested and analysed, configurations 6-4-4-1 and 6-14-1 demonstrated the best performance levels for moisture removal rate and effectiveness respectively for the regenerator. The results informed the decision for choice of these configurations for comparison of various parameters.

The $R^2$ values for the regenerator MRR model ranged from 0.82 to 0.985, 0.82 to 0.991, 0.78 to 0.991 and 0.78 to 0.975 during training, validation, testing and overall respectively. It was noted that the finest MRR performance prediction was best achieved by configuration 6-4-4-1 at 0.975, validating at epoch-8 with a value of 1.7735 x$10^{-8}$ as shown in Figure 3a. In similar sequence, the regenerator effectiveness was predicted within ranges 0.83-0.999, 0.82 - 0.999, 0.85 - 0.993 and 0.82 - 0.991 respectively. Structure 6-14-1 produced the finest results at 0.991 attaining an optimum performance prediction level of 3.3323 x $10^{-7}$ at epoch-5 as seen in Figure 3b.

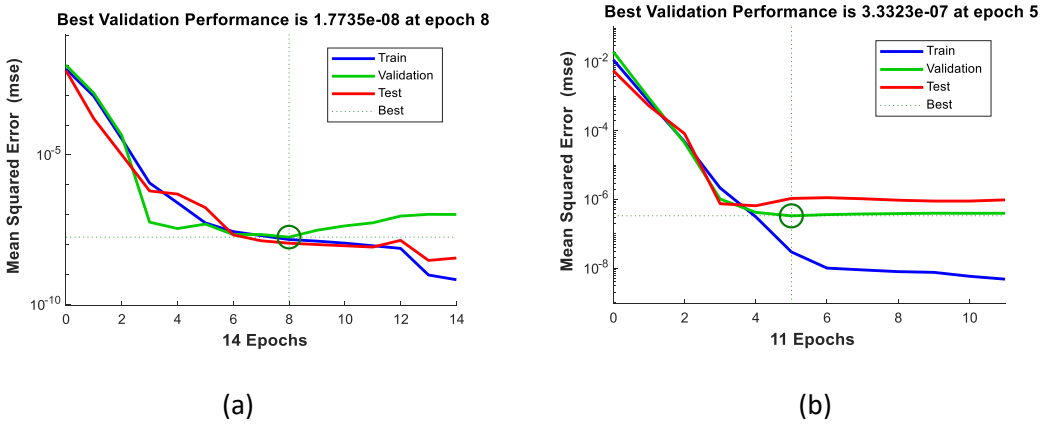


**Figure 3** The best-fit validation outcome for the regenerator (a) MRR (b) effectiveness

The regenerator MRR and effectiveness were best predicted at training output settings of 1*target+0.0034 and 1*target-0.000057 respectively. Other detailed presentation of testing, validation and overall outputs are shown in Figures 4 and 5. The training target being the experimental data, corroboration stopped at epochs 3 and 5 respectively at which point the corresponding $R^2$ values were 0.984 and 0.999 respectively.

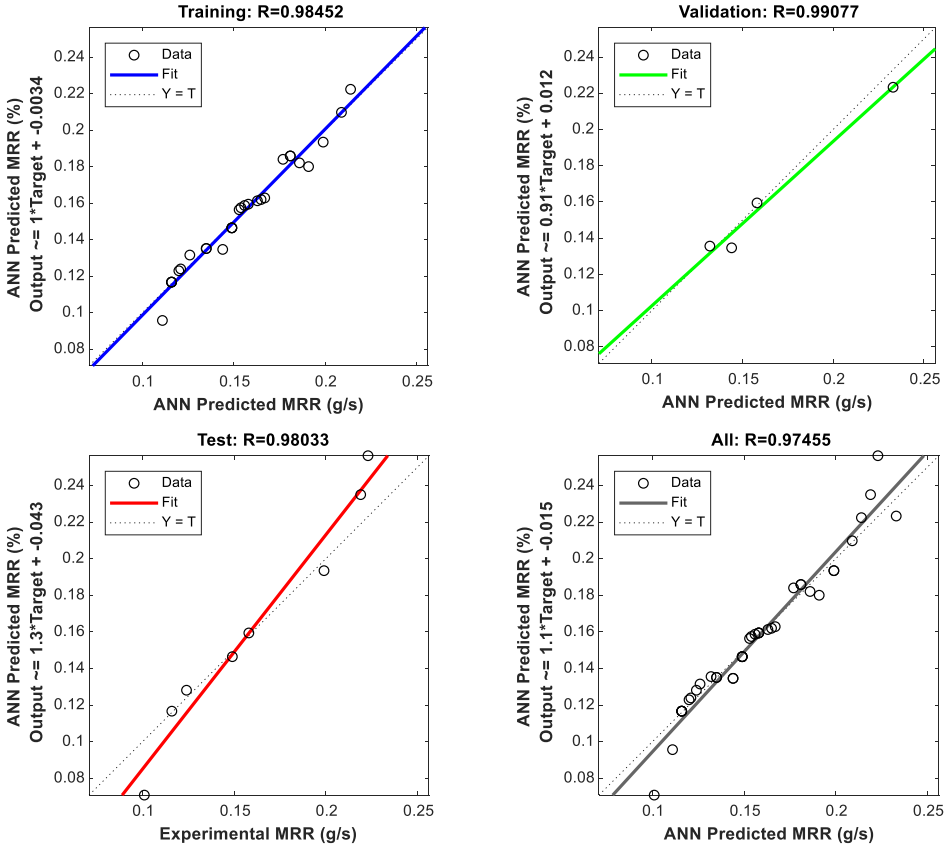


**Figure 4** The 6-4-4-1 ANN structure training regression validation halt at epoch 3 for MRR

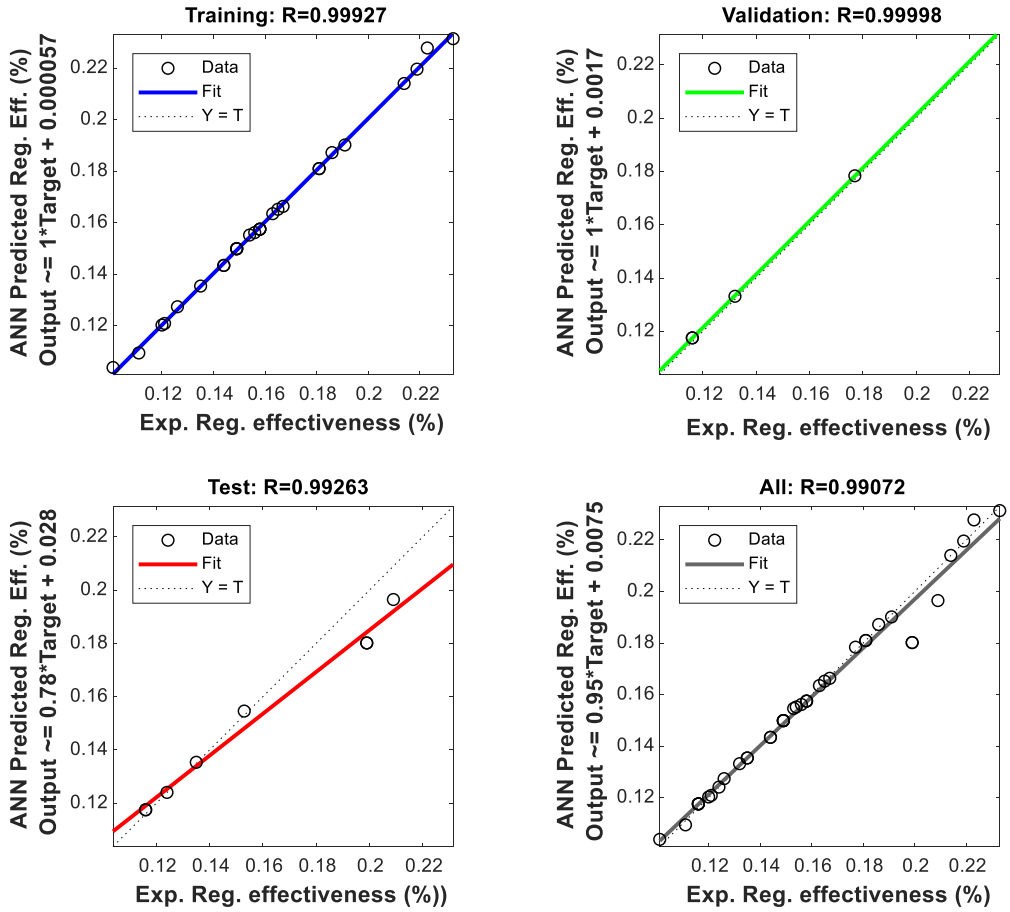


**Figure 5** The 6-14-1 ANN structure training regression validation halt at epoch 5 for effectiveness

## 6. MODEL AND EXPERIMENTAL RESULTS COMPARISON

The regenerator performance was characterized by MRR and effectiveness subjected to varying inlet temperatures of air and desiccant solution as well as inlet air humidity ratio. The training process was terminated when the iterations peaked at the defined total epochs of 25 000 or upon attainment of the least error on validation procedure, whichever came first. As a result, based on the comparison between the experimental and predicted results for MRR and effectiveness, the following findings were made.

The experimental and predicted regenerator MRR were plotted side by side against the number of testing in Figure 6 for structure 6-4-4-1. The highest MRR experienced occurred at a point of highest desiccant temperature as dictated by the solar radiation. However, on evaluation, the predicted and experimental profiles aligned perfectly with a maximum and mean difference being 0.18 g/s and 0.11 g/s respectively. As presented in Figure 7, the regenerator effectiveness was also computed and plotted for structure 6-14-1. Again, the profiles agreed well with a few negligible disparities with a mean and maximum difference of 0.6% and 1% respectively.

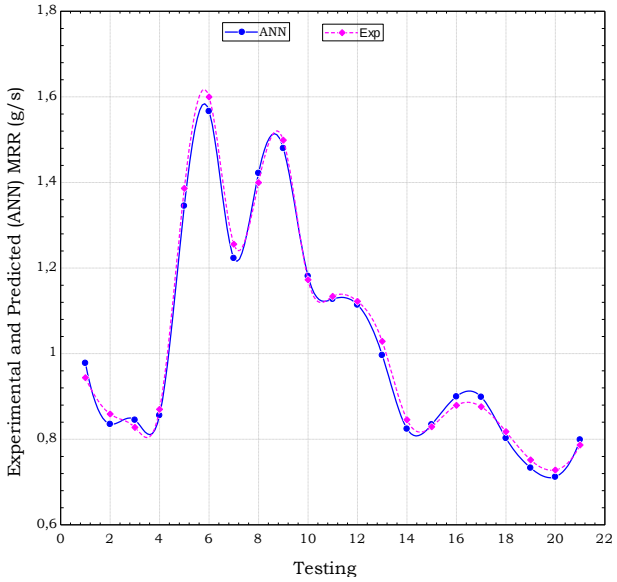


**Figure 6** The degree of accuracy between experimental and ANN predicted MRR values

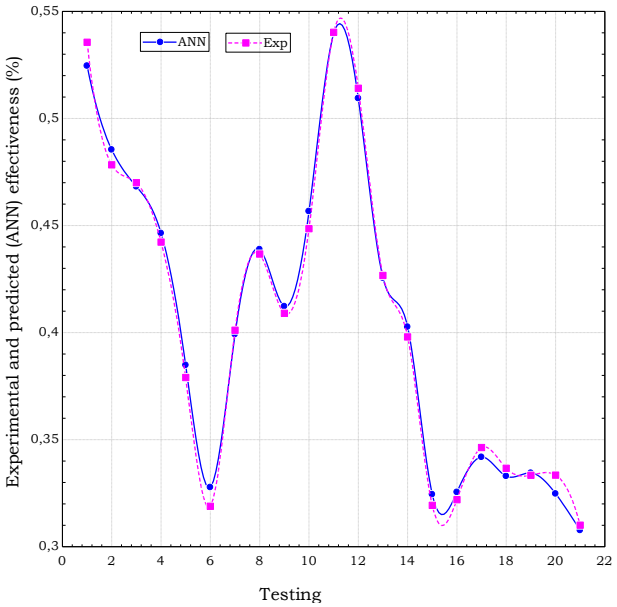


**Figure 7** The degree of accuracy between experimental and ANN predicted effectiveness

Since the humidity ratio (HR) of inlet air is essential in the design of LDAC systems, the humidity ratio at inlet conditions was monitored and recorded and used for training the neural network algorithm to mimic exact experimental outcomes. The respective outcomes of the predicted parameters were compared to those obtained from experimental processes. The variation of MRR and effectiveness against inlet air HR was plotted for the regenerator as shown in Figure 8. The MRR was observed to increase with as HR increased up to a maximum value of 1.47 g/s corresponding to 0.03 $kg_{H2O}/kg_{dryair}$ then slightly declined. The algorithm predicted the experimental values to maximum and mean accuracies of 0.0925 % and -0,012 % respectively. On the effectiveness, higher values were initially recorded up to HR of 0.018 $kg_{H2O}/kg_{dryair}$ then began to decline steadily. The maximum and mean accuracies of 4.14 % and 0.53 % respectively were realized in the prediction of experimental results by the neural network algorithm. The highest effectiveness obtained was 70 %, this value falling below 0.03 $kg_{H2O}/kg_{dryair}$.

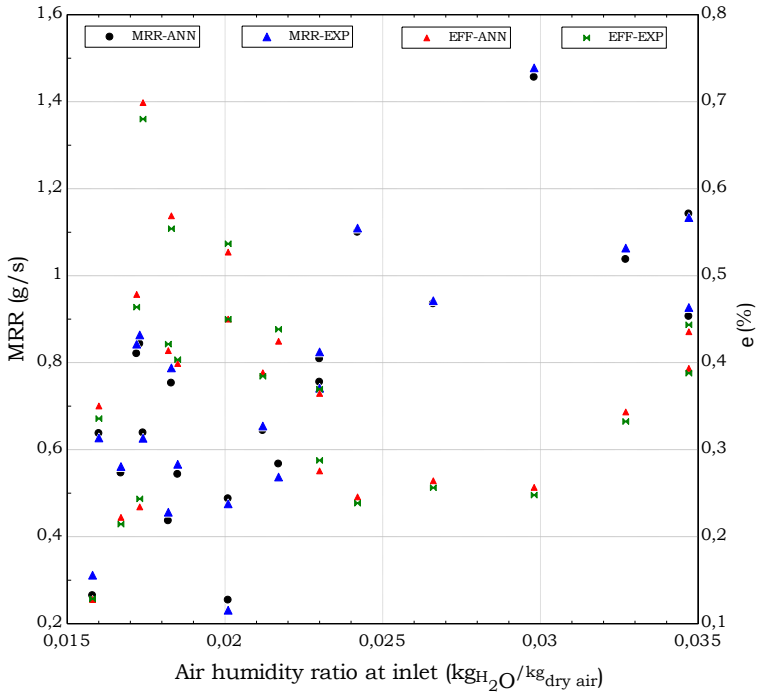


**Figure 8** The variation of MRR and effectiveness in relation to humidity ratio of air at inlet conditions

## 6.1. Effect of inlet desiccant temperature

The effect of inlet desiccant temperature variation of the regenerator was plotted as shown in Figure 9. The MRR displayed low sensitivity to changes in desiccant temperature at entry to the regenerator. However, beyond 32 $^{o}$C a diminishing trend was realized. In other words, MRR reduced with increase in temperature beyond this point. The highest difference between predicted and measured temperature was 3.496 %. From the above findings, it can be concluded that the ANN model precisely predicted the experimental inlet desiccant temperature with an average deviation of -0.5290 %. However, some see-saw variations were observed where the model didn't come close and these were attributed to minor discrepancies in experiments and oversimplification of the algorithm.

Of more interest was how the regenerator effectiveness varied with change in inlet desiccant temperature as a stimulant for heat and mass transfer. An increase in desiccant temperature resulted in improved regenerator effectiveness. This implied that desiccant at elevated temperature readily lost water vapour to the atmospheric air which resulted in a re-concentration to near initial conditions in readiness for re-circulation to the dehumidifier. This temperature increase could be provided by any renewable source or waste heat. In this case a hybrid PV/T was used. The variation of regenerator effectiveness is clearly evident in Figure 10 which shows a side-by-side comparison of the ANN generated values with those from the experiment. The maximum and mean deviations attained were 2.61 % and 0.21 % respectively, implying a near perfect fit.

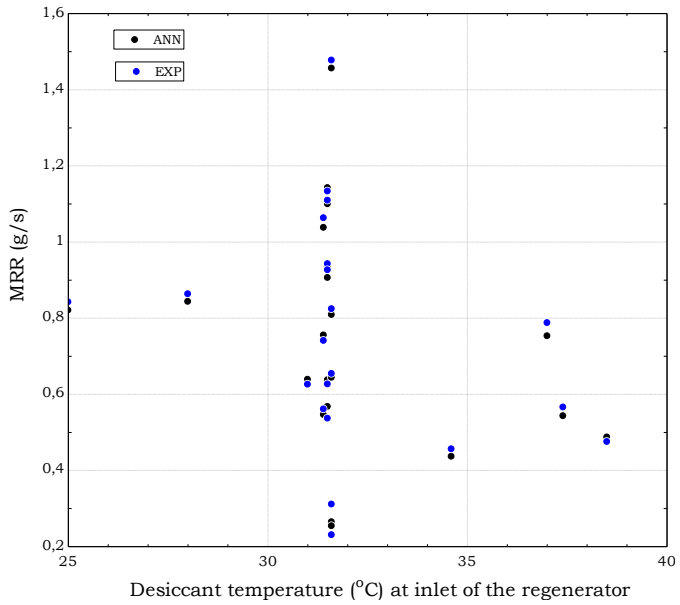


**Figure 9** The effect of inlet desiccant temperature on moisture removal rate of the regenerator MRR

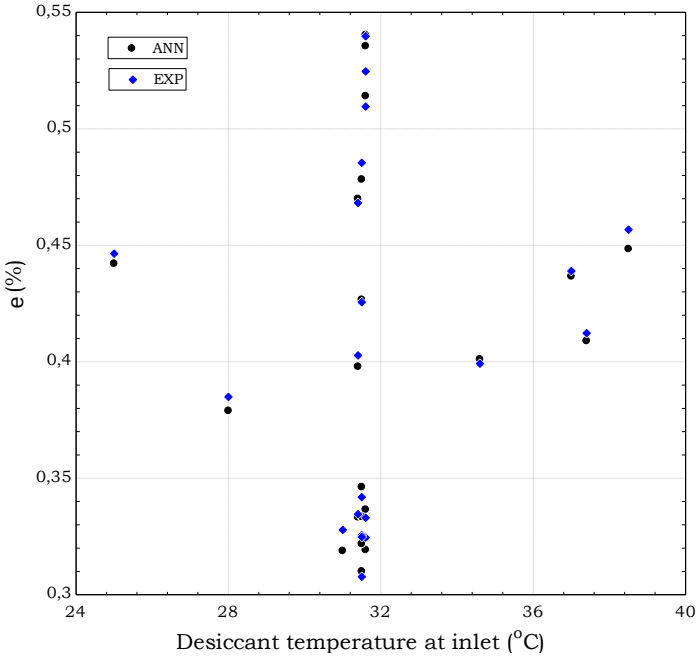


**Figure 10** Effect of inlet desiccant temperature on the effectiveness of the regenerator

## 6.2. Effect of inlet air temperature

In the regenerator, water vapour is expelled from the desiccant and absorbed in the air which is then exhausted to the atmosphere. The regenerator moisture removal rate varied proportionally with the air temperature, as depicted in Figure 11. The more the temperature escalated, the more the moisture removal rate showed an upward trend. This trend continued to a level of 30 $^{o}$C then a slight reduction ensued. However, up to the 40 $^{o}$C mark, the MRR was still well over 1 g/s. Again, the predicted MRR values matched perfectly with the calculated values from measured data. Although there were some negligible variations, the highest MRR was 1.5 g/s with a mean and highest difference of -0.12 % and 3.2 % respectively. The deviations were insignificant compared to the maximum allowable value of 20 %, hence the algorithm was deemed a success in this case.

The highest regenerator effectiveness achieved was 70 % with air temperature at room temperature of 25 $^{o}$C as shown in Figure 12. Beyond this point the effectiveness reduced significantly. The effectiveness outcomes of the ANN model were matched with the experimental data and found to be within mean and maximum deviation of -0.23 % and 2.1 % respectively. The insensitivity of effectiveness to air temperature was generally due to the air properties at room temperature which made it favourable for water vapour absorption by the liquid desiccant. In contrast, for the regeneration process, the higher desiccant temperatures resulted in higher effectiveness hence better performance.

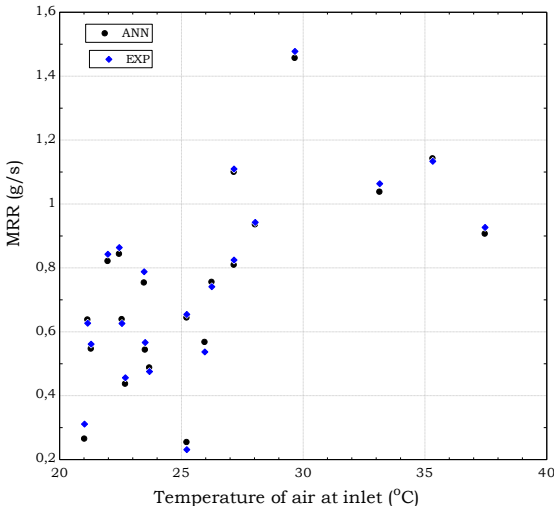


**Figure 11** Effect of the regenerator inlet air temperature on MRR

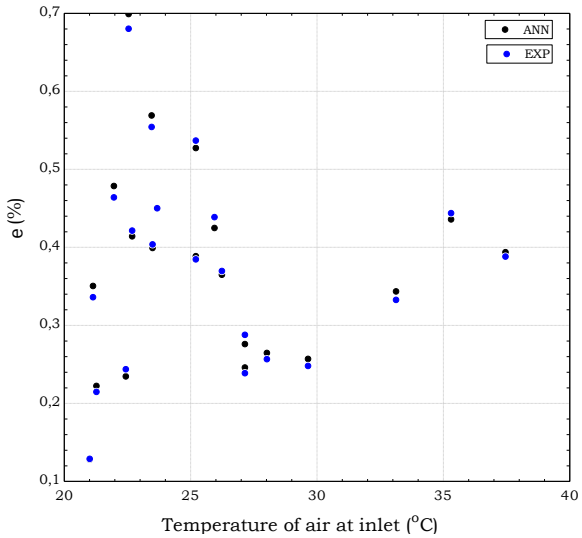


**Figure 12** The effect of inlet air temperature on effectiveness of the regenerator

## 7. CONCLUSION

Moisture removal rate and effectiveness were used as the performance analysis parameters for a solar adiabatic liquid desiccant regenerator. Using the reinforcement technique of supervised learning, error correction and perceptron convergence theorem, an ANN algorithm was developed and implemented in MATLAB. A regression analysis was performed on various ANN structures during training and the respective coefficient of determination $R^2$ established which then formed the basis for choosing the best combination with the best-fit. Data from the previous experimental results were used to train, test and validate the ANN algorithm. In order

to avoid oversimplification and/or over-complication of the model, the quantity of neurons and the number of layers were carefully chosen for exact accuracy of the algorithm. From the respective outcomes, the regenerator performance was best predicted by patterns 6-4-4-1 and 6-14-1 for MRR and effectiveness respectively. Hence, the results discussed for various items and comparisons were based on these configurations. From an in-depth detailed analysis of the algorithm performance and upon comparison of the ANN generated results to those from experiments, a number of conclusions were drawn, as presented below.

The predicted and experimental regenerator MRR profiles aligned perfectly, with the maximum and mean difference being 0.18 g/s and 0.11 g/s respectively. The regenerator effectiveness profiles agreed well with a few negligible disparities with a mean and maximum difference of 0.6 % and 1 % respectively. The algorithm predicted the experimental MRR values to maximum and mean accuracies of 0.0925% and -0,012 % respectively. The maximum and mean accuracies of 4.14 % and 0.53 % respectively were realized in the prediction of experimental regenerator effectiveness by the neural network algorithm. Overall, the prediction was deemed perfect since deviations were negligible and within acceptable limits. The ANN model precisely predicted the experimental regenerator MRR with respect to inlet desiccant temperature with an average deviation of -0.5290 % while the highest difference was 3.496 % between predicted and measured temperature.

As the stimulant for heat and mass transfer in the regenerator, the effectiveness varied with change in inlet desiccant temperature. The side-by-side comparison of the general trends as predicted by the ANN algorithm against the experimental values revealed maximum and mean deviations of 2.61 % and 0.21 % respectively. While the regenerator moisture removal rate varied proportionally with the air temperature, the predicted MRR values matched perfectly with the calculated values from measured data, with the mean and highest difference being -0.12 % and 3.2 % respectively.

The regenerator effectiveness outcomes of the ANN model were matched with the experimental data and found to be within a mean and maximum deviation of -0.23 % and 2.1 % respectively. In all the aforementioned cases, the mean and maximum differences between the ANN model and experimental values were way below the allowable limit of 5%, hence the algorithm was deemed to be successful and could find use in air conditioning scenarios. The ANN algorithm's capability and flexibility test of processing unforeseen inputs was accurate with negligible deviations in predicting the regenerator effectiveness and MRR within all ranges of temperature and concentrations.

## REFERENCES

[1] Anil, K. J., Mao, J., and Mohiuddin, K. M. Artificial Neural Networks: A Tutorial. *IEEE Transactions on Neural Networks*, **21**(3), 1996, pp. 31-44.

[2] McCulloch, W. S. and Pitts, W. A Logical Calculus of Ideas Immanent in Nervous Activity. *Bull Mathematical Biophysics*, **5**, 1943, pp. 115-133.

[3] Rosenblatt, R. Principles of Neurodynamics. New York: Spartan Books, 1962.

[4] Minsky, M. and Papert, S. Perceptions: An Introduction to Computational Geometry. Cambridge, Mass.: MIT Press, 1969.

[5] Hopfield, J. J. Neural Networks and Physical Systems with Emergent Collective Computational Abilities. *Proceedings of the National Academy of Sciences of the United States of America*, **79**, 132(f), 1982, pp. 2554-2558.

[6] Werbos, P. Beyond Regression: New Tools for Prediction and Analysis in the Behavioural Sciences. PhD thesis, Department of Applied Mathematics, Harvard University, Cambridge, Mass, 1974.

[7] Rumelhart, D. E. and McClelland, J. L. Parallel Distributed Processing; Exploration in the Microstructure of Cognition. Cambridge, Mass.: MIT Press, 1988.

[8] Gandhidasan, P. and Mohandes, M. A. Prediction of Vapour Pressures of Aqueous Desiccants for Cooling Applications by Using Artificial Neural Networks. *Applied Thermal Engineering*, **28**, 2008, pp. 126-135.

[9] Gandhidasan, P. and Mohandes, M. A. Artificial Neural Network Analysis of Liquid Desiccant Dehumidification System. *Energy*, **36**(2), 2011, pp. 1180-1186.

[10] Mohammed, T. H., Sohif, B. N., Sulaiman, M. Y., Sopian, K., and Abduljalil, A. A. Artificial Neural Network Analysis of Liquid Desiccant Dehumidifier Performance in a Solar Hybrid Air-Conditioning System. *Applied Thermal Engineering*, **59**, 2013, pp. 389-397.

[11] Mohammed, T. H., Sohif, B. N., Sulaiman, M. Y., Sopian, K., and Abduljalil, A. A. Artificial Neural Network Analysis of Liquid Desiccant Regenerator Performance in a Solar Hybrid Air-Conditioning System. *Sustainable Energy Technologies and Assessment*, **4**, 2013, pp. 11-19.

[12] Mohammed, T. H., Sohif, B. N., Sulaiman, M. Y., Sopian, K., and Abduljalil, A. A. Implementation and Validation of an Artificial Neural Network for Predicting the Performance of a Liquid Desiccant Dehumidifier. *Energy Conservation and Management*, **67**, 2013, pp. 240-250.

[13] Zeidan, E. B., Aly, A. A., and Hamed, A. M. Investigation on the Effect of Operating Parameters on the Performance of Solar Desiccant Cooling System Using Artificial Neural Networks. *International Journal of Thermal Environment Engineering*, **1**, 2010, pp. 91-98.

# Chapter8

# CONCLUSIONS AND RECOMMENDATIONS

## 8.1 Conclusions

The endothermic and exothermic reactions occurring during moisture exchange between the air and desiccant solution in the dehumidifier and regenerator vessels give rise to a simultaneous heat and mass transfer phenomena. Consequently, the heat and mass transfer process from analysis appear to coupled and cannot be delinked but analysed together under the influence of different variables to establish the aggregate operational performance of the dehumidifier and regenerator vessels. Moisture removal rate and effectiveness provide the most effective criteria for operational performance characterization of liquid desiccant dehumidifier and regenerator operating under adiabatic conditions. However, the heat and mass transfer coefficients indicate how best the moisture is absorbed or expelled from the air and desiccant, respectively. Based on the results of the comprehensive experimental and theoretical modelling studies conducted in this work, the following conclusions can be drawn;

From the considered sub-tropical climatic conditions, the experimental findings have provided in-depth insights into the application of solar energy and square channelled packing in the design and optimization of liquid desiccant and regeneration set-ups. For the given inlet conditions, increased inlet air humidity produced increases in inlet air enthalpies and reduction in outlet air enthalpies during both regeneration and dehumidification process. On the contrary, the desiccant solution enthalpies reduced at inlets and increased at outlets of both dehumidifier and regenerator vessels while the incoming air humidity increased. The increase in inlet air humidity ratio also significantly reduced regenerator effectiveness and MRR, while causing increased dehumidifier effectiveness and MRR. The increase in L/G ratio caused an increase in dehumidifier MRR and decrease in regenerator MRR. In contrast, the dehumidifier effectiveness was reduced while that of the regenerator is improved. Varying the airmass flow rate progressively upwards, improved the regenerator effectiveness by 15% while, that of the dehumidifier reduced by 43%. The MRR generally showed low sensitivity to the air and LiBr flow rates. The desiccant concentration significantly affected the dehumidifier MRR and effectiveness. As the solution concentration increased, the MRR decreased significantly by up to 4 kg/s. The effectiveness improved with increased LiBr concentration by up to 5% while the regenerator MRR decreased with increase in concentration within the same range.

Sets of reliable and consistent data upon which theoretical simulation models can be validated and empirical correlations developed have been provided. For optimal operation of the LD dehumidification and regeneration, a balance must be struck between the air and desiccant flow rates as well as concentration. These flow rates in-turn affect the heat and mass transfer coefficients and Lewis number.

The 3D predictive numerical thermal model based on falling liquid stream with constant thickness in counter-flow configuration was developed and solved by a combination of separative appraisal and stepwise iterative technique. The hybrid solution technique involving separative evaluation and iterative process allows for adjustments of model elements to suit the scheme under consideration. The numerical model showed that during the dehumidification and regeneration processes, an increase in airflow rate per unit length and desiccant solution flow rate per unit area resulted in increased thermal and mass exchange coefficients but with varying proportions. As the Lewis number increased, both the heat and mass transfer constants decreased significantly for both the dehumidifier and regenerator vessels. Comparisons conducted at various levels of input and output of the experimental and predicted dehumidifier and regenerator MRR, effectiveness, heat and mass transfer coefficients revealed sublime conformity. The underlying findings of this study, provided insights into the design and optimization.

The use of a multivariate Markov chain model in weather prediction is uncommon. This technique, as shown in the study, has provided perfect sets of artificial weather data with several input variables specific to subtropical climates. The artificial parameters, coupled with the analytical model, were used to theoretically predict the performance of solar-powered LD regenerator with great success. Even though much more computer time and memory were required during the iterative solution process of the model, the prediction of MRR and effectiveness was within the acceptable mean deviation of $\pm$ 20%. The precision of forecasting of categorical sequences was due to the associated computational accuracy, effective application and increased sequential phases. Stochastically generated artificial weather data can reliably be implemented in the solar energized system of LD dehumidification and regeneration.

The artificial weather data was applied in theoretical analysis of desiccant regeneration system powered by solar energy via a hybrid PV/T. From the air and desiccant temperature profiles at entry and exit of the regenerator, the highest inlet temperature attained was 67.22$^o$C with a corresponding outlet temperature of 36.14$^o$C. The regenerator effectiveness improved proportionally with air and desiccant mass flow rates. However, the maximum effectiveness of 69.3% was achieved at a corresponding air flow rate of 0.0847 kg/min, beyond this value, the effectiveness begun to drop due the system's reliance on the solar energy. The optimum flow mix for

effective regeneration was therefore established to be 0.847 and 0.00331 kg/min for air and desiccant solution, respectively. The liquid desiccant solution concentration by mass increased by 30% during peak hours when solar radiation was at its maximum. Increase in air and desiccant mass flow rates caused an exponential increase in the overall mass transfer coefficient over the regeneration period. The comparison of predicted heat transfer coefficients and experimental values showed an average deviation within the range of ±20%. The theoretical model revealed that, PV/T module could significantly raise desiccant temperature to required levels for regeneration process.

The artificial neural network (ANN) technique has been shown to offer a high degree of flexibility in the external domain suitable for complex computations and prediction with less time and little energy intake. The ANN technique has been used in this study with great success. As opposed to the complex mathematical models, a much faster and efficient process was achieved concerning the prediction of MRR and effectiveness of both dehumidifier and regenerator especially with a multi-layered algorithm trained based on supervised learning and error correction principle. The results have shown that the 6-4-4-1 and 6-14-1 conflagrations worked better for the regenerator MRR and effectiveness prediction, while configurations 6-12-12-1 and 6-6-6-1 worked well for the dehumidifier. In both scenarios, the percentage mean deviation between experimental and predicted results was less than ±5%. The fitness and elasticity of the ANN algorithm to predict unforeseen inputs with insignificant deviations under all ranges of temperature and concentration is paramount

## 8.2 Recommendations for future research

Considering the broadness of the subject area, the highlighted limitations of this research and despite the promising overall results obtained, some aspects still remain uncovered. The following suggestions and recommendations drawn from the study are put forth for further future research.

- From the experimental study, the square channelled ceramic cordierite (CC) packing material was used in the dehumidifier and regenerator. However, the biochemical reactions and biodegradability of LiBr and ceramic cordierite was not considered and can be proposed for further investigations.
- For incontestable accuracy, it is recommended that the predictive analysis should be validated with practical values of the geographical location under consideration; otherwise, a wide wedge between the predicted and measured values is likely to occur.

- Other liquid desiccants other than LiBr may also be tested on a PV/T to establish the applicability and proportions of concentrations achievable in a counterflow regenerator.
- This study only considered the counterflow configuration of the dehumidifier and regenerator. However, it is proposed that other configurations such as co-flow and cross-flow may be considered and evaluated to see their performance.

# REFERENCES


Al-Farayedhi, A. A., Gandhidasan, P., and Al-Mutairi, M. A. (2002). Evaluation of heat and mass transfer coefficients in a gauze-type structured packing air dehumidifier operating with liquid desiccant. *International Journal of Refrigeration*, 25:330–339.

Bravo, J., Rocha, J. A., and Fair, J. R. (1986). Pressure drop in in structured packings. *Hydrocarbon Processes*, 56(3):45 – 59.

Chung, T. W., Ghosh, T. K., and Hines, A. L. (1996). Comparison between random and structured packings for dehumidification of air by lithium chloride solutions in a packed column and their heat and mass transfer correlations. *Industrial and Engineering Chemistry Research*, 35(1):192–198.

Conde, M. (2004). Properties of acqueous solutions of lithium and calcium chlorides: formulations for use in air conditioning equipment design. *International Journal of Thermal Science*, 43:367–382.

de Lucas, A., Donate, M., and Rodriguez, J. F. (2003). Vapour pressures, densities, and viscosities of the (water+lithium bromide+potassium acetate) system and (water+lithium bromide+sodium lactate) system. *Journal of Chemical Engineering*, 48:18 – 22.

Dwyer, T. (2014). Liquid desiccants for dehumidification in building air conditioning systems. Journal 71, CIBSE.

Eduardo, C., Nóbrega, L., Carvallo, N., and Brum, L. (2013). *Desiccant-Assisted Cooling: Fundamentals and Applications*. Springer, London, 3rd edition edition.

Ertas, A. and Kiris, I. (1992). Properties of a new liquid desiccant solution-lithium chloride and calcium chloride mixture. *Solar Energy*, 49.

Gandhidasan, P. (2002). Prediction of pressure drop in a packed bed dehumidifier operating with liquid desiccant. *Applied Thermal Engineering*, 22:1117–1127.

Gandhidasan, P. (2004). A simplified model for air dehumidification with liquid desiccant. *Solar Energy*, 76:409–416.

Kaita, Y. (2001). Thermodynamic properties of lithium bromide-water solutions at high temperatures. *International Journal of Refrigiration*, 24:371 – 90.

Koronakia, I., Christodoulakia, R., Papaefthimioua, V., and Rogdakisa, E. (2014). Critical review of coupled heat and mass transfer models for a liquid desiccant

adiabatic dehumidifier and regenerator. *Advances in Building Energy Research*, 8:117–136.

Lazzarin, R. M., Gasparella, A., and Longo, G. A. (1999). Chemical dehumidification by liquid desiccants: theory and experiment. *International Journal of Refrigeration*, 22:334–347.

McNelly, L. (1979). Thermodynamic properties of aqueous solutions of lithium bromide. *ASHRAE Trans*, 85:412 – 34.

Mei, L. and Dai, Y. J. (2008). A technical review on use of liquid-desiccant dehumidification for air conditioning application. *Renewable and Sustainable Reviews*, 12:662–689.

Morillon, V., Debeaufort, F., Jose, J., Tharrault, J. F., Capelle, M., and Blond, G. (1999). Water vapour pressure above saturated salt solutions at low temperatures. *Fluid Phase Equilib*, 155:297 – 309.

Park, Y., Kim, J.-S., and Lee, H. (1997). Physical properties of the lithium bromide+1, 3-propanediol+water system. *International Journal of Refrigiration*, 20(5):319–325.

Yao, Y. and Liu, S. (2014). *Ultrasonic Technology for Desiccant Regeneration*. Wiley and Sons, Singerpore.

Younus, A., Gandhidasan, P., and AL-Farayedhi, A. A. (1198). Thermodynamic analysis of liquid desiccants. *Solar Energy*, 62.

Yuan, Z. and Herold, K. E. (2005). Thermodynamic properties of aqueous lithium bromide using multiproperty free energy correlation. *International Journal of HVAC and Refregiation Research*, 11:377–393.

# AppendixA

## Basic Properties of Lithium Bromide (LiBr)

LiBr is the most common desiccant solution in air conditioning systems. It is made by mixing lithium carbonate and hydrobromic acid ( an aqueous solution of hydrogen bromide). This reaction results in precipitation of LiBr and water. The chemical formulation of the described response is thus;

$$LiOH + HBr \rightarrow LiBr + H_2O \tag{A.1}$$

The resulting LiBr solution has the following constant properties;

Table A.1: Thermophysical properties of LiBr

| **Property** | **Value** | **Unit/formula** |
|---|---|---|
| Molar mass | 86.845 | $g/mol$ |
| Density | 3.464 | $g/m^3$ |
| Melting point | 552 | $^oC$ |
| Boiling point | 1265 | $^oC$ |
| Solubility | Water | $H_O$ |
| | Methernol | $CH_3OH$ |
| | Pyridine | $C_5H_5N$ |
| | Ethernol | $C_2H_5OH$ |
| | Ethers | Assorted |

### A.0.1 Solubility boundary

Figure A.1 shows the soluble capability of LiBr. The line spanning from A-B-C-D is referred to as crystallization transition boundary for different hydrates formed in the process.

The following relationships define this crystallization line formulated by(Conde, 2004).

$$T(x_{s,LiBr}) = T_L + \frac{T_R - T_L}{x_R - x_L}(x_{s,LiBr} - x_L) + T_t \sum_{i=1}^{N} a_i (x_i - x_L)^{m_i} (x_R - x_{s,LiBr})^{n_i} \tag{A.2}$$

$$x_{s,LiBr}(T) = x_L + \frac{x_R - x_L}{T_R - T_L}(T - T_L) + \sum_{i=1}^{N} b_i \left(\frac{t - t_L}{T_t}\right)^{m_i} \left(\frac{T_R - T^{n_i}}{T_t}\right) \tag{A.3}$$

$$x_{s,LiBr} = \frac{\xi_{s,LiBr}/M_{LiBr}}{\xi_{s,LiBr}/M_{LiBr} + (1 - \xi_{s,LiBr})/M_{LiBr}} \tag{A.4}$$

Where $x_{s,LiBr}$ and $\xi_{s,LiBr}$ represent the molar and mass fraction of salt in the solution respectively; $M_{LiBr}$ and $M_{LiBr}$ are molar masses in $kgmol^{-1}$ of LiBr and $H_2O$ respectively;

The $H_2O$ three-point temperature $T_t = 273.16$ K was initially randomly taken as the reference temperature to work out the dimensionless constants $a_i$ and $b_i$.

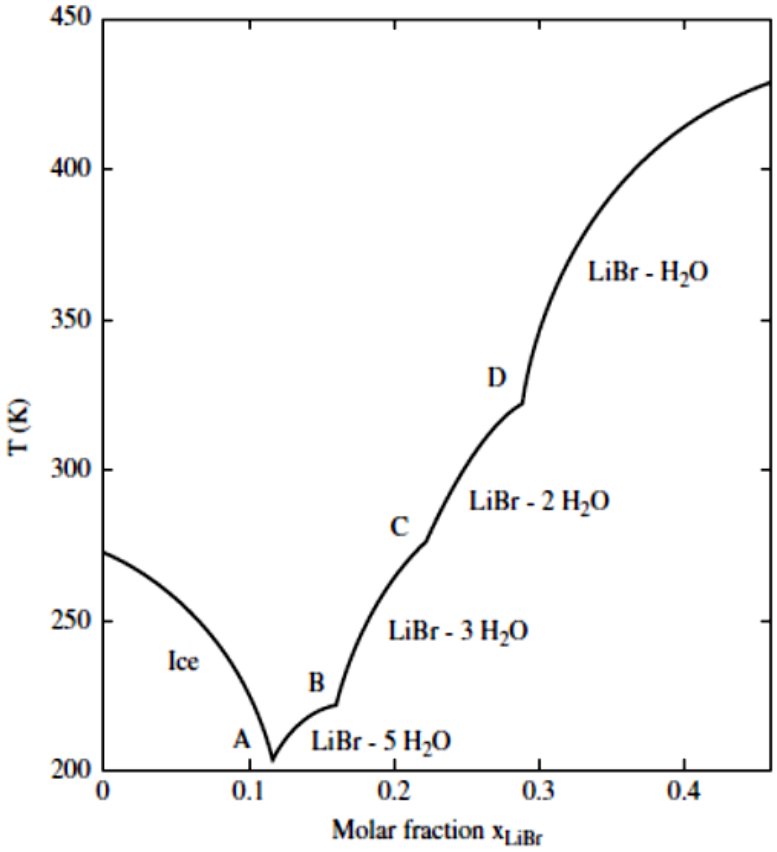


Figure A.1: Solubility boundary for LiBr aqueous solution

Table A.2: Constants for solubility boundary equation of LiBr based on equation A.2

| i | **LiBr-5$H_2O$**[a] | | | **LiBr-3$H_3O$**[b] | | | **LiBr-2$H_2O$**[c] | | |
|---|---|---|---|---|---|---|---|---|---|
| | $\mathbf{a}_i$ | $\mathbf{m}_i$ | $\mathbf{n}_i$ | $\mathbf{a}_i$ | $\mathbf{m}_i$ | $\mathbf{n}_i$ | $\mathbf{a}_i$ | $\mathbf{m}_i$ | $\mathbf{n}_i$ |
| 1 | $2.61161\times10^{1}$ | 1 | 1 | $2.47039\times10^{1}$ | 1 | 1 | $1.62375\times10^{1}$ | 1 | 1 |
| 2 | $2.38994\times10^{4}$ | 1 | 3 | $4.65459\times10^{3}$ | 1 | 3 | $2.47098\times10^{3}$ | 1 | 3 |
| i | **LiBr-$H_2O$**[d] | | | **Freezing area**[e] | | | | | |
| | $\mathbf{a}_i$ | $\mathbf{m}_i$ | $\mathbf{n}_i$ | $\mathbf{a}_i$ | $\mathbf{m}_i$ | $\mathbf{n}_i$ | | | |
| 1 | $1.00743\times10^{1}$ | 1 | 1 | $1.33842\times10^{1}$ | 1 | 1 | | | |
| 2 | $3.94593\times10^{3}$ | 1 | 4 | $-4.3929\times10^{1}$ | 2 | 1 | | | |
| 3 | | | | $4.02577\times10^{3}$ | 3 | 1 | | | |
| 4 | | | | $-505236\times10^{4}$ | 4 | 1 | | | |
| 5 | | | | $3.28383\times10^{5}$ | 5 | 1 | | | |

Table A.3: Constants for solubility boundary equation of LiBr based on equation A.3

| i | **LiBr-5$H_2O$**[a] | | | **LiBr-3$H_3O$**[b] | | | **LiBr-2$H_2O$**[c] | | |
|---|---|---|---|---|---|---|---|---|---|
| | $\mathbf{b}_i$ | $\mathbf{m}_i$ | $\mathbf{n}_i$ | $\mathbf{b}_i$ | $\mathbf{m}_i$ | $\mathbf{n}_i$ | $\mathbf{b}_i$ | $\mathbf{m}_i$ | $\mathbf{n}_i$ |
| 1 | -6.17446 | 1 | 1 | -7.17618E-1 | 1 | 1 | -1.06305 | 1 | 1 |
| 2 | -1.4677E+1 | 3 | 1 | -1.02551E+1 | 3 | 1 | -1.90921E+1 | 3 | 1 |
| i | **LiBr-$H_2O$**[d] | | | **Freezing area**[e] | | | | | |
| | $\mathbf{b}_i$ | $\mathbf{m}_i$ | $\mathbf{n}_i$ | $\mathbf{b}_i$ | $\mathbf{m}_i$ | $\mathbf{n}_i$ | | | |
| 1 | -9.25082E-1 | 1 | 1 | 1.22335 | 1 | 1 | | | |
| 2 | -7.2234E+1 | 3 | 1 | -1.67781 | 1 | 2 | | | |
| 3 | | | | -2.65346E+2 | 1 | 4 | | | |
| 4 | | | | -1.93594E+3 | 1 | 5 | | | |
| 5 | | | | -5.16209E+3 | 1 | 6 | | | |

For both cases;

$$\begin{cases} {}^{a}T_L = 202.8K & T_R = 222.4K & X_L = 0.1175 & X_R = 0.1604 \\ {}^{b}T_L = 222.4K & T_R = 277.11K & X_L = 0.1604 & X_R = 0.2213 \\ {}^{c}T_L = 277.1K & T_R = 322.2K & X_L = 0.2213 & X_R = 0.2869 \\ {}^{d}T_L = 322.2K & T_R = 429.15K & X_L = 0.2869 & X_R = 0.4613 \\ {}^{e}T_L = 273.16K & T_R = 202.84K & X_L = 0.0000 & X_R = 0.1175 \end{cases}$$

### A.0.2 Vapour Pressure (Pa)

Founded on Gibbs free-energy essential formulation, Yuan and Herold (2005) developed a novel thermodynamic property correlation models for aqueous LiBr which have been adopted for this work and enshrined in the computation software: the expressions are presented as follows;

$$\left(\frac{\partial g}{\partial \xi}\right)_{T,p} = \mu_{LiBr} - \mu_w \tag{A.5}$$

$$\mu_{LiBr}(\xi, T, P) = g + (1-\xi)\left(\frac{\partial g}{\partial \xi}\right)_{T,p} \tag{A.6}$$

$$\mu_w(\xi, T, P) = g - \xi\left(\frac{\partial g}{\partial \xi}\right)_{T,p} \tag{A.7}$$

$$\begin{aligned} g(\xi,T,P) = (A_0 + A_1\xi + A_2\xi^2 + A_3\xi^3 + A_4\xi^{1.1}) + T(B_0 + B_1\xi + B_2\xi^2 + B_3\xi^3 + B_4\xi^{1.1}) \\ +T^2(C_0 + C_1\xi + C_2\xi^2 + C_3\xi^3 + C_4\xi^{1.1}) + T^3(D_0 + D_1\xi + D_2\xi^2 + D_3\xi^3 \\ +D_4\xi^{1.1}) + T^4(E_0 + E_1\xi) + \left(\frac{F_0 + F\xi}{T - T_0}\right) + p(V_0 + V_1\xi + V_2\xi^2 + V_3T \\ +V_4\xi T + V_5\xi^2 T + V_6T^2 + V_7\xi T^2) + \ln T(L_0 + L_1\xi + L_2\xi^2 + L_3\xi^3 \\ +L_4\xi^{1.1}) + T\ln T(M_0 + M_1\xi + M_2\xi^2 + M_3\xi^3 + M_4\xi^{1.1}) \end{aligned} \tag{A.8}$$

The respective chemical strengths (in J/g) of $LiBr$ and $H_2O$ in the solvent are represented by $\mu_{LiBr}$ and $\mu_w$. $g$ in this case stands for Gibbs function while $\xi$ is the mass fraction of LiBr at temperature $T$(K) and ambient pressure $p$ (kPa).

By use of multi-property curve fit technique, the constant coefficients in the equation can be obtained by prudently solving for optimum vapour pressures at several points. The correlations give decent accuracy within liquid concentration span cascading from unadulterated water all the way to crystallization line with a corresponding temperature range of 5$^o$C to 250$^o$C. Some of the vapour pressure values obtained are presented in table A.4

Table A.4: Gibbs function quantities for computing LiBr solution vapour pressure generated from equation A.8

| | **0** | **1** | **2** | **3** | **4** |
|---|---|---|---|---|---|
| $A_i$, $i = 0...4$ | 5.506219979E+3 | 5.213228937E+2 | 7.77493056 | -4.575233382E-2 | -5.792935726E+2 |
| $B_i$, $i = 0...4$ | 1.452749674E+2 | -4.984840771E-1 | 8.836919180E-2 | -4.870995781E-8 | -2.905161205 |
| $C_i$, $i = 0...4$ | 2.648364473E-2 | -2.311042091E-3 | 7.55976620E-6 | -3.763934193E-8 | 1.176240649E-3 |
| $D_i$, $i = 0...4$ | -8.526516950E-6 | 1.320154794E-6 | 2.791995438E-11 | — | -8.511514931E-7 |
| $E_i$, $i = 0,1$ | -3.840447174E-11 | 2.625469387E-11 | — | — | — |
| $F_i$, $i = 0,1$ | -5.159906276E+1 | 1.114573398 | — | — | — |
| $L_i$, $i = 0...4$ | -2.183429482E+3 | -1.266985094E+2 | -2.364551372 | 1.389414858E-2 | 1.583405426E+2 |
| $M_i$, $i = 0...4$ | -2.267095847E+1 | 2.983764494E-1 | -1.259393234E-2 | 6.849632068E-5 | 2.767986853E-1 |
| $V_i$, $i = 0...4$ | 1.1767416161E-3 | -1.002511661E-5 | -1.695735875E-8 | -1.497186905E-6 | 12.538176345E-8 |
| $V_i$, $i = 5...7$ | 5.815811591E-11 | 3.057997846E-9 | -5.129589007E-11 | — | — |

Statistics: Mean vapour pressure error = 2.97%; $R^2$ = 0.999993; Specific heart = 0.389%; No of data points = 1800; Specific volume = 0.178%

### A.0.3 Specific Heat Capacity (j/kg$^o$C)

The expression for computing specific heat capacity of an aqueous LiBr solution in terms of mass fraction $\xi$ and temperature $T$(K) was formulated as follows;

$$c_{s,LiBr} = -2T(C_0 + C_1\xi + C_2\xi^2 + C_3\xi^3 + C_4\xi^{1.1}) + 6T^2(D_0 + D_1\xi + D_2\xi^2 + D_3\xi^3 + D_4\xi^{1.1}) \\ -12T^3(E_0 + E_1\xi) - 2\left(\frac{F_0 + F_1\xi}{(T - T_0)^3}\right) - 2pT(V_6 + V_7\xi) + \frac{1}{T}(L_0 + L_1\xi + L_2\xi^2 + L_3\xi^3 + L_4\xi^{1.1}) \\ -(M_0 + M_1\xi + M_2\xi^2 + M_3\xi^3 + M_4\xi^{1.1}) \tag{A.9}$$

### A.0.4 Density (kg/m$^3$)

The following equation gives the expression for computing density of LiBr. The corresponding values of the respective coefficients are listed in table A.5 for both specific heat capacity and density.

$$\rho = (V_0 + V_1\xi + V_2\xi^2 + V_3T + V_4\xi T + V_5\xi^2 T + V_6T^2 + V_7\xi T^2)^{-1} \tag{A.10}$$

Table A.5: Typical quantities for computing specific heat capacity and density function of LiBr solvent from equations A.9 and A.10

| i | 0 | 1 | 2 | 3 | 4 |
|---|---|---|---|---|---|
| $C_i$ | 2.648364473E-2 | -2.311041091E-3 | 7.55973662E-6 | -3.763934193E-8 | 1.176240649E-3 |
| $D_i$ | -8.52651695E-6 | 1.3015479E-6 | 2.7919954388E-11 | — | -8.511514931E-7 |
| $E_i$ | -3.840447174E-11 | 2.625469387E-11 | — | — | — |
| $F_i$ | -5.159906276E+1 | 1.114573398 | — | — | — |
| $V_{0-4}$ | 1.176741611E-3 | -1.002511661E-5 | -1.695735975E-8 | -1.497186905E-6 | 2.538176345E-8 |
| $V_{5-7}$ | 5.815811591E-11 | 3.0579997846E-9 | -5.129589007E-11 | — | — |
| $L_i$ | -2.183429482E+3 | -1.266985094E+2 | -2.364551372 | 1.389414858E-2 | 1.583405426E+2 |
| $M_i$ | -2.267095847E+1 | 2.983764494E-1 | -1.259393234E-2 | 6.849632068E-5 | 2.767986853E-1 |

### A.0.5 Dynamic Viscosity

Dynamic viscosity is an essential property that gives a measure of fluid's resistance to flow. For LiBr, this quantity was computed using the following equation A.11 as follows

$$\ln \mu_{s,LiBr} = \sum_{i=1}^{4}\sum_{j=1}^{2} a_{ij}x^{j-1}T^{i-1} \tag{A.11}$$

The corresponding values of i and j are given in table A.6

Table A.6: Values of $a_{ij}$ in equation A.11

| i j | 1 | 2 | 3 | 4 |
|---|---|---|---|---|
| 1 | 15.434 | -1.796 | -454.0 | -1645.0 |
| 2 | -1.497E-1 | 8.581E-2 | -3.187 | -11.190 |
| 3 | 3.211E-4 | -4.050E-4 | -6.116E-3 | 2.286E-2 |
| 4 | -2.398E-7 | 6.025E-7 | 2.69E-6 | -1.336E-5 |

### A.0.6 LiBr property routines

The properties subroutines of aqueous $LiBr/H_2O$ solution as fed in the Engineers Equation Solver (EES) software are outlined in this section. The simple routines are premised on the guideline from the Sorption Systems Consortium (SSC)based at the University of Maryland, USA.

Some of the relevant function routines, units and procedures are outlined in table A.7

Table A.7: List of LiBr routines

| **Functions** | **output units** | **Routine** |
|---|---|---|
| Thermal conductivity | W/mK | k = Cond_LiBr(T,X) |
| Dynamic viscosity | cP | $\mu$ = Visc_LiBr |
| Specific heat capacity | J/gK | cp = Cp_LiBr(T,X,P) or Cp_sat = Cp_LiBr(T,X) |
| Enthalpy | J/g | h = h_LiBr(T,X,P) or h_sat = LiBr(T,X) |
| Chemical potential(water) | J/g | $\mu_w$ = uw_LiBr(T,X,P) |
| Chemical potential(LiBr) | J/g | $\mu_{LiBr}$ = us_LiBr(T,X,P) |
| Volume | $m^3$/kg | v = v_LiBr(T,X,P) |
| Entropy | J/gK | s = s_LiBr(T,X,P) or s_sat = s_LiBr(T,X) |
| Saturation pressure | kPa | P_sat = Psat_LiBr(T,X) |
| Saturation temperature | $^o$C | T_sat = Tsat_LiBr(P,X) |
| Saturation mass fraction | – | X_sat = Xsat_LiBr(T,P) |
| Crystallization temperature | $^o$C | T_cryst = Tcryst_LiBr(X) |
| Flash calculation | – | CAll Flash_LiBr(h, P, x:Q,T) |
| **Procedures** | | |
| Partial Gibbs function | J/g | CALL LiBrpart_g(T,X,P:g, dgdx, mu_w, mu_s) |
| Partial enthalpy | J/g | CALL LiBrpart_h(T,X,P:h, dhdx, h_w, h_s) |
| Partial entropy | J/gK | CALL LiBrpart_s(T,X,P:s, dsdx, s_w, s_s) |
| Partial volume | $m^3$/kg | CALL LiBrpart_v(T,X,P:v, dvdx, v_w, v_s) |
| Flashing process | – | CALL LiBr_flash(h, P, x_in: q, T, x, hl, hv) |

**Input units**: Tc - $^o$C, X - Mass fraction of LiBr, P - kPa

**Note**: LiBrCp, LiBrCh and LiBrCs apply an overload in a way that if the value of P is not included then, saturation condition is assumed and computed.

The respective property units are chosen based on the $UnitSystem Command or within the Unit system dialogue. However, wherever there is a need, the conversion may be initiated.

### A.0.7 Transport Properties

The correlations were developed for various transport properties based on the available data from literature and experiments conducted. A summary of some factors are presented in this section;

#### A.0.7.1 Viscosity

$$\ln \mu = A_0 + A_1 X^2 + \frac{B_0}{T} + \frac{B_1 X^2}{T} + \frac{C_0}{T^2} + \frac{C_1 X^2}{T^2} \tag{A.12}$$

Where the constants are specified as:

$A_0$ = -2.3212641667148; $A_1$ = 3.190587778753

$B_0$ = -609.44957160372; $B_1$ = 963.16370163469

$C_0$ = 372994.85578423; $C_1$ = -35211.99698739

And the units are; $\mu$ (cP), T(K), X (LiBr mass fraction)

Tested with the experimental data, this equation gives $R^2$ value of 0.994273 over he chosen data range. For instance, for T = 20$^o$C (293 K), X = 0.35 $\Rightarrow$ $\mu$ = 1.987 cP

#### A.0.7.2 Thermal Conductivity

The correlation for thermal conductivity K (W/m-K)was developed as;

$$k = A_0 + A_1 X + B_0 T + B_1 T X + C_0 T^2 + C_1 T^2 X + D_0 T^3 + D_1 T^3 X \tag{A.13}$$

Where:

$A_0$ = -0.880453887702949; $A_1$ = 0.883985046484968

$B_0$ = 0.00898659269884302; $B_1$ = -0.007666522227789178

$C_0$ = -1.55427759660091E-05; $C_1$ = 1.38873506415764E-05

$D_0$ = 7.3203107999836E-09; $D_1$ = -6.31953452062666E-09

This correlation generated an $R^2$ = 0.9866 over most data points. For instance, at X = 0.35, T = 20 $^o$C (293 K) $\Rightarrow$ k =0.4873 w/m-K

#### A.0.7.3 Crystallization Temperature

The correlation for crystallization temperature adopted for the study was formulated as follows;

$$x = A_0 + A_1 T + A_2 T^2 \tag{A.14}$$

where the range of the constants values are tabulated as follows;

Table A.8: Constants for solubility boundary equation of LiBr based on equation A.3

| $i$ | $A_i$ | | |
|---|---|---|---|
| | **65 < x < 72** | **57 < x < 65** | **48 < x < 57** |
| 0 | 62.64 | 59.95 | 56.56 |
| 1 | 0.048 | 0.052 | 0.23 |
| 2 | 0.00024 | 0.0035 | 0.0014 |

## A.0.8 Thermodynamic properties of aqueous LiBr solution

Based on the best fit of Gibbs function on experimental data, a wide range of expressions for thermodynamically consistent properties can be derived which are. These properties include specific heat, chemical concentration, volume entropy and enthalpy;

### A.0.8.1 Enthalpy

Given the three independent properties, e.g. temperature, pressure and concentration; the enthalpy can be evaluated. However, because the effect of pressure is negligibly small, the P term can be ignored, and the software still calculates the enthalpy using an overload in the routine to extract properties at saturation pressure. It follows that the routine becomes;

h = h_ LiBr(T,x) or h_ LiBr(T,x, P)

Typical calculation; for T = 20$^o$C (293 K), x = 0.35 $\Rightarrow$ h = 63.37 j/g

### A.0.8.2 Specific heat capacity

cp = cp_ LiBr(T,x) or cp_ LiBr(T,x,P)

Typical calculation; for T = 20$^o$C (293 K), x = 0.35 $\Rightarrow$ cp = 2.372 j/g

### A.0.8.3 Entropy

s = s_ LiBr(T,x) or s_ LiBr(T,x,P)

Typical calculation; for T = 20$^o$C (293 K), x = 0.35 $\Rightarrow$ s = 0.1923 j/g-K

### A.0.8.4 Specific volume

v = v_ LiBr(T,x)

Typical calculation; for T = 20$^o$C (293 K), x = 0.35 $\Rightarrow$ v = 0.0006323 m$^3$/kg

#### A.0.8.5 Chemical potential

**CALL** g_LiBr(Tc,x,P;g,dgdx, mu_w, mu_s)
$\mu$_w = uw_LiBr(Tc,x,P)
$\mu$_s = us_LiBr(Tc,x,P)

$$g_w = \mu_w = g - x\left(\frac{\partial g}{\partial x}\right)_{p,T} \tag{A.15}$$

$$g_s = \mu_s = g + (100 - x)\left(\frac{\partial g}{\partial x}\right)_{p,T} \tag{A.16}$$

Typical calculation; for T = 20$^o$C (293 K), x = 0.35, P =0.8071 kPa $\Rightarrow$ g = -2.337 J/g, dg/dx = 3.758 J/g, g_w = -191.6 J/g, g_s = 186.9 J/g

The property of the mixture can be obtained by summing up the partial properties as follows;

$$g = \frac{(100 - x)g_w + xg_s}{100} \tag{A.17}$$

#### A.0.8.6 Partial enthalpy

**CALL** h_part_LiBr(Tc,x,P;h,dhdx, h_w, h_s)

$$h_w = h - x\left(\frac{\partial h}{\partial x}\right)_{p,T} \tag{A.18}$$

$$h_s = h + (100 - x)\left(\frac{\partial g}{\partial x}\right)_{p,T} \tag{A.19}$$

Typical calculation; for T = 20$^o$C (293 K), x = 0.35, P =0.8071 kPa $\Rightarrow$ h = 63.57 J/g, dh/dx = 1.944 J/g, h_w = 44.25 J/g, h_s = 166.8 J/g

Again, the property of the mixture can be obtained by summing up the partial properties as follows;

$$h = \frac{(100 - x)h_w + xh_s}{100} \tag{A.20}$$

#### A.0.8.7 Partial entropy

**CALL** s_part_LiBr(Tc,x,P;s,dsdx, s_w, s_s)

$$s_w = s - x\left(\frac{\partial s}{\partial x}\right)_{p,T} \tag{A.21}$$

$$s_s = s + (100 - x)\left(\frac{\partial s}{\partial x}\right)_{p,T} \tag{A.22}$$

Typical calculation; for T = 20$^o$C (293 K), x = 0.35, P =0.8071 kPa $\Rightarrow$ s = 0.1853 J/g-K, ds/dx = -0.006176 J/g-K, s_w = 0.4942 J/g-K, h_s = 166.8 J/g

Again, the features of the mixture can be obtained by summing up the partial properties as follows;

$$s = \frac{(100 - x)s_w + xs_s}{100} \tag{A.23}$$

#### A.0.8.8 Partial volume

**CALL** v_part_LiBr(Tc,x,P;v,dvdx, v_w, v_s)

$$v_w = v - x\left(\frac{\partial v}{\partial x}\right)_{p,T} \tag{A.24}$$

$$v_s = v + (100 - x)\left(\frac{\partial v}{\partial x}\right)_{p,T} \tag{A.25}$$

Typical calculation; for T = 20$^o$C (293 K), x = 0.35, P =0.8071 kPa $\Rightarrow$ v = 0.6523 cm$^3$/g, dv/dx = -0.006975 cm$^3$/g, v_w = 1.001 cm$^3$/g, v_s = 0.3033 cm$^3$/g

Again, features of the mixture can be obtained by summing up the partial properties as follows;

$$v = \frac{(100 - x)v_w + xv_s}{100} \tag{A.26}$$

#### A.0.8.9 Saturation properties

P$_{sat}$ = P_LiBr(T,X)

T$_{sat}$ = T_LiBr(P,X)

X$_{sat}$ = X_LiBr(Tc,P)

For instance; T = 20$^o$C (293 K), x = 0.35 $\Rightarrow$ P =0.7901 kPa $\Rightarrow$ v = 0.6523 kPa,

# AppendixB

# Editing Certificates

## B.1 Paper 3

**DR RICHARD STEELE**
BA, HDE, MTech(Hom)
**HOMEOPATH**
Registration No. A07309 HM
Practice No. 0807524
**Freelance academic editor**
**Associate member: Professional Editors' Guild, South Africa**

110 Cato Road
Glenwood, Durban 4001
031-201-6508/082-928-6208
Fax 031-201-4989
Postal: P.O. Box 30043, Mayville 4058
Email: rsteele201@outlook.com

---

**EDITING CERTIFICATE**

Re: **Andrew Y. A. Oyieke**
Journal article: **Stochastic generation of artificial weather data for subtropical climates using higher-order multivariate Markov chain model**

I confirm that I have edited this article and the references for clarity, language and layout. I returned the document to the author with track changes so correct implementation of the changes and clarifications requested in the text and references is the responsibility of the author. I am a freelance editor specialising in proofreading and editing academic documents. My original tertiary degree which I obtained at the University of Cape Town was a B.A. with English as a major and I went on to complete an H.D.E. (P.G.) Sec. with English as my teaching subject. I obtained a distinction for my M.Tech. dissertation in the Department of Homeopathy at Technikon Natal in 1999 (now the Durban University of Technology). During my 13 years as a part-time lecturer in the Department of Homoeopathy at the Durban University of Technology I supervised numerous Master's degree dissertations.

Dr Richard Steele
**21 April 2019**
*per email*

# B.2 Paper 6

**DR RICHARD STEELE**
BA, HDE, MTech(Hom)
**HOMEOPATH**
Registration No. A07309 HM
Practice No. 0807524
**Freelance academic editor**
**Associate member: Professional Editors' Guild, South Africa**

110 Cato Road
Glenwood, Durban 4001
031-201-6508/082-928-6208
Fax 031-201-4989
Postal: P.O. Box 30043, Mayville 4058
Email: rsteele@telkomsa.net

---

**EDITING CERTIFICATE**

Re: **Andrew Y. A. Oyieke**
Journal article: **PERFORMANCE PREDICTION OF AN ADIABATIC SOLAR LIQUID DESICCANT REGENERATOR USING ARTIFICIAL NEURAL NETWORK**

I confirm that I have edited this article and the references for clarity, language and layout. I am a freelance editor specialising in proofreading and editing academic documents. I returned the document to the author with track changes so correct implementation of the changes in the text and references is the responsibility of the author. My original tertiary degree which I obtained at the University of Cape Town was a B.A. with English as a major and I went on to complete an H.D.E. (P.G.) Sec. with English as my teaching subject. I obtained a distinction for my M.Tech. dissertation in the Department of Homeopathy at Technikon Natal in 1999 (now the Durban University of Technology). During my 13 years as a part-time lecturer in the Department of Homoeopathy at the Durban University of Technology I supervised numerous Master's degree dissertations.

Dr Richard Steele
**15 January 2019**
*per email*

# AppendixC

# Acceptance letters

## C.1 Paper 1



International Journal of Low-Carbon Technologies - Decision on Manuscript ID IJLCT-2020-007.R1

From: International Journal of Low-Carbon Technologies (onbehalfof@manuscriptcentral.com)

To: youngoyieke@yahoo.com; youngoyieke@gmail.com

Date: Tuesday, April 28, 2020, 08:18 PM GMT+2

28-Apr-2020

Dear Mr. Oyieke,

It is a pleasure to accept your revised manuscript entitled "A review of coupled heat and mass transfer in adiabatic liquid desiccant dehumidification and regeneration systems; Advances and opportunities" in its current form for publication in the International Journal of Low-Carbon Technologies.

You will receive your official acceptance date from Oxford University Press once you have signed your licence to publish. (N.B. If you are a UK-based author and are looking to comply with the HEFCE policy on open access in the Research Excellence Framework, you should use the official acceptance date when depositing in your repository).

Thank you for your fine contribution. On behalf of the Editors of the International Journal of Low-Carbon Technologies, we look forward to your continued contributions to the Journal.

Sincerely,
Professor Saffa Riffat
Editor in Chief, International Journal of Low-Carbon Technologies

# C.2 Paper 2



## International Journal of Low-Carbon Technologies - Decision on Manuscript ID IJLCT-2019-128.R1

From: International Journal of Low-Carbon Technologies (onbehalfof@manuscriptcentral.com)

To: youngoyieke@yahoo.com; youngoyieke@gmail.com

Date: Sunday, March 1, 2020, 01:11 PM GMT+2

01-Mar-2020

Dear Mr. Oyieke,

It is a pleasure to accept your revised manuscript entitled "Experimental assessment of heat and mass transfer characteristics of solar-powered adiabatic liquid desiccant dehumidifier and regenerator" in its current form for publication in the International Journal of Low-Carbon Technologies.

You will receive your official acceptance date from Oxford University Press once you have signed your licence to publish. (N.B. If you are a UK-based author and are looking to comply with the HEFCE policy on open access in the Research Excellence Framework, you should use the official acceptance date when depositing in your repository).

Thank you for your fine contribution. On behalf of the Editors of the International Journal of Low-Carbon Technologies, we look forward to your continued contributions to the Journal.

Sincerely,
Professor Saffa Riffat
Editor in Chief, International Journal of Low-Carbon Technologies

# C.3 Paper 3

**IAEME Publication**
(Publishers of High Quality Peer Reviewed Refereed Scientific, Engineering & Technology, Medicine and Management International Journals)

**www.iaeme.com**
**editor@iaeme.com**
**iaemedu@gmail.com**

**INTERNATIONAL JOURNAL OF MECHANICAL ENGINEERING AND TECHNOLOGY (IJMET)**

www.iaeme.com/ijmet/index.asp

**SCOPUS INDEXED JOURNAL**

http://iaeme.com/IJMET/IJMET_Scopus.asp

**Journal Impact Factor (2019): 10.6879 Calculated by GISI (www.jifactor.com)**

**ISSN Print**: 0976 - 6340 **ISSN Online**: 0976 - 6359

## Official Acceptance of Research Paper

**Paper ID:** IJMET/10/04/2019/IJMET_43259 **Date:** 25-April-2019

Dear **Andrew Y. A. Oyieke and Freddie L. Inambao**

We would like to inform you that your paper titled **"STOCHASTIC GENERATION OF ARTIFICIAL WEATHER DATA FOR SUBTROPICAL CLIMATES USING HIGHER-ORDER MULTIVARIATE MARKOV CHAIN MODEL"** has been accepted for publication in **International Journal of Mechanical Engineering and Technology (IJMET),** Volume 10, Issue 04, (April 2019) issue of the journal based on the Recommendation of the Editorial Board without any major corrections in the content submitted by the researcher.

This letter is the official confirmation of acceptance of your research paper.

**Your research work is licensed under a Creative Commons Attribution 4.0 (International) License (CC BY-NC 4.0). Hence no need to submit the Copyright form.**

Your research paper will be appearing in IJMET, Volume 10, Issue 04, April 2019.

**International Journal of Mechanical Engineering and Technology (IJMET)**
**Journal Impact Factor (2019): 10.6879 Calculated by GISI**
**ISSN Print: 0976 – 6340**
**ISSN Online: 0976 – 6359**

Review Comments are attached along with the mail.

Kindly send the Publication fee of **$ 575/- (Online only).** The Online Only mode includes online publication of paper, indexing of paper in more than 20 search engines and soft copy of the publication certificate.

You can transfer the money and send the scan copy of payment made evidence through e-mail.

Plot: 03, Flat- S 1, Poomalai Santosh Pearls Apartment, Plot No. 10, Vaiko Salai 6th Street, Jai Shankar Nagar, Palavakkam, Chennai - 600 041, Tamilnadu, India. Mobile: +91-9884798314, E-mail: editor@iaeme.com

# C.4 Paper 4



## International Journal of Low-Carbon Technologies - Decision on Manuscript ID IJLCT-2018-010.R1

From: International Journal of Low-Carbon Technologies (onbehalfof@manuscriptcentral.com)

To: youngoyieke@yahoo.com; youngoyieke@gmail.com

Date: Monday, June 18, 2018, 02:44 PM GMT+2

18-Jun-2018

Dear Mr. Oyieke,

It is a pleasure to accept your revised manuscript entitled "Interfacial Heat and Mass Transfer Analysis in Solar Powered, Packed-bed Adiabatic Liquid Desiccant Regeneration for Air Conditioning" in its current form for publication in the International Journal of Low-Carbon Technologies.

You will receive your official acceptance date from Oxford University Press once you have signed your licence to publish. (N.B. If you are a UK-based author and are looking to comply with the HEFCE policy on open access in the Research Excellence Framework, you should use the official acceptance date when depositing in your repository).

Thank you for your fine contribution. On behalf of the Editors of the International Journal of Low-Carbon Technologies, we look forward to your continued contributions to the Journal.

Sincerely,
Professor Saffa Riffat
Editor in Chief, International Journal of Low-Carbon Technologies

# C.5 Paper 5



## International Journal of Low-Carbon Technologies - Decision on Manuscript ID IJLCT-2019-002.R1

From: International Journal of Low-Carbon Technologies (onbehalfof@manuscriptcentral.com)

To: youngoyieke@yahoo.com; youngoyieke@gmail.com

Date: Monday, April 8, 2019, 10:26 PM GMT+2

08-Apr-2019

Dear Mr. Oyieke,

It is a pleasure to accept your revised manuscript entitled "Multilayered Artificial Neural Network for performance prediction of an adiabatic solar liquid desiccant dehumidifier" in its current form for publication in the International Journal of Low-Carbon Technologies.

You will receive your official acceptance date from Oxford University Press once you have signed your licence to publish. (N.B. If you are a UK-based author and are looking to comply with the HEFCE policy on open access in the Research Excellence Framework, you should use the official acceptance date when depositing in your repository).

Thank you for your fine contribution. On behalf of the Editors of the International Journal of Low-Carbon Technologies, we look forward to your continued contributions to the Journal.

Sincerely,
Professor Saffa Riffat
Editor in Chief, International Journal of Low-Carbon Technologies

# C.6 Paper 6

**IAEME Publication**
(Publishers of High Quality Peer Reviewed Refereed Scientific, Engineering & Technology, Medicine and Management International Journals)

**www.iaeme.com**
**editor@iaeme.com**
**iaemedu@gmail.com**

**INTERNATIONAL JOURNAL OF MECHANICAL ENGINEERING & TECHNOLOGY (IJMET)**
**Scopus Indexed Journal**
www.iaeme.com/ijmet/index.asp

**Paper ID: IJMET_10_03_073** **Date: 21-Mar-2019**

## *Certificate of Publication*

This is to certify that the research paper entitled **"PERFORMANCE PREDICTION OF AN ADIABATIC SOLAR LIQUID DESICCANT REGENERATOR USING ARTIFICIAL NEURAL NETWORK,"** authored by **"Andrew Y. A. Oyieke and Freddie L. Inambao,"** had been reviewed by the Editorial Board and published in **"International Journal of Mechanical Engineering & Technology (IJMET), Volume 10, Issue 03, March 2019, pp. 679-693; ISSN Print: 0976-6340 and ISSN Online: 0976-6359; Journal Impact Factor (2019): 10.6879 Calculated by GISI (www.jifactor.com); InfoBase Index IBI Factor for the year 2015–16 is 3.46; Thomson Reuters' Researcher ID: B-7384-2016".**

*Chief Editor*

Plot: 03, Flat- S 1, Poomalai Santosh Pearls Apartment, Plot No. 10, Vaiko Salai 6th Street, Jai Shankar Nagar, Palavakkam, Chennai - 600 041, Tamilnadu, India.
E-mail: editor@iaeme.com